THE SOURCE OF URANIUM AND VANADIUM AT THE LANGER HEINRICH AND KLEIN TREKKOPJE URANIUM DEPOSITS – GENESIS AND CONTROLLING FACTORS FOR URANIUM MINERALIZATION

A THESIS SUBMITTED IN FULFILMENT OF THE REQUIREMENTS FOR THE DEGREE OF MASTER OF SCIENCE

UNIVERSITY OF NAMIBIA

BY

Abraham Iilende

(Department of Geology)

9507566

November 2012

Main Supervisor: **Dr. A. F. Kamona (University of Namibia)**

Co-supervisors: **Dr. B. Hambleton – Jones (Consulting Geologist)**

Dr. A. G. Marlow (Consulting Geologist)

Abstract

The Langer Heinrich and Klein Trekkopje U deposits are located within the Namib Desert in Central Namibia. Both deposits are hosted by calcretes developed within palaeo-channel systems of Tertiary age. The sources of both U and V in the two deposits and the reasons why the two deposits differ in terms grade and tonnage have remained unclear to many researchers. The study aimed to resolve these uncertainties. During the study, the geology of the area was reviewed and a number of research methods were employed. U and V concentrations and the mineralogy of various rocks in the catchment area were analyzed by ICP-MS, XRF and thin sections. Leachability of various rocks was studied through the analysis of mineralogy, texture, structures, etc.

This study found that the Bloedkoppie granite, which is located in the catchment area for Langer Heinrich, contains about 5 – 15 ppm U and 5 – 20 ppm V. The Tinkas schist, which forms most of the bedrock in the catchment area for the Langer Heinrich deposit, contains 3 – 6 ppm U and 120 – 160 ppm V. The Bloedkoppie granite is considered to represent the source of U for the Langer Heinrich deposit. It is deeply weathered due to its relatively high proportion of ferromagnesian minerals, compared to average granites. The fluid which mobilized U and V from the Bloedkoppie granite also mobilized V from the Tinkas schist.

In the case of Klein Trekkopje, the main source of U was the Klein Spitzkoppe granite, Gross Spitzkoppe granite and some Damaran leucogranites. V is considered to

be derived from the Kuiseb schist, which contains about 100 – 160 ppm V. The Klein Spitzkoppe granite contains about 10 - 20 ppm U and about 1-3 ppm V whereas the Gross Spitzkoppe granite contains about 15 – 25 ppm U and 3 – 5 ppm V.

The catchment area for Langer Heinrich had more V than that of Klein Trekkopje, and V was found to be a key factor in the precipitation of carnotite. The geomorphology around the Langer Heinrich deposit (Etusis and Schieferberge mountains) is more favourable for constriction and ponding of subsurface water unlike that of Klein Trekkopje, which lacks resistant rocks which would restrict the fluids.

Oxidizing conditions were fully achieved at Langer Heinrich because there were less saline marine fogs and the subsurface water spent longer periods of time in ponds, resulting in lengthy interaction with air and seasonal rains. By contrast, at Klein Trekkopje, oxidizing conditions were regularly offset by the inflow of highly saline marine fogs and by the fact that poor constriction and ponding resulted in subsurface water moving faster downstream and having less time to interact with oxidizing atmospheric air and rain waters. As a result V^{4+} could not be effectively oxidized to V^{5+}, which is a pre-requisite for the precipitation of carnotite. Controlling factors for U precipitation in calcretes are redefined in the context of Langer Heinrich and Klein Trekkopje U deposits. Multiple sources of V are proposed. Exploration for calcrete – hosted U deposits could therefore start with investigations of the catchment, by gaging the availability of U and V as well as the suitability of the geomorphology and palaeo-climate.

Definition of Notations and abbreviations

PPL	Plane Polarized Light
Bloed	Bloedkoppie granite
Tink	Tinkas schist
AB	Abbabis basement gneiss
LCALC	Mineralized calcrete at Langer Heinrich
TCALC	Mineralized calcrete at Klein Trekkopje
GSS	Gross Spitzkoppe stock
Klein Sp	Klein Spitzkoppe granite
SP – CL	Clay samples derived from the Klein Spitzkoppe granite
Gross Sp	Gross Spitzkoppe granite
Dol	Karoo Dolerite
Sc	Kuiseb schist
(x)Sc	Metagabbro near the Klein Trekkopje U deposit
Qtz	quartz
Kfs	k-feldspar
Plag	plagioclase feldspar
Bt	biotite
Ms	muscovite
Amp	amphibole

Hbl	hornblende
Mi	microcline
Z	zircon
Ol	olivine
Opx	orthopyroxene
Cpx	clinopyroxene
Grt	garnet
Rt	rutile
Cal	calcite
GSN	Geological Survey of Namibia

Table of Contents

LIST OF FIGURES:

LIST OF TABLES

Acknowledgements:

I wish to thank Dr. Fred Kamona for providing academic supervision for this research project. I also wish to thank my two industry supervisors, Dr. Brian Hambleton – Jones and Dr. Alan Marlow for continuous supervision during the entire research. Dr. Hambleton – Jones provided guidance in the field and Dr. Marlow provided general guidance regarding relevant literature. Dr. Rob Bowell, like Dr. Marlow, also assisted in discussing several aspects of the research (especially groundwater geochemistry) and giving guidance about the relevant literature. My special gratitude goes to Dr. Peter Schreck for assisting with thin section studies and discussions on related matters. I also thank Dr. Erik van Noort for providing uranium and vanadium data for the area around Marenica uranium exploration project. Dr van Noort also led a couple of field trips around Marenica. I am also grateful for the contributions by Mr. Berti Roesener of Areva and Mr. Andrew Reid of Paladin who helped to organize and guide several tours on the Trekkopje and Langer Heinrich mines, respectively. I thank Dr. Stephen Frindt for undertaking a trip with me to the Gross Spitzkoppe granite and for continuous guidance about Cretaceous anorogenic intrusions.

I further wish to thank Mr. Vladimir Osiuuk of SWA Uranium (Pty) Ltd and Mr. Greg Symons of Symons Geophysical Services for organizing and guiding tours to uranium tenements belonging to SWA Uranium (Pty) Ltd and for providing exploration data in those areas. The two gentlemen also assisted in defining the course of the palaeo-channels from the Spitzkoppe area, some through Marenica, to Klein Trekkopje. Their

work provided insight into the morphology of the palaeo-channels around that area. I acknowledge generous support from Ms. Ute Schreiber of the Geological Survey of Namibia for assisting in preparing several maps during the study. I also appreciate the contribution by Prof. Judith Kinnaird of Wits University, who spent her precious time discussing the research topic in Windhoek with me. I also wish to express my gratitude to Mr. Edison Tjikune, the Ministry of Mines and Energy's IT expert, for assisting with the editing of pictures and tables in the thesis. In addition to Mr. Tjikune, I also wish to thank Mr. Toivo Kamati, an IT expert, for his selfless contribution towards the editing of this document. I thank my office team for carrying out the day to day tasks, despite limited input from my side during the project. Finally I thank my family for allowing me to focus most of my attention to the project while neglecting them during the research period.

CHAPTER 1 : INTRODUCTION

Namibia has for many years been one of the most favourable exploration destinations for international investors, particularly due to its high prospectivity for uranium. Currently Namibia is ranked as the world's fourth biggest uranium producer after Kazakhstan, Canada and Australia. In the last 6 years, uranium exploration activities have intensified in Namibia, especially in western Namibia where calcrete hosted uranium deposits are known to occur.

Both the Langer Heinrich and Klein Trekkopje deposits are located in the Namib Desert, in Central Namibia (Fig. 1). The Desert forms a 60 km wide belt of sand dunes and basement rock outcrops over a distance of 1,900 km along the Atlantic coast. The desert rises from sea level to elevations of approximately 975 m at the base of the foothills of the central Plateau. Trekkopje is situated in the central part of the desert, whilst Langer Heinrich is situated on the eastern side of the desert towards the slopes extending upwards to the Central Plateau.

The calcrete hosted Langer Heinrich and Trekkopje uranium deposits in the Namib Desert represent two different types of secondary uranium deposits. Langer Heinrich is a narrow, high grade, low tonnage deposit with average grades in the order of 600 ppm although high grade pods in excess of 5000 ppm have been reported. By contrast Trekkopje is a wide, low grade, large tonnage deposit with average grades in the order of 120 ppm. It has been estimated that the Trekkopje channel contains about 84

000 tons of U_3O_8 at a grade of 104 ppm (Macpherson, 2008) while the Langer Heinrich channel contains a total resource of about 79 000 tons of U_3O_8 at a grade of 600 ppm (Borshoff, 2009). The Langer Heinrich deposit stretches over 15 km and is 1,1 km wide. Trekkopje stretches for about 30 km and is about 5 km wide.

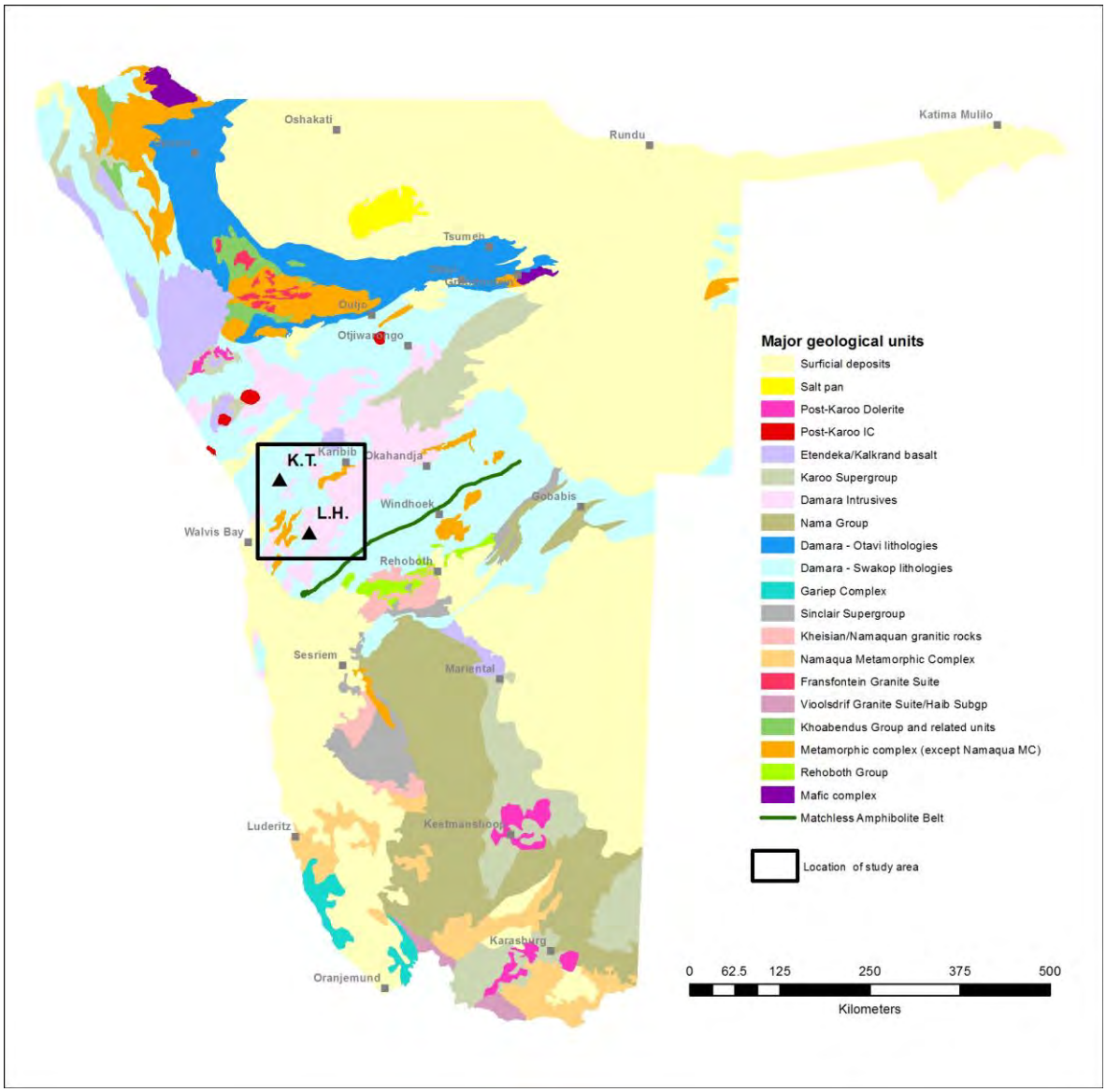

Fig . 1: Simplified geological map showing the location of the study area within Namibia. K.T. refers to the location of the Klein Trekkopje U deposit, and L.H. refers to the Langer Heinrich U deposit.

Figure 1 shows the catchment areas for both the Langer Heinrich and Klein Trekkopje uranium deposits. The Langer Heinrich deposit is covered by Mining Licence 140 held by Paladin Energy (Pty) Ltd, while the Klein Trekkopje deposit is covered by EPL 2218 which has since been converted into a mining licence, held by Areva.

The Langer Heinrich deposit is located about 80 km east of the major seaport of Walvis Bay. The Klein Trekkopje deposit is situated 70 km east of Swakopmund and 80 km northwest of the Langer Heinrich deposit. A smaller uranium prospect (7000 tU_3O_8, 98 ppm U) occurs 5 km to the east of the Klein Trekkopje deposit and it is known as the Trekkopje prospect. The two uranium occurrences (Trekkopje and Klein Trekkopje) together extend over a distance of nearly 30 km by 5 km within one primary drainage system. This study did not focus on the Trekkopje prospect.

The Langer Heinrich deposit forms a single sinuous channel extending for 15 km with a maximum width of only 1,100 m. At Langer Heinrich a number of higher grade pods exist within a single lower grade mineralized envelope.

The Langer Heinrich and Klein Trekkopje uranium deposits characterize an important style of uranium mineralization in Namibia, which is calcrete hosted secondary uranium mineralization formed in extremely arid conditions. The main knowledge gap associated with these calcrete – hosted U deposits is the fact that the sources of U and V are unclear. Furthermore, the controlling factors responsible for this type of U mineralization and their level of significance have not been fully understood. The main objective for this research is therefore to determine the sources of uranium and

vanadium for the Langer Heinrich and Trekkopje deposits and to establish the role played by factors such as Eh, pH, geochemistry of both source rocks and subsurface water, climate and geomorphology in concentrating carnotite within the two different depositional environments. This objective will lead to the establishment of a sound geological model, which enables exploration companies to improve the way they explore for these calcrete – hosted U deposits.

This study was aimed at reviewing the two deposits, assessing their differences and attempting to present them in the context of two end members of a continuum of calcrete hosted uranium mineralization. As stated earlier, the main objective for the study was to ascertain the source of U and V for the two deposits and to uncover the reasons for the difference in characteristics between the two deposits.

The study covered the Langer Heinrich and Klein Trekkopje uranium deposits and their perceived catchment areas. At Langer Heinrich the catchment area was fairly simple, comprising bedrock of predominantly Bloedkoppie granite, Tinkas schist and Etusis quartzite. However, at Klein Trekkopje, the catchment area was much broader, extending as far east as the Spitzkoppe granites which are about 40 km northeast of the deposit itself.

A common dilemma when exploring for secondary calcrete - hosted uranium has been whether to apply the Langer Heinrich “restricted channel” model or the Klein Trekkopje “wider sheet wash style” model. This research has defined and quantified specific geological and geochemical observations, which can assist in choosing the

correct exploration model for the area in question. Several publications, for instance Hambleton-Jones (1976) and Hartleb (1988), have described the two uranium deposits since the 70's, but they have focused on each individual deposit and no effort was ever made to compare the two deposits. Little attention has been paid to the geology of the catchment areas, the source of ions required to form carnotite or the Eh/pH conditions prevailing during the formation of the two uranium deposits. These various geological and geochemical parameters were reviewed in an attempt to establish some criteria for distinguishing between the two deposits.

Due to the fact that a number of researchers have investigated the geological aspects within the study area in the past, the writer decided to use data from such researchers. Although the writer's research topic is different, some data from previous researchers have proven to be useful. These data include the set from Hambleton–Jones (1978), pp208 – 212; Frindt's 2004 whole rock analytical data for the Gross Spitzkoppe granite, pp848-850; Kandara's whole rock analytical data for the Klein Spitzkoppe granite; Youlton's 2006 groundwater data for the Klein Trekkopje area; and Bowell's 2008 groundwater data. Finally, the writer also made use of groundwater analysis by Bittner (2009). There were hardly any limitations of the study because the study area was accessible at all times and the relevant information was either available or obtainable.

1.1 Methodology

The first step was the review of publications which exist on secondary uranium deposits and source rocks for U and V. The study also touched on primary U deposits, albeit to a lesser extent. Ultimately the main method of analyzing the data was by way of thin section studies and plotting correlation diagrams between V and U on the one hand and various other elements considered to play a critical role in the formation of secondary U minerals in a sedimentary environment. Geological maps used for the study were prepared by Ute Schreiber of the Geological Survey of Namibia. Photos of outcrops, critical samples and the two pits were also taken during the study.

1.1.1 Field sampling

The writer started sampling in March 2010 and within about three weeks, a total of 49 rock samples were collected. Subsequently, another 4 samples were also collected. Most of the samples were collected mainly from the catchment areas for the two mines, i.e. Langer Heinrich and Klein Trekkopje. The samples were analyzed by ALS Chemex in Johannesburg by ICP-MS.

In total 53 rock samples were collected during the study. The sample coordinates were recorded by using a GPS (Tables 7 and 8). It is worth noting that only a few samples were collected from those lithologies for which sufficient data is already available from previous researchers (e.g. Gross Spitzkoppe granite). The sample population was as follows: Bloedkoppie granite (12 samples); Tinkas schist at Langer

Heinrich (7 samples); mineralized calcrete at Langer Heinrich (6 samples); Abbabis felsic gneiss (5 samples); Klein Spitzkoppe granite (6 samples); granite derived clay at Klein Spitzkoppe (2 samples); Gross Spitzkoppe granite (3 samples); Karoo dolerite updrainage from Klein Trekkopje (2 samples), Kuiseb schist around Klein Trekkopje (5 samples); amphibolite (3 samples) and mineralized calcrete at Klein Trekkopje (2 samples). The 2 samples from dolerite and another 2 samples from granite derived clay at Klein Spitzkoppe were collected for the purpose of thin section and XRD studies, respectively. No ICP tests were conducted on these four samples.

1.1.2 Geochemical analysis

Each of the first 49 samples was cut into two pieces. The one set of samples was sent to ALS Chemex Laboratory in Johannesburg for Induced Coupled Plasma tests. The remaining set was used for thin section studies at the Geological Survey of Namibia. The four samples collected in the final round from the Karoo dolerite and weathered Klein Spitzkoppe Granite were analyzed by X-Ray Diffraction at the Geological Survey of Namibia. XRD analyses were performed by the Geological Survey of Namibia on five different rock types, namely Bloedkoppie granite (Bloed11), Klein Spitzkoppe granite, weathered Klein Spitzkoppe granite (SP-CL-1 & SP-CL-2) Tinkas schist around Langer Heinrich (Tink 7) and calcrete from the Langer Heinrich ore body (LCALC1). The samples were pulverized in an agate mortar and exposed on a silicon sample tray. The analyses were conducted at room temperature (25˚C) with an X-ray Diffractrometry instrument (Bruker D8 Goniometer). A copper X-ray tube was used for monochromatic

radiation. The main reason for the XRD analyses was to determine the type of clays found within the Klein Spitzkoppe granite.

Table 1: Sample coordinates, Langer Heinrich catchment area.

SAMPLE ID.	**LITHOLOGICAL UNIT**	**COORDINATES (**geographic coordinate system**)**	
Bloed1, Bloed2, Bloed3, Bloed4, Bloed5 & Bloed6	Bloedkoppie granite	S22˚48’46.1”	E015˚22’12.4”
Bloed7, Bloed8, Bloed9, Bloed10, Bloed11 & Bloed12	Bloedkoppie granite	S22˚50’14.6”	E015˚22’51.8”
Tink1, Tink2, Tink3, Tink4, Tink5, Tink6 & Tink7	Tinkas schist	S22˚48’34.5”	E015˚19’29.6”
LCalc1, LCalc2, LCalc3, LCalc4, LCalc5 & LCalc6	Langer Heinrich Calcrete (mineralized)	S22˚48’49.1”	E015˚18’48.8”
AB1, AB2, AB3, AB4 & AB5	Abbabis felsic gneiss	S22˚34’45.8”	E15˚02’29.5”

Table 2: Sample coordinates, Klein Trekkopje catchment area.

SAMPLE ID.	**LITHOLOGICAL UNIT**	**COORDINATES**	
Sp1 & Sp2	Klein Spitzkoppe granite	S21˚53’31.7”	E15˚02’29.5”
Sp3, SP4, Sp5 & Sp6	Klein Spitzkoppe granite	S21˚54’48.0”	E15˚02’19.8”
Gross 1 & Gross 2	Gross Spitzkoppe granite	S21˚50’07.8”	E15˚10’01.0”
Gross 3	Gross Spitzkoppe granite	S21˚5014.7	E15˚12’01.5”
		UTM Coordinate system	
TCALC 1 & TCalc2	Klein Trekkopje calcrete (mineralized)	0486133	7548279
Sc1, Sc2 & Sc3	Kuiseb schist	048429	7544274
2Sc1, 2Sc2 & 2Sc3	Amphibolite/ metagabbro near Klein Trekkopje	0482402	7544846

According to Lindelani Mugivi, who works for ALS Chemex, the following methodology was used at ALS Chemex to analyze 49 of the samples sent by the writer:

ME-MS61r (REE Add-on package to ME-MS61)* Ultra-Trace Level Method Using ICP-MS and ICP-AES:

Sample Decomposition:

$HF\text{-}HNO_3\text{-}HClO_4$ acid digestion, HCl leach (GEO-4A01)

Analytical Method:

Inductively Coupled Plasma - Atomic Emission Spectroscopy (ICP - AES) Inductively Coupled Plasma - Mass Spectrometry (ICP-MS)

A prepared sample (0.25 g) is digested with perchloric, nitric, hydrofluoric and hydrochloric acids. The residue is topped up with dilute hydrochloric acid and analyzed by inductively coupled plasma-atomic emission spectrometry. Following this analysis, the results are reviewed for high concentrations of bismuth, mercury, molybdenum, silver and tungsten and diluted accordingly. Samples meeting this criterion are then analyzed by inductively coupled plasma-mass spectrometry. Results are corrected for spectral interferences.

NOTE: Four acid digestions are able to dissolve most minerals; however, although the term "*near-total*" is used, depending on the sample matrix, not all elements are quantitatively extracted.

Results for the additional rare earth elements will represent the acid leachable portion of the rare earth elements.

The detection limits used by ALS Chemex Laboratory are as shown Appendix 1

1.1.3 Mineralogical studies

Covered thin sections were prepared in the Geological Survey of Namibia, using Logitec equipment. The covered thin sections were used to determine the mineralogy of the various samples, using an Olympus polarizing microscope at the Geological Survey of Namibia.

A portable XRF was also used to carry out a broad based survey for vanadium concentrations in the Tinkas and Kuiseb schists as well as in the Karoo dolerite. The Tinkas schist was surveyed around the Langer Heinrich mine, whereas the Kuiseb schist and the Karoo dolerite were surveyed around the Klein Trekkopje deposit.

A ground radiometric survey was carried out by the writer on the Bloedkoppie, Salem, Klein Spitzkoppe and Gross Spitzkoppe Granites. The instrument used in this exercise was a hand held scintillometer and the idea was to determine the radiation intensity for the granites and the homogeneity of their respective uranium concentrations. The values for the radiometric intensities are given in counts per second (cps).

A number of photos were taken in the field especially in the two pits, Langer Heinrich and Klein Trekkopje. More photos were also taken in the catchment area, especially the Bloedkoppie granite, Schieferberge schist, Etusis quartzite, Klein Spitzkoppe granite, Gross Spitzkoppe granite, Kuiseb schist, Salem granite and Karoo dolerite.

1.1.4 Additional data for the study

In order to avoid re-inventing the wheel and for the sake of completeness, the writer has partly used two geochemical data sets belonging to Kandara (1998) and Frindt (2004) for the Klein Spitzkoppe and Gross Spitzkoppe granites, respectively. The data was used to plot correlation diagrams between various elements. The writer has also used drilling data (XRF) from Chetty (1999) for the mineralized calcretes at Klein Trekkopje by plotting various correlation diagrams. Chetty did some work for a uranium exploration company by the name of Gulf Western Trading at the time. Furthermore, the writer has used existing groundwater data for the Langer Heinrich area from Bittner (2009) to plot correlation diagrams. These diagrams for ground water data would enable researchers to understand which elements in the ground water contribute to the precipitation of U and V. Similarly, existing groundwater data for the Klein Trekkopje area from Youlton (2006) were also used during the study.

CHAPTER 2 : LITERATURE REVIEW OF SECONDARY URANIUM DEPOSITS

2.1 The nature and occurrence of surficial uranium deposits

The World Nuclear Association has defined surficial uranium deposits as young (Tertiary to Recent) near-surface uranium concentrations in sediments or soils. These deposits usually have secondary cementing minerals including calcite, gypsum, dolomite, ferric oxide, and halite. In these deposits, uranium mineralization is found in fine-grained surficial sand and clay, cemented by calcium and magnesium carbonates. According to the World Nuclear Association, surficial uranium deposits comprise about 4% of the world uranium resources. In Western Australia, calcrete deposits are believed to represent about 4% of Australia's total resources of uranium. Calcrete deposits form where uranium - rich granites were deeply weathered in a semi-arid to arid climate. The main surficial uranium deposits in Namibia include Langer Heinrich, Klein Trekkopje and Marenica.

In Western Australia, where similar deposits are found, the main deposits include Yeelirrie, Lake Way, Centipede, Thatcher Soak and Lake Maitland. Other surficial uranium deposits have also been reported from South Africa, Botswana, Argentina and Somalia (World Nuclear Association, 2010). According to Toens (1984), in Hambleton-Jones (1984), the most common factor for these deposits is that uranium mineralization is almost invariably in the form of carnotite. Toens (1984) also suggested that valley – fill deposits, such as Langer Heinrich, Trekkopje, Tubas, and Aussinanis in Namibia,

have the greatest economic potential of all 8 types of surficial uranium deposits listed by Hambleton – Jones (1976) (Fig. 8). By definition, valley-fill deposits belong to the class of fluviatile deposits and are characterized by very deep channels. They are followed in depth by flood plain deposits, delta deposits and finally by playa deposits, which are the shallowest (Hambleton – Jones, 1984).

The playa deposits represent the lowest energy levels of the palaeo-current, while the valley-fill deposits represent the highest energy levels. Toens (1984) compared surficial uranium deposits in the Namib Desert to the ones in Western Australia, in terms of the drainage patterns. He observed that in Namibia, for instance, the water in the Tumas channel could travel many tens of kilometers before gradually disappearing in the sand. According to him, in Western Australia flow is subsurface, and many drainages terminate in playas.

In 1999, Gulf Western Trading requested MINTEK to carry out a mineralogical and chemical characterization of 40 samples originating from the Klein Trekkopje uranium deposit. Their data is contained in Tables 19 and 20. The company was attempting to understand the mode of occurrence and relationships between uranium, vanadium and strontium. The investigation found that in general, high uranium values were associated with high vanadium values (Chetty et al., 1999). It was also found that vanadium occurred mainly in carnotite. However, two other vanadium-bearing phases were found. These are believed to be oxides containing thorium as a predominant element with calcium and some silica.

It was also found that most of the carnotite was hosted by clay. Strontium occurred as celestite ($SrSO_4$) while barium occurred as barite ($BaSO_4$). Barite was mainly found to be associated with feldspar, which suggests that barium was primarily associated with feldspar when sulphate-rich water came into contact with the feldspar grains. Ba was derived from Ca-rich feldspars. The relationship between strontium and uranium did not show a clear positive correlation like the one between vanadium and uranium. The study found that carnotite was associated with fine grains (< 20 μm) in the samples. Other minerals of less significance found in the ore include celestite, monazite, zircon, fluorite and iron-hydroxides.

At Klein Trekkopje, carnotite appears as a yellow to greenish mineral within the sediments cemented either by calcite or gypsum. Carnotite constitutes 95% of the ore, and about 5% of uranium is believed to be contained in other minerals like tyuyamunite $Ca(UO_2)_2(VO_4).6(H_2O)$, urancalcarite $Ca(UO_2)3(CO_3)(OH)_6).6(H_2O)$ and soddyite $(UO_2)_2SiO_4.2(H_2O)$ (Roesener, 2010 personal communication).

2.2 Chemistry of ore forming elements

It is worthwhile to look at the chemistry of both U and V so that their chemical behaviour in magmatic fluids, in meteoric water and in rocks can be predicted.

2.2.1 Uranium

Maassen (1982) tabulated uranium concentrations in various rock types in order to indicate the lithologies which naturally carry more uranium than others.

Table 3: Average uranium abundance in common rocks (Maassen, 1982).

Rock Type	**Ppm**
Average “cosmic”	0.01 – 0.1
Average Crust	2.7 – 3.6
Granites	> 4.0
Inter. Igneous Rocks	1.9
Plateau Basalts	0.5
Ultramafic	0.01
Grey Shales	4.0
Black Shales	53.0
Limestones	4.0
Amphibolites	2.4
Granulites	0.6
Archean Shields	0.7
Paleozoic Crust	1.3
Alkalic Igneous Rocks	0.1 – 30.0

Table 4: U concentrations in various granitoids (after Marlow 1981).

Rock name	Average U Concentration (ppm)
Namibfontein red granite	3.5
Salem granite	2.9
Stinkbank leucogranites	7
Ida dome alaskite	40
Otjua red granite	112.6
Goanikontes alaskite	150
Valencia alaskite	34
Rossing alaskite	298

From Table 3, it can be seen that granites generally contain 4 ppm uranium or more. Looking at the data in tables 3 and 4, it can be seen that most granitoids studied by

Marlow (1981) in the Namib Desert have average U concentrations well above 4 ppm which is considered by Maasen (1982) as the average U concentration in granites. The only granitoids with U concentration below 4 ppm are the Salem granite and the Stinkbank leucogranites. Some of the granitoids in table 4 (e.g. Rossing, Goanikontes and Ida dome alaskites) are known to have high grade zones and have historically been targeted by mining companies.

Most of the rocks in the Namib Desert are anomalously U-rich. The geological map of Namibia shows that the Namib Desert is full of different types of granitoids and many of these Damaran granitoids are strongly radiogenic. It can therefore be expected that there is no shortage of uranium for the formation of secondary, calcrete - hosted, uranium deposits in this part of the world. Some of the rocks of the Namib Desert and higher on the plateau regions, which have uranium concentrations above crustal averages include Abbabis Basement gneisses, Damara - aged granites and Cretaceous granites such as Brandberg, Klein Spitzkoppe, Gross Spitzkoppe, etc. (Marlow, 1981 and Frindt et al., 2004a).

According to Skirrow et al. (2009) uranium occurs in minerals predominantly in hexavalent (U^{+6}) and tetravalent (U^{+4}) states. Because of its heterovalent state, uranium is highly sensitive to the oxidation conditions of the environment. Metal ions and ligands can be classified into acids (those which accept electrons) and bases (those with available electrons), (Skirrow et al., 2009). The ions U^{+4}, U^{+6} and Th^{+4} are hard acids

and hence tend to complex more readily with hard bases such as F^-, OH^-, NO_3^-, CO_3^{2-}, HCO_3, SO_4^{-2}, HSO_4, PO_4^{-3}, HPO_4^{-2} and $H_2PO_4^-$ (Skirrow et al., 2009).

Skirrow et al. (2009) tabulated uranium species, grouping them into oxy and hydroxyl species, carbonate species, phosphate species, sulphate species, fluoride species and chloride species.

Table 5: Aqueous complexes of uranium (Skirrow et al., 2009).

COMPLEX TYPE	URANIUM SPECIES
Simple and oxy and hydroxyl	U^{+3} , U^{+4}, $U(OH)^{+3}$, $U(OH)_2^{+2}$, $U(OH)_3^{+1}$, $U(OH)_4$, $U(OH)_5^{-1}$, $U_2(OH)_5^{+3}$, UO_2^{+1}, UO_2^{+2}, $UO_2(OH)_2^{+1}$, $UO_2(OH)_2$, $UO_2(OH)_3^-$, $UO_2(OH)_2^{+2}$, $(UO_2)_3(OH)_5^+$
Carbonate (uranyl)	UO_2CO_3, $UO_2(CO_3)^{-2}$, $UO_2(CO_3)_3^{-4}$
Phosphate (uranous and uranyl)	$UHPO_4^{+2}$, $U(HPO_4)_2$, $U(HPO_4)_3^{-2}$, $U(HPO_4)_4^{-4}$, $UO_2(HPO_4)$, $UO_2(HPO_4)_2^{-2}$, $UO_2(H_2PO_4)^+$, $UO_2(H_2PO_4)_2$, $UO_2(H_2PO_4)_3^-$
Sulphate (uranous and uranyl)	$U(SO_4)_2$, $UO_2(SO_4)$, $UO_2(SO_4)_2^{+2}$, USO_4^{+2}
Fluoride	UF^{+3}, UF_2^{+2}, UF_3^+, UF_4, UF_6
Chloride	UCl^{+3}, UO_2Cl^+

Although uranium can exist in a vast number of complexes, previous research has already established that in the groundwater of the Namib Desert, uranium is held as a carbonate complex (Bowell et al., 2009).

Maassen (1982) also indicated that uranium's high solubility in the surficial environment is due to the oxidation of U^{4+} to the U^{6+} as UO_2^{2+} in aerated or near surface oxidizing environments according to the equation $UO_2(S) + 2H^+ + 1/2O_2(aq) = UO_2^{2+} + H_2O$.

Because the complexes uranyl dicarbonate, uranyl tricarbonate and uranyl acid phosphate are all stable at pH values above 7.5, uranium is most mobile in alkaline aqueous environments (Maassen, 1982).

2.2.2 Vanadium

V is not a common element but economic deposits have been found mainly in magnetite layers in the upper zone of the Bushveld Igneous Complex (Bowell et al., 2010). It is usually used as an alloying metal for cutting and other tool steels. Its oxidation states of +5, +4, +3 and +2 are easily produced sequentially by reduction of solutions of vanadium salts since the reduction potentials for the different states are more or less evenly and quite widely spaced (Bowell et al., 2010).

2.2.3 Oxidation of vanadium:

According to Bowell et al., (2010) the reaction which is most relevant to the Namib Desert's groundwater is as follows:

$$2V^{2+} + 2.5O_2 + 3H_2O \rightleftharpoons 2H_3VO_4$$

The acid chelate $2H_3VO_4$ then reacts with the uranium to form a uranyl vanadyl complex.

This is the most common reaction, and it would be catalyzed by strong oxidizing couples such as Fe^{2+}, Fe^{3+}, Mn^{2+} or Mn^{5+} (the latter may explain the high Mn concentration in certain calcrete ores).

2.2.4 Previous experiments about the behavior of vanadium

In the olden days, Notestein (1918) observed during his experiments that vanadium in its high oxidation states (e.g. V^{5+}) is a very powerful oxidizing agent. His experiment in this regard was a solution consisting of potassium sulphate and uranyl sulphate. He added vanadium pentoxide to this solution and a bright yellow precipitate started to settle at the bottom of the bottle. In his opinion, this yellow precipitate was carnotite.

2.2.5 Previous research on Uranium

The data presented in Table 6 demonstrate the different degree to which uranium partitions into accessory minerals during fractional crystallization of a granitic magma:

Table 6: Uranium content for accessory minerals (isomorphic substitution in crystal lattice), after Skirrow et al., (2009).

MINERAL	**COMMON RANGE (PPM, U)**
Allanite $(Ca,Ce)_2Fe^{+2},Fe^{+3})Al_2O.OH[Si_2O_7][SiO_4]$	30-1000
Apatite $Ca_5 (PO_4)_3 (OH,F,Cl)$	5-100
Epidote $(Ca,Fe^{+3})Al_2O.OH[Si_2O_7][SiO_4]$	20-200
Garnet $Ca_3Al_2Si_3O_{12}$	6-30
Ilmenite $FeTiO_3$	1-50
Magnetite Fe_3O_4	1-30
Monazite $(Ce,La,Th)PO_4$	500-3000
Titanite $CaTi[SiO_4](O,OH,F)$	10-700
Xenotime YPO_4	300-35,000
Zircon $ZrSiO_4$	100-6000

Looking at Table 6, it can be seen that the accessory minerals which carry most U are xenotime, zircon, monazite and allanite. However xenotime tends to occur mainly in carbonatites while zircon, monazite and allanite are very common in granitoids, which makes them more relevant to this study. The catchment areas for Langer Heinrich and Klein Trekkopje U deposits consist of granitoids rather than carbonatites.

During fractional crystallization of a granitic magma, the light rare earth elements partition heavily into monazite while the heavy rare earth elements tend to partition into zircon (Frindt et al. 2004a). It follows therefore that research into whether uranium is leachable in a particular granitoid, can be carried out by examining its relationship with rare earth elements. A strong positive correlation between rare earth elements and uranium suggests that there is a lot of uranium locked up in these accessory minerals and consequently leaching of uranium becomes difficult in such granite. By contrast, a poor correlation between the accessory minerals and uranium suggests that most of the uranium resides outside resistant accessory minerals and can be liberated easily during erosion.

The uranium liberated in this way can be deposited downstream, resulting in potential secondary uranium deposits. Therefore in the next chapters, various granitoids will be investigated in this manner to see if they have potential to generate uranium deposits downstream. Miller (2009) tabulated several elements according to their ionic radius size and their charge (Table 7). Elements whose ionic radii are closely similar will substitute for each other during crystallization of a given magma. Furthermore, elements

which share the same charge and Group tend to substitute for each other during crystallization.

Table 7: Elements likely to substitute with each other depending on charge and size of ionic radii, after Miller 2009.

Group I (+)	Group II (2+)	Group III (3+)	Group IV (4+)	Group V/VI (5+)	Group VIII (2+, 3+)
Li 0.78	Be 0.34	B 0.20			
Na 0.98	Mg 0.78	Al 0.57	Si 0.39		
K 1.33	Ca 1.06		Ti 0.64		Fe 0.83, 0.67
Rb 1.49		Eu 1.13	Zr 0.87	Nb 0.69	
Cs 1.65			Sn 0.74	Ta 0.68	W 0.68
			Th 1.10		
			U 1.05		

Mg & Fe is one of the most common substitutions. Table 7 explains why, for instance, Rb and K tend to occur together and enriched in highly differentiated granitoids because of their similarity of ionic charge and radius. The table also explains why for instance, uranium tends to be associated with elements such as thorium or zirconium due to the similarity of charge.

Miller (2009) also listed common uranium minerals in granites and their locations (see below). The common primary U minerals include Uraninite – UO_2; Betafite - (U, Ca)(Nb, Ta, Ti) $_3O_9.nH_2O$; Uranyl silicate – U, Th, Si, Ca (coffinite) and brannerite. The common secondary minerals in granites include Uranophane – $Ca[UO_2]_2[SO_3]_2(OH)_2.5H_2O$ and Uranyl silicate – U, Th, Si, Ca (coffinite).

Regarding ground water, Bowell et al. (2010) tried to understand the groundwater geochemistry for the Namib Desert (Fig. 2), but his interpretations were very brief. According to Bowell et al. (2010), the deposit with the highest salinity is Mile 72, followed by Tubas, Trekkopje and Langer Heinrich. The reason behind this apparently relates to the distance from the sea, with Trekkopje and Langer Heinrich the furthest from the coast, Tubas being 40 km and Mile 72 at the coast. Uranium is present in many of the ground waters. Bowell et al. (2010) went further to argue that in terms of a correlation, a positive correlation can be observed for uranium with redox potential (Eh), high carbonate and lower sulphate and chloride, pH, and potassium in groundwaters (Bowell et al., 2010).

The chemistry of groundwater for Namibian calcretes promotes the stabilization of the species, $UO_2(CO_3)_2^-$ and for vanadium, $VO_2(OH)_4^-$ (Bowell et al., 2010).

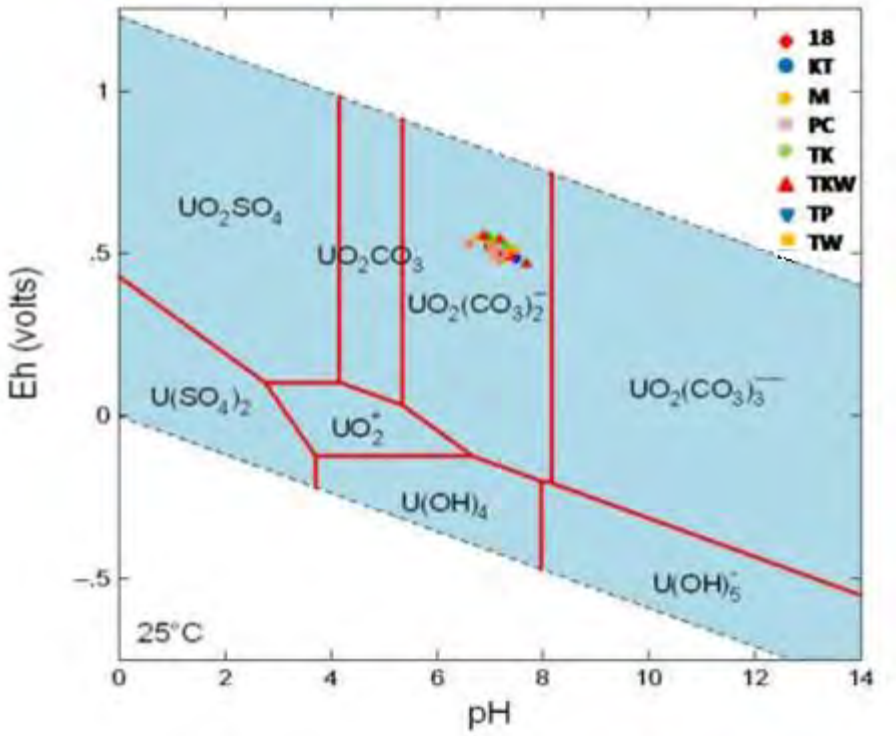

Fig . 2 : Eh-pH diagram for the system U-H-O-S-Cl (from Bowell et al., 2010). The symbols 18, KT, M, PC, TK, etc, represent various sample numbers for the groundwater in the Namib Desert. The pH – Eh for these samples plot in the field where the stable uranium species is $UO_2(CO_3)^{2-}$.

Figure 2 indicates that in all ground water samples of the Namib Desert plotted by Bowell et al. (2010), U is carried as a carbonate complex. According to Hartleb (1988), the combination of uranyl– and potassium-ions with vanadate-ions will result in the precipitation of carnotite according to the following reaction:

$$2K^+ + 2UO_2^{2+} + 2(HVO_4)^{2-} + 2H_2O \quad \rightleftharpoons \quad 2KUO_2VO_4.3H_2O + 2H^+$$

Carnotite is stable within a broad pH range around a neutral pH value. It is therefore not surprising that carnotite is one of the most common secondary uranium minerals within calcrete type deposits.

Hartleb (1988) also observed that calcification is achieved through the following reaction in the groundwater: $Ca^{2+} + 2HCO_3^- \rightarrow CaCO_3 + CO_2 + H_2O$.

The calcium carbonate was added as a bi-carbonate to the clastics and its deposition facilitated by the loss of carbon dioxide and water.

2.3 General favourable criteria for carnotite precipitation

Carlisle et al., (1978) have documented uranium favourability criteria deduced from the Australian and Namibian studies as follows:

1. Adequate source terrain, deeply weathered;
2. Anomalous groundwater uranium and vanadium contents;
3. Large catchment area;
4. Low drainage gradients;
5. Very limited runoff;
6. Nonpedogenic calcrete;
7. Absence of soil carbonate deposition or other uranium fixing processes in the catchment area;
8. Evaporative concentration of uranium, vanadium, and potassium drainages;

9. Constricted, shallowing, or upwelling groundwater flow within the valley calcrete area due to bedrock or impermeable sediment barriers;

10. Reconcentration of carnotite;

11. Stabilization of carnotite; and

12. Moderate to low relief and tectonic stability.

The next four diagrams (Figures 3 – 5) by Carlisle et al. (1978) demonstrate idealized genetic processes of carnotite precipitation in calcrete/gypcrete. These Figures illustrate the role of CO_2, H_2O, SO_4^{2-}, and bedrock highs in the formation of calcrete/gypcrete - hosted U mineralization. The loss of CO_2 and H_2O through evapo-transpiration promotes the precipitation of carnotite in ground water because abundant CO_2 in the water would lead to the ongoing complexing of uranyl ion with the CO_3^{2-} ion, which means U stays in solution (Carlisle et al., 1978). Figure 5 shows how the chloride and sulphate ions are added to groundwater through the introduction of marine fogs. According to Carlisle et al. (1978), the continuous introduction of the chloride and sulphate ion will retard the precipitation of carnotite because both the pH and Eh get decreased.

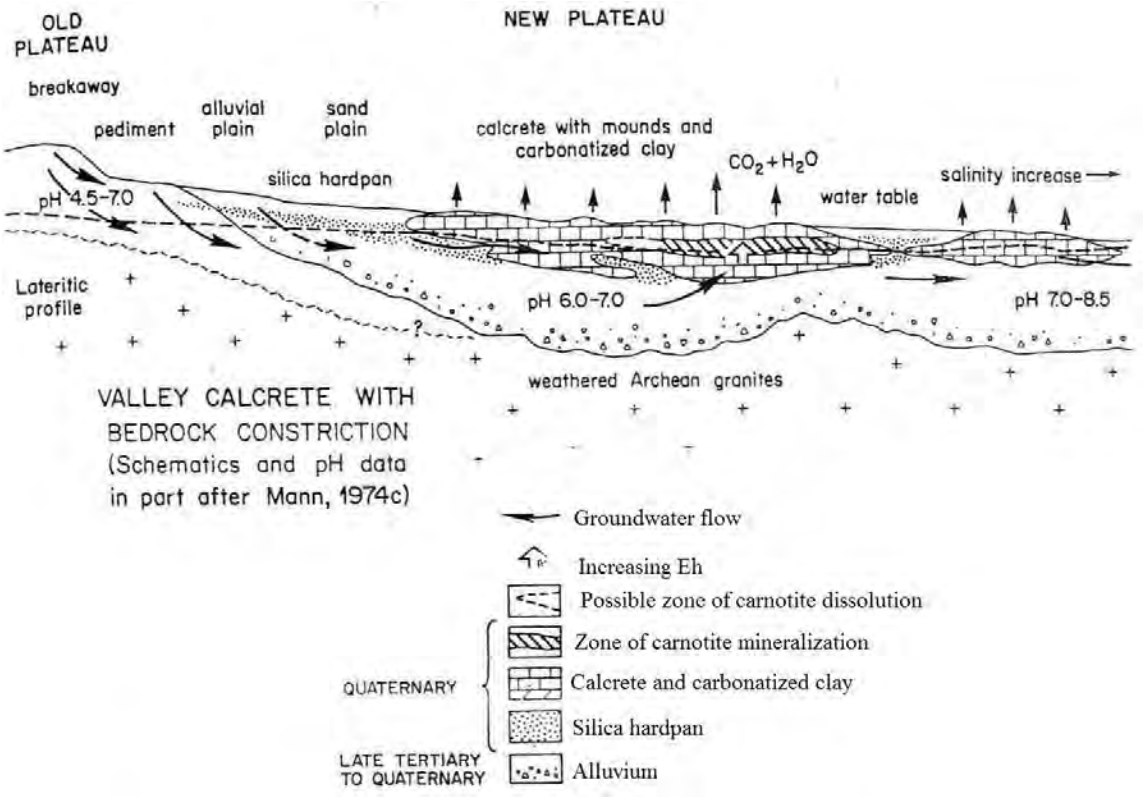

Fig . 3 : Schematic models for nonpedogenic, U-bearing calcrete, Western Australia and Namibia (from Calisle et al. 1978).

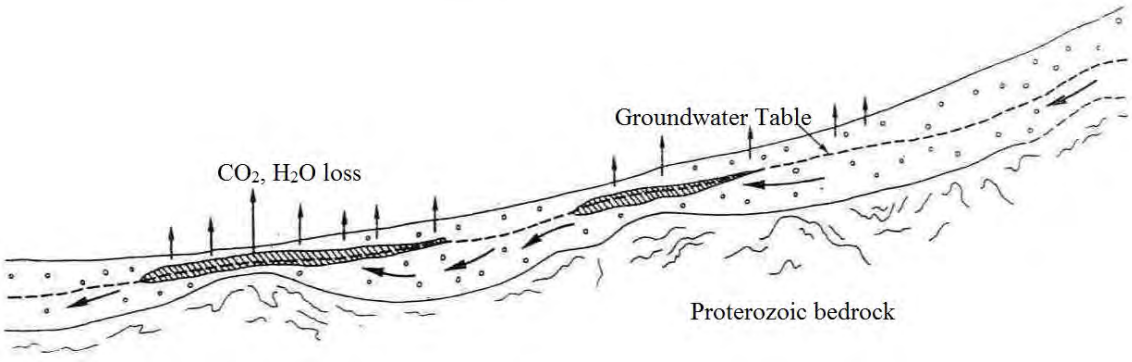

Fig . 4 : Schematic model showing the influence of geomorphology on U mineralization (mineralization is associated with bedrock highs), (after Carlisle 1978).

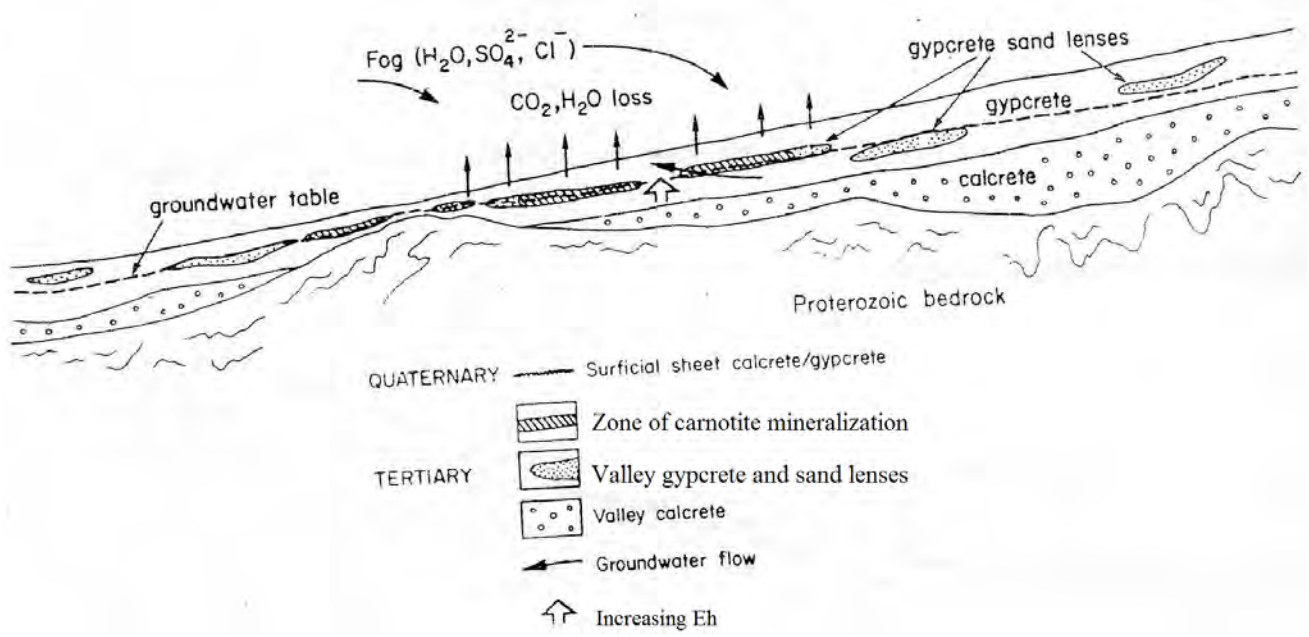

Fig . 5 : Gypcrete type model for secondary U mineralization (from Carlisle 1978). This model is applicable to the Klein Trekkopje U deposit.

In all the three Figures (3-5), U mineralization appears to be exclusively associated with bedrock highs. Similarly, the loss of water and carbon dioxide due to evaporation takes place in areas of bedrock highs. This highlights the significance of geomorphology in the process of U precipitation.

Figure 6 below shows the idealized process of leaching, transportation of uranium and vanadium and finally, precipitation of carnotite (Mann and Deutscher, 1978). It shows a catchment area comprising uranium-rich granites and vanadium-rich mafic rocks. The Figure also shows how this catchment area is weathered, resulting in the enrichment of U, K and V in the subsurface water in the channel. Finally, Figure 10

shows how a Yeelirie type deposit is formed in a pond situated behind a natural barrier (bedrock high).

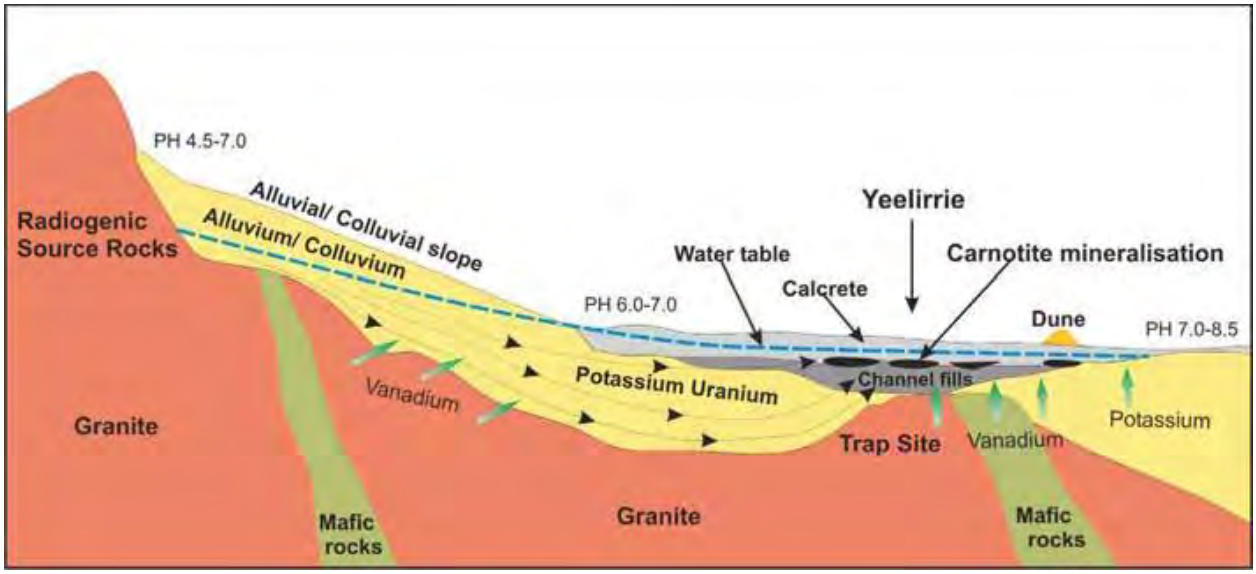

Fig . 6 : Idealized model of valley-fill calcrete uranium mineralization: example from the Yeelirrie deposit of Western Australia (after Mann and Deutscher 1978).

Uranium mineralization at Yeelirrie is typically carnotite, a potassium uranyl vanadate ($K(UO_2)_2(VO_4)_2.3H_2O$) and is commonly cemented by secondary minerals including calcite, gypsum, dolomite, ferric oxide and halite. Uranium deposits in calcrete (calcium and magnesium carbonates) are the largest of the surficial deposits. These usually form in regions where deeply weathered, uranium-rich granites occur in a semi-arid to arid climate. In Figure 6, the mafic rocks are considered to be the main source of V which formed the Yeelirrie deposit. Just like in Figures 3 – 5, U mineralization in Figure 6 is associated with bedrock high. Examples from Western Australia occur in

valley-fill sediments along Tertiary drainage channels (e.g. Yeelirrie and Lake Mason) and in playa lake sediments (e.g. Lake Maitland). Bowell et al. (2010) suggests that the mineralogy of the overburden within the Yeelirrie drainage channel is dominated by quartz, saponite, gypsum and calcite with lesser amounts of illite / Al smectite, kaolinite, dolomite and feldspar. The calcrete is apparently dolomitic at depth.

In magmatic systems, uranium tends to be adsorbed onto the surfaces of biotite crystals, held as inclusions in accessory minerals such as zircon and monazite, or held in inter-granular spaces, e.g. between quartz and feldspar grains (Marlow, 1981). In the structure of biotite, uranium appears to cling onto the positions otherwise occupied by Fe and K. This explains the close association between uranium and these two elements in igneous rocks. Certain high level granites have pink orthoclase, this colour is due to iron oxide distributed within the orthoclase and which has the effect of occluding uranium (Hambleton - Jones, 1976). Orthoclase weathers easily in carbonated water (Hambleton – Jones, 1976).

In sedimentary systems, aqueous sulfur dioxide has the effect of reducing V^{5+} to V^{4+}. Several experiments carried out in the past to establish the behaviour of uranium and vanadium have resulted in significant findings. One of the findings was that clay minerals, especially montmorillonite, play a vital role in concentrating uranium in a sedimentary environment (Hambleton – Jones, 1976). In a sedimentary environment, both uranium and vanadium are adsorbed onto the surfaces of clay minerals before carnotite precipitation takes place. These experiments have also shown that vanadium, in

its high oxidation states, is a very powerful oxidant and will readily precipitate uranium from solution (Hostetler and Garrels, 1962). The vanadium experiment carried out by Hostetler and Garrels (1962) is considered to be significant in relation to the formation of the Langer Heinrich uranium deposit, which formed as a result of unique abundance of vanadium in the palaeo-groundwater.

According to Mann and Deutscher (1978), the secondary uranium deposits in Western Australia illustrated above are slightly different from the ones in the Namib Desert. Some of them, like Lake Maitland, were formed as a result of subsurface water coming into contact with saline brines in a lake environment. Because of this scenario, the calcrete cement in these deposits usually shows minerals such as dolomite and halite, which owe their existence to the brines in the lake.

Hambleton – Jones (1976) has indicated that granites with high leachable U characteristically contain the following primary minerals, mainly orthoclase feldspar and biotite with minimal muscovite and amphiboles, e.g. Bloedkoppie Granite. However, oligoclase is also common in many U-bearing granites. On the other hand, granites with low leachable U characteristically contain the following primary minerals, higher proportion of plagioclase feldspar, muscovite in preference to biotite and presence of amphiboles, e.g. Donkerhoek granite. Accessory non-leachable minerals e.g. monazite and zircon are common to both in different proportions.

2.4 Palaeo-climate

It is quite important for one to understand the palaeo-climate for the Namib Desert because climate is one of the key factors in the formation of calcrete hosted U deposits. In Namibia the winds from the SSW blow throughout the year (Wilkinson, 1990). According to the same literature, these winds drive the north-flowing Benguela Current and generate maximum upwelling of cold bottom water adjacent to the coast.

Rainfall at Swakopmund over 35 years has been measured at 18mm/annum and increases to 150 mm/annum further inland (Hambleton – Jones, 1978). Most of the precipitation in the Namib Desert is from fogs blown inland from the sea, and amounts to 130 mm/annum. These marine fogs are carried by winds driven by the north easterly Benguela current.

Ward (1987) summarized the stratigraphy for the Central Namib as follows:

150 Ma: Break up of Gondwana.

130 Ma: Opening of South Atlantic, starting at Southern Cape.

127 Ma: Escarpment starts to form.

80 Ma: South Atlantic and escarpment formed. Rapid erosion at first; sediment deposition 4 km off Orange River and 3 km off Walvis Bay.

65 – 60 Ma: Well developed erosional landscape with resistant inselbergs: Tumas, Kamberg, etc.

50 – 15 Ma: Formation of dunes, interdune areas and pans of the Tsondab Sandstone formation, south southwest winds, similar to today's regime. Infilling of deep depressions by eroded material from the escarpment. Dunes much higher than today.

15 Ma: Wetter climate (at least semi-arid with strong seasonal runoffs) introducing alluvial fans, braided river systems: forming today's terraces; Karpfenkliff Conglomerate Formation i. e. not incised drainage systems in broad depressions.

7 – 5 Ma: End of wetter period (0.5 1 million years): calcareous soils (calcareous duricrusts) formed. Annual rainfall 350 - 450 mm.

5 – 3 Ma: General phase of upwarping and continental uplift, with its axis coincident with today's escarpment. Rivers cut deep gorges into the calcretes, conglomerates and sandstones. Accumulation of the dune sands of the Namib Sand Sea, from sand brought down by the Orange River, washed northwards by the longshore current funneled onshore and blown into the main Namib Sand Sea.

1 – 0 Ma: several cycles of sediment buildup alternating with erosion, preserved as river terraces (e.g. Oswater Conglomerate Formation). Evidence points to the fact that dunes were already present. These were instrumental in moving the mouth of the Kuiseb River from Sandwich Harbour to its present position, i.e. climate generally arid with wetter intervals forming pans and tufa deposits.

Today: Large linear dunes move 0 – 2 m per year, the coastal crescentic dunes move approximately 1 – 10 m per annum. A narrow dune belt is established between Walvis Bay and Swakopmund. In conclusion, Ward (1987) remarked that the last few million years were wetter, and therefore terrigenous sediment transport was probably higher.

Sedimentation which led to the formation of calcrete - hosted uranium mineralization in the Namib Desert took place mainly during the Tertiary and Quaternary periods. During these periods, a sequence of events took place. An erosional episode, which started as far back as Paleocene, was followed by a depositional episode, then by calcification and finally by carnotite precipitation (Hartleb, 1988). The age of carnotite for most calcrete hosted uranium deposits has been calculated to be Late Pleistocene (Hartleb, 1988). This scenario suggests that conditions in the Namib Desert were not favourable for the formation of significant calcrete - hosted uranium deposits until the Pleistocene Epoch. Alternatively, uranium deposits could have formed prior to the Pleistocene period (Hambleton - Jones, 1976) but were subsequently eroded during periods of massive rainfall and sea level changes.

The beginning of aridification of the Namib Desert is believed to have started around the Pliocene Epoch (Wilkinson, 1990). In his publication Wilkinson (1990) further mentioned that several paleontologists studied fossil records to arrive at this estimate. This indicates evaporites in the Namib Desert, such as gypsum and calcite are of Pliocene age or younger. Apart from the usual northeasterly wind in the Desert, a hot,

strong westerly wind also occurs. This wind is responsible for hot winter days in towns like Swakopmund.

Wilkinson (1990) used ^{14}C dating to document the fact that the Namib Desert has undergone phases of aridity of varying intensity. The ^{14}C dating was carried out in the Rossing and Tinkas caves.

Table 8: Climatic fluctuations within the recent Namib Desert (after Ward 1984).

Climatic periods	**Date (No. of years before present)**
Distinct return to aridity	25,000 – present
A short return to wetter conditions	27,000 – 25,000
Aridity	34,000 – 27,000
Wetter conditions	49,000 – 34,000

The age for uranium mineralization at Klein Trekkopje has been estimated at 30 000 years (Hambleton – Jones 1976), which conforms to the 34 000 – 27 000 years period of aridity constrained by Wilkinson (1990) in Table 6.

CHAPTER 3: REGIONAL GEOLOGY

Both the Langer Heinrich and Klein Trekkopje palaeo-channels have been eroded in rocks of the Neoproterozoic Damara Orogenic Belt, which forms the bedrock to most of the Namib Desert (Miller, 2008). These rocks unconformably overly the 2 Ga Mesoproterozoic Abbabis Basement Complex of granite gneiss (Miller, 2008). The sedimentary rocks of the Damara Belt consist of arenites and argillites of the Nosib Group, overlain by pelitic sediments and carbonates of the Swakop Group. During metamorphism between 550 Ma and 450 Ma (Mc Dermott, 1986; Miller, 2008), Nosib and Swakop Group sedimentary rocks were partially mobilized and granitized and then intruded back into the Damara Supergroup to form what is today known as the Damara granites. These various Damaran granitoids have variably weak to strongly radiogenic characteristics.

According to Miller (2008), the Damara Supergroup is the most extensive stratigraphic unit in Namibia, deposited mainly in a NE-trending Damara Belt of Central Namibia and the N-trending Kaoko Belt of NW Namibia. Its evolution is believed to have begun at around 850 Ma with the deposition of more than 6000 m of sedimentary rocks and bimodal, peralkaline volcanic rocks of the Nosib Group in two intra-continental rifts, in half grabens marginal to the rifts and in laterally extensive basins beyond the zones of rifting. The areal extent and the geology of the study area are shown in Figure 7.

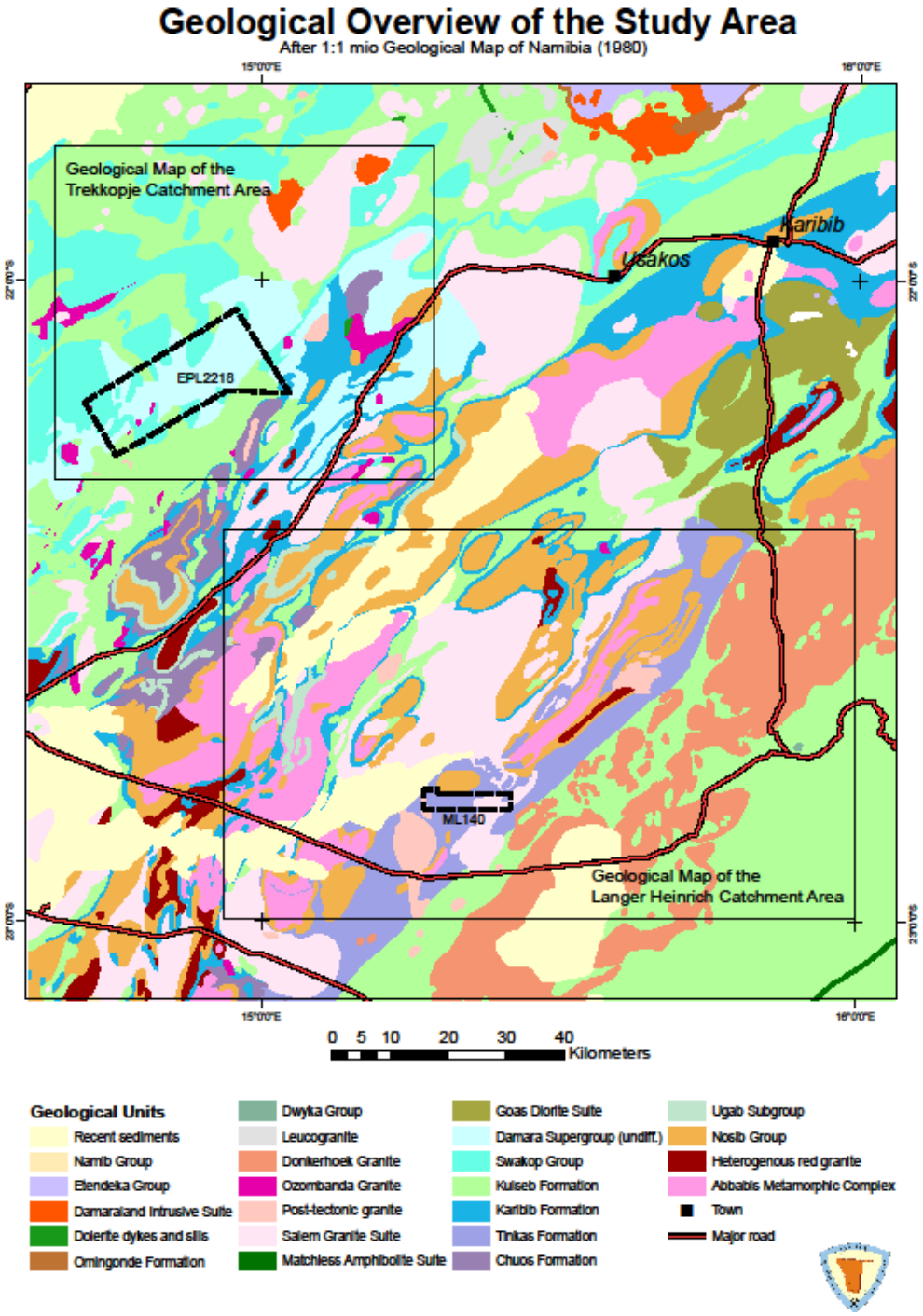

Fig . 7: Geological overview of the study area.

ML 140 represents the mining licence over the Langer Heinrich U deposit and EPL 2218 represents current licence over the Klein Trekkopje U deposit (Fig. 7).

The first snowball-Earth glaciation produced the Chuos Formation at about 750 Ma (Miller, 2008). The second glacial episode produced the Ghaub Formation. Miller (2008) also observed that the northern rift of the Damara Belt has deepened throughout spreading and is believed to have as much as 17 km of sedimentary and volcanic rocks.

In the immediate vicinity of the Langer Heinrich uranium deposit, the predominant rock types are mainly Abbabis gneiss, Bloedkoppie granite, Nosib Group quartzite and Tinkas schist. The Karibib marbles do not outcrop anywhere near the deposit. Around the Klein Trekkopje uranium deposit, the predominant sedimentary sequences are the Karibib marble and Kuiseb schist, while the quartzites, conglomerates and sandstones of the Nosib Group are conspicuously absent. Damara - aged granites, as well as those of the Cretaceous age are present in both areas. The Nosib Group is a sequence of siliciclastic sediments such as quartzites, conglomerates and sandstones. The Swakop Group is mainly a sequence of shallow marine (carbonate) as well as deep marine sediments (schists). The stratigraphy of the Damara Belt is summarized in Table 9.

Table 9: Summarized stratigraphy of the Damara Supergroup (based on data from Marlow (1981), Mc Dermott (1986) and Miller (2008)).

SUPERGROUP	AGE (Ma)	GROUP	FORMATION	ROCK TYPES
Damara Supergroup	Up to 650	Swakop	Kuiseb (incl. Matchless member)	Biotite schist, amphibolites
			Karibib	Carbonates
			Ghaub	Diamictite & glaciomarine sediments
			Arandis	Schist, calc-silicate & dolomite
			Chuos	Tillites & diamictites
			Rossing	Carbonates, quartzites, conglomerates & pelites
	1000 – 900	Nosib	Khan	Calcareous, feldspathic sandstones
			Etusis	Quartzites

3.1 Overview of Cretaceous magmatism

During the breakup of the Gondwana Supercontinent around 135 – 125 Ma, the Damara Supergroup was intruded by anorogenic peralkaline, slightly peraluminous topaz - bearing granites (Frindt et al., 2004a). These granites (e.g. Gross Spitzkoppe and

Erongo) have average uranium contents in the order of 15 – 30 ppm. Cretaceous magmatism is linked to the rising Tristan mantle plume, (Frindt et. al., 2004a). The Tristan plume, from early Cretaceous to the present, can be traced through an offshore Walvis Ridge, spanning some 500 km in width. According to Miller (2008), some complexes are slightly older (Paresis – 137 Ma; Cape Cross – 140 Ma) than the Etendeka Group whereas several complexes have gabbroic and/or granitic phases of syn – Etendeka age. Etendeka basalts and quartz latites are believed to be 132 Ma and most mafic and silicic Cretaceous intrusions are coeval with Etendeka volcanism.

Incision of most palaeo-channels in the Namib Desert took place between 80 Ma to 50 Ma, following uplift in that part of the African continent which in turn was driven by the opening of the South Atlantic (Bowell et al., 2009).

A number of north-south trending Karoo - aged dolerites and felsic dykes were also emplaced in response to the crustal relaxation related to the disintegration of Gondwana. The Langer Heinrich valley is a portion of an east-west trending palaeo-channel which transects the Bloedkoppie granite in the east, then the Tinkas schist before its northern bank is formed by the Nosib/Khomas contact and finally the valley is eroded into the Tinkas schist again, for the rest of its westward course (Hartleb, 1988). The Klein Trekkopje channel has been eroded into the Spitzkoppe granites, Kuiseb schist, Damaran granites, Karibib marbles and Karoo dolerites.

3.2 Morphology of the palaeo-channels

The morphology of the palaeo-channels is very crucial in understanding the source of uranium and vanadium, but more so for uranium. At Langer Heinrich, the channel morphology is almost obvious, whereas at Klein Trekkopje deposit the palaeo-channel network in the catchment area is more anastomozing. Figure 8 shows eight different secondary U deposits and/or prospects. The Figure also shows an interesting feature, the western cut-off line, west of which there are no calcrete-hosted uranium deposits. Hambleton – Jones (1984) suggested that there might have been deposits to the west of this feature, but they were probably eroded during periods of sea transgressions.

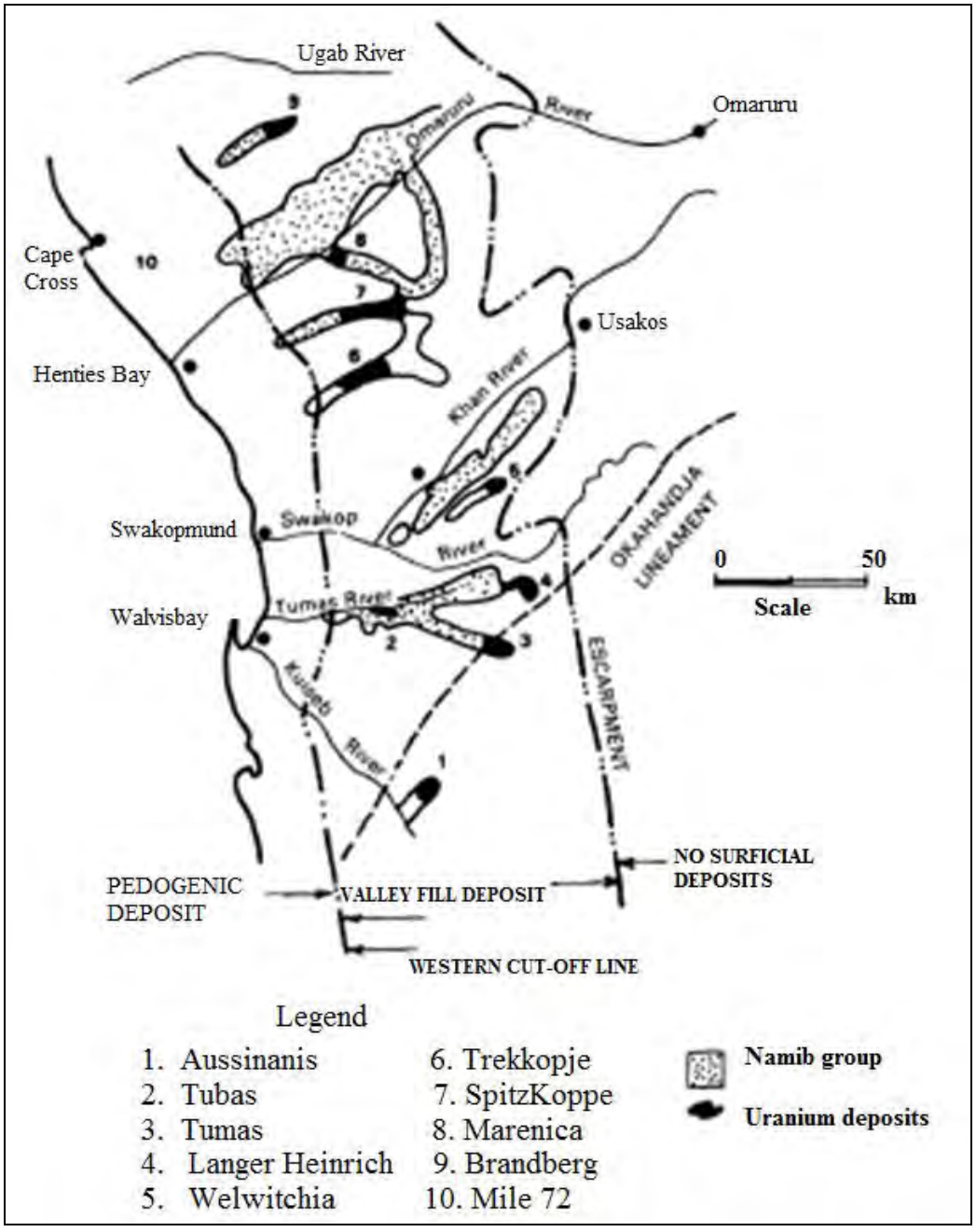

Fig . 8 : A map showing the distribution of calcrete-hosted carnotite deposits in central Namibia, after Hambleton-Jones (1984).

The Langer Heinrich palaeochannel is best observed on a hyperspectral image (Fig. 9) where, the various colours reflect the different mineralogical units. The boundaries of the mineralized calcrete at Langer Heinrich are shown as white polygons. The predominant mineral that defines these calcretes is calcite mapped in red. Residual illite partially covers some of the calcrete and in the eastern most polygon the presence of dolomite may show a change in calcrete facies.

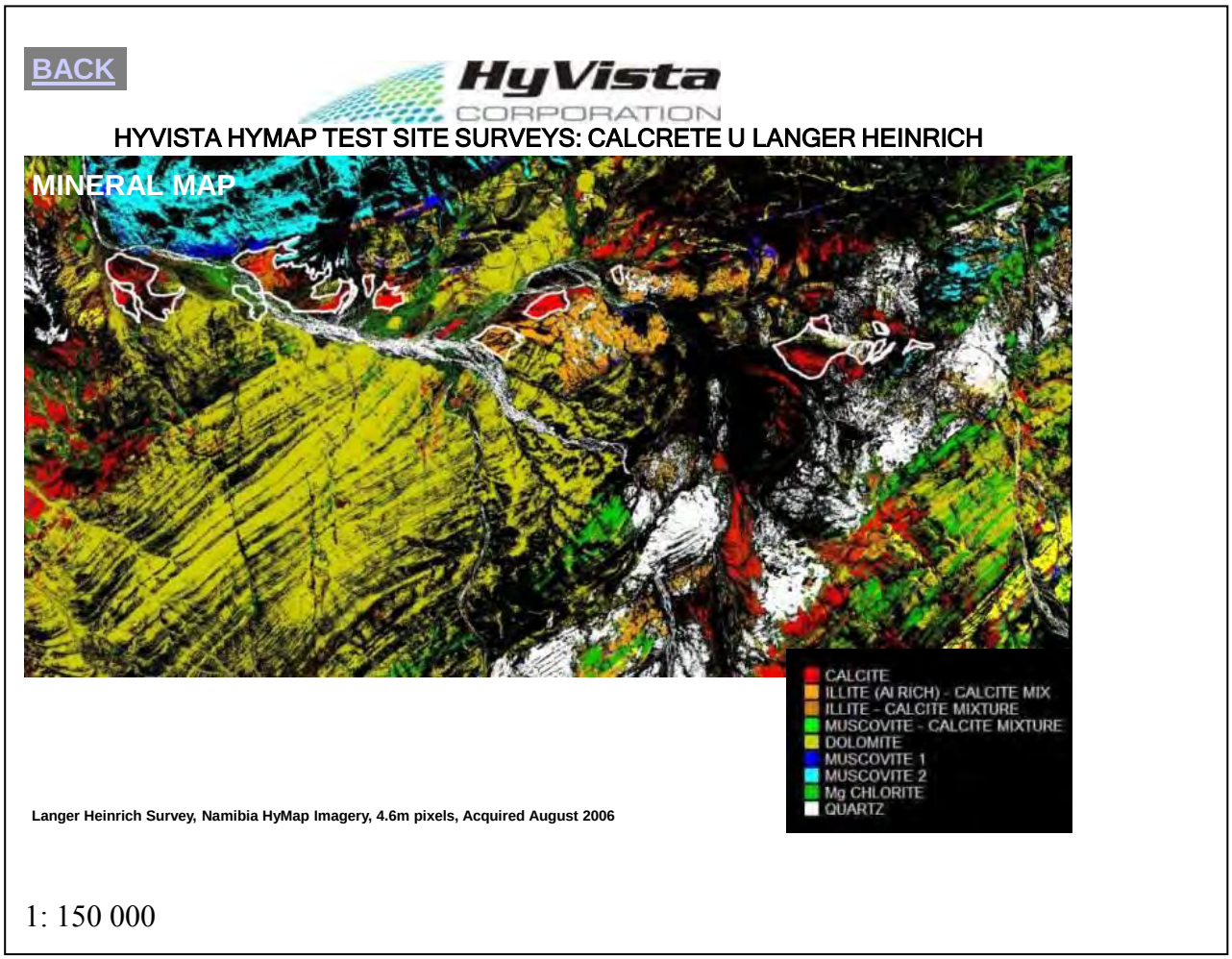

Fig . 9 : Hyperspectral map for the area around the Langer Heinrich area showing how different minerals/ lithologies have a different hyperspectral response (after Hussey, 2006).

From the hyperspectral map (Fig. 9), it can be seen that the Langer Heinrich palaeo-channel is well constrained and much simpler than other more complex palaeo-channel systems in the Namib Desert. The lithology with a strongly developed northeasterly foliation is the Tinkas schist. Figure 9 shows clearly that for the most part, the Langer Heinrich channel is cutting through the Tinkas schist. What is also interesting on this image is the abundance of Mg chlorite within the main bedrock of the Tinkas schist. The Bloedkoppie granite occupies most of the area in the center of the image, where various tributaries are converging into the main channel. The Bloedkoppie granite shows no foliation in the image above. The circular bluish lithology in the northwestern corner of Figure 9, represents the Etusis quartzite. The palaeochannel hosting the Klein Trekkopje U deposit is described at length in chapter 4. However, there seem to be a couple of channels connecting to it according to Figure 8, one from Marenica and the other from the direction of the Spitzkoppe granites.

CHAPTER 4 : SEDIMENTARY CHARACTERISTICS AND MINERALIZATION

Sedimentary characteristics such as physical properties observed on sediments are critical in understanding the type of current, provenance and climate which existed at the time of erosion and deposition. The sedimentary features are best exposed in the two pits namely, Langer Heinrich and Klein Trekkopje (Fig. 10). The disintegration of Gondwana Supercontinent was followed by uplift in the west of the Supercontinent and then by erosion. The major erosional episode started about 60 million years ago (Hartleb, 1988).

4.1 Langer Heinrich

At Langer Heinrich, mineralization is hosted by fluviatile sediments of the channel (Fig. 11). The sequence consists of arkose, conglomerates and fanglomerates at the top. Several visits were made by the writer to the Langer Heinrich uranium mine, and surrounding areas. The dominant geomorphological features are the Langer Heinrich mountain (Etusis quartzite) to the north of the channel and the Schieferberge mountain (Tinkas schist) to the south and opposite the Etusis mountain. Refer to the hyperspectral image of the Langer Heinrich channel (Fig. 9). The bulk of the mineralization lies between these two mountains. The Schieferberge mountain (shown in green colour, northwestern corner of the spectral image) is composed of quartz rich Tinkas schist and its high relief is a clear indication of how resistant it was to erosion. The low lying parts of the Tinkas schist are more biotite - rich.

Etusis mountain is composed of Etusis quartzite. Etusis quartzite is by far the most resistant lithology in the area and together with the Schieferberge in the south, formed the constriction for the subsurface water heading to the Atlantic Ocean in the west. Due to the highly resistant nature of the two lithologies, the Langer Heinrich channel was forced to meander and form ponds within the intervening constriction. The groundwater trapped in these subsurface ponds was continuously leaching vanadium from the schist. In addition, U and K were being continuously concentrated in groundwaters sourced from the catchment area which is dominated by the Bloedkoppie granite. Locally, the resistant lithologies also formed bedrock highs, thereby focusing the subsurface water upwards and exposing it to evapo-transpiration. The channel gradient is very low and there is very limited runoff. The elevation of the base of the deposit descends from 710 m above sea-level in the east to 550 m above sea-level in the west over a distance of 14 km, having a gradient of 1.14% (Hartleb, 1988).

Fig.10: The Langer Heinrich open pit, which can be up to 10 m deep.

U mineralization in the pit is not only restricted to calcrete, but in places it is found a few metres into the weathered schist bedrock.

Fig . 11: Carnotite disseminated within the conglomerate matrix at Langer Heinrich uranium mine.

The six samples (Lcalc1 – Lcalc6) taken from the mineralized calcretes at Langer Heinrich represent an immature conglomerate with poorly sorted and poorly rounded clasts in carbonate cement. In thin section, the carbonate in the cement is clearly visible by its characteristic rhombic cleavage, while the matrix shows a yellowish tint. The yellowish tint is due to uranium mineralization (Fig.11).

The arkose can be subdivided into clay at the bottom, grading into a clay grit and finally into a calcareous grit. The clay grit occurs below the water table and has very low

calcite cement. The calcareous grit consists of quartz, feldspar chips, minor rock fragments and a micaceous sandy matrix. It contains about 18% calcite cement (Maasen, 1982). The conglomerate which overlies the calcareous grit consists of rounded to subrounded quartz, quartzite clasts and granite pebbles in a matrix of sand and grit, cemented by calcite. The fanglomerate consists of coarse subangular to angular clasts of schist, quartzites and granites in a poorly sorted matrix of sand and grit. Becker and Hogarth (2005) observed that the carbonate cement at Langer Heinrich can be anything between 5 - 35% in general. Average calcite concentrations are reported to be about 15%, decreasing to about 5% below the water table.

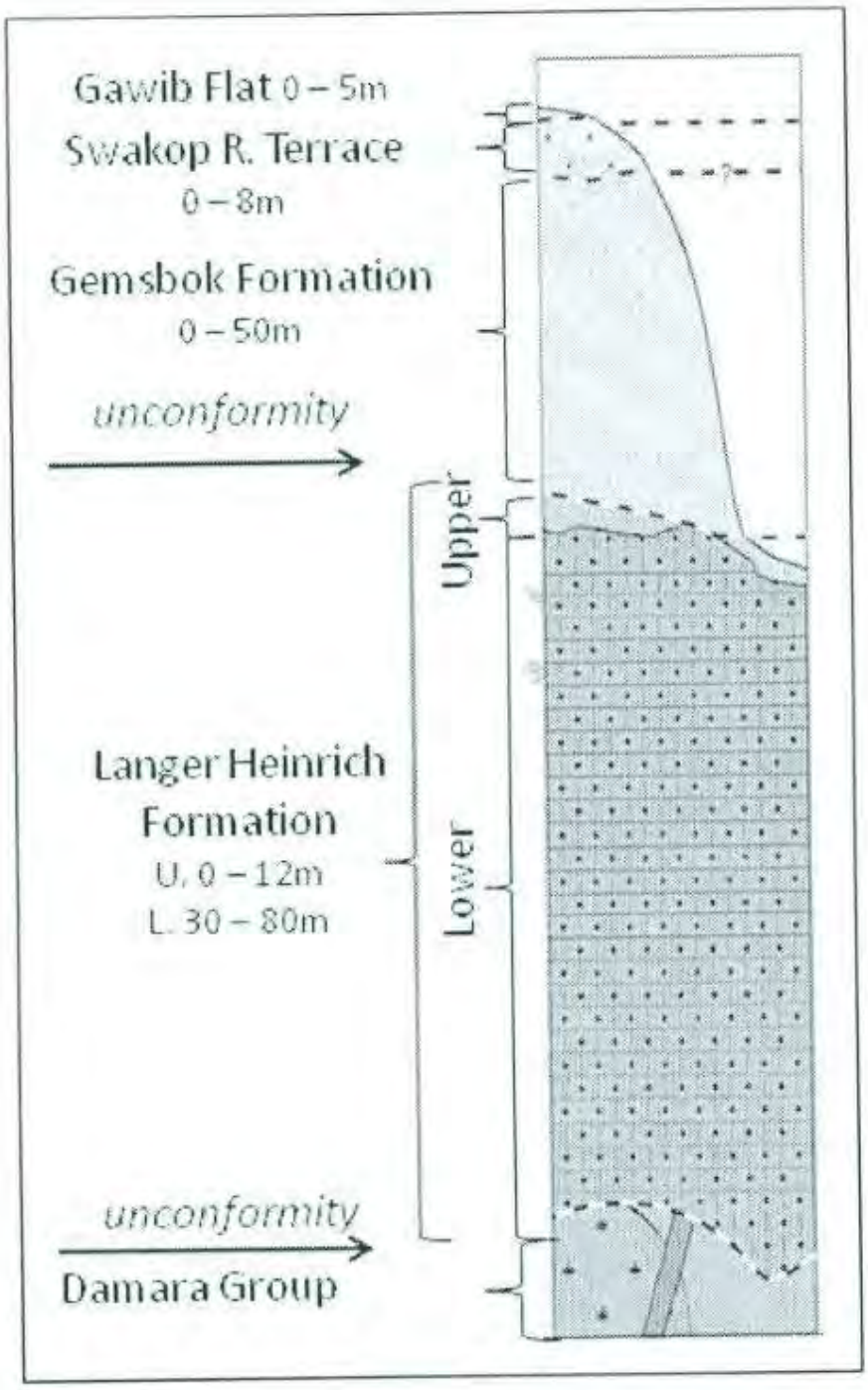

Fig. 12: Idealized composite profile showing the stratigraphy of Cenozoic sediments within the Langer Heinrich area (after Becker and Karner, 2007).

The Langer Heinrich Formation described above is overlain by the Gemsbok Formation (Fig. 12) although there is an unconformity between the two Formations. This sequence is overlain by the Swakop River Terraces and Gawib Flats on top. The Gemsbok Formation is largely conglomeratic with quartz and feldspar constituting the detrital material and calcite cement in places (Becker and Karner, 2007). The Gemsbok Formation has no uranium mineralization.

Mineralization in the Langer Heinrich Formation occurs mainly within the calcareous grit and the conglomerate as disseminations in fractures and on surfaces of clasts (Fig. 11). Carnotite appears as a uniform bright canary yellow mineral in surface outcrop, though it may have a greenish tint locally (Hartleb, 1988). The ore comprises carnotite-rich, sub-horizontal, clastic rock units, which vary from conglomerates through grits and sands to micaceous claystones. In general the ore becomes finer grained with depth and hence ore beneath the water table is mainly conglomeratic, gritty or sandy micaceous claystones (Becker and Hogarth, 2005). In hand specimen and in thin section the ore is largely a clast supported, calcrete cemented, immature conglomerate (Fig. 11 and 13). The ore consists mainly of carnotite but tyuyamunite is also present (Kinnaird 2011, personal communication). In some areas mineralization can be found a couple of metres into the schist bedrock. This suggests that subsurface groundwaters in the channel, enriched in uranium have penetrated deep into the schist which facilitated precipitation of ore minerals due to its elevated vanadium content.

According to Hambleton-Jones (1976), the U^{6+} and V^{5+} complexes have very strong electronic bonding characteristics. The strength of this bond and the availability of ions will determine what uranyl mineral will precipitate. For example, in the presence of sufficient K, U and V carnotite will preferentially form, but when there is a short-fall of K and there is Ca available then tyuyamunite will form. The latter has the weaker electronic bond between the two.

The calcrete at Langer Heinrich consists mainly of calcite and dolomite but at Trekkopje the calcrete contains calcite and strontianite (Hambleton–Jones, 1976). This indicates there were different groundwater conditions during the formation of the two ore bodies. The presence of clay minerals in the Langer Heinrich calcrete, as reported by Hambleton–Jones (1976), is an important controlling factor because clay minerals, especially montmorillonite have a powerful adsorption capacity for uranium and other metals. However from a mining perspective, too much clay can present severe metallurgical difficulties during extraction, as they do not release uranium as easily.

According to Becker and Karner (2007), carnotite occurs as finely disseminated specks, as blebs up to 20 mm and as coatings in open pore spaces which are irregularly distributed within the matrix of all host lithologies within the valley. This suggests that porosity of the rock is one of the controlling factors for carnotite precipitation. In fact Becker and Karner (2007) remarked that carnotite occurs preferentially in the less cemented portions of the host sediment. Mineralization occurs as an undulating 1 m to 30 m thick layer shaped like a subterranean meandering river (Fig. 14). In cross-section,

grade distribution within a layer is a series of broad concentric ellipsoidal shells, with highest grades in the central core and decreasing towards the bottom, top and banks of the channel (Becker and Hogarth, 2005). This observation by Becker and Hogarth (2005) is reminiscent of the formation of ponds prior to the precipitation of carnotite.

In a typical pond, carnotite precipitation will decrease with depth because the deeper it gets, the lower the rate of evapo-transpiration. On the other hand, carnotite precipitation will decrease from the middle of the pond towards the surface because the closer it is to the earth surface, the more oxidizing it gets. As it will be discussed in the next chapters, carnotite precipitation is most intense near the water table where there is fluctuation in the groundwater conditions between weakly oxidizing and strongly oxidizing. Near the earth surface there is no fluctuation in the groundwater conditions and the environment is purely oxidizing.

It is apparent that the strongest precipitation is at the core of the ellipsoid as observed by Becker and Hogarth (2005). Becker and Hogarth (2005) also observed that after surveying the channel, it was found that high grade zones are found within deeper parts of the channel. This statement should not be misinterpreted or generalized to mean that carnotite precipitation is enhanced with depth. It simply means within the 1 – 30 m depth, mineralization is found where ponds existed in the past and these correspond to mini-depressions.

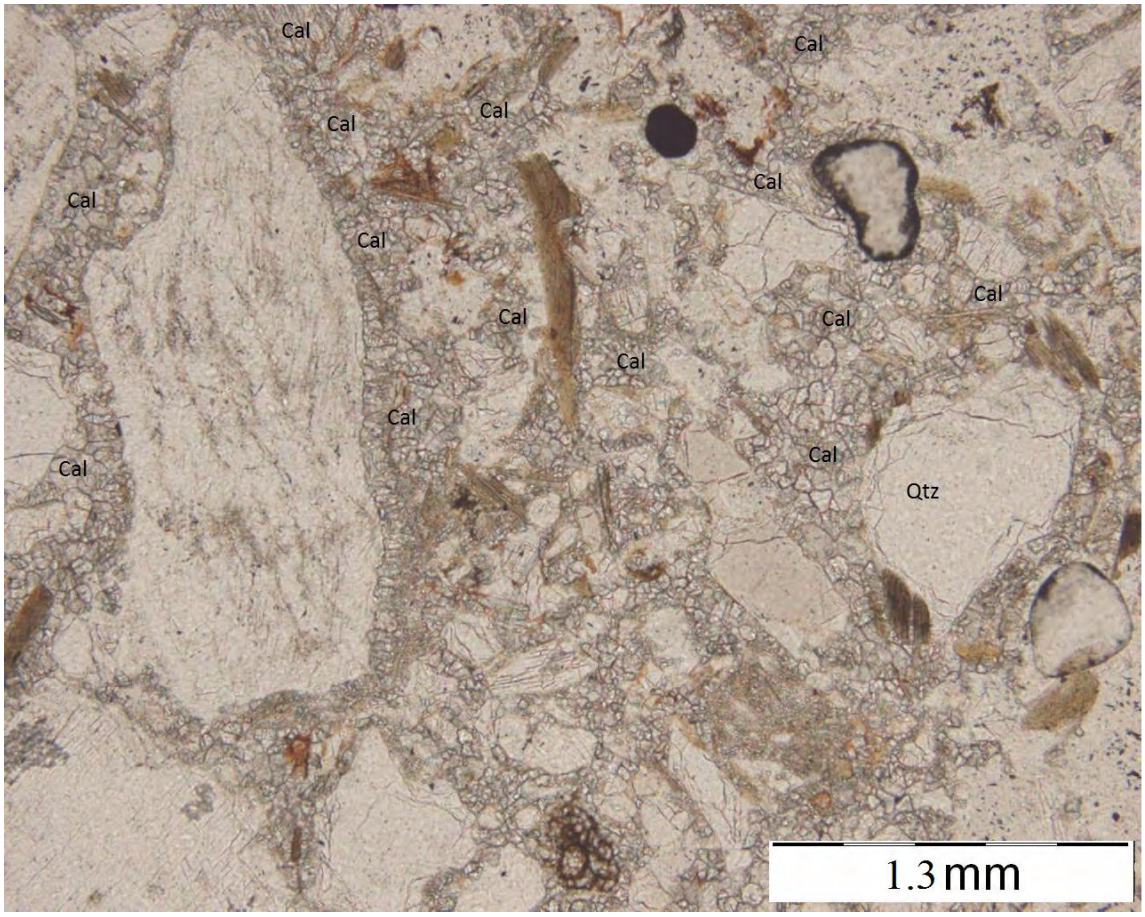

Fig . 13 : Calcretized conglomerate (sample LCALC 2) from Langer Heinrich ore body (PPL). Detrital grains have been pushed apart by lime cement. The picture shows quartz (Qtz) – rich fragments in a calcite (Cal) matrix.

Figure 13 shows how a mineralized clast - supported conglomerate looks in thin section. The calcite cement can be seen from its characteristic rhombic cleavage, around the clasts. The dark yellow mineral seen in fractures and around the clasts is carnotite. Sometimes carnotite occurs as disseminations within the matrix.

(a)

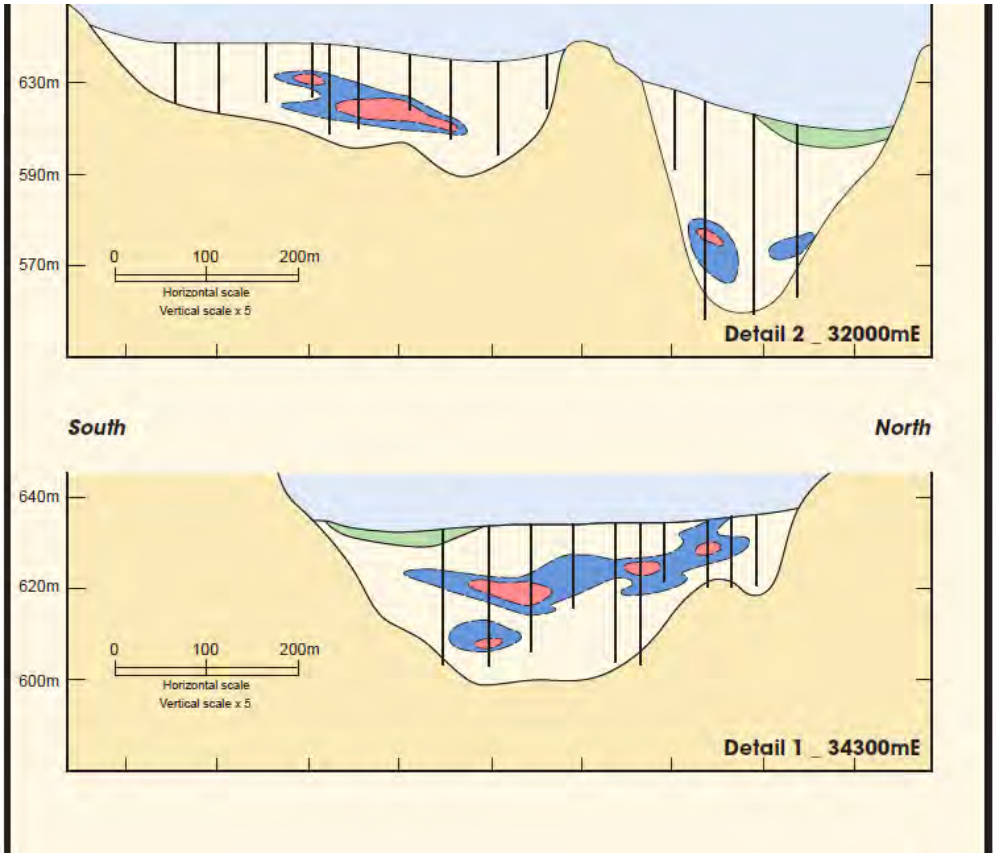

(b)

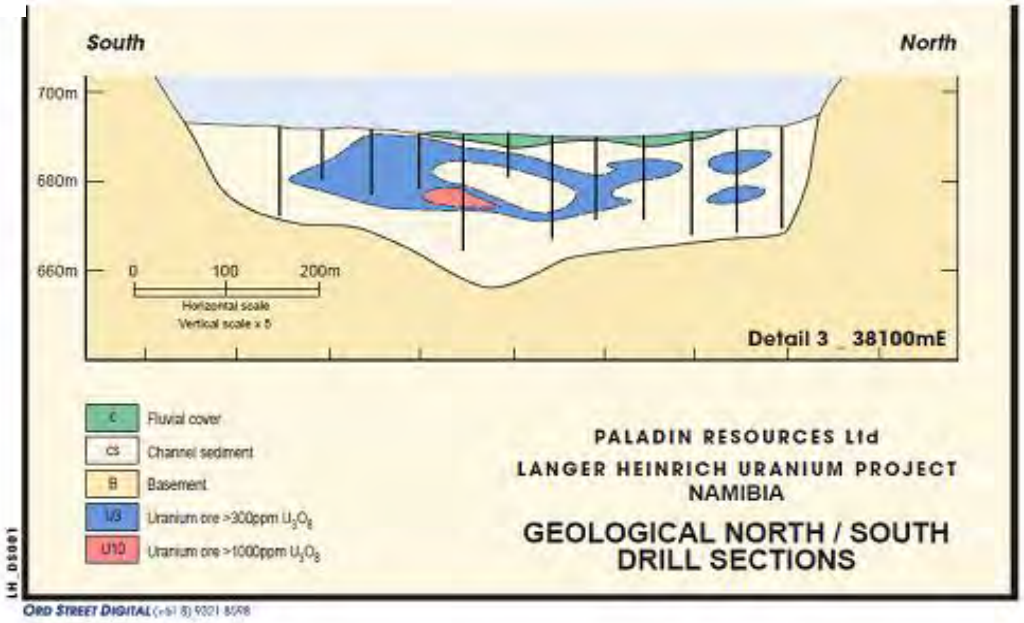

Fig . 14 : (a) and (b): North – south cross sections for the Langer Heinrich uranium deposit illustrating the Palaeo-geomorphology around the Langer Heinrich deposit (after Becker and Hogarth 2005).

The three cross sections in Figure 14 show the relationship between uranium mineralization and the geomorphological features. From the cross sections, it can be seen that high grade zones (coloured in red) are located within areas of channel narrowing and ponds. Perched ponds favour evapo-transpiration and deeper ponds will not result in significant uranium mineralization because evapo-transpiration is only effective down to about 30 m. These shallow or perched ponds have been referred to as bedrock highs in earlier literature.

The Langer Heinrich deposit is comparable to Yeelirie in Australia. One major difference between the Yeelirrie and Langer Heinrich deposits is that the established source of vanadium for the former is granitoids and some mafic rocks of the Yilgram Block whereas the source of vanadium for Langer Heinrich is schists and to a lesser extent granitoids.

4.2 Klein Trekkopje

To date, the channel network between the Spitzkoppe mountains and the Klein Trekkopje U deposit has not been fully delineated and it remains a subject of debate. Figure 15 was prepared with the use of electro-magnetic data collected and analyzed by Greg Symons, a geophysicist who was working for uranium exploration companies in that area then. The aim of this exercise was to outline the course of the palaeo-channels in the catchment area for the Klein Trekkopje U deposit.

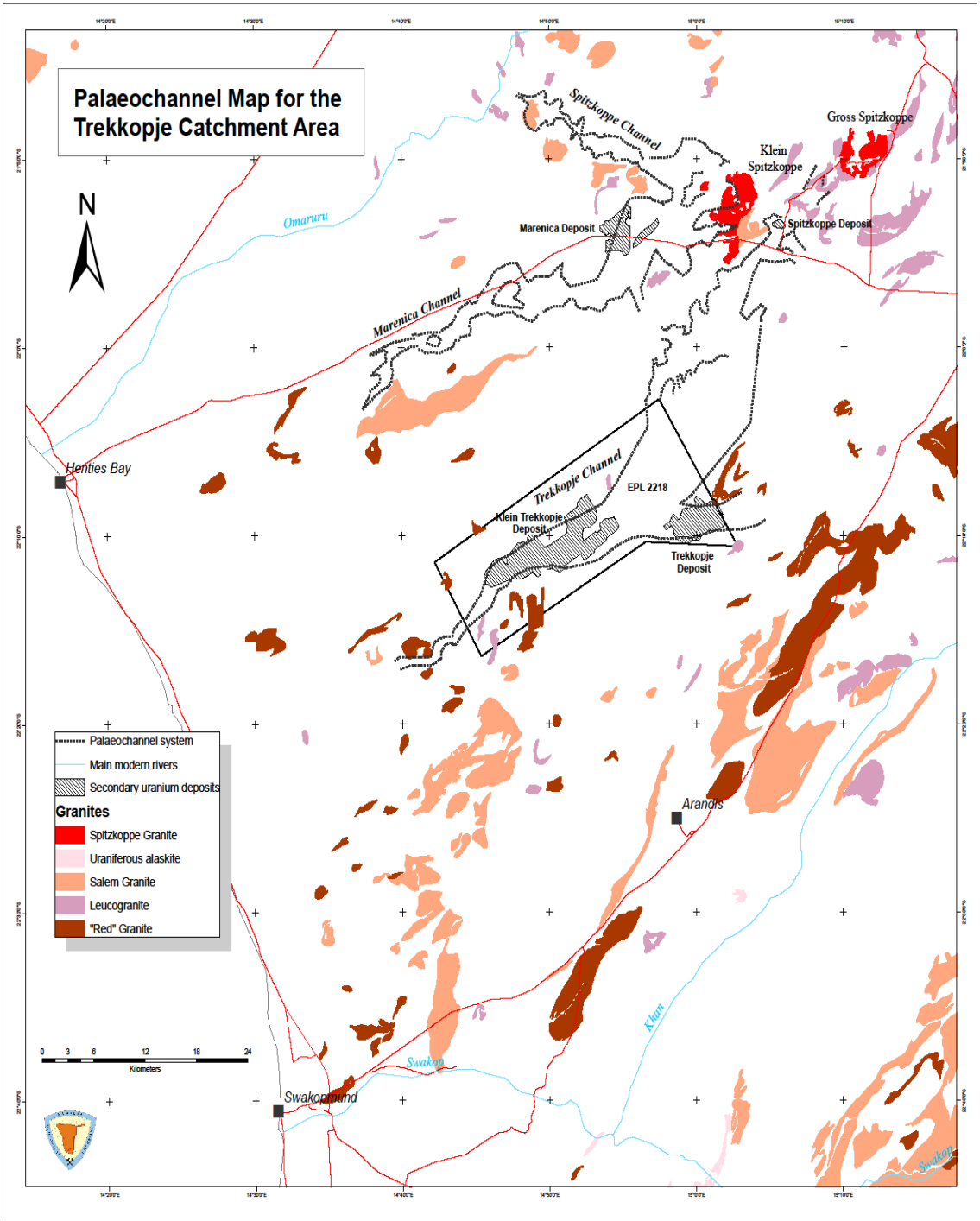

Fig . 15 : A map of western Namibia showing the morphology of the palaeo-channels as well as granitoids around the Klein Trekkopje area.

Figure 15 shows the general morphology of the palaeo-channels between the escarpment, around the Spitzkoppe mountains, and the coast line. It also shows the geographic location of various granitoids in the area. The EM surveys carried out by Greg Symons in 2009 show that the main channels leading to the Klein Trekkopje U deposit can be traced back to the Spitzkoppe mountains. According to Greg Symons there are three main palaeo channels, namely the Spitzkoppe channel, the Marenica channel and the Trekkopje channel. The Spitzkoppe channel starts at the Spitzkoppe mountains and runs towards the Omaruru river.

The Marenica channel also starts at the Spitzkoppe mountains, passes the Marenica U deposit and continues towards the sea but ends before it reaches the sea. The Trekkopje channel in the south starts between the Gross Spitzkoppe and Klein Spitzkoppe mountains, continues in a southwesterly direction, through the Klein Trekkopje U deposit, then continues towards the sea but ends before it reaches the sea. There is a possibility that the Marenica channel did connect with the Trekkopje channel (Fig. 15). There is also a smaller channel running from the side of the Trekkopje prospect towards the Klein Trekkopje deposit (Bittner, 2006). Figure 16 shows the main geological features within the Klein Trekkopje uranium deposit. Bedrock consists mainly of Karibib marble, Damara aged granite and Karoo dolerite. Figure 16 shows bedrock can occasionally be a sandy unit and weathered remnants of original rocks.

From observation of the morphology of the palaeo-channels as outlined in Figure 15, it appears there is a watershed between the Klein Spitzkoppe granite and the

Trekkopje palaeo-channel. This suggests that the Trekkopje channel was sourcing material from the Gross Spitzkoppe side and from the Damara - aged leucogranites situated between Klein Spitzkoppe and Gross Spitzkoppe granites. This drainage system was responsible for the formation of the Spitzkoppe uranium prospect situated southwest of Gross Spitzkoppe and about 8 km east of Klein Spitzkoppe granite (Fig. 15). Therefore the main source of uranium for the Spitzkoppe U deposit is Gross Spitzkoppe granite, with limited input from the Damara - aged leucogranites situated in that area.

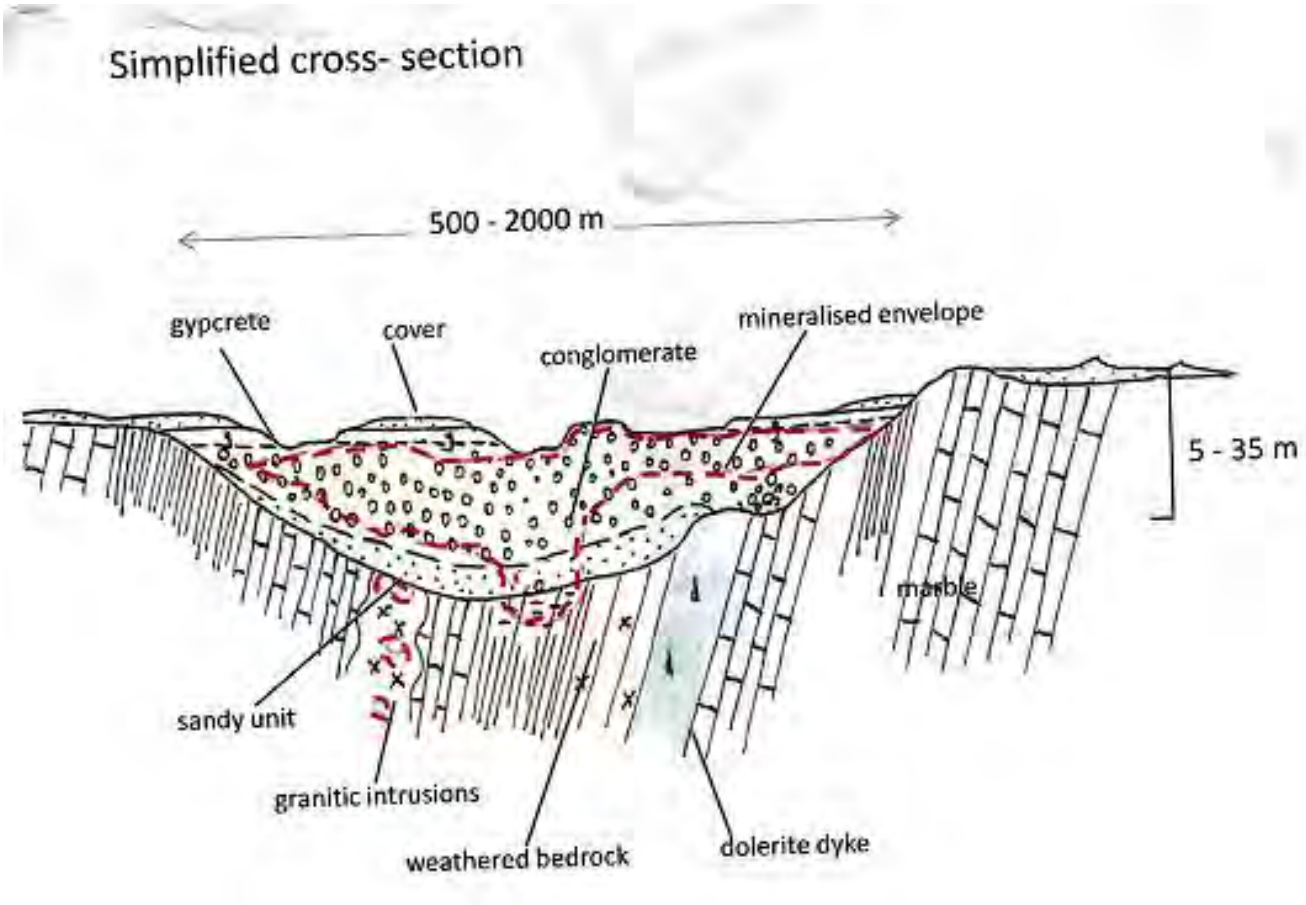

Fig . 16 : Stratigraphic profile for the Klein Trekkopje U deposit, with the mineralized envelope coloured in red (after Pedley 2007).

The conglomeratic clasts in the palaeo-channel valley-fill consist of poorly sorted, angular to sub-angular, basement debris (marbles, gneisses, granite, quartz, dolerite, and pegmatite). The valley-fill sediments are highly variable and consist of alternating layers with variable thickness of conglomerate, grit, sand, clay-grit, and clay. The sediments are largely conglomeratic (~80%), with minor lenses of sand (~10%) and clay (~5%), interspersed with rare boulders and cobbles (<5%). This variable lithology reflects rapid changes in water velocity, with erratic deposition of bed loads noted throughout prospective horizons. The sediments are poorly consolidated, ranging from friable in the upper zones to massive and weakly lithified at depth. Later cementation by calcium carbonate has produced a hard compact rock beginning at depths of one to two meters or more.

At Klein Trekkopje mineralization occurs between depths of 0-25 m with the bulk of the mineralization at less than 10 m depth. This contrasts with Langer Heinrich where mineralization occurs down to a depth of 30 m. The writer made several visits to the Klein Trekkopje deposit in 2010 and 2011. As at Langer Heinrich, mineralization occurs along fractures and as coatings on pebbles (Fig. 17). Similarly high grade pods are found to be associated with bedrock highs, indicating a strong geomorphological control on mineralization. In the pit, carnotite is mainly bright yellow but greenish varieties were also found.

Fig. 17: A sample from the mineralized conglomerates at Klein Trekkopje, showing carnotite as a yellow mineral within the matrix and as coatings on pebbles.

At Klein Trekkopje there are two palaeo-channels converging around marble and this is where most of the mineralization is located. Drilling within the deposit has also exposed a dolerite dyke immediately below one of the spots where good uranium grades are located (Kinnaird, 2011 personal communication). Hambleton–Jones (1976) identified two generations of calcite precipitation. According to him the first generation calcite is barren while the second one is coeval with carnotite precipitation. He dated this second generation calcite together with mineralization at 30 000 yrs. Closely similar ages (68 000 yrs) have been estimated for the uranium mineralization at Langer Heinrich (Kinnaird, 2011, personal communication). These ages indicate that calcrete hosted uranium mineralization in the Namib Desert is very recent. Since mineralization at Klein Trekkopje is believed to be related to a salinity boundary, it is likely that the first

generation calcite was probably precipitated at a time when the groundwater at Klein Trekkopje had not yet reached the required levels of salinity. It could also mean that the first generation calcite was precipitated at a time when U-rich fragments had not yet been deposited around Klein Trekkopje.

4.3 Discussion

Judging from the quantity of material eroded from the escarpment since the breakup of the Gondwana continent (more than 900m), it is evident that most of the watersheds or basement highs in the Namib Desert are of late Tertiary to Quaternary age. Therefore during the late Cretaceous to early and even mid-Tertiary, the ancestral Trekkopje channel might have sourced material from the Klein Spitzkoppe granite as well. Observation of Figure 15 indicates that the 7000t U_3O_8 deposit located at Trekkopje was not sourced from the Spitzkoppe Mountains because there is basement high between the catchment area for this small prospect and the main Trekkopje channel. This suggests that the low grade uranium prospect at Trekkopje was formed by sourcing uranium from the Damara aged granites to the north east of the prospect. Nevertheless, the palaeo-channel responsible for the formation of the Trekkopje prospect finally joins the main Trekkopje channel and drains towards the Klein Trekkopje uranium deposit. This indicates part of the uranium deposited at Klein Spitzkoppe, was sourced from the area around the Trekkopje prospect.

While one channel runs from the area around the Trekkopje prospect towards the Klein Trekkopje deposit (Bittner, 2006), another channel, which is not shown on Figure

15, appears to run from the side of the Trekkopje prospect subpararell to the main Trekkopje channel but outside the mining tenement. This appears to be the target of EPL 3573 which URAMIN demarcated to the south of the main tenement. This channel was delineated by EM and radiometric surveys conducted by URAMIN, the mineral right holder for both Trekkopje and Klein Trekkopje uranium occurrences during 2007/2008.

As alluded to earlier, a small palaeo-channel appears to have been draining from the main Marenica channel into the Trekkopje channel. This indicates that during the early Tertiary period, the area of Klein Trekkopje was being fed with uranium from many directions and sources. Progressive erosion of basement highs defined by competent resistant lithologies resulted in the drainage channels changing course, as they meandered around these resistant lithologies. Therefore the watersheds as seen today in the Namib desert should not be construed to have been there throughout the erosional episode.

Regarding vanadium, although metapelites are the most likely source, it is clear that granitoids (especially Damaran - aged) have also contributed vanadium to the subsurface waters. The drilling data from Marenica (appendix 4) have shown that some Damaran granites are very rich in vanadium, in some boreholes, reaching values above 150 ppm. Potential for future discovery of secondary uranium deposits in the Trekkopje channel system can be expected to the east of the URAMIN's mining tenement, i.e. between Spitzkoppe Mountains and the Klein Trekkopje deposit. To the west of the Klein Trekkopje deposit, the groundwater conditions are considered to be too saline to

have formed significant concentrations of carnotite. Moreover, the channel becomes more and more unrestricted, the closer it comes to the sea. An unrestricted channel cannot form ponds in which the subsurface water can stay for a long time, in order to precipitate carnotite (Carlisle et al., 1978).

The Marenica palaeo-channel appears to have sourced material from the Klein Spitzkoppe granite during most of its history. However, during the early Tertiary it might have had input from the Gross Spitzkoppe granite and the Damaran granites between Klein Spitzkoppe and Gross Spitzkoppe granites. It appears the Marenica channel had sufficient amounts of uranium, being very close to the source granite, but the geomorphology was not ideal for the precipitation of vast amounts of carnotite. Apart from the uranium trapped between two granite domes, to form what is today known as the Marenica deposit, most of the uranium was transported further to the west due to a lack of mechanical traps. Potential for more secondary uranium exists in the Marenica area and slightly further west. Exploration should be targeting areas around favourable geomorphological features like dolerite dykes and granite domes.

Regarding the Spitzkoppe channel, just like with the other two channels, it was probably draining from as far as Gross Spitzkoppe in the early Tertiary although it was draining from the Klein Spitzkoppe granite for most of its history. The Spitzkoppe palaeo-channel is located in a good position because it was sourcing material from the Klein Spitzkoppe granite directly. It also dissects a fairly rugged terrain, which is reminiscent of the Langer Heinrich palaeo-channel. However one key ingredient appears

to be missing for it to be classified as being prospective for secondary calcrete-hosted uranium deposits. This channel seems to be set too deep into the hinterland and too far from areas which can be reached by marine fogs.

A limited amount of marine fogs is necessary as it makes the groundwater conditions moderately saline. Moderate salinity helps to destabilize uranyl carbonate complexes in the subsurface water, thereby concentrating uranium. However, extremely high salinity is a problem because it leads to a low oxidation state and acidic conditions. This subsequently inhibits the precipitation of carnotite (Mann and Deutscher, 1978). The scarcity of gypcrete or dolocrete in the Spitzkoppe channel system points to a historical lack of marine fogs in the area. In the absence of active marine fogs in most parts of the Spitzkoppe channel, a salt lake would be necessary to trigger carnotite precipitation as in the case of Yeelirrie, in Australia (Mann and Deutscher, 1978). However no salt lake is known in the Spitzkoppe channel system and the potential for a significant calcrete-hosted uranium deposit is slim.

Apart from the palaeo-channels indicated in Figure 15, another palaeo-channel to the northwest of the Gross Spitzkoppe granite has been detected by Greg Symons. According to him this channel might have transported material from as far as the Erongo granite complex. The Erongo granite is known to have higher uranium concentrations than both Klein Spitzkoppe and Gross Spitzkoppe granites. Average values of 30 – 40 ppm U have been reported (Frindt. et al., 2004a). A possibility therefore exists that part

of the uranium found in the three main palaeo-channels shown in Figure 15 might have been derived from as far as the Erongo granite during the early Tertiary.

The presence of poorly rounded clasts at both Langer Heinrich and Klein Trekkopje suggests that the bulk of the fragments in the channels came from a proximal source. Nevertheless, the presence of well rounded quartz clasts especially at Klein Trekkopje indicates that some of the material in the channel came from a distal source. The poorly sorted fragments in both channels indicate the varying energy for the current which existed during the erosional episode.

Uranium mineralization is characterized by carnotite at both Langer Heinrich and Klein Trekkopje but the latter has a few other minerals such as tyuyamunite. The groundwater system at Klein Trekkopje had more total contained U than the Langer Heinrich system because of the former's widespread catchment area but the channel width prevented smooth precipitation of carnotite at Klein Trekkopje.

Regarding the palaeo-geomorphology, the geology of the bedrock was studied in detail. The geomorphology around the Langer Heinrich deposit appears to be highly favourable for uranium precipitation. The Langer Heinrich Mountain and the quartz - rich portions of the Schieferberge schist were responsible for constraining the fluids at Langer Heinrich. Both of these lithologies were therefore responsible for the formation of perched ponds, which enabled carnotite precipitation to take place effectively.

At Klein Trekkopje, there were fewer resistant geomorphological features and this resulted in the low U grades in that deposit. In general, the geomorphology around the Klein Trekkopje deposit was far less favourable for the precipitation of uranium, compared to Langer Heinrich.

The range of colours observed in the mineralized calcretes, especially at Klein Trekkopje, is a clear indication that the Eh/pH conditions for the groundwater has been oscillating between a weakly oxidizing environment and a more strongly oxidizing one. As a result, part of the vanadium has not been oxidized from V^{4+} to V^{5+}, hence the greenish colours.

4.4 Summary

Sedimentary characteristics for the channel fill especially at Klein Trekkopje indicate that U and V were sourced from both proximal and distal sources. Precipitation of carnotite appears to have been smoother and uninterrupted at Langer Heinrich compared to Klein Trekkopje, where a number of negative factors were at play. Although the total contained U in the Klein Trekkopje channel is far higher than the one at Langer Heinrich, the opposite can be said about the grades. This is clear demonstration that in the formation of a calcrete-hosted U deposit, there are so many factors at play that the availability of U and V in the catchment alone does not necessarily guarantee the formation of a secondary calcrete-hosted U deposit downstream.

CHAPTER 5 : GEOLOGY AND PETROLOGY OF THE CATCHMENT AREAS

Geological and mineralogical features for various rocks in the catchment area for the two U deposits were examined in the context of their ability to contribute either U or V towards the formation of the two deposits. The results are presented in this section.

It is worth noting that the sedimentary fill, in the channels downstream from the Spitzkoppe granites, is poorly sorted and coarse-grained, which indicates rapid transport and deposition. Because of this high rate of erosion and deposition, there was insufficient time to leach this material in the source area but was subsequently leached of V and U after deposition in the channel (Hambleton-Jones, 1976).

5.1 Langer Heinrich catchment area

Figure 18 shows the general geology of the Langer Heinrich catchment area. It also shows the mining licence area with an L shape and the locations from which rock samples were taken. The main rock types in the catchment area are the Schiefeberge schist, Bloedkoppie granite and Etusis quartzite.

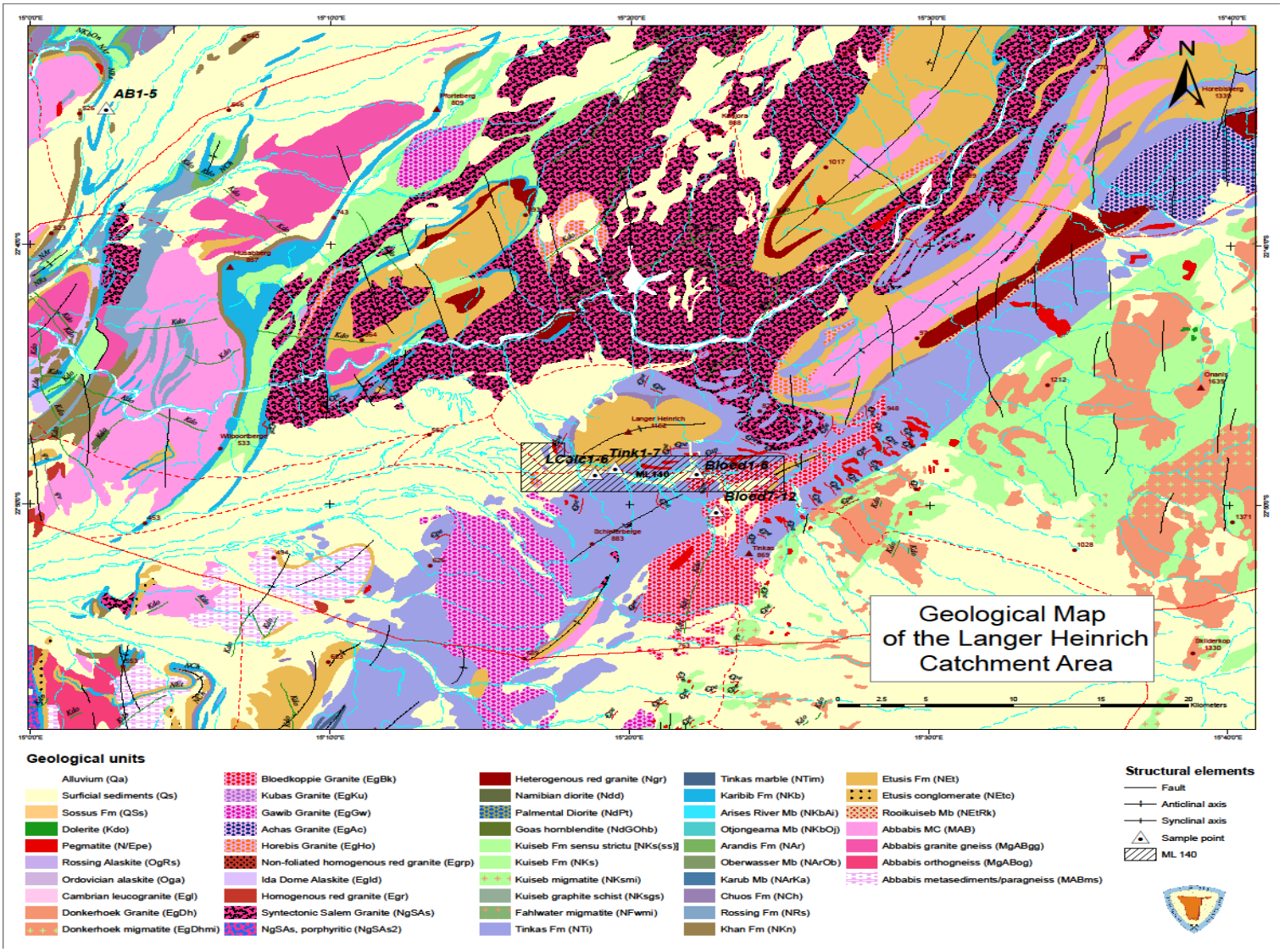

Fig . 108 : A geological map showing geographic locations for the sample points in the Langer Heinrich catchment area.

5.1.1 Bloedkoppie granite

The Bloedkoppie granite occupies most of the catchment area for the Langer Heinrich uranium deposit (Fig. 18). In outcrop, the granite is generally coarse-grained and deeply weathered. Felsic dykes crosscut the main lithologies of the Bloedkoppie granite. The granite appears jointed, which would have assisted meteoric water to percolate through it and leach uranium out. The Bloedkoppie granite also contains xenoliths of the Tinkas schist. The contact between the xenoliths and the Bloedkoppie is very sharp, clearly indicating that the granite did not assimilate the schist when it intruded the schist. The following Figures (Fig. 19 (a) – (c)) are presented in order to show the extent to which the Bloedkoppie granite has been weathered.

(a)

b)

(c)

Fig . 119 : Outcrops of the Bloedkoppie granite showing: (a) tafoni; (b) both tafoni and alveoles, with Dr Hambleton – Jones, for scale and (c) deeply weathered granite (Dr Kamona for scale).

The weathering features shown in Figure 19 (a) – (c) indicate that the Bloedkoppie granite has undergone intense weathering during erosion, and this resulted in the formation of the hollows which are called tafoni and alveoles.

Fig. 19 (d): An aplite dyke cross-cutting the Bloedkoppie granite.

Contrary to what we see in the Spitzkoppe granites, aplite dykes show higher radiation intensity than the host granite. The aplite dykes vary from 5 to 20 cm but on average they are about 15 cm in width (Fig. 19 (d)). They appear more whitish than the main granite in outcrop and generally contain more quartz than the main granite. In thin section (e.g. samples Bloed1 and Bloed2), the Bloedkoppie granite typically consists of 45% K-feldspar, 33% quartz, 15% plagioclase, 5% biotite with accessory muscovite, chlorite and amphibole. The K-feldspar is mainly microcline. Both plagioclase and K-

feldspar crystals show clear alteration to micas, mainly chlorite and muscovite. The style of alteration indicates that both the late stage magmatic fluids and meteoric water have acted on the early formed crystals to cause alteration. There is no primary muscovite in the granite. The content of biotite in the Bloedkoppie granite appears to be lower than that of the Spitzkoppe granites.

The pegmatite veins show higher radiation intensity than the main granite. The scintillometer shows 89 cps on the main granite and just above 100 cps on pegmatite veins. The confirms the findings of Kamona (2011), who reported that these cross-cutting pegmatite veins have average U concentrations of 23 ppm, while the main granite has about 10 ppm U.

(a)

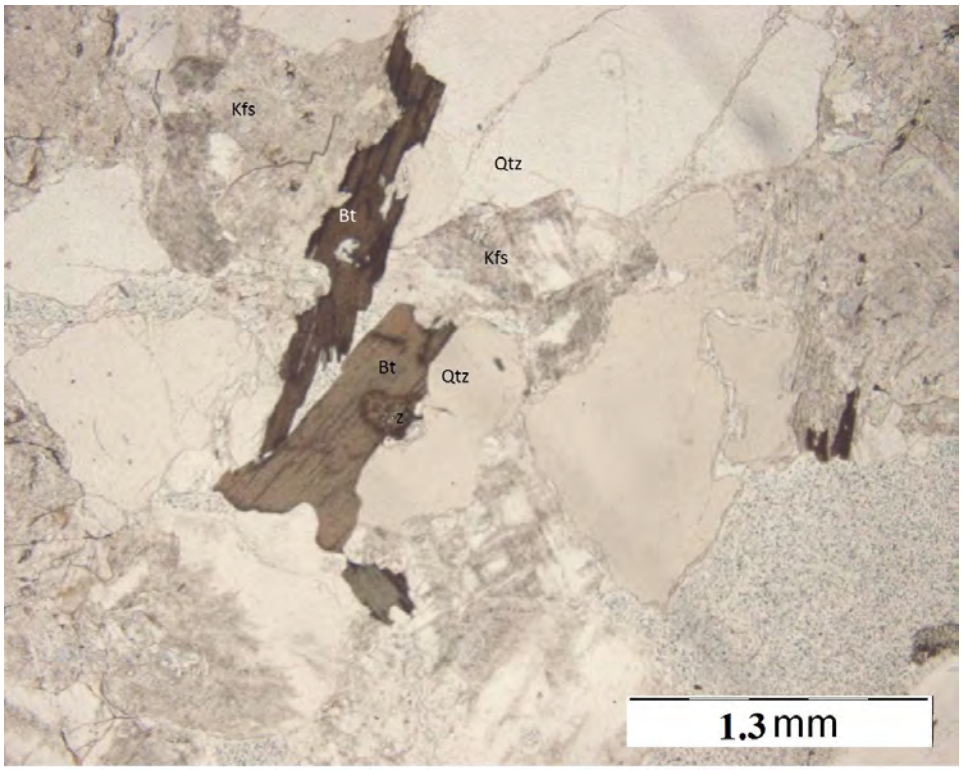

(b)

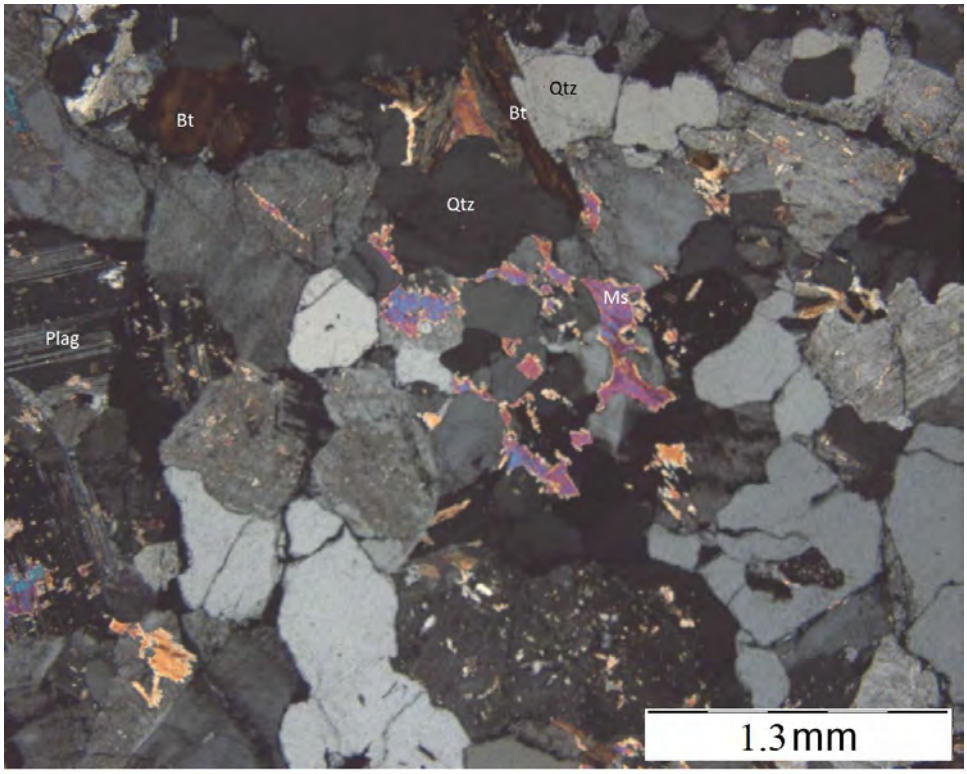

Fig . 20: Photomicrograph of the Bloedkoppie granite, sample Bloed 6 showing (a) radiation haloes in biotite (Bt) crystals (PPL) ; (b) feldspars weathering to muscovite (Ms) or sericite (crossed nicols). Quartz (Qtz) crystals can also be seen.

Biotite in the Bloedkoppie granite shows alteration to chlorite and is riddled with radiation haloes (Fig 20). The sub-circular radiation haloes reflect the presence of uranium-bearing accessory minerals like monazite and zircon, which occur as inclusions in biotite.

5.1.2 Tinkas schist

In hand specimen, the Tinkas schist is a medium- to coarse-grained amphibole - biotite schist. Parts of the schist are more biotite-rich while other parts are more quartz-rich. The Tinkas schist forms more than 60% of bedrock for the Langer Heinrich palaeo-channel. The schist has been highly metamorphosed during the Damara Orogenesis, resulting in intense foliation.

In thin section the Tinkas schist typically contains about 25% biotite, 30% amphiboles and 45% quartz (Fig. 21). Both biotite and amphibole crystals are aligned along the same direction and in the groundmass of quartz. The oxides appear to be randomly distributed in the matrix. Because of the compression during the Damara Orogeny, the quartz crystals also appear to be elongated, aligned along the same direction as the biotite and amphibole crystals. In thin section, quartz shows dramatic strain extinction due to deformation.

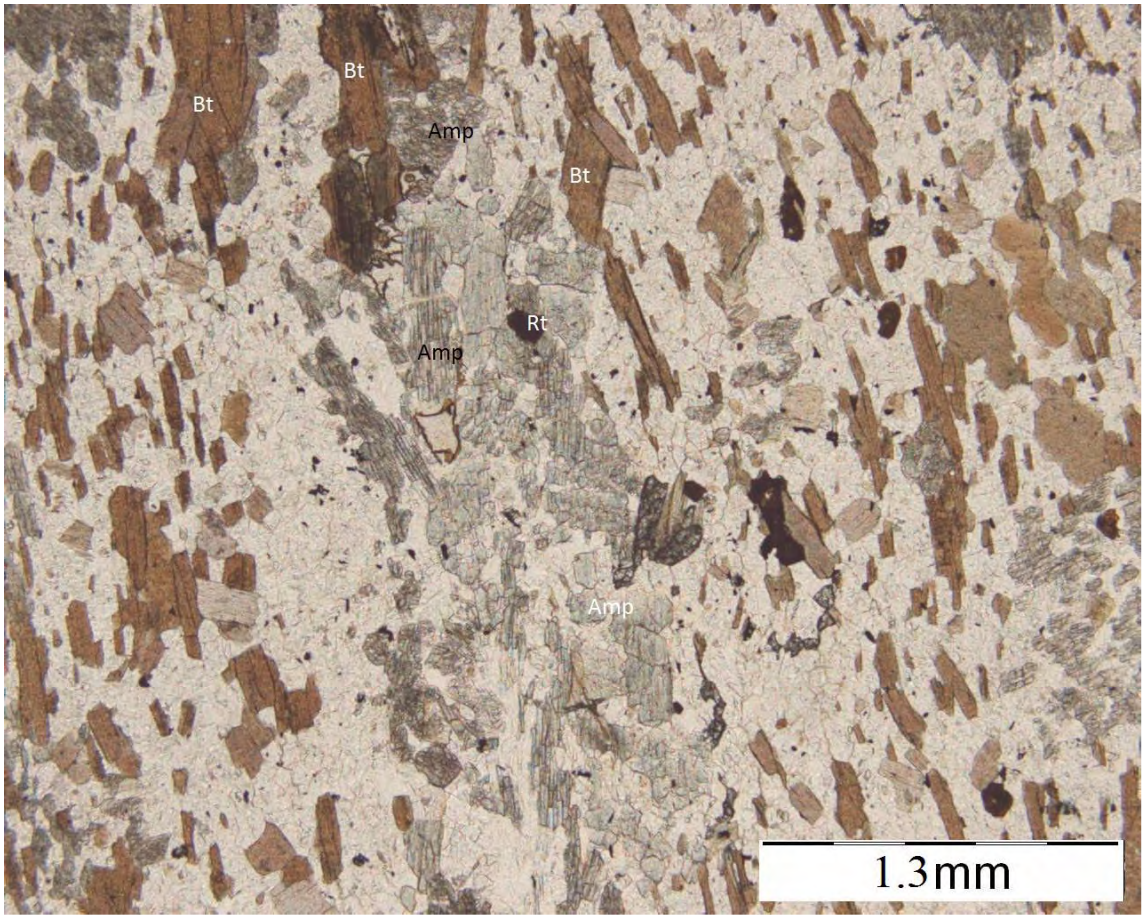

Fig . 21: Photomicrograph of the Tinkas schist around Langer Heinrich, sample Tink 2 (PPL) showing the alignment of the biotite (Bt) and amphibole (Amp) crystals.

5.1.3 Abbabis Metamorphic Complex

The 2 Ga Abbabis Basement complex was sampled near Arandis (Fig. 18), where it is well exposed. There is a major unconformity between the Abbabis gneiss and the Damara Supergroup. According to Marlow (1981) the Abbabis gneiss is about 2 Ga in age while deposition of the Nosib, which is the base of the Damara Supergroup, is dated at around 1 Ga. The purpose of sampling the Abbabis gneiss was to test the U and V concentrations even though it does not immediately underlie either of the two

catchment areas. Abbabis felsic gneisses are coarse grained in hand specimen. They appear whitish to greyish in colour and in general are less weathered than the Bloedkoppie granite. In thin section the felsic gneiss (e.g. AB3) typically consists of 60% quartz, 10% plagioclase, 20% K-feldspar, 5% biotite and 5% pyroxenes (Fig. 22). The pyroxenes are a combination of about 60% clinopyroxene and 40% orthopyroxene. The quartz crystals appear highly deformed in thin section.

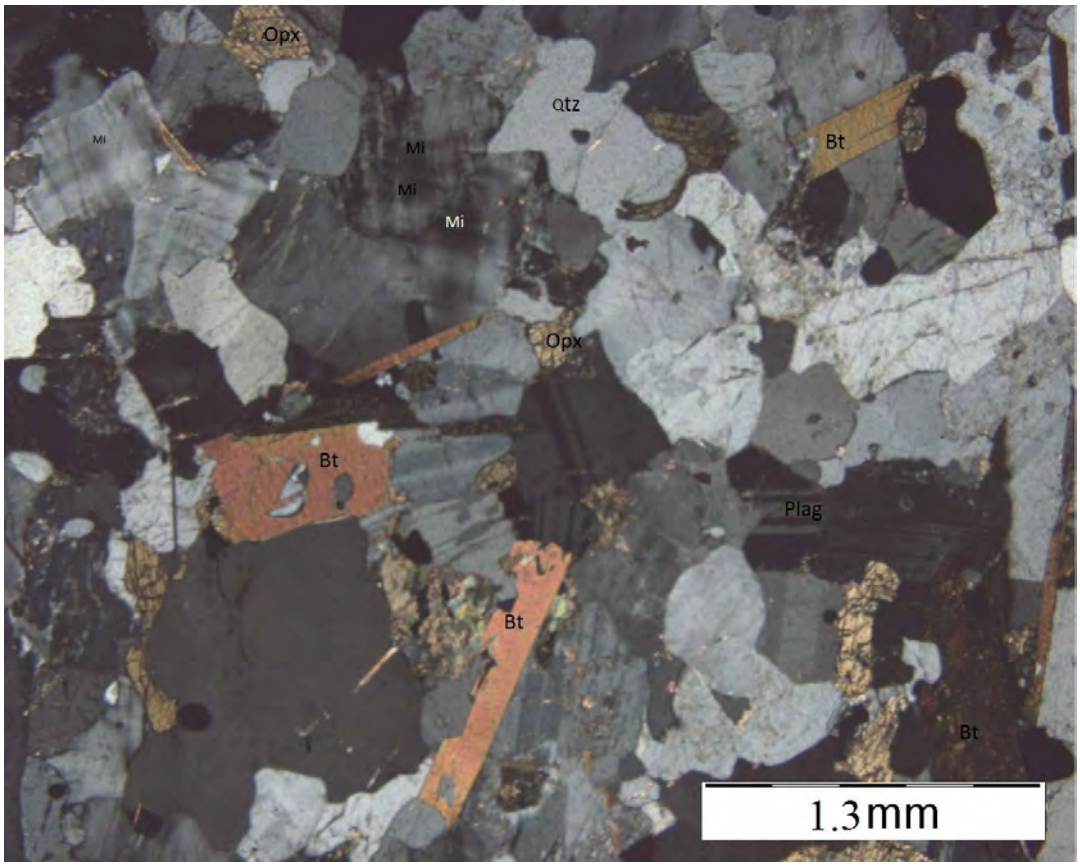

Fig . 22 : Photomicrograph of the Abbabis gneiss, sample AB3 (crossed nicols) showing strained quartz (Qtz) with amoeboid shape, cross-hatched microcline

5.2 Klein Trekkopje catchment area

The main rock types in the catchment area for the Klein Trekkopje U deposit include Karibib marble, Kuiseb schist, Damara aged leucogranites, Salem granite, Karoo dolerite, Klein Spitzkoppe granite and Gross Spitzkoppe granite (Fig. 23).

5.2.1 Klein Spitzkoppe granite

This granite has three distinct lithological units, a medium-grained porphyritic granite, a coarse-grained biotite granite, and a whitish fine-grained microgranite. Aplite and lamprophyre dykes cross-cut the main granite in places. Two dimension stone quarries, one in the south and another one to the north of the granite, were used as the main observation points during the study because this is where all the igneous, structural and weathering features are best exposed.

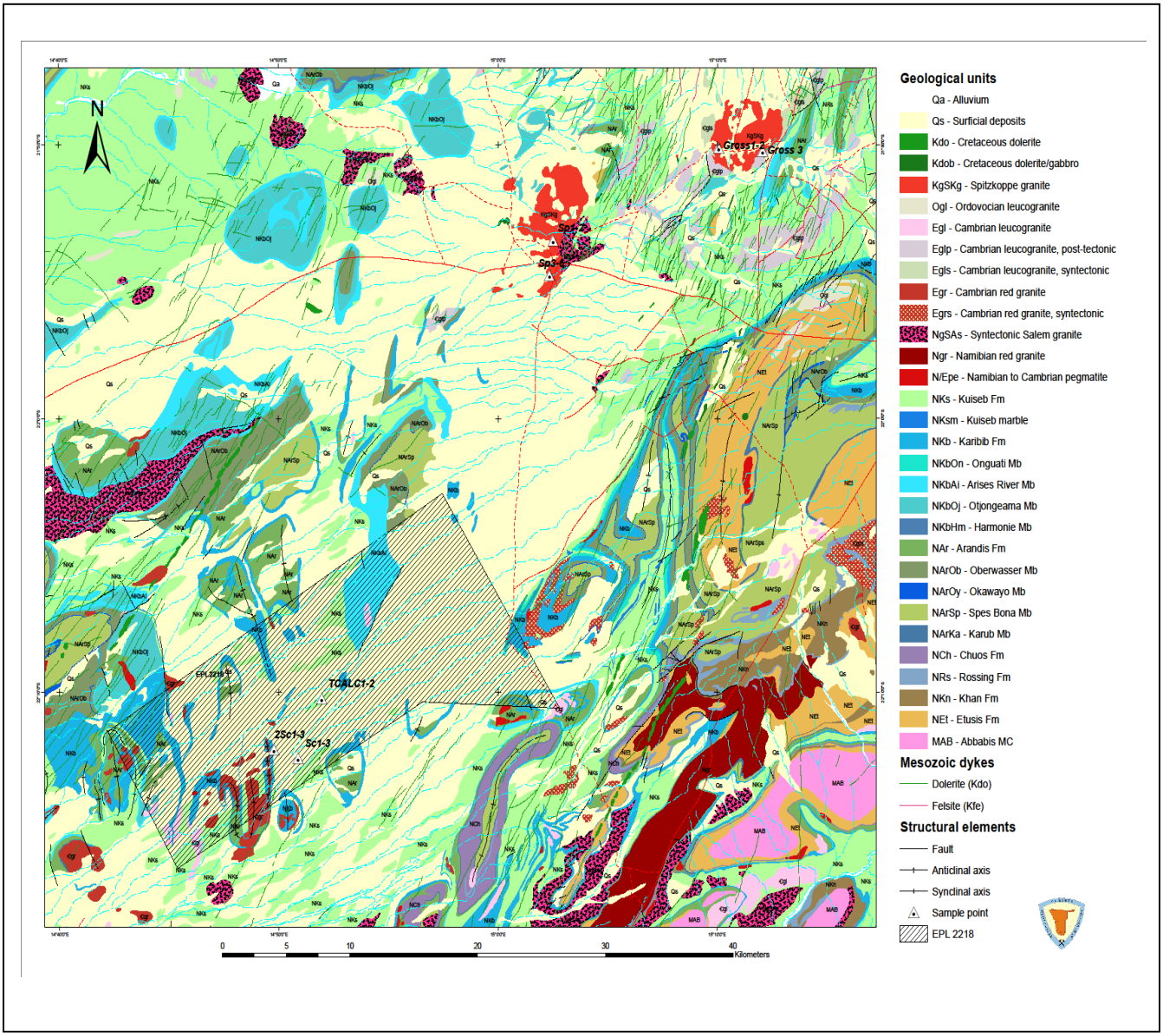

Fig . 23 : A geological map showing the geographic locations for the sample points in the Klein Trekkopje catchment area.

Figure 23 shows the geology of the catchment area for the Klein Trekkopje U deposit which has been described in detail under the Regional geology and Introduction chapters. The mining licence boundary is also shown in Figure 23.

Fig . 24: An outcrop of the Klein Spitzkoppe granite, decomposing into clay at the bottom (southern quarry).

Figure 24 shows palaeo-weathering of the coarse-grained biotite bearing Klein Spitzkoppe granite. Below, feldspars have completely decayed into clay. The picture shows Greg Symons checking the radiation intensity of the granite block with a scintillometer. The writer's main focus on this stock was to study the structures and weathering features as these provide an indication on the extent to which uranium had been leached. The quarries on this granite belong to African Granite (Pty) Ltd, a mining

company owned by a Karibib resident Franz Wittreich. In terms of structure, the Klein Spitzkoppe granite is intensely faulted and jointed. In the southern quarry, which is up to 15 m deep, the granite shows clear oxidation (Fig. 26 (a) – (c)). Secondary minerals include goethite, hematite and clay minerals. The depth and the intensity of this palaeo-weathering clearly indicates that the degree of leaching has been extremely high. The XRD tests have revealed that the dominant clay mineral at Klein Spitzkoppe granite is montmorillonite.

Fig . 25: An aplite dyke in the main medium-grained biotite bearing Klein Spitzkoppe granite (southern quarry).

At this location (Fig. 25), the main granite and the aplite dyke report 120 cps and 105 cps respectively. The difference in radiation intensity once again clearly shows that

the aplite dyke represents a more evolved melt depleted in U and Th. This is the melt which remains after U/Th fixing phases such as biotite, zircon, monazite have crystallized. The residue which formed the aplite dyke has less biotite, zircon, monazite, etc., and hence less U and Th. In general the main granite at Klein Spitzkoppe reports about 160 – 170 cps. The assay report shows the main granite containing about 12 ppm U while the aplite dyke contains 7 ppm U.

Fig . 26: (a) :Weathering features in the southern quarry, Klein Spitzkoppe granite (southern quarry).

In Figure 26 (a), there are two distinct weathering features, each indicating a specific intensity of weathering or oxidation. Part of the granite is still fresh and unweathered. The second part has weathered, to produce a reddish colour, which shows lower

radiation intensity than the fresh granite on a hand-held scintillometer. A third portion of the granite has weathered to a greyish yellow colour. The reddish part consists mainly of hematite whilst the greyish yellow part consists mainly of goethite and hence is highly weathered.

Fig . 26 : (b) Sample SP 9 showing oxidation in the Klein Spitzkoppe granite.

There are two samples of granite shown in Figure 26 (b). The one sample is fairly fresh and the other more oxidized and thus reddish. The two samples were taken from the same outcrop. There is a common belief that at a concentration of less than 20 ppm or so, U tends to substitute in accessory minerals like zircon and monazite rather than forming its own minerals (Miller, 2009; Kinnaird personal communication, 2011). This

study has shown that this is not always true because U locked up in accessory minerals cannot be easily liberated during erosion to form some of the secondary deposits we see today like Langer Heinrich, Trekkopje, Marenica, etc.

In Namibia most of the granitoids which have been shown to be the sources of U for the secondary deposits have less than 20 ppm U on average. A quick check with a scintillometer in the field (S21˚54’41.3”; E015˚02’21.1”) reveals that the fresh sample (SP9) in Figure 26 (b) above gives a radiation intensity of 230 cps, whilst the weathered sample of the same outcrop reports 160 cps. In geochemical terms, this represents a difference of about 8 ppm U. This is an indication that even without serious mechanical erosion, meteoric water percolating through a granite can wash out some U and send it into the groundwater systems. It is therefore likely the uranium in this outcrop of the Klein Spitzkoppe granite was loosely held, most probably adsorbed onto the surfaces of biotite crystals or contained between grain boundaries as uranyl silicate instead of being locked up in accessory minerals. The writer has not undertaken an ICP-MS analysis on this particular fresh sample but similar samples reported about 16 ppm U.

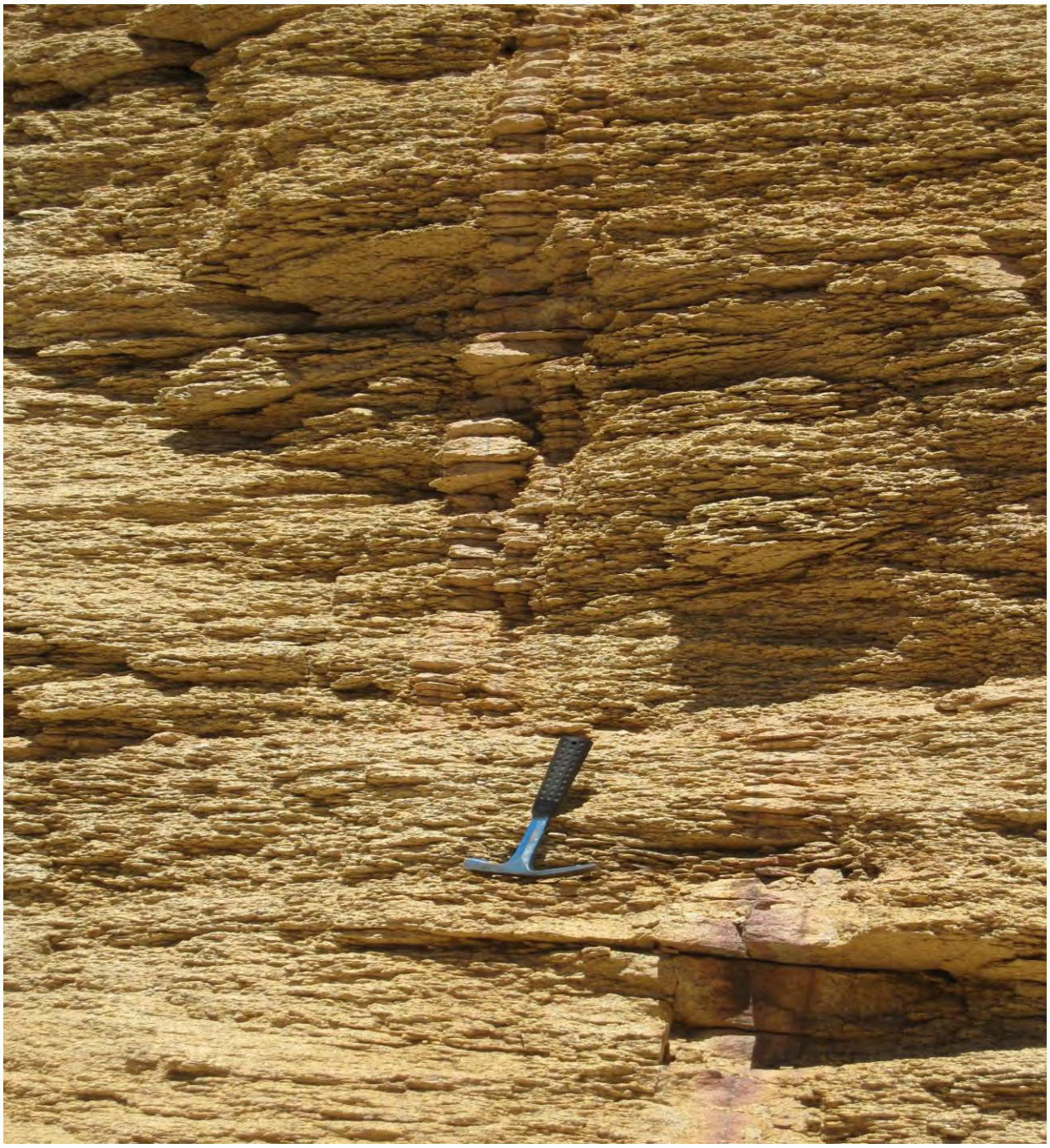

Fig . 26 : (c) A sheared aplite dyke in the weathered Klein Spitzkoppe granite, southern quarry.

Figure 26 (c) shows an aplite dyke in the bottom right corner displaced by sinistral shearing within a deeply weathered main granite of the Klein Spitzkoppe stock. The hammer handle is right on the shear zone. The same dyke can be seen in the middle of the picture, albeit slightly weathered, to the left of the hammer and towards the top of the picture. Sub-vertical joints are prevalent in the Klein Spitzkoppe granite. These kinds of structures serve as conduits for water flow and as a result they play a vital role in leaching U from the granite.

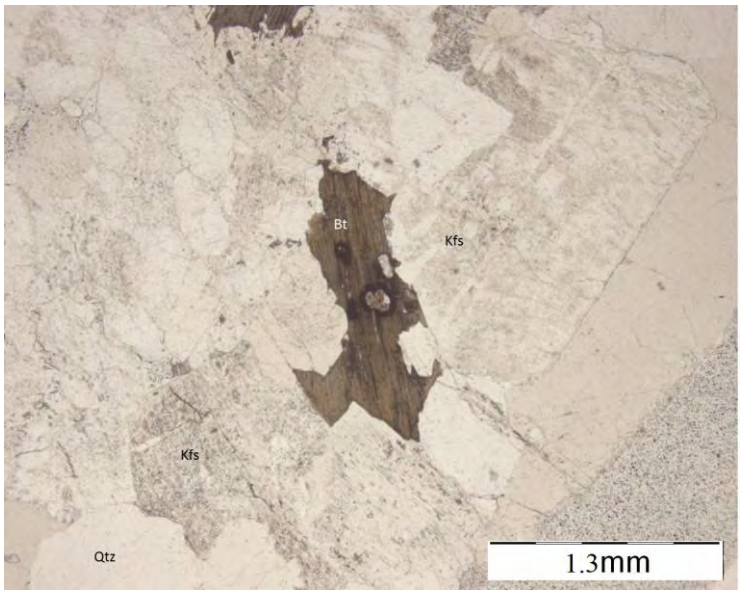

(a)

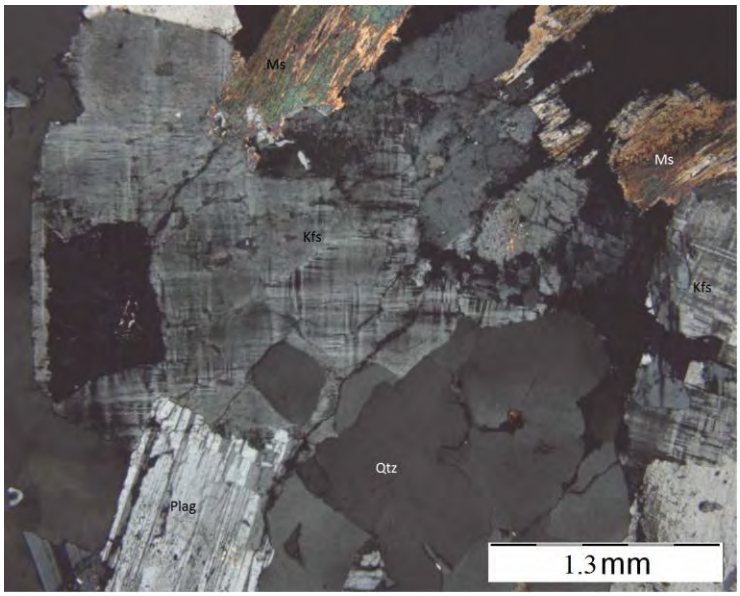

(b)

Fig . 27 : Photomicrograph of the medium-grained microgranite, sample SP6 showing (a) radiation haloes in a biotite (Bt) crystal (PPL); (b) microcline (Mi), biotite (Bt), K-feldspars (Kfs), with cross-hatched twinning and quartz (Qtz) with strained extinction (crossed nicols).

In thin section, the medium-grained microgranite comprises about 40% K-feldspar, 35% quartz, 6% biotite, 7% muscovite and 8% albite (Fig. 27 (a) & (b)). The feldspars appear to be relatively unaltered compared to the ones observed in the Bloedkoppie granite earlier. The quartz crystals also appear to show strain extinction in thin section. The biotite is riddled with radiation halos. The only mineral which shows some degree of alteration in these thin sections is muscovite.

The Klein Spitzkoppe granite consists of two main types of granite, a coarse-grained biotite granite and a medium-grained microgranite (Kandara, 1998). In hand specimen, the medium-grained micro-granite appears more whitish and less weathered than the coarse-grained. The coarse-grained biotite granite constitutes about 75% of the entire stock. The medium- to fine-grained micro – granite is distinctly different to the coarse grained biotite granite in thin section. The microgranite has much more quartz and K – feldspars and far less biotite. The medium coarse-grained granite and a finer-grained variety are both quarried for dimension stone.

5.2.2 Gross Spitzkoppe granite

The Gross Spitzkoppe granite is situated about 15 km north east of the Klein Spitzkoppe granite discussed earlier (Fig. 23). The two granites are situated along the same structural lineament on the Damaran Belt and are believed to be genetically related (Frindt et al. 2004a). The Gross Spitzkoppe stock consists mainly of three main types of granite: a marginal medium- to coarse-grained granite (comprising about 5% of the

stock), a coarse-grained biotite granite (70%) and porphyritic biotite granite (23%), (Frindt et al., 2004a).

As with the Klein Spitzkoppe granite, the minerals show no visible alteration in thin section. This is an indication that the degree of chemical weathering was quite low in these granites. The intensity of radiation halos in the biotite means any phases crystallizing after biotite in the Gross Spitzkoppe granite would be depleted in U as most of the U is already taken up by biotite as well as by accessory minerals within the biotite. The relatively low U concentrations observed in the pegmatite dykes, which cross-cut the main Gross Spitzkoppe granite should be seen in this context. Some of the K-feldspar crystals have radiation halos, but the intensity is much lower than it is in the biotite. In outcrop, the Gross Spitzkoppe granite shows typical features of physical weathering but features such as alveoles and tafoni observed in the Bloedkoppie granite are non-existent.

Fig . 28 (a) : Northward view of the Gross Spitzkoppe granite showing classic foliation.

The NNE trending foliation in Figure 28 (a) shows evidence of how the granite was emplaced during sinistral shearing which led to the opening of the South Atlantic. According to Frindt et al. (2004a), the granite is about 125Ma +/- 1Ma.

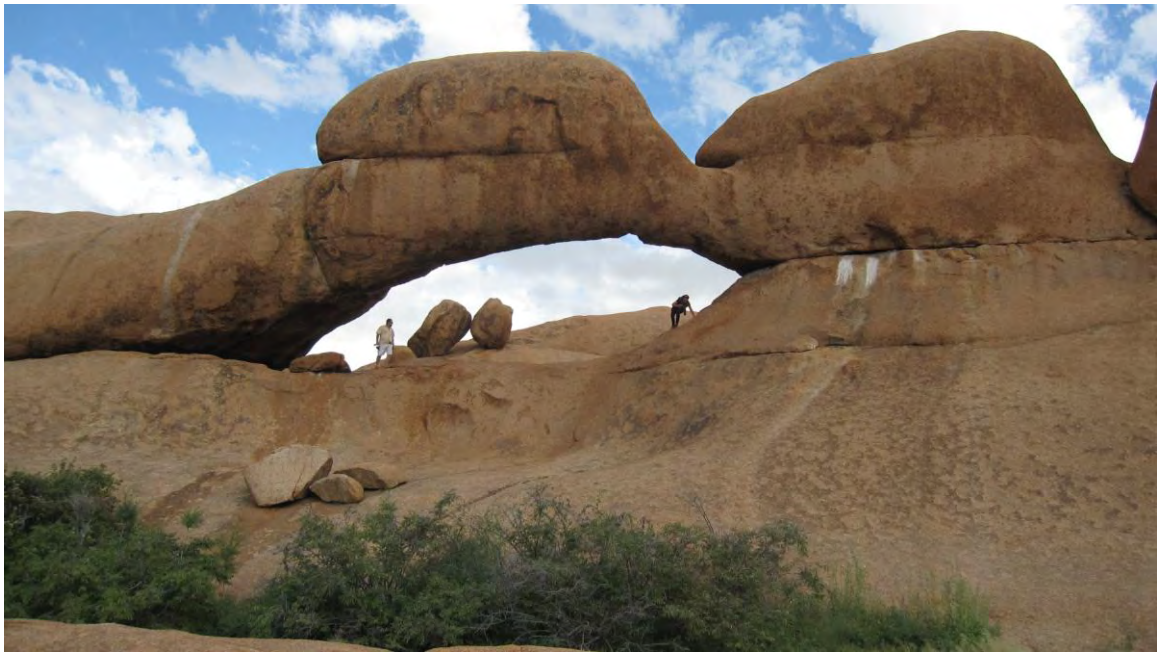

Fig . 28 : (b): A famous erosional feature “the Bridge” in the coarse grained biotite granite of the Gross Spitzkoppe granite.

The feature locally known as “the Bridge” is one of most famous tourist destinations within the Spitzkoppe granites. It shows the extent of mechanical weathering, which took place in the granite. No alveoles or tafoni were observed in these outcrops.

Fig. 28 (c): Inclusions of basaltic material (black spots) in the marginal phase of the main Gross Spitzkoppe granite.

The black spots in Figure 28 (c) represent basaltic material, which is evidence of bimodal magmatism during the break up of the Gondwana Supercontinent. Kandara (1998) also reported a number of lamprophyric dykes intruded into the Klein Spitzkoppe granite. This is evidence of bimodal magmatism during the formation of the two granites.

Fig. 28 (d): Porphyritic feldspathic granite of the Gross Spitzkoppe Stock, showing radiation intensity of 192 cps, which equates to about 15 ppm.

A quick radiometric survey of the porphyritic granite at Gross Spitzkoppe shows an average of 170 - 190 cps, while the coarse-grained biotite granite reports about 200 – 220 cps.

Fig. 28 (e): Biotite schlieren (massive biotite) within the marginal granite of the Gross Spitzkoppe stock.

The biotite schlieren display a radiation intensity of about 385 cps, about twice as much radioactivity as the porphyritic granite. This indicates that most of the U in this granite is associated with biotite. According to Frindt (2004b), the biotite schlieren are full of accessory minerals such as zircon and allanite. According to him, these minerals are completely metamict due to intense radiation. The schlieren gives 28 ppm U (Frindt et al., 2004a). Hambleton-Jones (1976) argues that the metamictization in this case will create small pathways for water to move through the crystals and leach U. According to him this will result in increased leachability of U in the granite.

Fig. 28 (f): An aplite dyke within the coarse-grained biotite granite, Gross Spitzkoppe granite.

The coarse-grained granite measures 200 cps and the dyke reports 160 cps on the scintillometer. Again this confirms that the dykes represent a late stage residual magma which is depleted in U. Geochemical analysis by Frindt (2004a) has shown that biotite-rich lithologies of the Gross Spitzkoppe granite contain in excess of 25 ppm U. By contrast, the aplite dyke contains only about 10 ppm U. In thin section, the Gross Spitzkoppe granite consists mainly of 40% Quartz, 30% biotite, 15% K-feldspar, 10% plagioclase feldspar and 5% accessory minerals such as zircon (as inclusions in the biotite). This is the average mineralogy although there are differences from one lithology to the other (e.g. Porphyritic granite differs from coarse-grained granite).

In thin section, the coarse grained biotite granite consists of 30% biotite, 35% quartz, 30% K- feldspar and 5% plagioclase. The biotite shows immense damage due to radiation. In many Damaran granitoids, U - bearing accessory minerals like zircon and monazite are contained as inclusions within biotite, (Marlow, 1981).

Fig. 28 (g): Gravels in the valley of Gross Spitzkoppe granite.

The gravels were derived directly from the GSS granites and yet their radiation intensity is only 105 cps, which is much lower than that of any of the three granites of the GSS. This suggests that part of the uranium has been washed away by meteoric water and carried downstream. The more fine-grained soils in the valley give 122 cps,

suggesting the uranium content may be influenced by the clay mineral content of the sediments.

Fig. 29: Salem granite in contact with Gross Spitzkoppe granite, showing very low radiation intensity.

Commonly the Salem granite has a higher plagioclase content than Spitzkoppe granites and the former has a lower U content. In general the Damaran-aged Salem granite ranges between 70 – 90 cps. Without analyzing them, it is clear their uranium content is too low to have contributed significant amounts of U to subsurface water. In geochemical terms this level of radiation translates into about 5 ppm U.

Table 10: Radiation intensity for various rocks of the Gross Spitzkoppe granite.

	ROCK TYPE	RADIATION INTENSITY (CPS)	ESTIMATED U CONC. (PPM)
Gross Spitzkoppe granite	Biotite schlieren	385	25
	Coarse-grained granite	200 – 220	16
	Porphyritic granite	170 – 190	13
	Aplite dyke	160	10
	Salem granite	70 – 90	5

The following Figures are from thin sections for the Gross Spitzkoppe granite (Fig. 30)

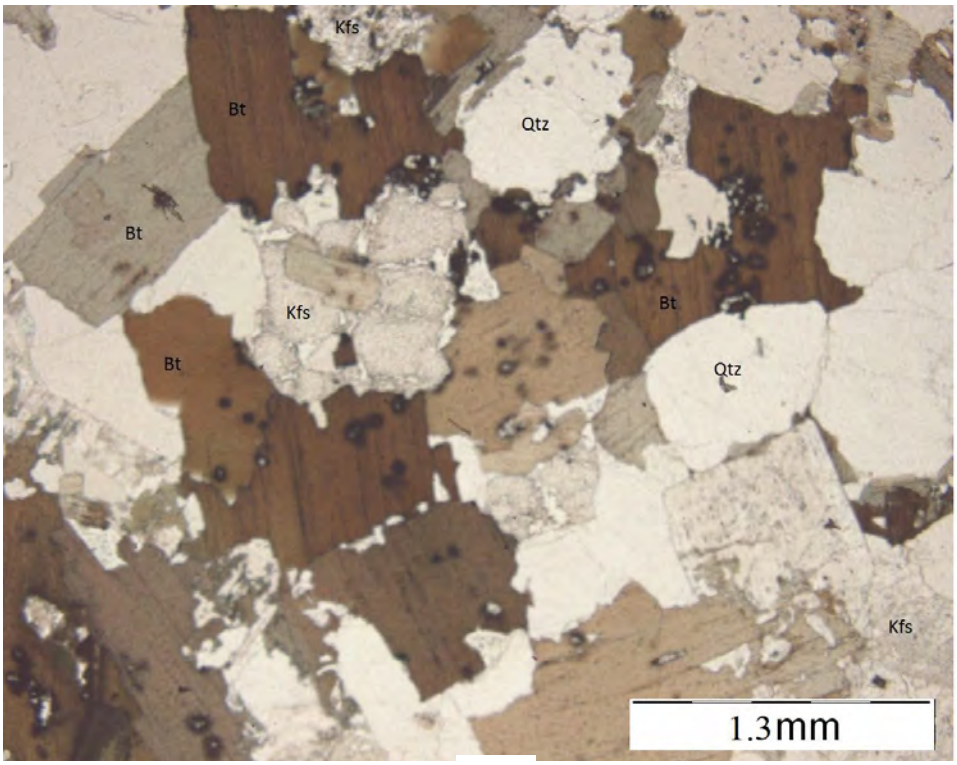

(a)

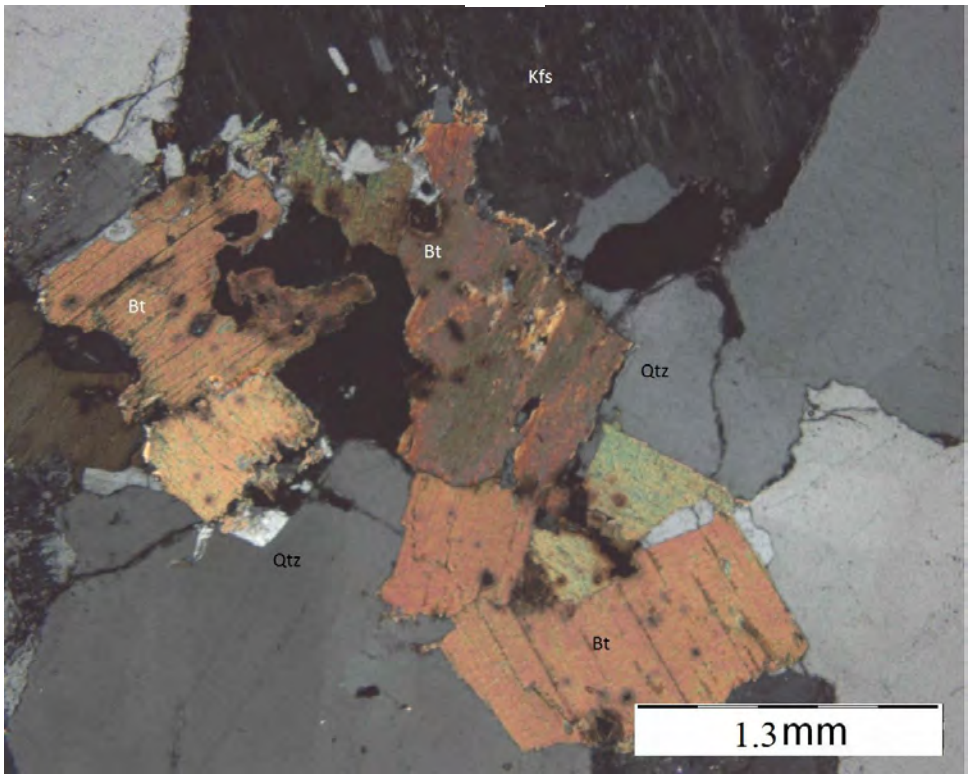

(b)

Fig. 30: Photomicrograph of the coarse-grained granite (Sample Gross 1), Gross Spitzkoppe granite, showing how the biotite (Bt) crystals are damaged by radiation to form circular radiation haloes. In (a) the quartz is very sutured (PPL). Plate (b) shows the K-feldspars (Kfs), quartz (Qtz) with sutured margins and faint strain extinction, while biotite is ragged (crossed nicols).

The high number of radiation halos in the biotite reflects a strong association between uranium and biotite during the latter's crystallization in a cooling magma.

Although in thin section, biotite crystals are the most visible, Marlow (1981) has documented the fact that accessory minerals such as monazite and zircon crystallize more or less at the same time as biotite and the uranium is actually associated with these accessory minerals. The fact that the accessory minerals are completely metamict means part of the U is trapped in them.

5.2.3 Karoo dolerite

The dolerite was sampled in the Trekkopje tenement, where it is well exposed. In hand specimen, the dolerite is medium to coarse-grained, with strongly interlocking grains. In thin section the dolerite consists of 20% olivine, 10% orthopyroxene, 30% clinopyroxene, 37% plagioclase and 2% opaque oxides (Fig. 31). Laths of plagioclase appear to be the last phase to crystallize. There is virtually no alteration despite the fact that the sample was taken at the surface where oxidation should have occurred. The portable XRF machine used by the writer in the field showed that the dolerite contains about 150 – 200 ppm V. These values correspond to the ones obtained by van Noort (2010).

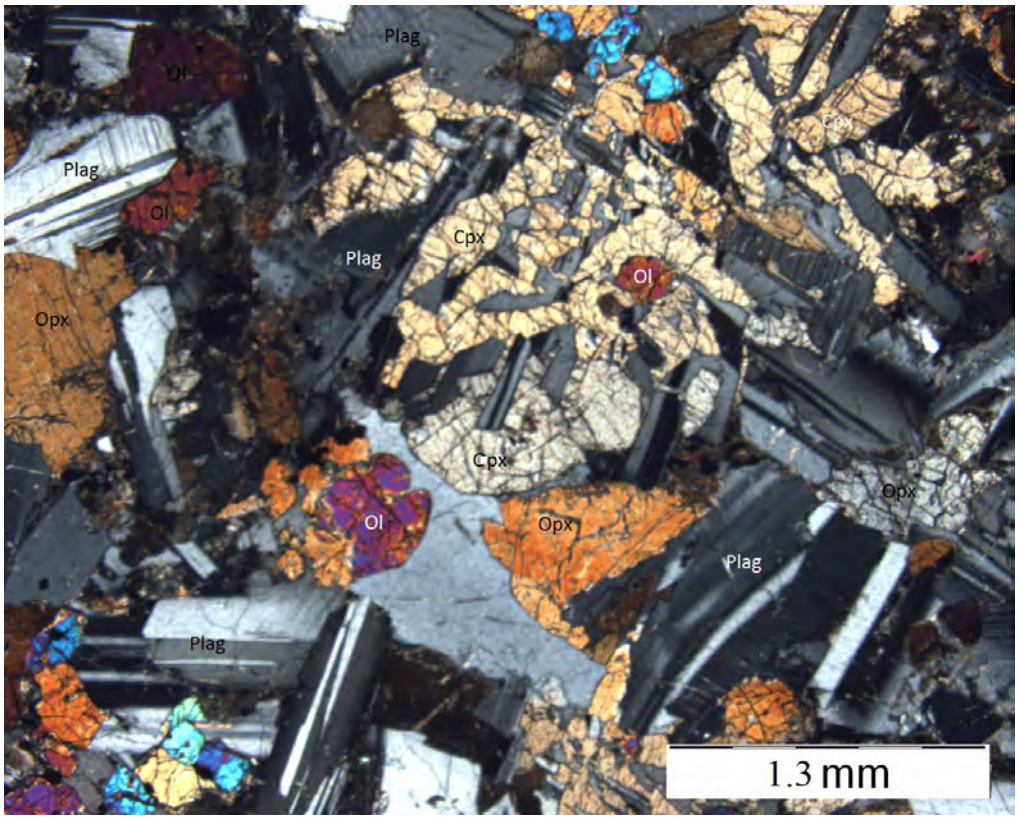

Fig. 31: Sample Dol 2 from Karoo dolerite (crossed nicols), near the Klein Trekkopje U deposit. The picture shows olivine (Ol), orthopyroxene (Opx), clinopyroxene (Cpx) and plagioclase feldspar (Plag).

5.3 Discussion

The geology for the Central Namib Desert supports the formation of calcrete hosted U deposits because of a number of factors. The structures, weathering features, U and V concentrations in the granitoids of the Namib Desert are clearly favourable for leaching during erosion.

Most granitoids with anomalously high U concentrations in the catchment area consist of quartz, microcline, albite, orthoclase and biotite. This kind of mineralogy, with the exception of quartz, is highly amenable to leaching during erosion. In general the higher the concentration of biotite and plagioclase feldspars, the higher the leachability. On the other hand, a high concentration of quartz and alkali feldspars will result in lower leachability. Other factors controlling the leaching of a specific rock include grain size, porosity, structures such as faults, permeability and the period for which a rock has been exposed to fluids. The concentration of U or V – fixing accessory minerals in a rock also affects the leachability of such a rock. The Bloedkoppie granite has undergone intense chemical and physical weathering and is highly leachable. Its aplite dykes have a higher U concentration than the main granite. The biotite crystals in this granite appear to host the bulk of the U. Parts of the Tinkas biotite schist have more quartz than others. Those parts with more quartz tend to be more resistant to weathering and stick out as high outcrops in the field.

The Abbabis gneiss has undergone a lower degree of chemical weathering compared to the Bloedkoppie granite. The Klein Spitzkoppe granite has also undergone both chemical and physical weathering but on the Gross Spitzkoppe granite, physical weathering is dominant. The two Spitzkoppe granites have more biotite than the Bloedkoppie granite and U appears to be associated with biotite, judging from the radiation haloes. Aplite dykes which have crystallized after biotite have lower U concentrations than the main granites. The Spitzkoppe granites have a lot of joints and

faults, which make them amenable to leaching during erosion. The dolerite dykes in the catchment area for the Klein Trekkopje have undergone more physical weathering and very little chemical weathering. The relatively high radiation intensity shown by biotite rich portions of all the granites demonstrates the strong association existing between U and biotite in any granite. Etusis quartzite is essentially composed of quartz and is highly resistant to both chemical and physical weathering. Other resistant lithologies which played the same role on the Klein Trekkopje catchment area include granite domes, marbles and dolerite dykes.

5.4 Summary

This study has shown that V in the pelitic sediments and in granitoids is highly leachable during erosion because of a number of factors already discussed. The study has also brought to light the fact that most of the U-bearing granitoids on the escarpment and in the Namib Desert itself contain plenty of leachable uranium. Granitoids such as Bloedkoppie, Klein Spitzkoppe, Damaran-aged granites and Abbabis felsic gneiss are all good sources of U during erosion. Certain portions of the Gross Spitzkoppe stock have a high concentration of resistant U bearing accessory minerals such as zircon, monazite and allanite. Because of this mineralogy, the Gross Spitzkoppe granite contains less leachable U than Klein Spitzkoppe granite despite the fact that the former has a higher absolute U concentration.

CHAPTER 6 : GEOCHEMISTRY OF SOURCE ROCKS AND GROUNDWATER

In this chapter, the geochemistry of rocks in the catchment areas, the calcretes and ground water is studied. The geochemical data collected by the writer is presented in Appendix 3. Various data sets from previous researchers are also presented in this chapter. The Klein Spitzkoppe and Gross Spitzkoppe granites are more enriched in alkalis compared to the Bloedkoppie granite.

6.1 Langer Heinrich catchment area

This catchment area consists mainly of Abbabis gneiss, Bloedkoppie granite, Tinkas schist and Etusis quartzite.

6.1.1 Bloedkoppie granite

Twelve samples collected by the writer from the Bloedkoppie granite gave an average of 5.5 ppm U and 10 ppm vanadium. It is important to note that the Bloedkoppie granite is deeply weathered and the results of these 12 samples, which were taken from the Bloedkoppie outcrops, may not be reflective of fresh material as they were taken close to surface. The true uranium and vanadium concentrations can be expected to be slightly higher than the values reported. In fact, Hambleton–Jones (1976) collected 11 samples from the Bloedkoppie granite and they returned 17 ppm uranium. These values were confirmed by Kamona (2011), who reported average U concentrations of 15 ppm after conducting a systematic survey for U and Th concentrations in the Bloedkoppie

granite. Unfortunately both Hambleton-Jones (1976) and Kamona (2011) did not assay for V.

From Table 11, it can be seen that not only is the Bloedkoppie granite enriched in uranium but it is also enriched in vanadium. Both the Bloedkoppie and the Tinkas schist were amenable to leaching as shown by the existence of large hollows in the outcrops of the Bloedkoppie granite. This indicates the granite's readiness to decompose in contact with water (Fig. 19 (a) – (c)). Hambleton-Jones (1976) referred to these hollows as tafoni. There are also smaller hollows, which he referred to as alveolus. In places the hollows are a couple of metres wide (Fig. 19).

The following data are for the samples taken by the writer from the Bloedkoppie granite:

Table 11: Geochemical data for the Bloedkoppie granite (ICP-MS).

Sample ID.	U (ppm)	V (ppm)	Th (ppm)	Ce (ppm)	La (ppm)	Zr (ppm)	Ti (%)	Fe (%)	Na (%)	Rb (ppm)	K (%)	Ca (%)	Mg (%)	Ta (ppm)	Be (ppm)	Al (%)	Nb (ppm)	P (ppm)
Bloed1	7.6	5	13.3	9.51	7	43.3	0.024	0.65	3.04	248	2.22	0.53	0.04	4.12	14.8	6.6	53.6	100
Bloed2	9	3	25.3	19.85	13.2	48	0.033	0.76	2.56	380	3.27	0.4	0.05	5.08	12.25	6.66	63.8	170
Bloed3	4.4	9	22.9	14.15	5.7	54.7	0.028	0.72	2.66	369	3.11	0.44	0.06	5.21	11.1	6.69	39.3	160
Bloed4	4.1	2	19.4	15.3	7.4	38.8	0.031	0.68	2.54	332	3.11	0.49	0.05	3.18	11	6.49	26.3	210
Bloed5	8.2	2	18.3	11.65	5.5	37.4	0.02	0.51	2.45	350	3.32	0.44	0.03	3.69	10.55	6.39	30	190
Bloed6	4.8	7	31.5	25.9	11.5	61.6	0.041	0.77	2.45	395	3.33	0.52	0.08	4.22	10.05	6.55	29.8	200
Bloed7	4.4	18	20.7	91.8	46.3	89.3	0.161	1.73	2.21	264	3.9	0.92	0.21	2.88	6.18	7.11	26.5	510
Bloed8	3.4	18	26.7	101	51.6	82.3	0.172	1.86	2.32	276	3.45	1.06	0.22	1.94	5.62	7.07	25.5	530
Bloed9	9.2	5	17.1	20.1	7	35.1	0.054	0.84	1.53	288	4.86	0.38	0.08	0.9	3.44	6.86	13.6	170
Bloed10	5	18	30.7	109.5	55.2	101	0.163	1.83	2.2	233	3.38	1.06	0.23	2.38	6.3	6.95	26.2	500
Bloed11	3.5	18	24.7	98.6	50.6	100	0.179	1.7	2.23	250	3.71	0.99	0.21	2.27	6.18	6.93	28.2	400
Bloed12	2.4	12	18	96.4	36.1	77.7	0.115	1.22	2.04	214	3.21	0.87	0.15	2.24	6.28	6.15	19.7	380
Average	**5.5**	**9.75**	**22.4**	**51.1**	**24.7**	**64.1**	**0.085**	**1.11**	**2.35**	**300**	**3.41**	**0.67**	**0.12**	**3.17**	**8.64**	**6.70**	**31.87**	**293.3**

The Bloedkoppie granite's concentrations for U and V are above those of average granites. Some leucogranites in the vicinity of the Klein Trekkopje deposit have given V concentrations as high as 100 ppm (appendix 3).

The Bloedkoppie granite has a lower content of biotite than the Spitzkoppe granites, particularly the Gross Spitzkoppe granite. It is known that biotite takes up a lot of U during fractional crystallization. Therefore a low content of biotite in the granitic magma means most of the U proceeds to residual fluids. The pegmatite dykes which later form from these residual fluids will therefore be highly enriched in U. This is the main reason why pegmatite dykes in the Bloedkoppie granite have higher U concentrations than the main granite. With the Spitzkoppe granite, the crystallization history is quite different. The granitic magma from which the Spitzkoppe granites were formed had a very high content of biotite during its crystallization process. Since biotite takes up plenty of U, any residual fluids left after the crystallization of biotite would have extremely low concentrations of U. The writer has observed that pegmatite dykes, which cross-cut the main Klein Spitzkoppe and Gross Spitzkoppe granites, have lower U concentrations than the main granites.

The writer's sampling exercise has shown that the Bloedkoppie granite contains in the order of 15 ppm V on average (Table 11). Therefore erosional water draining from the Bloedkoppie granite is carrying V in addition to U. When the groundwaters at Langer Heinrich finally make contact with the Tinkas schists, which is known to contain about 160 ppm vanadium, the resulting effects are predictable. Once oxidizing

conditions are achieved, there will be plenty of V^{5+} in the system. Therefore at Langer Heinrich, precipitation of carnotite was likely to have been achieved easily. The fact that the Langer Heinrich deposit is dominated by bright yellow carnotite, rather than greenish or bluish varieties as at Klein Trekkopje, is strong evidence that the Langer Heinrich deposit was formed in a much more oxidizing environment, where V^{5+} predominates over V^{4+} and V^{3+}.

In Figures 32 (a) – (q), the relationships between various key elements and U in the Bloedkoppie granite are examined. The relationship between some elements and V in the granite is also examined in Figure 32 (r) – (t). These Figures are helpful in understanding how U and V behaved in the granitic magma which produced the Bloedkoppie granite.

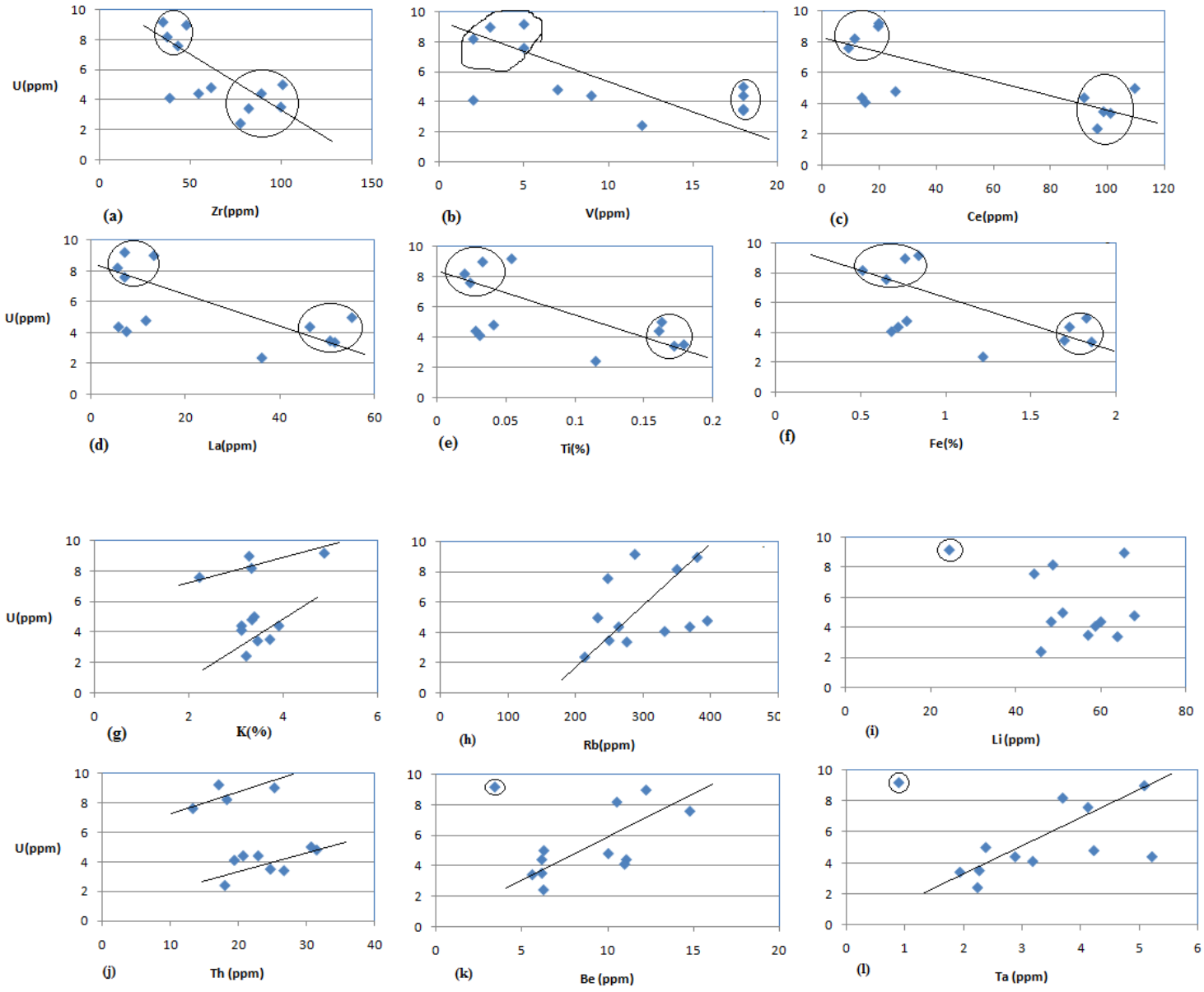

Fig .32 (a) – (l): Correlation diagrams for the Bloedkoppie granite showing the relationship between various elements and U.

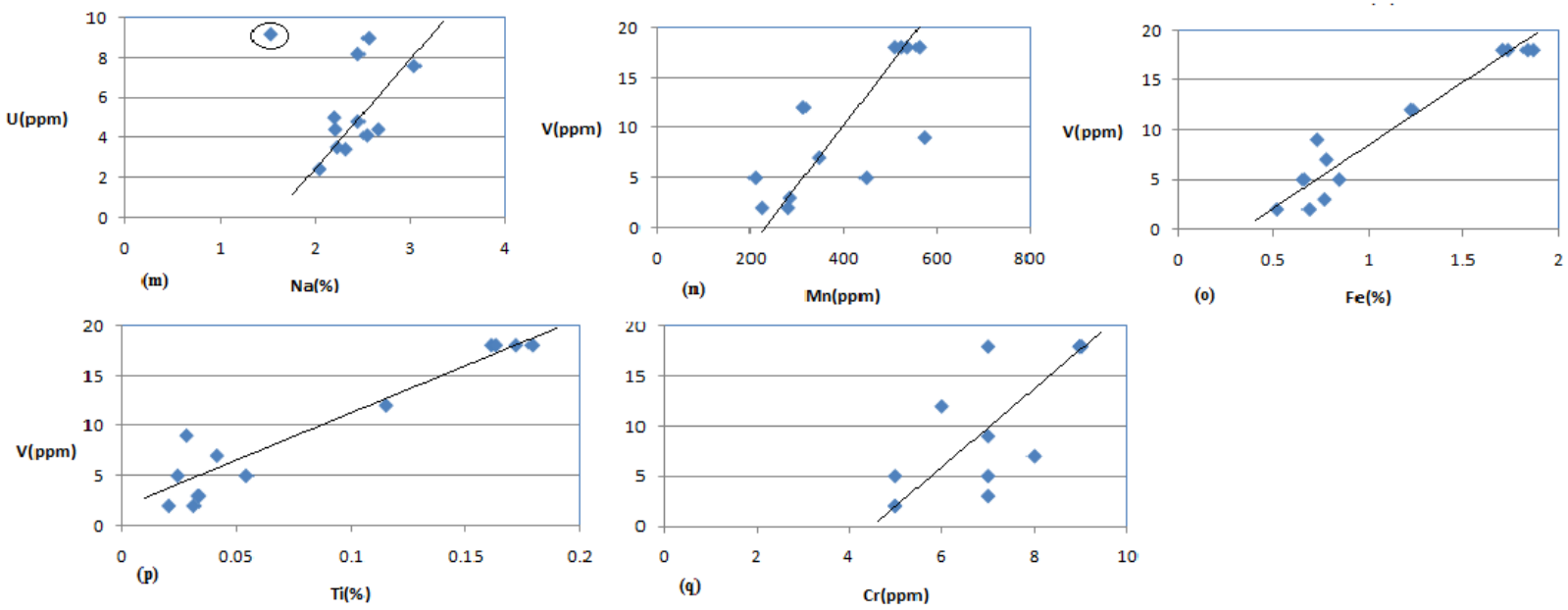

Fig. 32: Correlation diagrams for the Bloedkoppie granite showing (m) the relationship between Na and U, (n) – (q) the relationship between various elements and V.

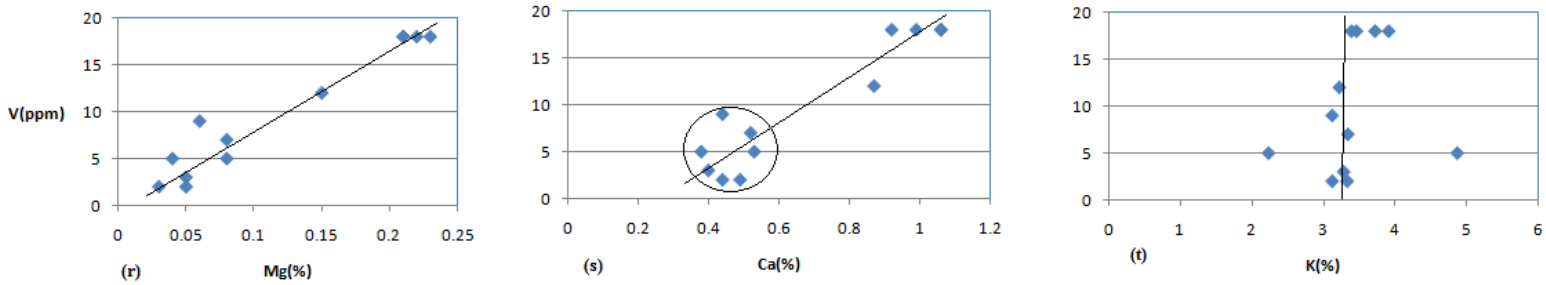

Fig. 32 (r) – (t): Correlation diagrams for the Bloedkoppie granite showing the relationship between various elements and V. The circles indicate cluster centres for the samples while the straight lines are drawn to show an estimated linear pattern which the sample points tend to follow.

Figure 32 (a) shows the relationship between Zr and U for the Bloedkoppie granite. The Figure shows that although there is no perfect correlation between Zr and U, in general high Zr concentrations are associated with low U concentrations. This suggests that most of the uranium in the Bloedkoppie granite is not associated with zircons. For the samples taken from the less evolved outcrops of the Bloedkoppie granite (low U), there is some degree of positive correlation between Zr and U. This suggests that in those outcrops, there is a lot of U locked up in zircons. However, since the majority of the samples tend to show a poor correlation between U and Zr, it seems the Bloedkoppie granite could be a good source of U. A poor correlation between these elements (i.e. Zr and Ce) and U suggests that most of the U is not locked up in resistant accessory minerals like zircons or monazite and could easily be liberated during erosion.

Figure 32 (b) shows that there is a negative correlation between V and U in the granite, whereby high U tends to be associated with low V. This is to be expected because naturally U, being incompatible with major silicates, tends to be enriched in more evolved parts of the granite. On the other hand V tends to partition into early forming ferromagnesian minerals and will hence be depleted in the more evolved portions of the granite. In a granite, V usually substitutes for Fe in minerals like biotite, magnetite and ilmenite. Samples Bloed 7-8 and Bloed 10 – 12 in Table 11 have high V values and are associated with low U values. The large variance in these V values suggests that the V concentration in the Bloedkoppie granite is not quite homogeneous.

Figures 32 (c) and 32 (d) show the Ce-U and La-U plots for the Bloedkoppie granite respectively. The Figures show that samples Bloed 11, Bloed 10 – Bloed 12 have low U concentrations associated with high Ce and La concentrations (Table 11). These samples were taken from an outcrop which is less evolved compared to the rest of the outcrops. This trend suggests that the more evolved parts of the Bloedkoppie Granite generally have less monazite and more U. However the lack of linear correlation in both Ce-U and La-U plots suggests that most of the U in the Bloedkoppie is not really locked up in monazite. Nevertheless, high Ce and La concentrations appear to be associated with low U in general suggesting that most of the U in this granite lies in more differentiated portions.

Figures 32 (e) and 32 (f) show the Ti-U and Fe-U plots respectively. The linearity for the sample points is very poor but low concentrations for these two elements are generally associated with high U concentrations and vice versa. This inverse relationship reflects the progressive depletion of Fe and Ti with fractionation as the two elements partition into silicates and oxides. Since earlier analysis has shown that most of the uranium in the Bloedkoppie granite is not held in accessory minerals either, it is likely that most of the uranium is held as inter-granular uranium, as uraninite or uranyl silicate (Marlow, 1981). This suggests that most of the U resides mainly between quartz and feldspar grains whilst the remaining small proportion may be held within biotite and accessory minerals. The Fe-U and the Ti-U plots for the Bloedkoppie granite look much the same, indicating a close association between Fe and Ti in a granitic

magma. The poor linearity in Figures 32 (e) and 32 (f) may also reflect the low content of biotite in the Bloedkoppie granite.

Figure 32 (g) shows the relationship between K and U. The Figure shows two sample populations with some degree of positive correlation between the two elements. The same positive correlation can be observed in Figure 32 (h), which shows the relationship between Rb and U. Both K and Rb values can be used to get an idea on the degree of fractionation in a granite. In the Bloedkoppie granite, the average Rb value is 300 ppm and the average strontium value is 72 ppm (appendix 3). This represents a Rb/Sr ratio of about 4.2, which is higher than the ratio for an average granite.

Figure 32 (i) shows that in the Bloedkoppie granite, there is no correlation between Li and U because the sample points are just scattered all over the plot, without any linear trend. Figure 32 (j) shows the relationship between U and Th. Two sample populations from the Bloedkoppie outcrops show some positive correlation between these two elements. This suggests that in weakly radiogenic granites, the Th:U ratio is likely to remain roughly constant.

Figures 32 (k) and 32 (l) show the Be-U and Ta-U plots. The two Figures show some degree of positive correlation with U. This is a coincidental correlation because all the three elements are incompatible in silicates and are usually enriched in residual melts during fractionation. The positive correlation between Na and U observed in Figure 32 (m) can again be explained in terms of fractionation. During fractionation, Na gets enriched while Ca gets depleted with progressive fractionation.

Figures 32 (n) to 32 (p) show how the three elements, Mn, Fe and Ti relate to V in the Bloedkoppie granite. The three plots appear to be closely similar and show some degree of positive correlation between the elements and V. This suggests that V is occupying sites otherwise occupied by Fe, Mn or Ti in a crystal lattice. Therefore in a given granitoid, V enrichment can be expected in silicates which are rich in Fe such as amphiboles, biotite and to a less extent K-feldspar. In accessory minerals, V can be expected in magnetite and ilmenite. The trend observed in Figures 32 (n) to 32 (p) suggests the more mafic minerals there are in a given rock type, the more V it will contain.

The outcrop with highest Ti content shows a negative correlation between Ti and U. This is to be expected because Ti is enriched in early crystallizing phases in which U is largely incompatible. However, outcrops with lower Ti concentrations are characterized by a slight positive correlation between Ti and U. The association between Ti and U in individual outcrops suggests the two elements are largely hosted within one mineral. The only major silicate which can host both Ti and U is biotite. If most U is hosted by biotite, then the Bloedkoppie granite is a good source of U because during erosion, biotite is completely destroyed to release U. These kinds of granites were likely formed by partial melting of a uranium-rich sedimentary package (Cuney, 2008).

Figure 32 (q) shows the relationship between Cr and V. Although high Cr concentrations are generally associated with high V concentrations, the linearity of sample points is quite poor compared to the Fe-V, Mn-V and Ti-V plots. This poor

linearity in Figure 32 (q) suggests that although both Cr and V are enriched in less evolved portions of the granite, the two elements are not substituting for each other in the Bloedkoppie granite. In the Bloedkoppie granite, average Cr concentrations nearly two times lower than V concentrations.

Figure 32 (r) shows high concentrations of Mg associated with high V concentrations. Figure 32 (s) also shows Ca and V nearly relating to each other in the same manner as Mg and V. The fact that high Ca values are associated with high V values can also be explained in terms of fractionation, just like in the case of Mg vs. V. However, the degree of linearity is much stronger between Mg and V than it is between Ca and V. Since most of the Ca is contained within plagioclase feldspar, a poor linearity between Ca and V may suggest that most of the V resides outside plagioclase feldspar and that the positive looking correlation between the two elements is simply a coincidence, having to do with the fact that both elements are depleted with progressive fractionation of a granitic magma. In an average granite, both Mg and Fe occur mainly in biotite and this could be the reason why the two elements tend to have a similar relationship with U. Where amphiboles are present, the two elements also occur together.

Figure 32 (t) shows that the K concentration is roughly constant across the entire Bloedkoppie granite, averaging about 3.3%.

The K/Ca ratio is about 6, again indicating the enrichment of K relative to Ca during magma evolution. This all points to the Bloedkoppie granite being a highly

evolved granite and hence potentially a good source of uranium as high uranium tends to be associated with high potassium from a general point of view.

The proportion of U-bearing accessory minerals (e.g. zircon & monazite), formed during the cooling of the Bloedkoppie magma is quite low. As mentioned earlier, a granite with a high concentration of uranium bearing accessory minerals like zircon, monazite and allanite will have a lot of uranium locked up in these minerals and during erosion, such uranium will not be liberated. The Bloedkoppie granite has low Zr, Ce and La concentrations, which further makes it a good source of uranium upon erosion. It was found to be a good source not only with respect to uranium but also vanadium. The water which eroded the Bloedkoppie granite was probably very corrosive and was able to mobilize both U^{6+} and V^{4+} into the groundwater. The same water also mobilized V^{4+} from the schist.

6.1.2 Tinkas schist

The data in Table 12 was collected by the writer. The Tinkas schist was sampled during the project because of its suspected high concentration of V, which might have been leached to contribute to the formation of the Langer Heinrich carnotite deposit downstream. Part of the reason for sampling this schist was also to study the degree of alteration both in hand specimen and in thin section.

Table 12: Geochemical data of the Tinkas Schist, around Langer Heinrich.

Sample No.	U (ppm)	V (ppm)	Ca(%)	K(%)	Mg(%)	Ti (%)	Mn (ppm)	S(%)	Zn (ppm)	Fe(%)	Cu (ppm)	Rb (ppm)
Tink1	3.3	134	9.74	2.12	2.2	0.416	966	0.02	101	5.05	37.3	101.5
Tink2	3.1	164	3.74	2.02	2.51	0.454	713	0.03	120	6.14	106.5	41.4
Tink3	3	124	10.65	1.76	2.41	0.4	745	0.05	106	5.41	43.4	91.4
Tink4	2.4	92	16	0.66	1.35	0.366	1700	0.04	93	3.06	8	38.3
Tink5	3.6	151	1.75	4.87	2.39	0.448	478	0.02	111	5.17	24.4	217
Tink6	6.5	164	6.08	2.51	2.15	0.447	788	0.03	133	5.89	79.2	91.6
Tink7	4.2	145	4.55	1.73	2.34	0.458	702	0.08	109	5.24	61	83.4
Average	3.73	139	7.5	2.24	2.2	0.416	870	0.04	110.4	5.14	51.4	95

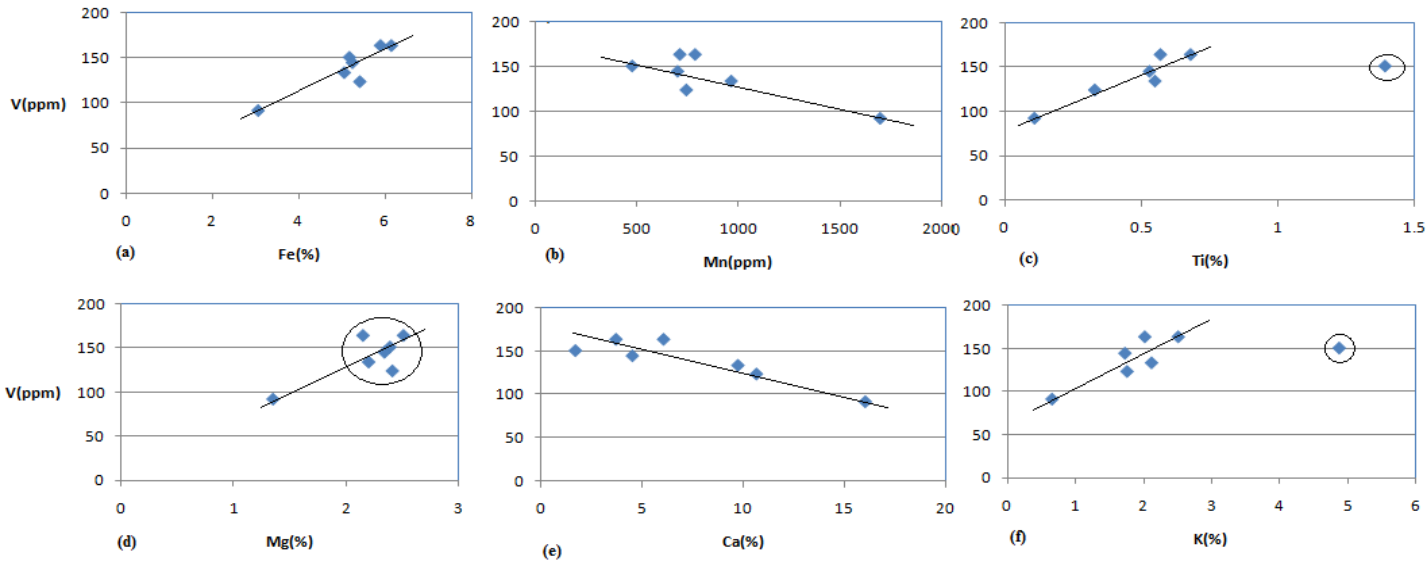

Fig. 33 (a) - (d): Correlation diagrams for the Tinkas Schist, showing the relationship between several elements and V.

Figures 33 (a) and 33 (c) show a strong positive correlation between V and the two elements Fe and Ti. This suggests that in the Tinkas schist, V occupies more or less the same sites in as Fe and Ti in the crystal lattices. However, contrary to the trend observed in the Bloedkoppie granite, Mn and V show a mild negative correlation. The average Mn concentration in the Tinkas schist is about 800 ppm, whilst the Bloedkoppie granite contains only about half of that. Looking at the V/Mn data pattern, there seems to be a possibility that during metamorphism of these pelitic sediments, Mn beats V in their competition to substitute for Fe in crystal lattices, because the highest V concentrations are associated with the lowest Mn concentrations. The fact that the Mn concentration in the schist is almost 6 times higher than that of V suggests that V is rarer than Mn in sediments.

Mg shows some positive correlation with V, while Ca shows a negative correlation with V according to Figures 33 (d) and 33 (e) respectively. Once again, the positive correlation between Mg and V may be explained by the fact that both elements are associated with Fe in hydrothermal as well as magmatic fluids. However, Ca and V do not behave the same and hence the negative correlation between V and Ca. The strong positive correlation observed in Figure 33 (f) between K and V is most likely a reflection of biotite's influence on V concentration in the schist. A relatively more biotite rich schist will carry more vanadium than others and because most of the K in the schist is contained within the biotite, K and V will show a positive correlation.

The Tinkas Schist has an average of 844 ppm Mn and 110 ppm Zn (Table 12). Upon weathering, these metal concentrations can contribute to a decreased oxidation state of the subsurface water. This in turn can lead to decomplexing of uranyl carbonate ions in the water. Concentrations of 7.5% Ca and 2.2% Mg (Table 12) in the Tinkas schist also suggest that upon weathering of silicates in this schist, the two elements would be in sufficient supply to precipitate calcite or dolomite. These concentrations would be topped up by different detrital material from other lithologies in the catchment area such as Bloedkoppie granite.

The Tinkas schist, which forms most of the bedrock for the Langer Heinrich channel, contains an average of 4 ppm U and 140 ppm V (Table 12). This indicates that there was enough V and U in the Tinkas schist and Bloedkoppie granite respectively, to form what is now seen as the Langer Heinrich U deposit. In fact the Bloedkoppie has about 15 ppm V, which increases the total V budget in the system.

Biotite-rich schist is important in a sense that it carries more vanadium and it also weathers more easily to release the vanadium. Biotite-rich schist forms hollows or ponds by weathering to form depressions in the bedrock. The quartz rich schist is more important as a geomorphological feature because it forms bedrock highs. Due to its resistance to erosion, the quartz-rich schist also causes the channel to meander, resulting in constrictions and the formation of ponds. Over a long period of time, uranium may be concentrated in these ponds and constrictions. Bedrock highs serve to elevate the water

table, causing ponding, which enhances evapo-transpiration and eventually carnotite precipitation.

The Tinkas schist around Langer Heinrich is a suitable catchment area because it contains about 13 times more V than the Bloedkoppie granite. The schist also reports a high concentration of Mg and in fact an XRD analysis of this schist has revealed the presence of magnesio-hornblende.

6.1.3 Abbabis Metamorphic Complex

The Abbabis basement gneiss was sampled primarily so that its V and U could be studied.

Table 13: Geochemical data for the Abbabis basement complex.

Sample No.	U (ppm)	V (ppm)	Ca(%)	K(%)	Mg(%)	Ti (%)	Mn (ppm)	Sr(ppm)	Zr (ppm)	Fe(%)	Cu (ppm)	Rb (ppm)
AB1	4.2	52	1.7	4.25	0.87	0.435	774	183.5	53.1	2.76	5.5	284
AB2	2.4	75	3.64	1.32	0.82	0.569	1080	272	29	1.97	0.8	48.6
AB3	4.1	70	1.84	4.32	0.72	0.407	908	196.5	71.9	3.46	1.4	195
AB4	1.3	4	0.73	5.34	0.1	0.038	131	133	34.1	0.39	3.3	281
AB5	0.7	3	1.43	4.49	0.06	0.025	89	128	38.8	0.32	1.7	230

Five samples of Abbabis gneiss reported an average of 2.5 ppm U and 40.8 ppm V. This U concentration is not anomalous and falls within common crustal levels but the V concentration is quite high (Table 13). The V contained in the Abbabis basement gneisses is likely to reside in both pyroxenes and biotite, i.e. wherever the Fe resides. These gneisses have high amounts of quartz and are unlikely to undergo significant chemical weathering during erosion. The fact that both feldspars and biotite appear quite

fresh in thin section is a reflection of their resistance to weathering. Therefore even if these gneisses were to be located along a palaeo-channel, they wouldn't lead to the formation of a calcrete hosted U deposit.

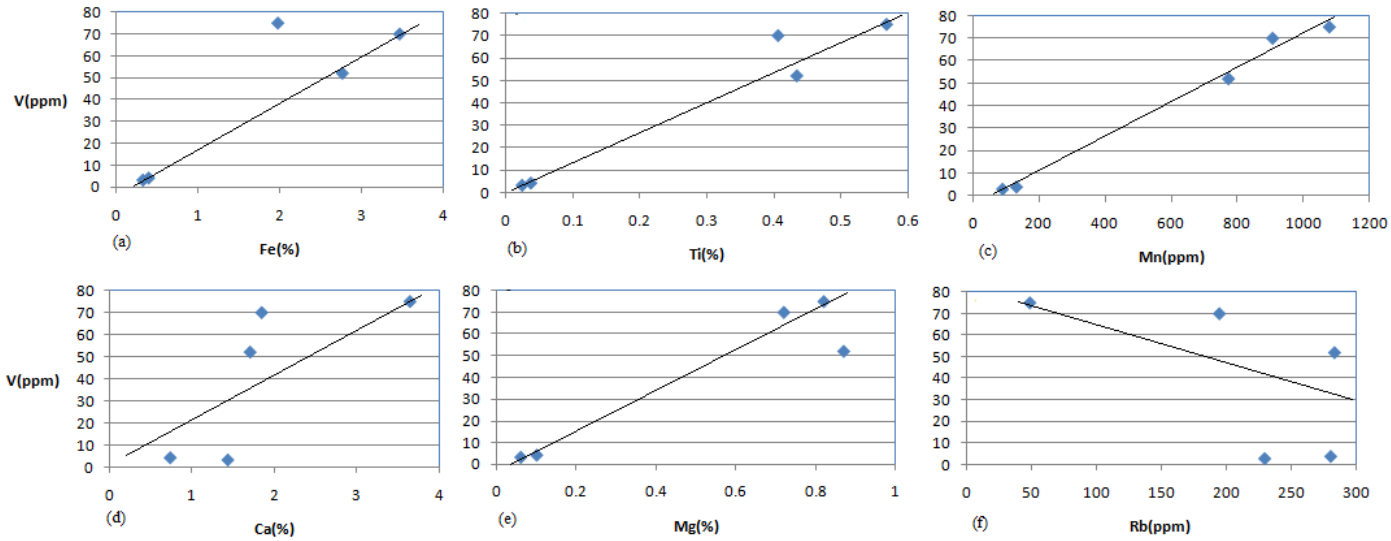

Fig . 34 (a) - (f): Correlation diagrams for the Abbabis Metamorphic Complex, showing the relationship between several elements and V.

In Figure 34, the data relating to the Abbabis Basement complex are presented. The purpose of plotting these diagrams was to examine high concentrations of V detected in the samples from these basement gneisses. Figures 34 (a) to 34 (c) and 34 (f) indicate that V is associated with Fe, Mn, Ti and to a less extent with Mg in these felsic gneisses. V shows a very poor correlation with Ca, the sample points indicate that in general high Ca values tend to be associated with high U. Rb also shows a poor correlation with V, but the sample points indicate that in general high Rb values tend to

be associated with low V. Five samples from the Abbabis basement reported an average of 2.5 ppm U and 40.8 ppm V.

The geochemistry of Etusis was not studied in detail because it is seen to be unimportant as a potential chemical trap. Marlow (1981) has reported uranium enrichment in certain parts of Etusis Formation, related to alaskite intrusions. These mineralized quartzites are located on Wolfkoppe 105, which is far from the Langer Heinrich catchment area. Marlow (1981) also attributed radioactivity in most parts of Etusis quartzite to Th rather than U. Due to the high resistance of quartzite to erosion, there is no way the quartzite could have contributed significant amounts of either uranium or vanadium to the subsurface waters. Therefore Etusis quartzite is only important as a geomorphological feature.

A similar phenomenon, regarding the effect of resistant lithologies, has been observed around the Marenica uranium project. At Marenica, the main uranium resource is found in a discrete channel between two granite domes. This indicates the importance of geomorphological control over uranium mineralization in a sedimentary environment. The other important geomorphological feature is the dolerite. However, the regional distribution of the dolerites is limited as they mainly occur as dykes sub-parallel to the coast line. Although dolerite intrusions can form bedrock highs, their ability to form constrictions and to narrow the channel is limited because they are generally not thick enough to form hills. Granite domes tend to be better as geomorphological features

because they form both bedrock highs as well as constrictions, thereby narrowing the channel.

6.1.4 Mineralized calcretes at Langer Heinrich

Mineralized calcretes were studied not only because they host carnotite mineralization but also due to the fact that they can be reworked and deposited downstream.

Table 14: Geochemistry of the mineralized calcrete at Langer Heinrich.

Sample No.	U (ppm)	Th (ppm)	V (ppm)	Ca(%)	K(%)	Mg(%)	Ba (ppm)	Sr (ppm)	Mn (ppm)	S(%)	Zn (ppm)	Fe(%)	Cu (ppm)	Rb (ppm)
LCalc1	154	3.6	53	10.8	2.03	0.31	240	156.5	130	0.1	21	0.68	7.4	82.1
LCalc2	160	3.7	47	9.6	2.07	0.28	250	163.5	139	0.06	35	0.76	7.9	83.5
LCalc3	2260	3.9	511	12.45	1.87	0.29	240	163.5	221	0.04	16	0.79	8.9	77.5
LCalc4	344	3.5	98	10.3	2.15	0.32	270	163	172	0.03	24	0.88	8.5	92.4
LCalc5	284	3.6	79	10.45	2.21	0.26	260	152.5	117	0.04	32	0.72	7.4	85.3
LCalc6	10100	4.2	2480	15.15	1.7	0.38	170	175	128	0.04	22	0.74	7.6	66.3
Average	2217	3.7	544.7	11.46	2.0	0.31	238.3	162.3	151.2	0.05	25	0.76	7.9	81.2

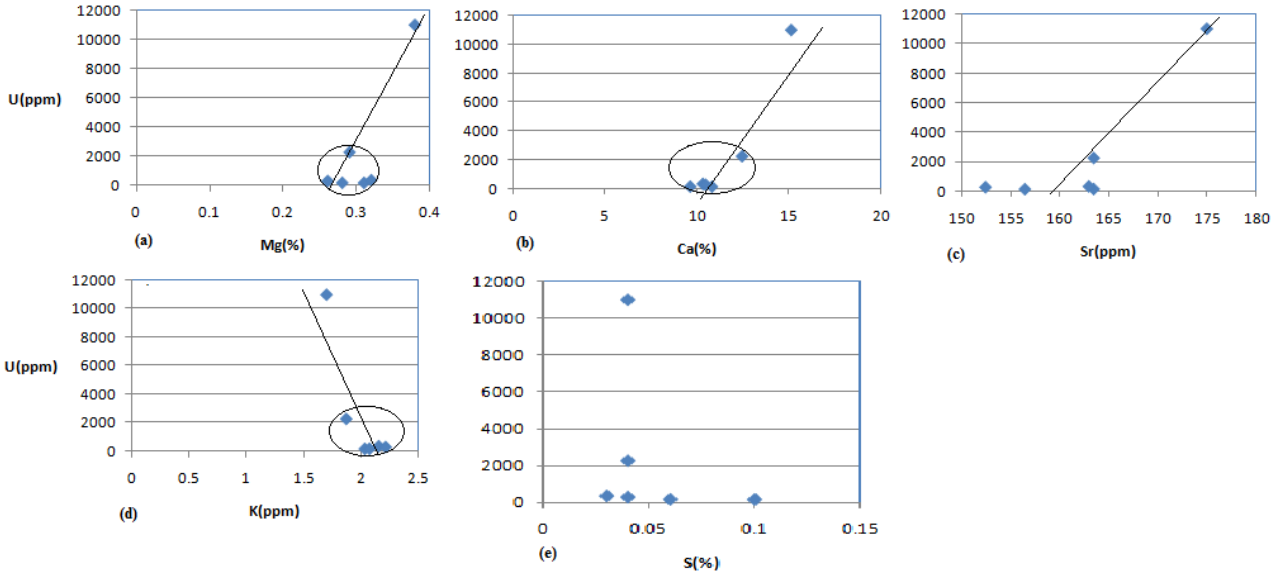

Fig. 35 (a) - (e): Correlation diagrams for mineralized calcretes at Langer Heinrich showing the relationship between several elements and U.

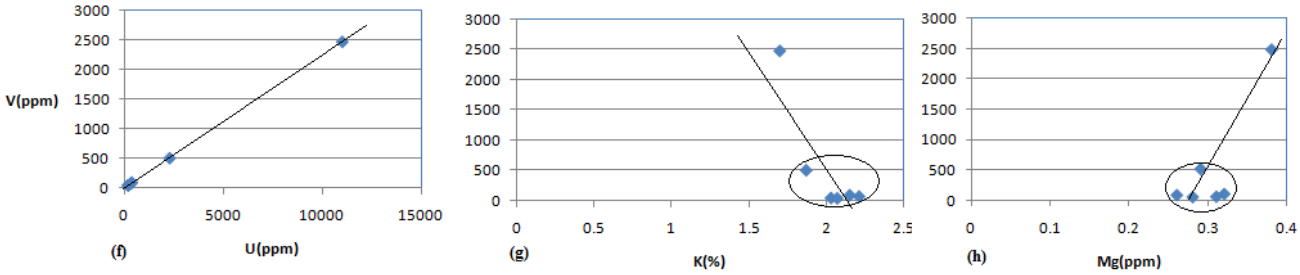

Fig. 35 (f) – (h): Correlation diagrams for mineralized calcretes at Langer Heinrich showing the relationship between several elements and V.

Figures 35 (a) to 35 (c) show the relationship between three elements, Mg, Ca, Sr and U. The three elements appear to show a positive correlation with U in the calcretes, whereby high concentrations for these elements are generally associated with high U concentrations. The correlation coefficient is 0.9, which is very close to unity. An association between uranium and calcium suggests that uranium precipitation in the form of carnotite is syngenetic with calcification. Since calcite is a product of evapo-transpiration, this correlation suggests that mineralization is largely driven by evapo-transpiration. Calcium is a commonly occurring element in the earth crust but a Ca-rich bedrock will speed up carnotite precipitation.

The six samples, from the Langer Heinrich mineralized conglomerates, do show an interesting feature regarding the relationship between Mg and U. The U concentration for four of the samples remains roughly constant despite the variation in Mg concentration. Sample LCALC3 has a U concentration of 2260 ppm. Another sample (LCALC6) has a U concentration in excess of 10 000 ppm or 1%. This reflects a very high content of carnotite in the two samples. The fact that high Mg is associated with high U suggests that Mg plays a role in facilitating carnotite precipitation. Since U in the groundwater is carried as a carbonate complex, Mg will attack this complex to scavenge the CO_3^{2-} ion and form $MgCO_3$. In this way, U is liberated and concentrated over time. This saturation of U, if accompanied by the saturation of K and V, will result in the precipitation of carnotite. This positive correlation between Mg and U indicates that an addition of Mg to the groundwater, would aid carnotite precipitation.

The same can be said about Sr, the only difference being the fact that Sr naturally occurs as a trace element in the crust and its influence on U precipitation is likely to be limited.

Figure 35 (d) shows a negative correlation between K and U in the calcrete. Since both elements make up carnotite, the relationship between the two elements was supposed to be positive. A more comprehensive sampling program may lead to such a finding. A negative correlation between K and U may suggest that there is a lot of K residing outside carnotite, probably in detrital fragments.

Figure 35 (e) shows the relationship between S and U. This relationship is not clear. In fact there may be a slight negative correlation between the two elements, whereby high uranium content is associated with low sulfur content. This suggests too much SO_4^{2-} and/or H_2S introduced by marine fogs or pyrite in bedrock could inhibit carnotite precipitation in the groundwater as it leads to a drop in pH.

Figure 35 (f) shows the relationship between U and V in the mineralized calcretes. The sample points show a strong positive correlation where linearity is almost 100%. This suggests that in the calcrete, U and V are contained purely within the same minerals, probably carnotite or tyuyamunite. Mg and K show a similar relationship with V as with U (Fig. 35 (g) and 35 (h)).

The assays in Table 14 show sufficient concentrations of Ca, Ba and Sr. However, the assays show very low concentrations of Mg, suggesting that most of the

carbonates exist in the form of calcite rather than dolomite. The average ratio of U:V in these samples is 4.07:1, which is roughly the same as the 4.7:1 U:V ratio in carnotite. This ratio suggests that most of the U and V in the conglomerates are held in carnotite and only negligible amounts are still in detrital material.

6.2 Klein Trekkopje catchment area

This catchment area has a wide variety of rocks but the ones which were sampled during this project, for the purpose of geochemical investigations, include Kuiseb schist, Klein Spitzkoppe granite and Gross Spitzkoppe granite, Karoo dolerite and the mineralized calcretes.

6.2.1 Klein Spitzkoppe granite

Geochemical analyses for various samples have been used, 6 collected as part of this project and 18 from Kandara (1998). These data are presented in Tables 15 and 16, respectively.

Table 15: Geochemistry for Klein Spitzkoppe granite.

Sample ID.	U (ppm)	V (ppm)	Th (ppm)	Zr (ppm)	Ti (%)	Fe (%)	K (%)	Na (%)	Ca (%)	Mg (ppm)
SP1	11.3	1	21.8	53.1	0.005	0.57	2.89	3.09	0.2	90
SP2	10.7	1	20.6	51.2	0.004	0.55	2.87	2.92	0.19	90
SP3	11.6	1	61.7	73.4	0.021	0.95	3.23	2.57	0.46	90
SP4	9.3	5	56.6	85.8	0.02	1.09	3.34	2.55	0.44	100
SP5	7.2	1	50.3	64.4	0.022	1.22	3.46	2.63	0.47	100
SP6	7.8	4	64.9	98.4	0.02	0.91	3.27	2.72	0.48	100
Average	9.6	2.2	46	71.1	0.02	0.88	3.2	2.75	0.37	95

Table 16: Geochemistry for Klein Spitzkoppe granite (after Kandara, 1998).

Sample ID.	U (ppm)	V (ppm)	Th(ppm)	Zr (ppm)	SiO_2 (%)	K_2O (%)	CaO (%)	MgO (%)	Ce(ppm)	La(ppm)	TiO_2(%)
JK03	7.2	<2	42.0	198.0	77.80	4.17	0.32	<0.01	64.80	22.80	0.02
JK54				25.0	73.45	3.40	0.05	0.09			0.01
JK58	9.4	<2	26.0	147.0	76.60	4.47	0.43	<0.01	56.20	21.10	0.01
JK100	19.6	<2	49.0	175.0	77.00	4.47	0.28	<0.01	80.40	32.80	0.05
JK103C				2.0	75.50	3.00	0.40	0.09			0.01
JK107	8.4	<2	54.0	166.0	76.30	4.40	0.55	<0.01	52.30	20.40	0.02
JK105	9.2	4.0	54.0	175.0	75.80	5.11	0.63	<0.01	88.60	35.30	0.08
JK66R	4.6	9.0	42.0	172.0	76.90	4.57	0.31	<0.01	74.30	25.80	0.00
JK94	6.9	<2	55.0	179.0	77.80	3.84	0.54	<0.01	101.00	38.80	0.02
JK106B	9.0	<2	58.0	195.0	75.50	5.03	0.74	<0.01	95.80	42.90	0.06
JK108	10.0	<2	55.0	230.0	76.30	4.59	0.75	<0.01	101.00	44.60	0.05
JK09A	12.4	<2	35.0	154.0	77.10	4.11	0.25	0.01	11.3	0.47	0.02
JK53	5.9	<2	27.0	138.0	77.10	3.97	0.20	<0.01	64.10	19.40	0.01
JK87	9.4	<2	60.0	234.0	74.60	5.12	0.77	<0.01	104.00	46.70	0.06
JK110A	9.1	<2	77.0	381.0	75.50	5.66	0.55	<0.01	182.00	93.10	0.10
JK110B	63.4	13.0	73.0	203.0	75.20	5.93	1.74	<0.01	49.90	23.80	0.02
JK44B	5.1	7.0	63.0	188.0	76.20	4.30	1.54	<0.01	107.00	45.80	0.02
JKBD				540.0	42.00	2.75	7.00	3.00			2.05
Average	12.6		51.3	194.5	74.2	4.38	0.95				

Tables 15 and 16 show that the Klein Spitzkoppe granite is highly siliceous and highly potassic. In the granite, the Mg concentration is extremely low. The XRD tests have further confirmed the thin section studies, which showed that the dominant feldspars in the Bloedkoppie and Klein Spitzkoppe granites are microcline and albite.

ICP-MS and ICP-AES results have shown that the more oxidized samples of the Klein Spitzkoppe granite have lower uranium concentrations. This is a further indication that meteoric water has washed uranium and possibly vanadium out of the granite into the channels. Using results from six samples taken by the writer and 15 samples taken by Kandara (1998), the granite reported an average of 12 ppm uranium and 2.5 ppm vanadium.

Figure 36 was plotted using a combination of data from Kandara (1998) and the writer. In this Figure, the blue dots represent the samples collected by Kandara (1998) and the red dots represent those samples collected by the writer.

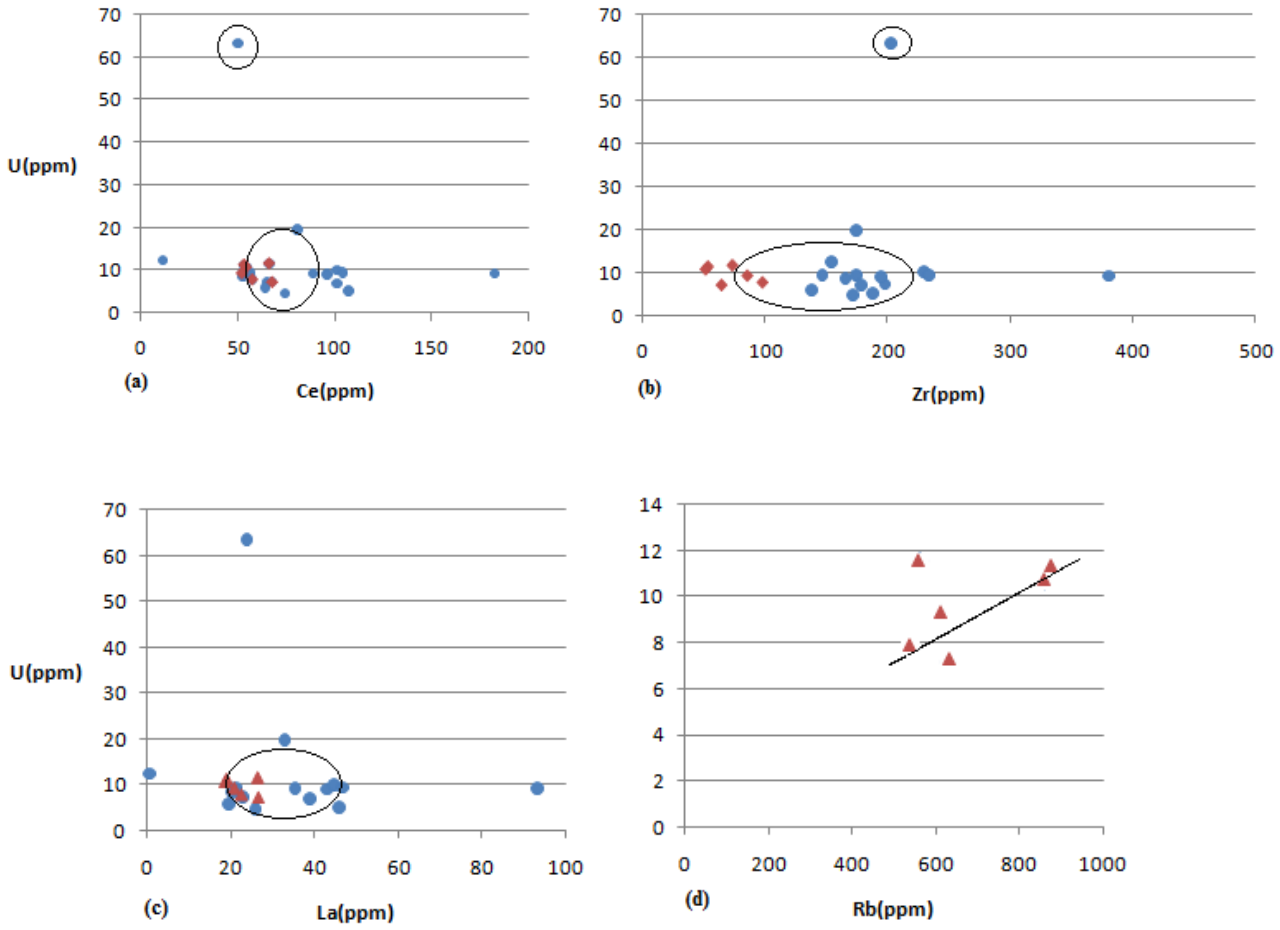

Fig . 36 (a) - (d): Correlation diagrams for the Klein Spitzkoppe granite showing the relationship between several elements and U.

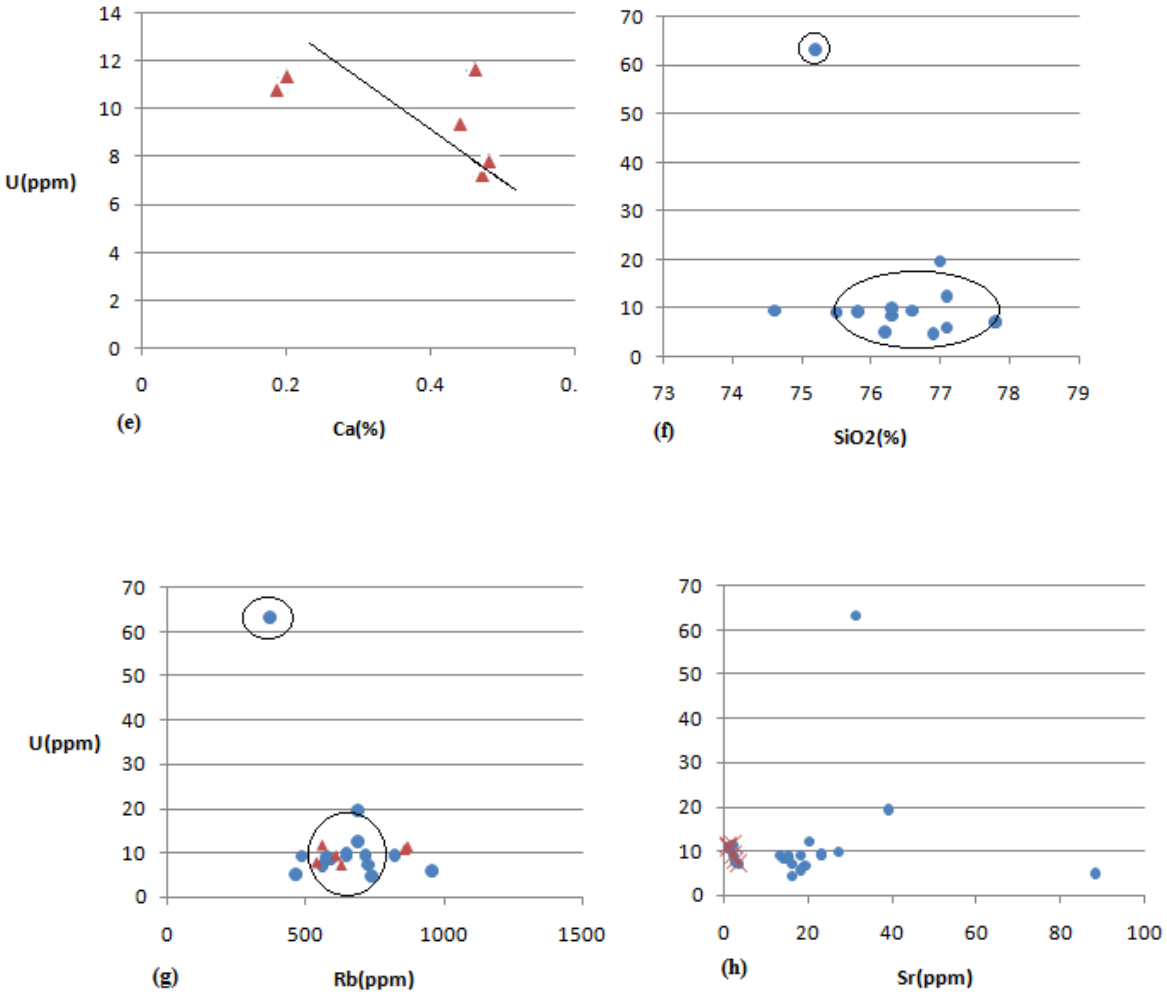

Fig. 36 (e) – (h): Correlation diagrams for the Klein Spitzkoppe granite showing the relationship between several elements and U.

Figures 36 (a) to 36 (c) show how Zr, Ce and La relate to U in this granite. These Figures indicate that concentrations for the three elements remain roughly constant throughout the granite and that there is no correlation between them and U. This indicates that most of the uranium in this granite is not locked up in refractory accessory minerals such as zircon, monazite or allanite. In Figure 36, the outlying sample point

with 63.4 ppm U was taken from a massive biotite pocket also called biotite schlieren in literature. This sample also shows a relatively elevated concentration of V (13 ppm). The sample with the highest Ce concentration is JK110A in Table 18 and the one with highest U concentration is JK110B. The relationship between Zr and U appears more or less similar to the one between Ce and U except that Zr shows wider scatter, ranging from 50 ppm to 250 ppm.

The relationship between Rb and U in Figure 36 (d) appears to show some degree of positive correlation, again suggesting progressive enrichment of U during fractionation of a granitic magma which does not have plenty of biotite.

Figure 36 (e) shows a very poor correlation between Ca and U although in general, high Ca values are associated with low U values. As with the Bloedkoppie granite, this trend reflects the fact that in a granitic magma, Ca gets depleted while U gets enriched with fractionation. Silica content appears to remain roughly constant, ranging mainly between 76% and 77%, according to Figure 36 (f). However, the sample with highest U value shows a relatively lower silica content, compared to the cluster centre. This trend can again be attributed to fractionation as silica is progressively enriched with fractionation while U is fixed by the crystallization of earlier phases such as biotite and some accessory minerals.

Figure 36 (d) (Rb-U plot) shows a combination of sample points from the writer and from Kandara (1998). The relationship is closely similar to the one between K_2O and U, which is not shown in the diagram above. This means in a granitic magma U may

get depleted with progressive fractionation. This trend is due to the fact that biotite, which is one of the early phases to crystallize in a granitic magma, captures a lot of U through adsorption. With further fractionation, biotite becomes less which results in less U. The poor correlation observed in Figure 36 (g) suggests that the mild positive correlation between Rb and U observed in Figure 36 (d) is localized and does not really apply to the entire Klein Spitzkoppe granite.

The Sr-U plot (Fig. 36 (h)) shows a mild positive correlation between the two elements again supporting the idea U is getting depleted with progressive fractionation in a granitic magma due to the decreasing concentration of biotite. The roughly constant uranium concentration suggests that on average uranium is homogeneously disseminated throughout the granite. This makes it a potentially good source of uranium during erosion.

6.2.2 Gross Spitzkoppe granite

The geochemistry of the Gross Spitzkoppe granite has been thoroughly studied by Frindt et al. (2004a) and most of his data was used by the writer in this study. Therefore, on the Gross Spitzkoppe Granite, the writer only collected few samples. On the following plots for the Gross Spitzkoppe granite, the red dots represent data collected by the writer (2010) and the blue dots represent data from Frindt (2004a).

Table 17: Geochemical data for the Gross Spitzkoppe granite.

Sample ID.	U (ppm)	V (ppm)	Th (ppm)	Zr (ppm)	Ti (%)	Fe (%)	K (%)	Ca (%)	Mg (ppm)
Gross1	16.9	3	94.3	137	0.073	1.48	4.04	0.67	0.03
Gross2	15.2	3	86.7	128.5	0.068	1.57	3.54	0.68	0.03
Gross3	11.4	9	92.3	81.4	0.108	1.96	4.45	0.11	0.1
Average	14.5	5	91.1	115.6	0.083	1.67	4.01	0.49	0.05

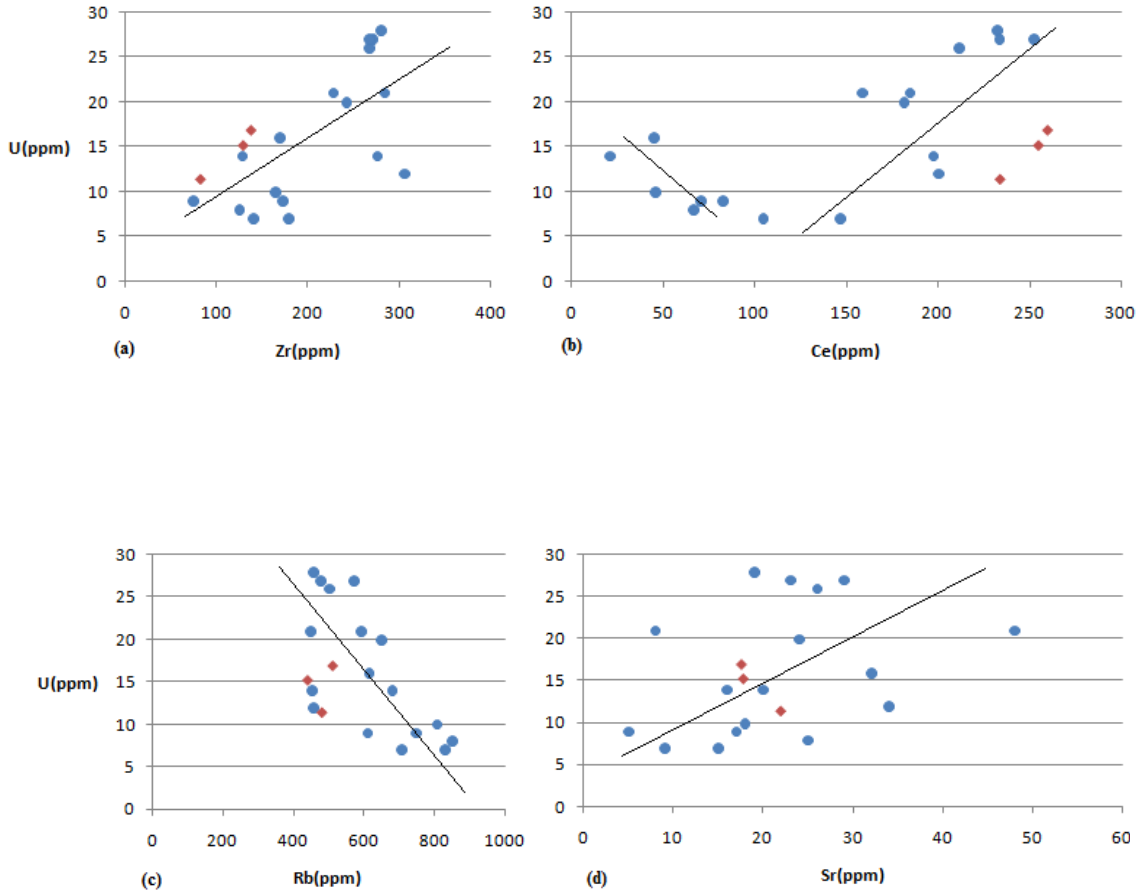

Fig. 37 (a) – (d): Correlation diagrams for the Gross Spitzkoppe granite showing the relationship between several elements with U.

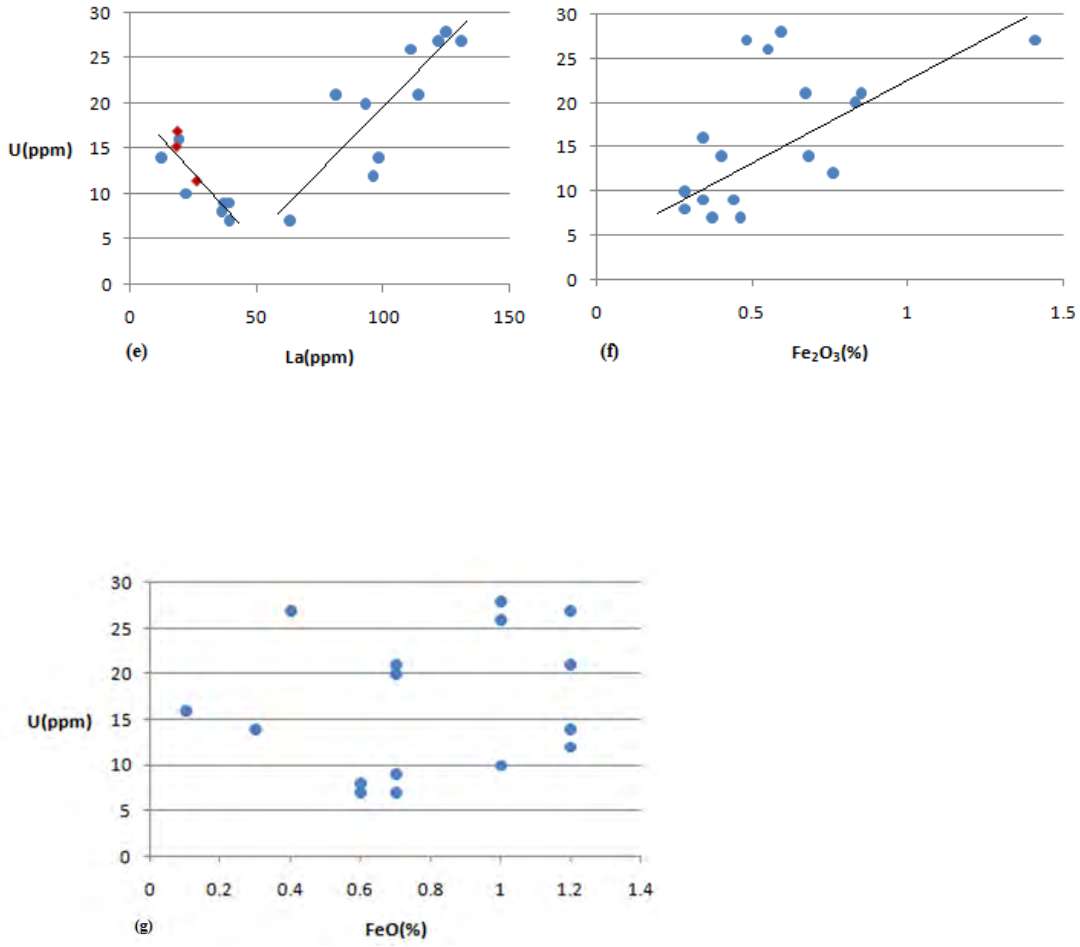

Fig. 37 (e) – (g): Correlation diagrams for the Gross Spitzkoppe granite showing the relationship between several elements with U.

Figure 37 (a) shows the relationship between Zr and U. Unlike in the case of Bloedkoppie and Klein Spitzkoppe granites, there is a very strong positive correlation between Zr and U in the Gross Spitzkoppe granite. This suggests that in the Gross Spitzkoppe granite, there could be a substantial amount of U locked up in zircons. On average Gross Spitzkoppe granite has a higher concentration of Ce and Zr than Klein Spitzkoppe granite. This means although the Gross Spitzkoppe granite has a higher absolute content of U, its amount of leachable U is lower than that of Klein Spitzkoppe or Bloedkoppie granite. According to Frindt (2004a), the zircon grains in the Gross Spitzkoppe granite have uranium concentrations in the order of thousands of ppm. He observed the same feature in the allanite grains, which have been totally blackened by radiation.

Figure 37 (b) shows an interesting relationship between Ce and U. When the Ce concentration is below 100 ppm, there is a negative correlation between Ce and U. However, when Ce concentrations are above 100 ppm, the two elements correlate positively. The same trend can be observed in Figure 37 (e) because the chemical behaviour of La is closely similar to that of Ce. The only difference is that the critical point on the La-U plot is 50 ppm and not 100 ppm. From Frindt (2004a), the samples which show a negative correlation in Figure 37 (b) are mainly the ones from aplite dykes and the porphyritic granite. Those samples which show a positive correlation in Figure 37 (b) are the ones which have undergone a limited degree of fractionation. They have relatively more biotite and more accessory minerals like monazite. The samples which

show a negative correlation are SF-101, SF-058, SF-141, SF-057, SF-071 and SF-083 (Frindt et al. 2004a). Since the majority of the samples in Figures 37 (b) and 37 (e) show a strong positive correlation, this is again an indication that there could be a significant amount of U trapped in monazite.

The Rb-U plot in Figure 37 (c) shows a negative correlation, while the Sr-U plot in 37 (d) shows a positive correlation. This is an indication that the early forming crystals such as biotite are depleting U in the melt and hence the drop in U concentration with fractionation. This trend was also observed in the Klein Spitzkoppe granite although it is much clearer in the Gross Spitzkoppe granite.

Figure 37 (g) shows the relationship between Fe^{2+} and uranium in the Gross Spitzkoppe granite. The samples are distributed randomly across the whole plot, suggesting that there is no correlation between the two elements. This shows once again that during differentiation of a reduced magma, U does not partition in the early forming crystals where Fe^{2+} is absorbed. These are minerals like amphiboles and the very early biotite.

Figure 37 (f) above shows some degree of positive correlation between Fe^{3+} and U. This confirms conclusions from laboratory experiments discussed earlier, which show that U tends to adsorb onto the surfaces of oxidized biotite much more than it does onto fresh biotite in a reducing environment. While the Gross Spitzkoppe granite contains less than 20 ppm U on average, values of up to 28 ppm U have been reported in places where massive biotite is found. The massive biotite is locally referred to as biotite schlieren

(Frindt et al., 2004a). The absence of any correlation between Fe^{2+} and U, and the positive correlation between Fe^{3+} and U in the Gross Spitzkoppe granite is an indication that U tends to associate with more evolved or oxidized biotite.

There is a positive correlation between Ti and U although the plot is not shown above. However in samples which have a relatively high concentration of Ti, there is virtually no correlation between the two elements. This suggests that the early formed crystals of biotite do not carry much uranium. It is notable that the Ti content for Klein Spitzkoppe granite is almost 30 times lower than that of the Gross Spitzkoppe granite. This demonstrates further that the Klein Spitzkoppe granite is more evolved than Gross Spitzkoppe granite.

Damara aged leucogranites in this area contain 60 – 110 ppm vanadium and 5 - 20 ppm uranium (appendix 4). These granites have therefore contributed both U and V to the subsurface water in the area. Erongo Energy Ltd, an Australian company which has been exploring for uranium since 2007 within the Erongo Complex has obtained average values of 2 ppm V from more than 100 samples. They obtained average values of between 15 – 20 ppm U, even though individual values of up to 100 ppm were found. On average, the Erongo granite Complex appears to have higher uranium grades and slightly lower vanadium grades than the Klein Spitzkoppe and Gross Spitzkoppe granites. This could be an indication that the degree of partial melting was higher around Erongo Granite compared to the two Spitzkoppe granites. The U/Pb ages for the Spitzkoppe granites and Erongo Complex are given as 125 Ma and 130 Ma respectively (Frindt, et

al., 2004a). The rare earth element patterns for the two granite suites, (i.e. Erongo and Spitzkoppe) suggest they have been derived from the same source.

During this project, dolerite intrusions were also studied. The purpose of studying the dolerite was first to assess its V concentration and, secondly, to check its degree of weathering in order to judge if it could have contributed V to the subsurface waters. Two schools of thought seem to exist regarding the dolerite's potential to contribute V to the subsurface water. While the majority of the researchers are of the view that the dolerite cannot contribute significant amounts of V to subsurface water (e.g. Hambleton – Jones (1976)), there are those who believe that weathering in the dolerite is intense enough to have caused the release of significant amounts of V (e.g. Bowell et al. (2010)). Hambleton-Jones (1976) believes that even if the dolerite were to weather deeply, it wouldn't release significant amounts of V because the V sits mainly in resistant accessory minerals such as magnetite.

The mineralogy and geochemistry of the Kuiseb schist is closely similar to that of the Tinkas schist which was discussed earlier. Therefore there is no need to re-open the discussion for this schist. Its uranium and vanadium concentrations are closely similar to those observed in the Tinkas schist. Because of these similarities, the Kuiseb schist will behave like the Tinkas schist during sedimentation. The only difference is that the Tinkas schist forms most of the bedrock at Langer Heinrich, while the Kuiseb schist forms less than half of the bedrock, where mineralization is found. The Kuiseb schist has a magnesium concentration about half that of the Tinkas schist (Table 18). It also has a

strontium concentration of about 70 ppm, while Tinkas contains about 900 ppm. Since magnesium and strontium have an affinity to the carbonate ion in the groundwater, they will contribute to the precipitation of carnotite.

Table 20 shows a comparison between Kuiseb and Tinkas schist, in terms of key elements, which contribute to the precipitation of carnotite:

Table 18: Comparison between Kuiseb and Tinkas schists.

Element	**Kuiseb schist**	**Tinkas schist**
Ca (%)	0.7	8
Mg (%)	1	2.3
Sr (ppm)	70	900
U (ppm)	3	4
V (ppm)	140	140
K (%)	1.3	2.5

Five samples from the Kuiseb Schist and six samples from the Tinkas Schist were analyzed (as shown in Appendix 3) and their averages used in Table 18 above. Comparing the two metapelitic sediments, it is clear that the Tinkas schist has far more calcium, magnesium, strontium and potassium than the Kuiseb schist. This makes the Tinkas schist a much more favourable bedrock in terms of the ability to precipitate carnotite. The process of carnotite precipitation is however driven by vanadium for the most part. Some elements contributing to the salinity of subsurface water could actually be sourced from bedrock through supergene leaching. However, in nature marine fogs tend to speed up this process of reaching the required levels of salinity more easily than bedrock.

6.2.3 Mineralized calcrete at Klein Trekkopje

The calcretes at Klein Trekkopje are closely similar to those at Langer Heinrich in physical appearance except that the former have gypcrete layers.

Table 19: XRF data for mineralized calcrete from Borehole KTK11, Klein Trekkopje (after Chetty et al., 1999).

Depth	SiO2(%)	TiO2(%)	Al2O3(%)	FeO(%)	MnO(%)	MgO(%)	CaO(%)	Na2O(%)	K2O(%)	Sr(%)	SO4(%)	CO3(%)	Cl(%)	V(ppm)	U(ppm)
0-1m	38	0.11	5.08	0.87	0.02	0.68	17.3	1.1	2.56	0.3	22.8	7.1	0.15	29	22
1-2m	46.8	0.08	5.96	0.69	0.01	0.72	15	1.28	2.77	0.22	14.1	6.8	0.18	46	20
2-3m	56.4	0.13	6.56	0.86	0.02	1.15	13.3	1.12	3.35	0.35	0.5	16.9	0.2	44	40
3-4m	60.2	0.11	7.54	0.86	0.02	0.98	11.6	1.19	3.8	0.16	0.5	11.8	0.12	40	35
4-5m	59.1	0.13	7.03	1.57	0.02	0.97	12.3	1.2	4.07	0.06	0.5	12.9	0.18	37	42
5-6m	54.8	0.11	6.69	1.52	0.02	1	15.5	1.05	3.36	0.22	0.5		0.15	57	111
6-7m	57.7	0.11	6.63	1.4	0.02	0.95	14.1	0.96	3.58	0.05	0.5	14	0.12	53	98
7-8m	56.6	0.14	6.74	1.42	0.02	1.02	13.2	1.16	3.54	0.13	0.5	15.2	0.13	43	60
8-9m	48.6	0.1	6.67	1.48	0.02	1.04	19.2	1.04	2.95	0.32	0.5	19.8	0.09	54	97
9-10m	51.6	0.1	6.73	1.2	0.02	0.83	17.1	1.05	3.23	0.36	0.5	18.8	518ppm	40	75
10-11m	46.7	0.1	5.53	0.69	0.02	0.86	19.9	0.8	2.41	0.41	0.5	21.7	426ppm	34	50
11-12m	32.9	0.1	3.87	0.76	0.02	0.85	12.3	0.82	2.25	0.1	0.5	20.2	350ppm	28	26
12-13m	48.2	0.12	5.99	0.68	0.02	0.48	18.7	0.84	2.3	0.03	0.5	21.4	115ppm	23	4
13-14m	39.1	0.13	5.14	0.95	0.03	0.46	15.4	0.98	2.5	0.03	0.5	20.8	78ppm	30	9
14-15m	48.7	0.12	6.58	1.09	0.03	0.49	17.6	1.11	3.3	0.03	0.5	19.6	143ppm	38	4
15-16m	46.5	0.25	8.08	2.25	0.03	0.97	17.3	0.99	0.11	0.02	0.5	19.1	54ppm	73	23

Table 20: XRF data of mineralized calcretes from Borehole TKP5, Klein Trekkopje (after Chetty et al., 1999).

Depth	SiO2(%)	TiO2(%)	Al2O3(%)	FeO(%)	MnO(%)	MgO(%)	CaO(%)	Na2O(%)	K2O(%)	Sr(%)	Cl(%)	SO4(%)	CO3(%)	U(ppm)	V(ppm)	LOI(%)
0-1m	56.5	0.14	7.11	0.76	0.03	0.46	15.2	1.16	3.87	0.07	0.07	1.2	16.8	4	18	13.5
1-2m	64.9	0.17	7.42	1.07	0.03	0.62	13.4	1.25	4.19	0.05	0.07	1.2	13.5	4	31	11.9
2-3m	63	0.2	7.09	0.91	0.02	0.71	15	0.96	3.86	0.04	0.1	1.3	15.3	6	40	14
3-4m	54.8	0.17	5.76	0.91	0.03	0.71	19.7	0.81	3.19	0.22	0.15	1.4	20.8	4	49	17.7
4-5m	58.4	0.18	6.54	1.12	0.03	0.77	17.1	0.93	3.49	0.33	0.1	1.5	17.2	4	73	14.9
5-6m	68.7	0.16	7.58	0.99	0.02	0.59	11.6	1.06	4.1	0.08	0.1	3.1	10	4	72	10.5
6-7m	63.6	0.02	7.84	0.71	0.02	0.54	13.7	1.2	4.43	0.05	0.1	4.6	12.4	4	47	12.5
7-8m	53.5	0.14	5.86	0.78	0.04	0.56	22.7	1.09	4.27	0.04	0.1	5.4	15.9	4	53	15.8
8-9m	46.7	0.13	6.99	0.66	0.02	0.59	18.5	0.94	3.17	0.04	0.11	6.1	18.8	11	49	17.9
9-10m	54.3	0.15	6.71	0.8	0.03	0.67	20.4	1.09	3.31	0.03	0.09	4	18.9	10	48	16.5
10-11m	48.6	0.13	6.73	1	0.03	0.7	14.6	1.19	3.56	0.06	0.16	9.1	14	201	92	16.7

11-12m	47.8	0.13	6.53	0.84	0.03	0.81	15	1.16	3.32	0.06	0.13	7.7	14.5	331	117	17.2
12-13m	45.3	0.11	6.41	0.8	0.03	0.81	17.6	1.02	3.23	0.04	0.13	4.5	18	239	93	17.7
13-14m	51.1	0.12	7.03	0.88	0.03	0.8	15	1.11	3.6	0.02	0.11	3.2	18.1	168	79	15.3
14-15m	53.4	0.17	7.39	1.12	0.03	1.03	13.5	1.09	3.59	0.02	0.15	1.7	16.7	81	70	14.9
15-16m	35.2	0.13	4.74	0.94	0.04	1.04	25.5	0.68	2.18	0.02	0.17	2.3	29.1	183	78	24.1
16-17m	51.5	0.15	7.22	1.06	0.03	0.98	15.3	1.04	3.4	0.03	0.12	0.9	17.9	48	56	15.5
17-18m	59	0.13	8.17	0.95	0.02	0.95	9.52	1.17	4.26	0.02	0.15	0.8	10.7	19	42	11.7
18-19m	57.9	0.16	7.92	1.14	0.03	1.06	10.1	1.26	4.01	0.02	0.13	0.7	13.8	16	51	12.4

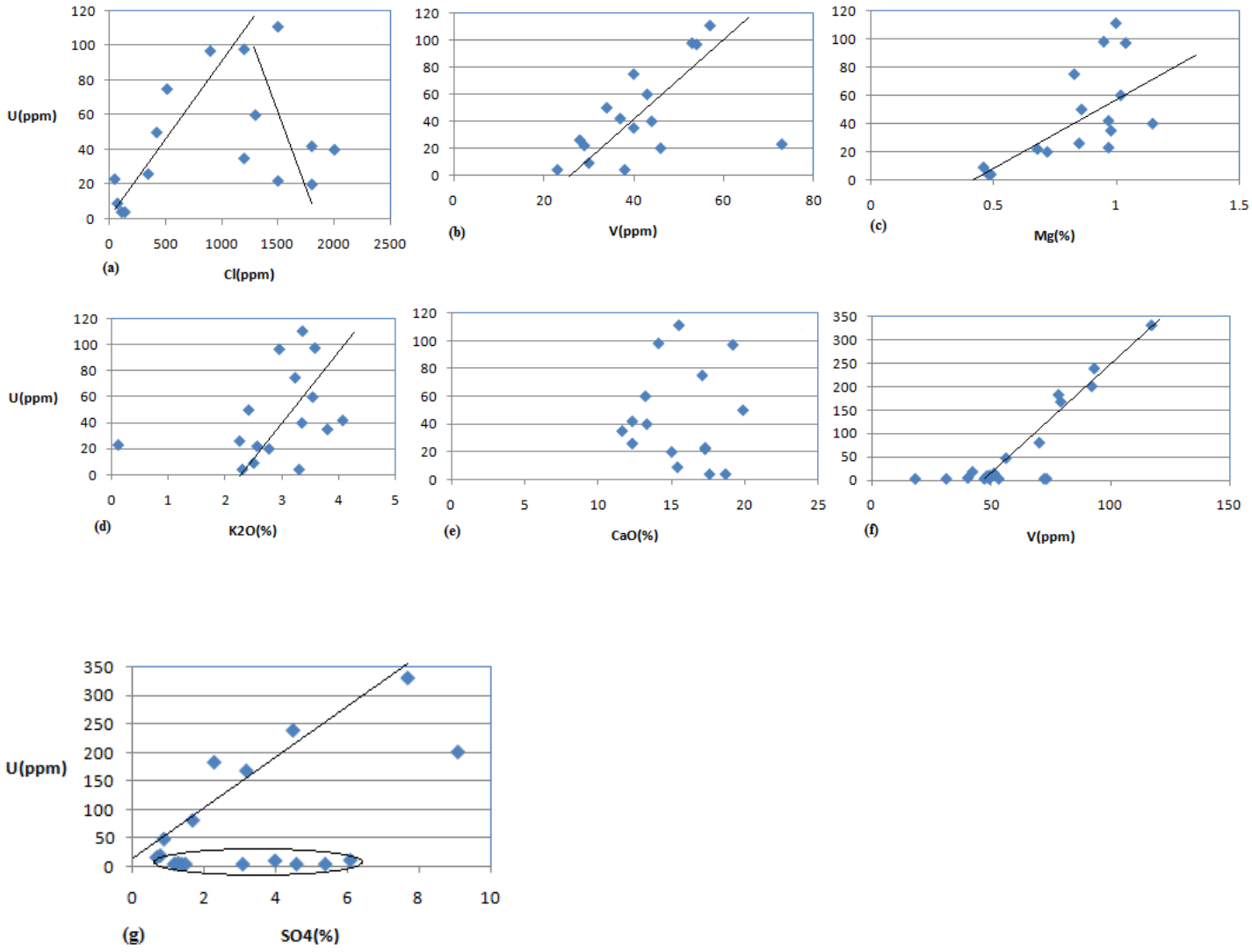

Fig . 38 (a) – (g): Correlation diagrams for mineralized calcretes at Klein Trekkopje, showing the relationship between several elements and U.

Figure 38 (a) shows the relationship between Cl and U. The Cl-U plot for the Klein Trekkopje ore body shows a very interesting feature. It indicates that for Cl concentrations between 0 and 1300 ppm chloride ion, the conditions are conducive to carnotite precipitation. However, above 1300 ppm Cl, carnotite precipitation starts to drop and becomes progressively inhibited as the concentration for the chloride ion

continues to increase. Figure 38 (a) somehow demonstrates the little effect of marine fogs on the groundwater conditions with respect to its ability to precipitate carnotite.

Chetty et al. (1999) analyzed data from two boreholes (KTK11 and TKP5) at Klein Trekkopje. From this data, it is evident that evapo-transpiration is an important factor in the process of carnotite precipitation because the highest U concentrations are found within shallow depths. It is also clear from the two boreholes that mineralization is associated with the palaeo-water table. This supports the view that salinity is most favourable for the precipitation of carnotite close to the water table.

The chloride and sulphate ion data also support the argument that salinity was one of the controlling factors in the process of carnotite precipitation at least in the Klein Trekkopje deposit. In borehole TKP5, there is a strong positive correlation between the concentrations for the sulphate ion and U (Fig. 38 (g)). This suggests that in some areas at Klein Trekkopje, a slight increase in pH might have contributed to the leaching of U from fragments in the channel. It might also be an indication that gypsum and carnotite precipitate under closely similar geochemical and climatic conditions. The sample points which are aligned horizontally with a very low U concentration in Figure 38 (g) are the ones from significant depths, where there is no gypsum. At Klein Trekkopje, although the most abundant sulphate is gypsum, other minerals such as barite (BaSO4) and celestite (SrSO4) have been reported (Hambleton – Jones, 1976).

The relationship between V and U (Fig. 38 (b) and 38 (f)) shows a strong positive correlation, which suggests that in the ore, vanadium occurs invariably within

carnotite. The Figures 38 (b) and 38 (f) represent two different boreholes. There is an inconsistency in one of the samples, whereby a high vanadium value (73 ppm) is associated with a very low uranium value (23 ppm). This sample happens to be the deepest, between 15 – 16 m. This inconsistency can only be explained by the fact that the deeper it is in the channel, the rate of evapo-transpiration is lower. This indicates that evapo-transpiration is an important factor in the process of carnotite precipitation.

The sharp increase in the uranium concentration between 5 – 7m appears to be driven by an increase in the vanadium concentration. Similarly, at the deepest level where the uranium concentration is expected to be lowest if evapo-transpiration was the only driving factor, the uranium concentration rises to 23 ppm. This was definitely caused by a sudden increase in the vanadium concentration from 38 ppm to 73 ppm. Vanadium is therefore a very important controlling factor in the precipitation of carnotite.

The Mg-U plot in Figure 38 (c) from Borehole KTK11 shows a positive correlation. In the Langer Heinrich ore body, the same trends were observed and this simply means that in general the magnesium concentration in the groundwater plays a role in the precipitation of uranium. The two diagrams indicate that the best uranium grades can be expected in samples with a magnesium concentration between 800 ppm and 1000 ppm. A magnesium concentration below 800 ppm probably suggests too low salinity which cannot result in the destabilization of uranyl carbonate complexes. Similarly, if the magnesium concentration is above 1000 ppm in a given groundwater

system, it could mean that the salinity is too high and as a result carnotite is more likely to be redissolved. However, it has been shown earlier by Youlton (2006) that the groundwater conditions at Klein Trekkopje support carnotite precipitation and not dissolution.

Figure 38 (d) shows the relationship between K and U in the Klein Trekkopje ore body. It shows a positive correlation between the two elements, whereby high K concentrations are generally associated with high U. Linearity is weak, which means there is a lot of K residing outside carnotite, probably in detrital minerals such as biotite and K-feldspar. Figure 38 (e) shows that there is no correlation between Ca and U. It is known that the groundwater in the Namib Desert has more calcium than sea water from the Atlantic Ocean (Hambleton–Jones, 1976). Therefore an inflow of marine fogs into the groundwater may dilute the calcium concentration in the subsurface water, thereby affecting the process of uranium mineralization negatively.

In the case of borehole KTK11, the level between 5 – 7m can be said to be the level around which the palaeo-water table was fluctuating. Not only is the U concentration highest at this level, but the chloride ion concentration is moderate and most suitable for carnotite precipitation.

6.3 REE geochemistry

The following Tables (21 – 26) contain REE data for various rock types in the catchment areas for both Langer Heinrich and Klein Trekkopje U deposits. The REE plots for these data are given in Figure 39.

Table 21: REE geochemistry for the Bloedkoppie granite.

Sample ID.	La (ppm)	Ce (ppm)	Pr (ppm)	Nd (ppm)	Sm (ppm)	Eu (ppm)	Gd (ppm)	Tb (ppm)	Dy (ppm)	Ho (ppm)	Er (ppm)	Tm (ppm	Yb (ppm)	Lu (ppm)
Bloed1	7	9.51	1.66	7	2.71	0.33	3.71	0.89	6.21	1.32	4.09	0.62	3.99	0.64
Bloed2	13.2	19.85	3.94	17.5	6.36	0.46	8.27	1.7	10.8	2.19	6.18	0.82	4.84	0.73
Bloed3	5.7	14.15	1.86	7.9	3.1	0.23	3.39	0.77	5.37	1.16	3.89	0.69	5.12	0.87
Bloed4	7.4	15.3	2	8.1	2.39	0.34	2.41	0.46	2.93	0.6	1.94	0.31	2.15	0.36
Bloed5	5.5	11.65	1.51	6.2	2.06	0.3	2.22	0.48	3.15	0.66	2.11	0.34	2.29	0.38
Bloed6	11.5	25.9	3.06	11.8	3.18	0.34	3.07	0.58	3.58	0.74	2.41	0.4	2.83	0.48
Bloed7	46.3	91.8	10.35	37.9	7.55	1.2	6.9	1.06	5.91	1.17	3.53	0.5	3.23	0.49
Bloed8	51.6	101	11.35	41.7	8.11	1.2	7.22	1.03	5.43	1.03	3	0.4	2.49	0.37
Bloed9	7	20.1	1.86	7	1.69	0.52	1.67	0.28	1.64	0.33	0.99	0.14	0.9	0.15
Bloed10	55.2	109.5	12.15	43.8	8.03	1.05	7.04	0.98	5.16	1	3.06	0.43	2.79	0.44
Bloed11	50.6	98.6	11.25	41.3	8.22	1.2	7.46	1.1	6.05	1.16	3.43	0.47	2.86	0.42
Bloed12	36.1	96.4	8.84	32.1	6.2	0.93	5.62	0.89	4.39	0.72	2.61	0.35	2.33	0.27
Average	**24.7**	**51.1**	**5.82**	**21.8**	**4.97**	**0.67**	**4.9**	**0.85**	**5.05**	**1.0**	**3.1**	**0.45**	**2.98**	**0.47**

Table 22: REE geochemistry for the Tinkas Schist.

Sample ID.	La (ppm)	Ce (ppm)	Pr (ppm)	Nd (ppm)	Sm (ppm)	Eu (ppm)	Gd (ppm)	Tb (ppm)	Dy (ppm)	Ho (ppm)	Er (ppm)	Tm (ppm	Yb (ppm)	Lu (ppm)
Tink1	28.5	71.8	8.3	32.8	7.15	1.32	6.7	1.16	5.8	0.92	3.36	0.44	3.06	0.36
Tink2	23.9	60.8	7.35	28.8	6.36	1.12	6.09	1.06	5.4	0.86	3.15	0.42	2.89	0.36
Tink3	22.5	56.3	6.68	27.1	6.2	1.2	5.7	1	5.03	0.82	3.01	0.4	2.72	0.33
Tink4	23.2	53.8	6.65	26.1	5.78	1.26	5.87	1.04	5.31	0.85	3.11	0.41	2.83	0.34
Tink5	25.2	57.5	6.97	26.4	5.05	1.37	4.54	0.68	3.11	0.52	1.93	0.25	1.8	0.23
Tink6	26.8	66.6	7.51	28.8	5.99	1.16	5.54	0.89	4.25	0.69	2.61	0.34	2.48	0.3
Tink7	26.5	71.3	7.79	29.6	6.11	1.2	5.66	0.92	4.64	0.76	2.84	0.38	2.7	0.34
Average	25.23	62.58	7.32	28.51	6.09	1.23	5.73	0.96	4.79	0.77	2.86	0.38	2.64	0.32

Table 23: REE geochemistry for Abbabis Complex.

Sample ID.	La (ppm)	Ce (ppm)	Pr (ppm)	Nd (ppm)	Sm (ppm)	Eu (ppm)	Gd (ppm)	Tb (ppm)	Dy (ppm)	Ho (ppm)	Er (ppm)	Tm (ppm	Yb (ppm)	Lu (ppm)
AB1	132.5	263	30.1	107.5	17.75	2.99	14.95	1.82	8.44	1.54	4.54	0.55	3.22	0.48
AB2	82.8	197	22.5	83.4	14.05	2.07	12.1	1.61	8.18	1.61	5.08	0.71	4.63	0.74
AB3	133.5	264	29.5	103	16.15	2.89	13.75	1.59	7.35	1.41	4.48	0.61	4.07	0.67
AB4	12.4	22.3	2.62	10	2.33	1.32	2.06	0.31	1.66	0.3	0.88	0.1	0.63	0.09
AB5	10.3	16.9	1.81	6.5	1.44	1.01	1.36	0.21	1.16	0.21	0.62	0.08	0.52	0.08
Average	74.3	152.6	17.31	62.1	10.34	2.05	8.84	1.11	5.36	1.01	3.12	0.41	2.61	0.41

Table 24: REE geochemistry for mineralized calcretes at Langer Heinrich.

Sample ID.	La (ppm)	Ce (ppm)	Pr (ppm)	Nd (ppm)	Sm (ppm)	Eu (ppm)	Gd (ppm)	Tb (ppm)	Dy (ppm)	Ho (ppm)	Er (ppm)	Tm (ppm	Yb (ppm)	Lu (ppm)
LCalc1	10.7	19.35	2.69	10	2.08	0.51	1.91	0.29	1.34	0.18	0.65	0.08	0.59	0.07
LCalc2	8.4	19	2.18	8.2	1.68	0.46	1.54	0.23	0.98	0.14	0.5	0.06	0.48	0.06
LCalc3	8.7	20.3	2.29	8.5	1.79	0.47	1.69	0.26	1.19	0.18	0.63	0.08	0.57	0.07
LCalc4	9.7	20.2	2.52	9.3	1.94	0.51	1.82	0.28	1.29	0.19	0.69	0.09	0.62	0.07
LCalc5	10	18.2	2.48	9.2	1.89	0.51	1.74	0.28	1.14	0.16	0.57	0.07	0.54	0.06
LCalc6	9.6	20.5	2.48	9.5	1.95	0.39	1.87	0.29	1.3	0.19	0.69	0.08	0.62	0.07

Table 25: REE geochemistry for the Klein Spitzkoppe granite.

Sample ID.	La ppm)	Ce(ppm)	Pr (ppm)	Nd (ppm)	Sm (ppm)	Eu (ppm)	Gd (ppm)	Tb(ppm)	Dy (ppm)	Ho (ppm)	Er (ppm)	Tm (ppm	Yb (ppm)	Lu (ppm)
SP1	18.9	53.1	7.46	27.2	9	0.02	7.23	1.73	12.1	2.6	10.35	2.33	19.4	3.22
SP2	18.5	54.2	7.58	27.4	8.92	0.02	6.77	1.59	11.1	2.38	9.47	2.07	16.9	2.84
SP3	26.3	65.9	9.12	37.4	11.75	0.07	11.8	2.59	18	4.08	14.5	2.56	17.8	2.82
SP4	20.7	52	7.12	29.6	10	0.08	10.25	2.23	15.5	3.56	12.8	2.28	16.1	2.61
SP5	26.5	67.5	9.56	41.1	14.2	0.08	14.25	3.1	21.5	4.93	17.8	3.24	23.1	3.81
SP6	22.4	57.3	7.97	33.5	11.5	0.07	11.75	2.65	18.85	4.36	15.75	2.83	20.1	3.25
Average	22.2	58.3	8.13	32.7	10.9	0.06	10.34	2.31	16.2	3.65	13.45	2.55	18.9	3.09

Table 26: REE geochemistry for mineralized calcretes at Klein Trekkopje.

Sample ID.	La (ppm)	Ce (ppm)	Pr (ppm)	Nd (ppm)	Sm (ppm)	Eu (ppm)	Gd (ppm)	Tb (ppm)	Dy (ppm)	Ho (ppm)	Er (ppm)	Tm (ppm	Yb (ppm)	Lu (ppm)
TCALC1	63.29	43.30	37.79	28.91	18.37	8.10	11.82	9.09	6.46	5.12	5.20	4.71	5.23	4.72
TCALC2	42.62	28.19	25.47	19.27	12.68	7.07	8.37	6.95	5.00	4.06	4.17	3.92	3.94	4.33

The REE plots may give insight into the provenance or precursor for a particular rock type. They may also provide understanding of either sedimentation or crystallization history. Since the concentrations of the key elements, U and V, in the

various rocks in the catchment area, the analysis of REE patterns is also aimed at comparing such patterns in the context of U and V concentrations.

The following plots (39 (a) – (h)) are aimed at examining these patterns more closely.

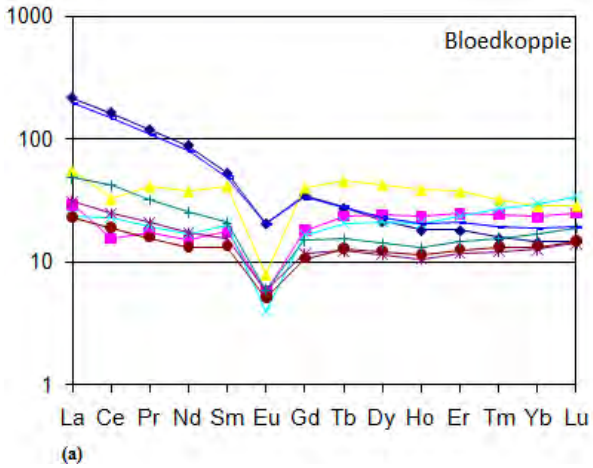

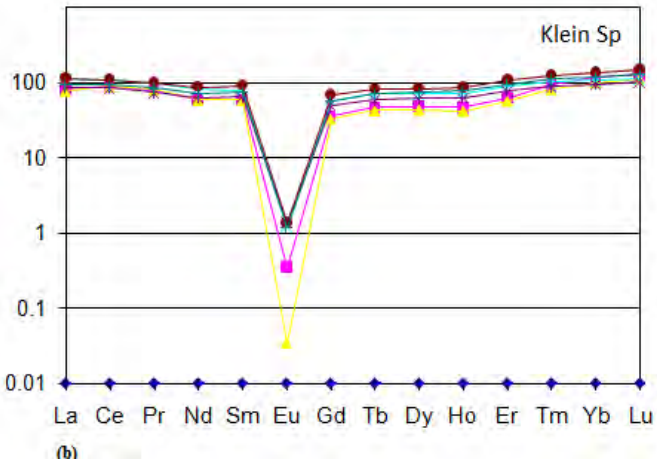

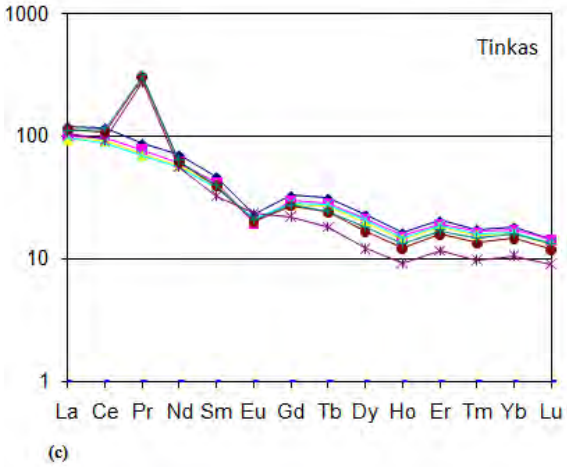

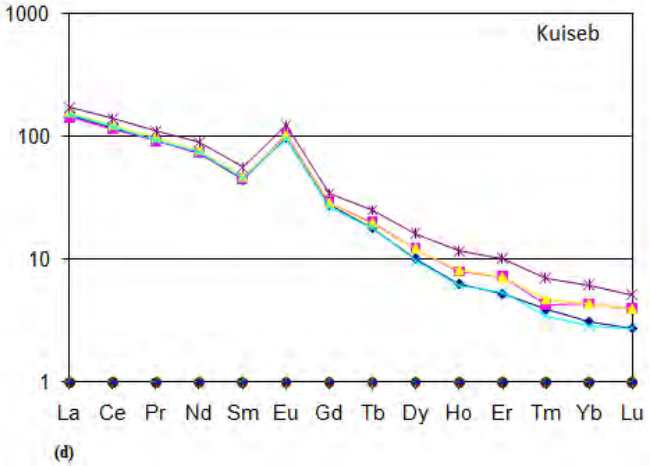

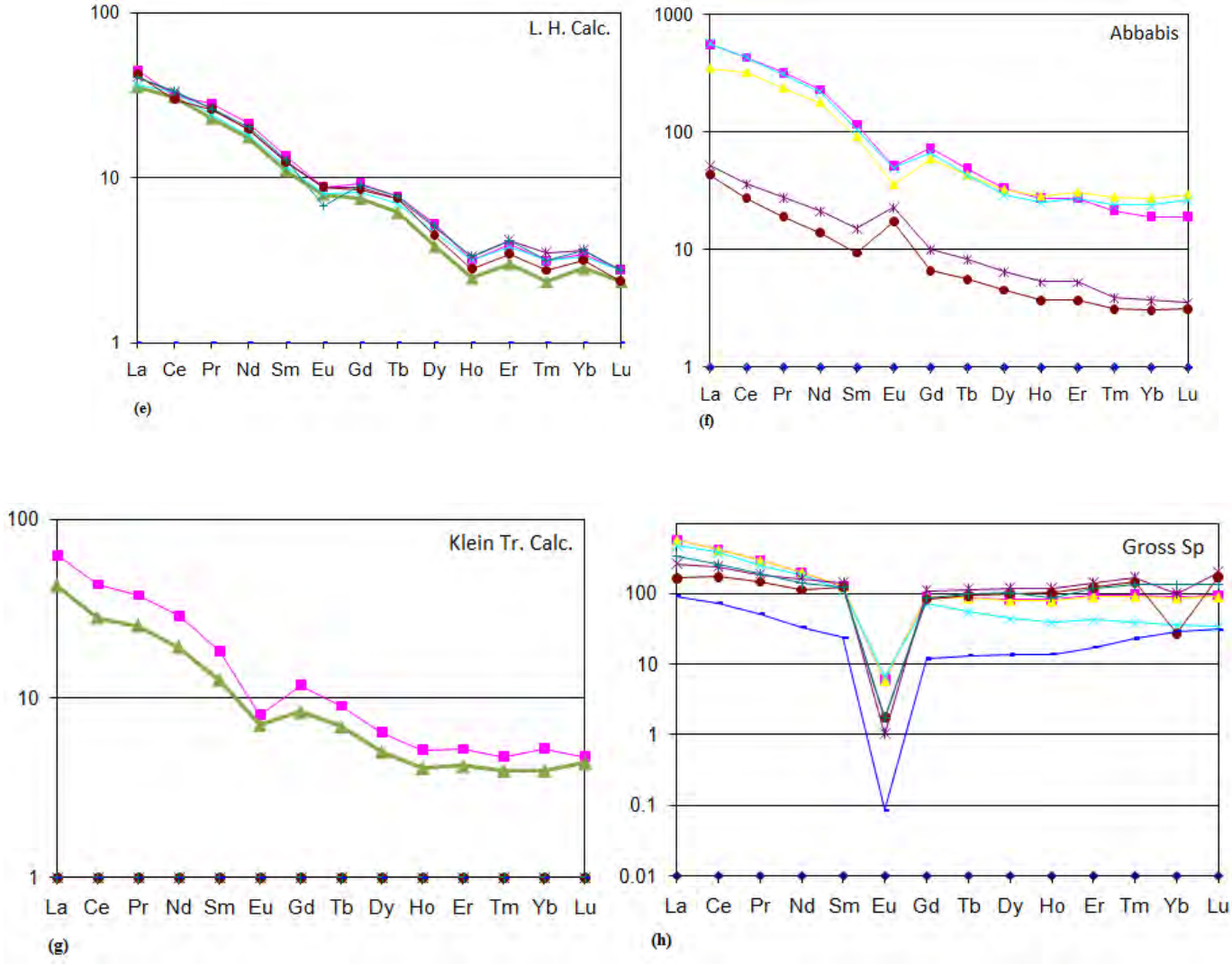

Fig. 39 (a) – (h): Chondrite-normalized REE patterns for various rock types in the catchment areas for Langer Heinrich and Klein Trekkopje. (a) Bloedkoppie granite; (b) Klein Spitzkoppe granite; (c) Tinkas schist; (d) Kuiseb schist; (e) mineralized calcrete at Langer Heinrich; (f) Abbabis Basement gneiss; (g) mineralized calcrete at Klein Trekkopje and (h) Gross Spitzkoppe granite. Each colour represents a specific sample from that particular rock.

Some samples of the Bloedkoppie granite show a prominent negative Ce anomaly while others have a prominent positive Ce anomaly. The same Ce anomaly is also observed in samples from the Langer Heinrich ore body. The Bloedkoppie granite is relatively enriched in LREE, especially samples Bloed 7 – 12 (Table 21) and this is accompanied by a relative depletion in HREE. Looking at Table 11, it can be seen that these samples have relatively high Zr (about 100 ppm). There are also some samples within the Bloedkoppie granite which have a have a flat REE pattern.

On average the Bloedkoppie granite has a prominent negative Eu anomaly, indicating a significant degree of differentiation.

In general there is no positive correlation between U and Zr, Ce, La & Ti, but samples from individual outcrops within the Bloedkoppie granite appear to show some mild correlation. Samples like Bloed 10 – 12 in Table 11 show a positive correlation between U and accessory minerals. This means that in those few cases where there is a high concentration of accessory minerals; U tends to be trapped in such minerals. The outcrops with the highest concentration of accessory minerals tend to have more biotite and plagioclase and less K-feldspar. They appear more weathered than the ones with high K-feldspars and high silica. Hambleton Jones (1976) observed that the Bloedkoppie granite has a REE pattern closely similar to those of Etusis sediments.

The REE patterns for the Tinkas schist resemble those of typical sediments, the only exception being the fact that some of the samples show a prominent Pr anomaly.

One of the samples (Tink 5), which show a positive Pr anomaly also shows a clear depletion of HREE.

The REE patterns for the Abbabis felsic gneisses indicate both a negative and a positive Eu anomaly. Samples AB1, AB2 & AB3 have much higher total REE than samples AB4 and AB5 (Table 23/ Fig. 39 (f)). This suggests that during metamorphism of the Abbabis, AB1, AB2 & AB3 represent the late stage metamorphic fluids, into which the REE have been remobilized. Samples AB4 and AB5 have a positive Eu anomaly and lower total REE. They therefore represent the early crystallizing portion of the metamorphic fluids.

The REE patterns for mineralized calcretes at Langer Heinrich show a progressive depletion of HREE. All samples have closely similar REE element plots. An enrichment of LREE suggests that detrital accessory minerals like monazite are abundant in the mineralized calcrete. Some samples show a negative Ce anomaly while others show a positive Ce anomaly (also found by Hambleton-Jones, 1976). This may indicate that part of the provenance for these calcretes was a laterite derived from the Bloedkoppie granite at some time in the past and now eroded away.

The REE pattern for the Klein Spitzkoppe granite (Fig. 39 (b)) appears fairly flat, with an average La/Lu ratio of about 10. The granite nevertheless has a prominent negative europium anomaly, suggesting that its magma was much more depleted in plagioclase and thus less basic than the magma which gave rise to the Gross Spitzkoppe granite, for instance. The average Eu concentration for Klein Spitzkoppe is 0.1265 ppm

(Table 25), while that of Gross Spitzkoppe is 0.224 ppm (Frindt et al. 2004a). The samples taken by the writer have also shown that the Klein Spitzkoppe granite is more potassic than the Gross Spitzkoppe granite. The K/Ca ratios are 9.7 and 8.2 for Klein Spitzkoppe and Gross Spitzkoppe granites respectively. Combined samples taken by the writer, Kandara (1998) and Frindt et al. (2004a) reported average Rb/Sr ratios of 31 and 27 for the Klein Spitzkoppe and Gross Spitzkoppe granites respectively. All these findings are a clear indication that the Klein Spitzkoppe granite is more evolved than the Gross Spitzkoppe granite. The fact that the REE pattern for the Klein Spitzkoppe granite is fairly flat is a clear indication that the granite has very little accessory minerals which would otherwise show an enrichment of LREE. This confirms earlier observations by the writer that most of the uranium in the Klein Spitzkoppe granite is leachable and not locked up in resistant accessory minerals.

The REE pattern for the Gross Spitzkoppe granite (Fig. 39 (h)) above shows a significant enrichment of light REE. This may suggest that the Gross Spitzkoppe granite is full of accessory minerals such as monazite and allanite. Thin section studies have revealed the presence of circular radiation haloes in biotite crystals. These circular features are reminiscent of U contained in zircons or monazite. The heavy REE tend to show a flat pattern like those of the Klein Spitzkoppe granite except that some samples in the Gross Spitzkoppe granite have a notable depletion of heavy REE like Dy and Ho. This depletion might reflect crystallization of zircons in earlier phases. The zircons are known to take up HREE during their crystallization. A pronounced Eu anomaly can be

observed in Figure 39 (h), almost similar to the one observed in the Klein Spitzkoppe granite. The fact that the Gross Spitzkoppe granite has more refractory accessory minerals than the Klein Spitzkoppe Granite means the former is likely to have more U trapped in these accessory minerals.

The REE patterns for the mineralized calcrete at Klein Trekkopje mine (Fig. 39 (g)) appear to have the same shape as those from the Langer Heinrich ore body. However there is one striking difference – the positive Ce anomaly observed in the mineralized calcretes at Langer Heinrich does not exist in the Klein Trekkopje calcrete. The negative Eu anomaly is slightly more prominent in the Klein Trekkopje calcrete compared to the Langer Heinrich calcrete. This probably reflects a slight abundance of detrital K-feldspar relative to plagioclase in the calcretes at Klein Trekkopje. Another unique feature in the Klein Trekkopje calcrete is that the REE pattern forms a mild concave upward shape. This is probably due to the fact that the Klein Trekkopje calcretes have less detrital zircons than the Langer Heinrich calcretes. The ore at Klein Trekkopje has about 23 ppm Zr on average whereas the Langer Heinrich ore has 35 ppm Zr.

6.4 Groundwater

Figure 40 shows the stability fields for several U and V phases under varying Eh/pH conditions. The carnotite stability field is very broad, which explains the reason why carnotite is usually the main U mineral in most calcrete hosted deposits. Different elements and compounds either contribute to the precipitation or dissolution of carnotite

in the water. This chapter, and its subsequent discussion, is dedicated to examining how the presence of various elements and compounds affect U in the groundwater. Elements and compounds which promote the precipitation of U are expected to have a negative correlation to it, whilst those that promote the solubility of U in the water will show a positive correlation with it.

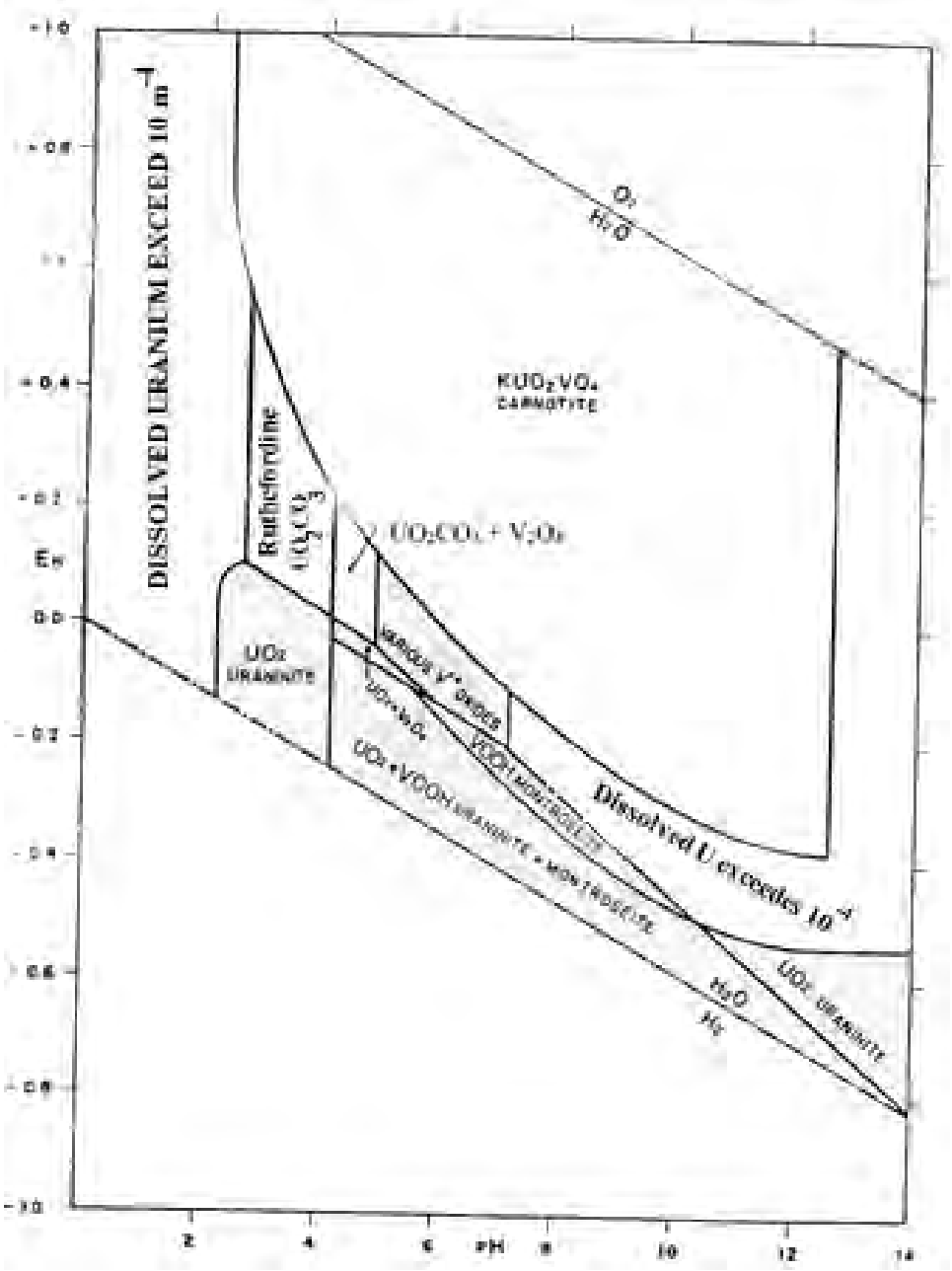

Fig . 40: Stability relations among some U and V compounds in water at 25˚C and 1 atmosphere total pressure. Total dissolved V species = 10-3; total dissolved carbonate species = 10-3; total dissolved K species = 10-3. (After Maasen 1982).

6.4.1 Groundwater around Langer Heinrich

Figure 41 was compiled by Bittner (2009). The data from the boreholes in this Figure are given in Appendix 5 and processed as part of this project, for the writer to have some understanding of the groundwater chemistry around the Langer Heinrich deposit.

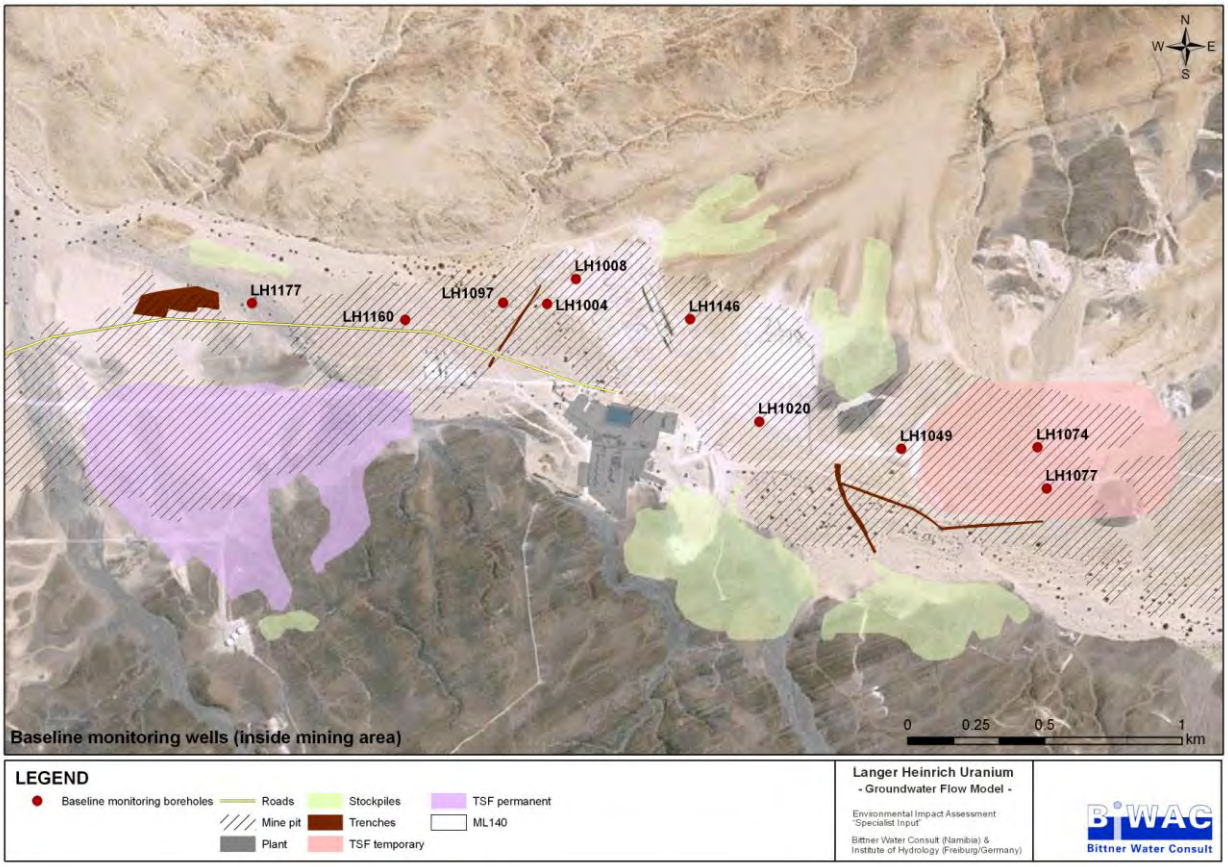

Fig. 41: A map showing water borehole positions around the Langer Heinrich U deposit (after Bittner, 2009).

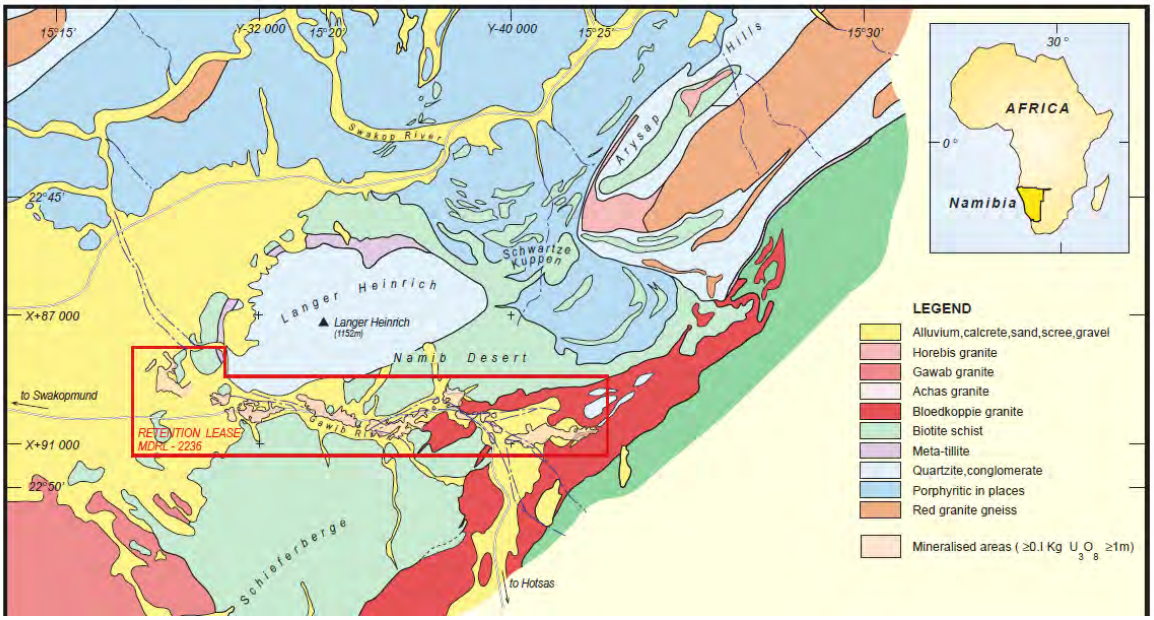

Fig. 42: Geological map for the Langer Heinrich area showing the demarcation of the mining licence area as well as U mineralization (after Becker and Hogarth, 2005).

Figure 42 shows the course of the Langer Heinrich palaeo-channel and the type of lithologies that it transgresses. The course of the ancestral Tumas River can also be seen on this Figure, coming from the direction of the Abbabis Basement gneiss in the west. From this map, it can be seen that high grade uranium mineralization occurs where there is narrowing of the channel and where the channel is meandering. The map also shows the degree of exposure of the Schieferberge schist (Tinkas).

The following correlation diagrams (Fig. 43) for the groundwater at Langer Heinrich were plotted using the data in appendix 5 (after Bittner, 2009).

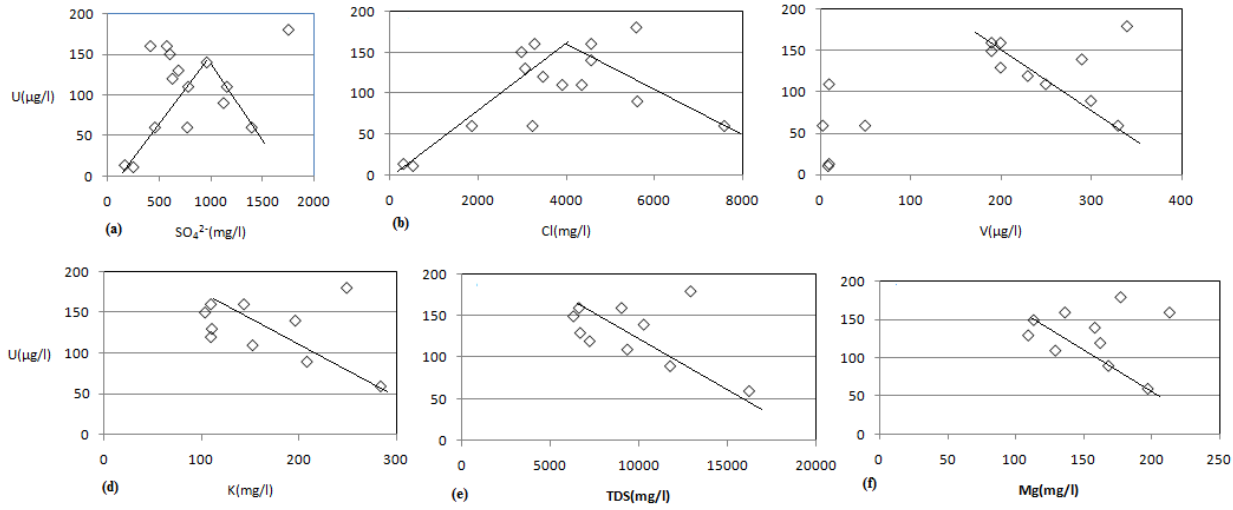

Fig. 43 (a) – (f): Correlation diagrams for groundwater at Langer Heinrich, showing the relationship between several elements and U.

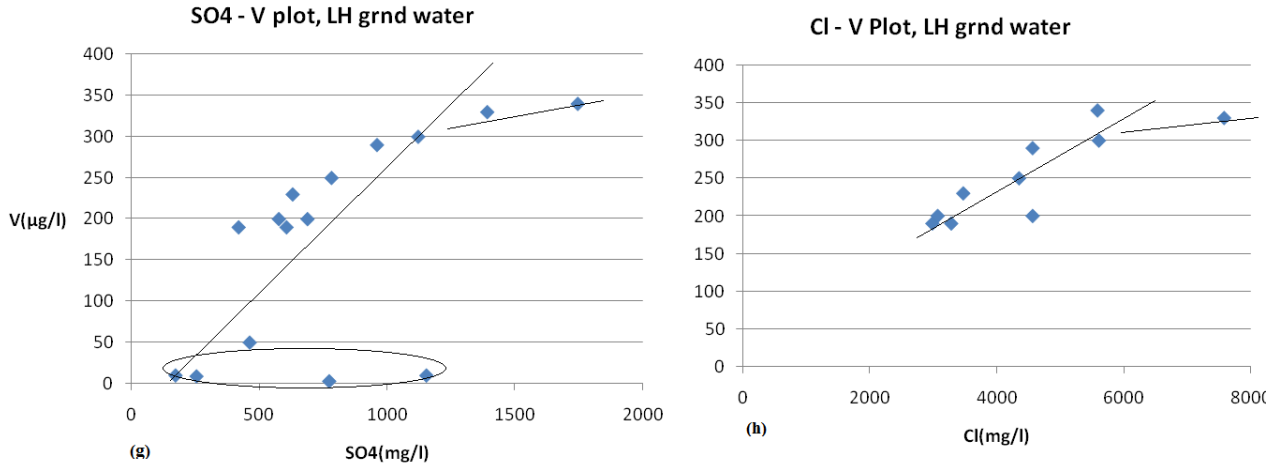

Fig. 43 (g)-(h): Correlation diagrams for groundwater at Langer Heinrich, showing the relationship how some ions relate to V.

Figure 43 (a) shows the relationship between the sulphate ion and U in the groundwater. The conical shape in this diagram both a positive and negative correlation can exist depending on the concentration for the sulphate ion. When the sulphate ion

concentration is below 100 mg/l, the U concentration increases together as the sulphate ion concentration increases. A fluid with a low concentration of sulphate ion will most likely have low salinity. That means there are not enough cations to facilitate the decomplexing of the uranyl carbonate complex and eventually precipitate U. as a result, U stays highly soluble in the water. However, a sulphate concentration above 1000 mg/l is reminiscent of high general salinity. This means apart from the sulphate ion, such a fluid has high concentrations of other cations which facilitate the decomplexing of the uranyl carbonate ion and eventually precipitate U. This will have the effect of dropping the U concentration in the water as salinity increases. The negative correlation observed in Figure 43 (a) beyond the 1000 mg/l sulphate concentration should be seen in that context.

The conical shape correlation observed in Figures 43 (b) and 43 (c) can also be explained from the point of view of general salinity. A low Cl content in the water suggests low general salinity, which means U solubility is high. A chloride concentration above 4300 mg/l as shown in Figure 43 (b) means the water has reached a salinity level capable of precipitating U. In Figure 43 (c), for V concentrations below 200 μg/l, there is virtually no correlation between V and U. However, above that concentration U shows a strong negative correlation with U. This means a V concentration above 200 μg/l will trigger the precipitation of U in the water and consequently deplete such water of U. An outlying value showing both high vanadium

and uranium concentrations probably points to a weakly oxidizing environment, struggling to precipitate carnotite.

Figure 43 (d) shows a negative correlation between K and U in the water, which means the higher the K concentration in the water, the higher the rate of carnotite precipitation and the higher the depletion of U in such water. In general uranium mineralization is not too sensitive to the lack of potassium in the water because tyuyamunite can still form as an alternative. The rock samples taken by the writer from the mine, show that the Tinkas schist has about 2.2% potassium while the Bloedkoppie granite has about 3.6%. Therefore any boreholes in the vicinity of any of the two lithologies will see an increase in the potassium concentration of the groundwater.

Figure 43 (e) shows a negative correlation between total dissolved solids (TDS) and U. TDS can be used as a measure of general salinity. This relationship between TDS and U therefore suggests that salinity plays an important role in the precipitation of U from groundwater. Mg also shows a degree of negative correlation with U in the water (Figure 43 (f)), again suggesting that the former contributes to the precipitation of the latter.

In general, the data in Appendix 5 indicates that the uranium concentration decreases from east to west. This suggests a major source for this element in the eastern part of the deposit. This is in line with the common belief that the Bloedkoppie granite, which is situated to the east, was the major source of uranium for the Langer Heinrich Deposit. The V concentration is highest in the vicinity of the Tinkas schist. This

supports common theories suggesting that the main source of vanadium for the Langer Heinrich deposit was the Tinkas schist. The concentrations for both the sulphate and chloride ions increase from the east to the west. This suggests that the main source of the two ions was the marine fogs, which are more active in the west or closer to the sea. In the modern day Swakop River, water samples from boreholes indicate that the concentrations for both U and V are much lower than those in the palaeo-channel. The U concentrations in the modern day rivers range mainly from 10 to 50 μg/l. The V concentrations in the modern day Swakop River ranges from 5 to 15 μg/l. These low metal concentrations in modern day rivers suggest that these aquifers are constantly recharged during the rainy season and that the water is close to being fit for human consumption.

Figure 43 (g) shows a strong, positive linear relationship between the sulphate ion and V. The water samples taken from the River bed have low V values, and do not show a positive correlation between the sulphate ion and V. The strong positive correlation between the sulphate ion and V probably suggests that V^{4+} is more mobile in water with a slightly low pH because a high sulphate ion concentration in the water usually means the pH is below 7. Figure 43 (h) shows a strong relationship between the chloride ion and V in the water, again indicating the chloride ion's possible contribution to the mobilization of V.

The Ca-U plot, though not shown above, shows a degree of negative correlation between the two elements, whereby relatively high calcium concentrations in the water

are associated with relatively low uranium concentrations. Calcium contributes to the decomplexing of the uranyl carbonate complex in the water, thereby leading to the concentration of uranium and eventual precipitation of carnotite and depletion of U in the water.

6.4.2 Groundwater around Klein Trekkopje

Appendix 6 presents analytical results of groundwater at Klein Trekkopje. Although the data from Youlton (2006) had many other elements apart from the ones tabulated, the writer only selected those elements that are most relevant to this study. The presence of strontianite in the ore body at the Klein Trekkopje deposit has been confirmed about 20 years ago (Hambleton – Jones, 1976).

The research carried out by Youlton (2006) has revealed that at Klein Trekkopje, areas of high carnotite grades in the calcretized conglomerates coincide with areas of high vanadium and magnesium concentrations in the groundwater. These areas also coincide with high water tables or bedrock highs.

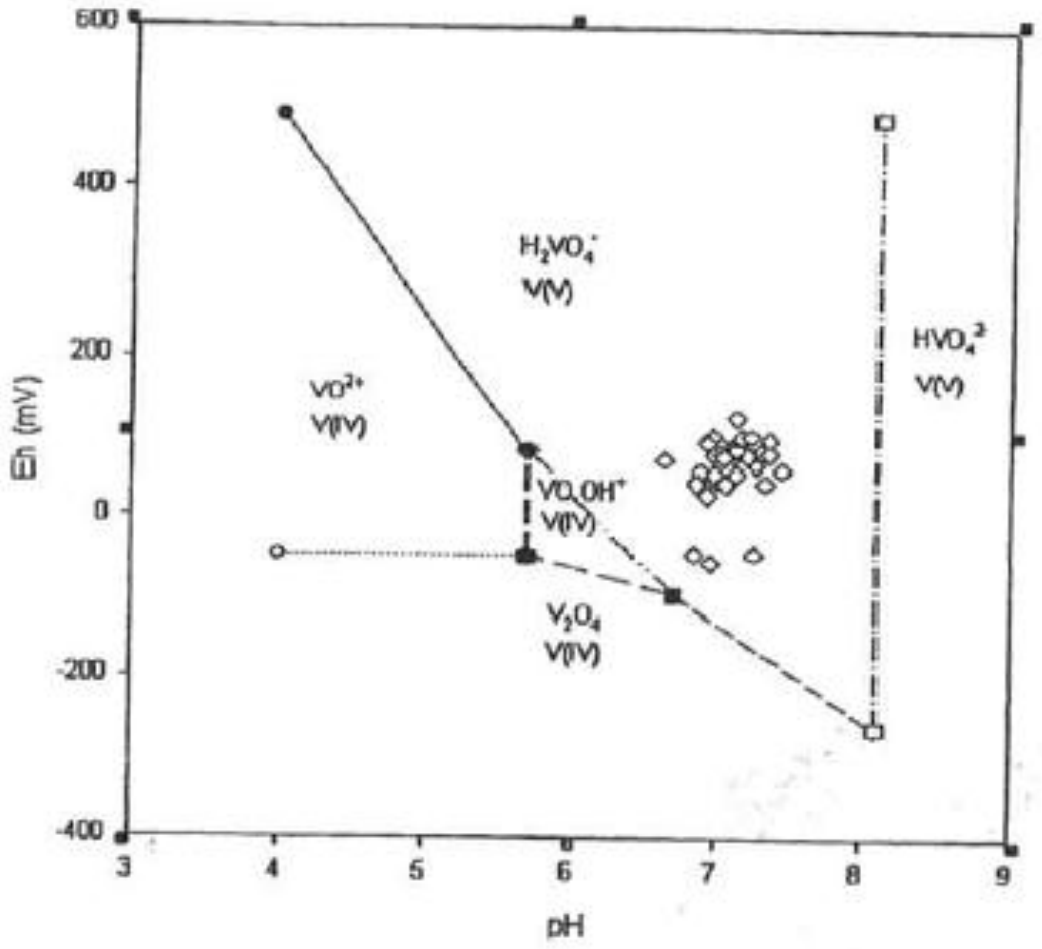

Fig . 44: Eh/ pH diagram, showing groundwater data for Klein Trekkopje area (after Youlton, 2006).

The data in Figure 44 plotted after Youlton (2006), indicate that most of the groundwater samples are plotting in the area of V^{5+}, which indicates groundwater conditions are largely oxidizing in the channels around the Klein Trekkopje deposit.

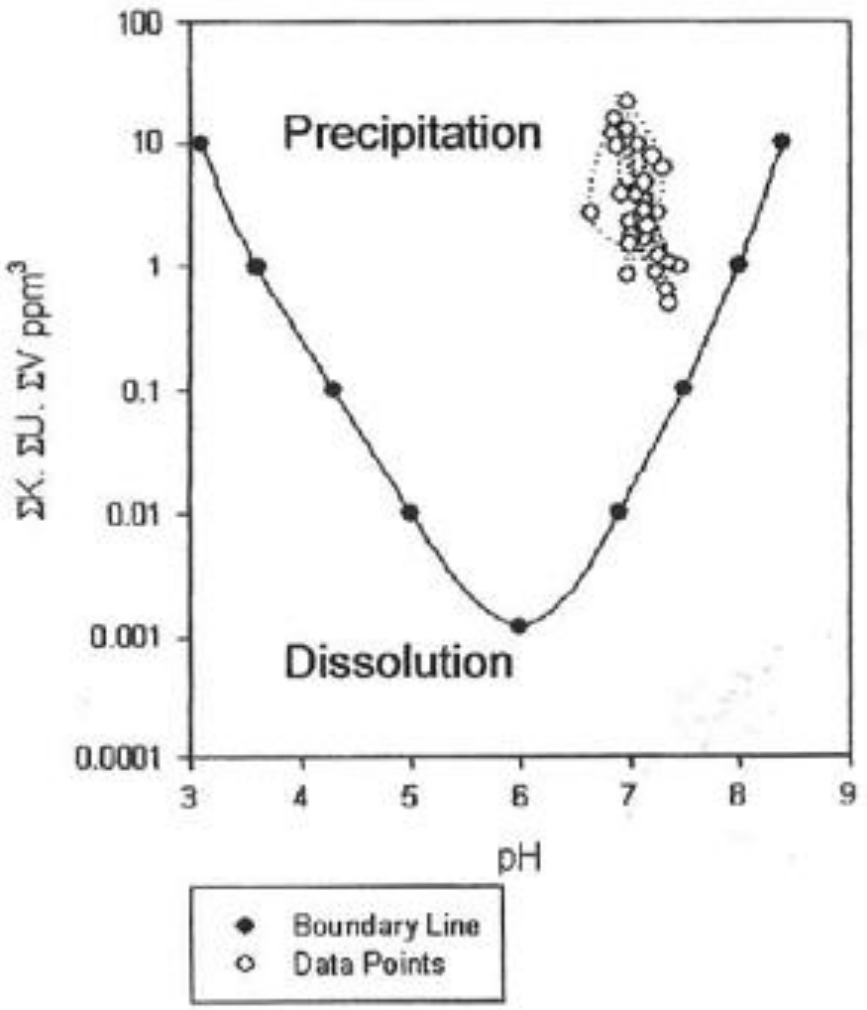

Fig . 45: Carnotite precipitation – dissolution diagram, showing positions for groundwater samples from Klein Trekkopje area (after Youlton, 2006).

The data in Figure 45, after Youlton (2006), indicate that for nearly all water samples analyzed, the groundwater conditions support the precipitation of carnotite rather than its dissolution. This indicates the Klein Trekkopje prospect is still in the process of forming.

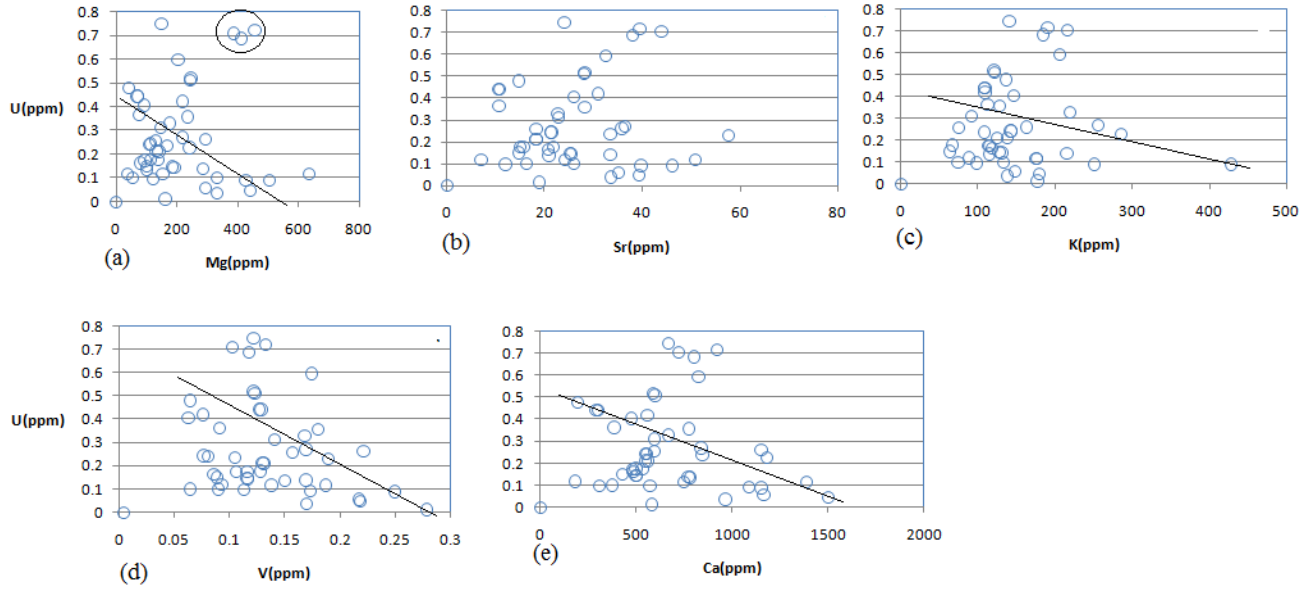

Fig. 46 (a) – (e): Correlation diagrams for the groundwater at Klein Trekkopje, showing how several elements correlate with U (data from Youlton (2006)).

Figure 46 illustrates the general chemical behaviour of certain elements in the groundwater at Klein Trekkopje. According to Figure 46, Mg, K, V and Ca all show a negative correlation with U in the water, which means these elements contribute to the precipitation of U and thereby depleting its concentration in the groundwater. Figure 46 (d) indicates that even if there are enormous amounts of U in the groundwater, it will remain in solution for as long as there is no powerful oxidizing agent like V. V is therefore a key ingredient in the entire precipitation process for calcrete hosted U. A source terrain with little amounts of U and high amounts of V could therefore have more potential than one with abundant U but little V.

K and V have a closely similar effect on U and this might be an indication that the two elements are both adsorbed onto clay minerals before the precipitation of carnotite takes place. Adsorption of vanadium onto clay minerals is thought to be an important process in the precipitation of carnotite (Hambleton – Jones, 1984). A deficiency in vanadium may lead to the formation of such minerals as urancalcarite and sodyite but these minerals are rarely significant. At Klein Trekkopje, for instance, they only constitute 5% of the ore and the rest is carnotite (Bowell et al., 2009). This may indicate these minerals are not very stable across a wide range of pH-Eh conditions like carnotite. However, Hambleton-Jones (1976) observed that uranium minerals form from increasing solubility products of the mineral species, starting with the least soluble forming first e.g. carnotite down to the most soluble UO_2CO_3. Secondly, the availability of ionic species – if there is insufficient vanadium, but available silica, then sodyite could form. As a parallel in the Karoo U deposits of South Africa, there is no vanadium but arsenic, so uranyl arsenates form.

The Sr-U plot in Figure 46 (b) does not show a clear correlation with U but in the writer's opinion this is due to the fact that the Sr concentrations in the water are much lower than those of Ca, Mg, and K. As a result, Sr does not seem to contribute a great deal to the precipitation of U in the groundwater.

Ca and U show a negative correlation, especially when calcium concentrations increase. At moderate concentrations of Ca in the groundwater, the two elements can co-exist without impacting on each other negatively. However as the Ca concentration increases, it contributes to the precipitation of U, which accompanies the precipitation of calcite. This happens because the two elements share the carbonate ion in solution. Excessive amounts of calcium in solution will lead to the calcium ion wrestling for the carbonate ion which is complexing with U, thereby causing the U concentration to increase to precipitation levels.

The other factor is that calcite only precipitates when there is enough heat to cause evapo-transpiration. The loss of water and carbon dioxide, which follows, will also lead to increased concentrations of U, K and V. Therefore the precipitation of calcite will always be accompanied by the precipitation of carnotite as the two minerals form under very similar chemical and climatic conditions.

6.5 Discussion

The main rock types in the study area have been analyzed for their U and V concentrations, either by the writer or by previous researchers. The results from the portable XRF measurements confirmed that vanadium enrichment, as obtained from the ALS Chemex assays, in the schists is not localized but largely homogeneous for the entire schist. The same transpired for the Karoo dolerite, which was drilled by van Noort

(2010). This survey has confirmed the homogeneity of uranium enrichment in the three granites, namely Bloedkoppie, Gross Spitzkoppe and Klein Spitzkoppe. The Salem granite did not show anomalous U concentrations in most cases.

The uranium concentrations for these rocks as well as their perceived leachability are tabulated in Table 27. As discussed earlier, the leachability is measured in the field by observing the extent to which a specific rock has undergone chemical and/ or physical weathering. In general, features such as mineralogy, texture, porosity, permeability and structures control leachability and are helpful in estimating the leachability of a given rock. These features have been described in Chapter 5.

Table 27: Observed U and V concentration ranges for various rock types in the study area (a combination of data from Marlow (1981); Mc Dermott (1986), van Noort (2010) and the writer (2011)).

ROCK TYPE	**AVERAGE V (ppm)**	**AVERAGE U (ppm)**	**LEACHABILITY DURING EROSION**
Bloedkoppie granite	5 – 15	5 – 18	Very good
Salem granite	40 – 50	2 -4	Very good
Donkerhoek granite	10 – 20	2 -4	Very good
Schieferberge schist	100 – 160	3 – 5	Good
Kuiseb schist	100 – 160	3 – 5	Very Good
Karoo dolerite	150 – 200	Close to 0	Very poor
Leucogranites (around Marenica)	30 – 200	5 – 40	Very good
Abbabis gneiss	40 – 70	2 – 5	Good
Klein Spitzkoppe granite	5	8 – 14	Good
Gross Spitzkoppe granite	5 - 8	10 – 18	Good
Etusis quartzite	5	2 – 5	Extremely poor
Alaskites	2 – 10	10 – 500	Good

The rating ranges from “very good” to extremely poor. Rocks which react to chemical weathering are rated as very good while those which are highly resistant to weathing are rated as extremely poor.

Comparing the Bloedkoppie granite with the Gross Spitzkoppe granite, for instance, it is obvious that the amount of U – bearing accessory minerals differs between the two granites. Bloedkoppie has an average 51 ppm Ce, while Gross Spitzkoppe has 160 ppm Ce. Bloedkoppie has about 78 ppm Zr while Gross Spitzkoppe has 196 ppm Zr.

Regarding the Klein Spitzkoppe granite, ICP-MS results for the medium-grained biotite granite give a lower U concentration, probably reflecting its lower biotite content. The coarse-grained biotite granite has a more pinkish colour in hand specimen. The fact that the coarse-grained biotite granite is more weathered than the fine- to medium-grained micro-granite, which has far less biotite, appears to suggest that biotite not only plays a role in hosting U but that it also facilitates weathering. It also appears that the grain size and grain type plays a role in facilitating weathering. The fine-grained, quartz rich granites always appear less weathered than the coarse-grained varieties which have more K- feldspars, more biotite and less quartz. This is understandable considering the fact that a fine-grained granite will be less permeable than a coarse-grained one. Similarly a quartz-rich granite will be less permeable than the one with less quartz.

It is likely that initially the magma which formed the Klein Spitzkoppe granite was part of a bigger magma chamber which also formed the Gross Spitzkoppe granite (Frindt et al. 2004a). The U is highest in the Erongo granite, which is to the eastern extreme of the catchment area, followed by the Gross Spitzkoppe granite and then by the Klein Spitzkoppe with the lowest U concentration. This systematic decrease in U concentration from east to west most likely reflects the possibility that during crustal relaxation, the degree of partial melting was decreasing towards the west.

Marlow (1981, p128-131) has observed an intimate relationship between the U phases and the accessory minerals, where euhedral uranyl silicate is intergrown with euhedral monazite and zircon in a radioactive red granite. Using an electron microprobe, Marlow (1981) further observed that in granites such as the Bloedkoppie granite, the most common U phases are uranyl silicate and uranophane. However, this scenario is slightly different for mineralized alaskites such as Rossing and Goanikontes. Marlow (1981, p133) observed that the common U phases in mineralized alaskites are uraninite, betafite and metaminct thorite. His work revealed that uraninite occurs interstitially or as euhedral inclusions in quartz, feldspar and biotite, commonly in association with zircon, monazite or Fe-oxide. Marlow's work is quite critical to this study as it unveils the way in which U occurs in source granites. This is of great help in predicting and understanding how U is leached from the catchment area during erosion.

Magnesium has been described by many researchers as one of the key ingredients required to facilitate the precipitation of carnotite through common ion effect. ICP results (appendix 3) indicate that the Tinkas schist has average magnesium concentrations between 2% and 2.5%. Without even taking into account the magnesium concentration for other lithologies or from marine fogs, it is clear that the subsurface waters in the Langer Heinrich channel had all the ingredients available for the precipitation of carnotite. However, magnesium only makes an impact in groundwater systems, which lack calcium. The presence of massive layers of calcrete at Langer Heinrich suggests that there was sufficient calcium in the system. Therefore carnotite precipitation at Langer Heinrich did not have to wait for the addition of magnesium to the system. The magnesium introduced to the groundwater only served as a bonus, unlike at Klein Trekkopje, where magnesium has been shown to play an integral role in mineralization.

Compared to Langer Heinrich, there was far more magnesium in the Klein Trekkopje channel. The Langer Heinrich ore body has about 0.3% Mg compared to about 0.9% in the Klein Trekkopje ore body. It means the ore at Klein Trekkopje has 3 times higher concentrations of magnesium than the one at Langer Heinrich. The same magnesium ratio was observed in the groundwaters in the vicinity of the two uranium deposits.

The abundance of Mg^{2+} in groundwater has been linked to uranium precipitation by Youlton (2006), as it contributes to decomplexing of the uranyl carbonate complex, thereby forming $MgCO_3$ and making U available for the formation of carnotite. This phenomenon has been observed at Klein Trekkopje, where high U appears to be associated with high Mg in the groundwater. Therefore the Tinkas schist was not only vital for the formation of carnotite through providing vanadium to the groundwater, but it may also have provided abundant magnesium to the groundwater.

A strong positive correlation between chlorine and vanadium in borehole KTK11 indicates that V is better mobilized by saline brines, rather than by fresh water. Once again, the relationship between the two elements suggests that carnotite precipitation at Klein Trekkopje was triggered by a salinity boundary.

From borehole KTK11 at Klein Trekkopje, it is clear that there are three main controlling factors for carnotite precipitation, namely the vanadium concentration, evapo-transpiration, which regulated the partial pressure of CO_2, and changes in redox conditions. The precipitation of carbonates of these elements reduces the partial pressure of CO_2 in the immediate environment, which can then have an influence on whether uranyl and vanadyl ions complex to form carnotite.

Hambleton – Jones (1984) has shown that there are no calcrete-hosted U deposits beyond the western cut-off line and argued that they have probably been eroded. This

could be partly true but the other reason, reflected by this study, is that groundwater conditions to the west of that line would be too saline for the precipitation of carnotite to occur.

6.6 Summary

The Bloedkoppie granite has both V and U concentrations which are high enough to make the Langer Heinrich U deposit. The Tinkas schist which has V concentrations above 100 ppm did boost the V concentration in the groundwater system at Langer Heinrich, which led to the smooth precipitation of carnotite.

In most granitoids, such as the Gross Spitzkoppe granite, U is associated with accessory minerals such as zircon and monazite, which in turn are contained as inclusions mainly in biotite. However, the Bloedkoppie granite has a lot U residing outside such accessory minerals. In most granitoids and pelitic sediments in the catchment area, V is associated with Fe and the two elements substitute for each other in minerals such as biotite, hornblende, magnetite and ilmenite. In general leachability and volume of a given rock appears to be more critical for the formation of a secondary U deposit than a high concentration of either U or V in such a rock.

The Spitzkoppe granites together with other Damaran-aged granitoids in the catchment area for the Klein Trekkopje U deposit had sufficient U to form the Klein Trekkopje deposit. The granitoids in this catchment area also had enough V to form the

Klein Trekkopje U deposit and this was boosted by the high V concentration in the Kuiseb schist. The abundance of S-bearing evaporites at Klein Trekkopje is an indication that marine fogs have been more active there than at Langer Heinrich, where the proportion of S-bearing evaporites is minimal. The REE patterns for granitoids in the catchment area resemble those of evolved granites, capable of carrying U as proto-ore. The groundwater chemistry at both Langer Heinrich and Klein Trekkopje demonstrates the significance of elements such as V, Mg and Cl in controlling the precipitation of carnotite.

CHAPTER 7 : MASS BALANCE CALCULATIONS

There is an ongoing debate regarding the size of source granitoids for both the Langer Heinrich and Klein Trekkopje uranium deposits. Some researchers like Hartleb (1988) believe that the Bloedkoppie granite is too small and that there might be an alternative source of uranium for the Langer Heinrich deposit. Similarly some researchers believe that the Spitzkoppe granites are too small and that they could not have provided all the U found at Klein Trekkopje today. This chapter aims to address these questions by evaluating the volumes for the source granitoids and their U concentrations and then comparing that with the U tonnage in the two deposits.

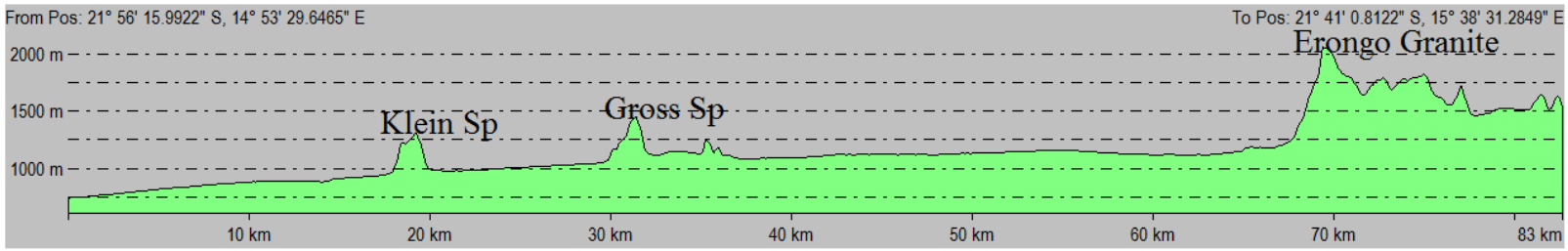

Fig . 47: NE – SW cross-section along the Damara structural grain, cutting through the Klein Spitzkoppe, Gross Spitzkoppe and Erongo granites.

Figure 47 shows a northeasterly cross-section along the Damara structural grain. The cross-section goes through the Klein Spitzkoppe granite, then Gross Spitzkoppe granite and finally through part of the Erongo complex to the extreme east. The highest point for the Gross Spitzkoppe granite corresponds to about 31 km, while the one for Erongo complex is about 70 km from the beginning of the cross-section. In the west of the cross-section, the average height for the Namib Desert' surface above sea level is shown.

7.1 Langer Heinrich

Borshoff (2009) on Paladin Energy's website put the Figure for mineable reserves in the Langer Heinrich deposit at about 80 000 tons of U_3O_8. This translates into 67840 tons of U metal. The density for an average granite is about 2.7 tons/m^3. Assuming that the U concentration in the Bloedkoppie granite is about 10 ppm, it follows that we would only need 6 784 000 000 tons of granite to produce the amount of uranium found in the Langer Heinrich deposit today. This tonnage is equivalent to 2 512 592 592.6 m^3 or 2.5 km^3 of granite. This would simply require the erosion of a small hill 2 km by 5 km, with a height of 250 m. The areal extent for the Bloedkoppie granite has been estimated to be 25 km^2 (Hartleb, 1988). Judging from the degree to which the Bloedkoppie granite has been eroded, there is no doubt that the Bloedkoppie granite was of such a size capable of producing the uranium for the Langer Heinrich deposit.

Field evidence clearly shows that the Bloedkoppie granite is the only uranium enriched granite, in the Langer Heinrich catchment area. The writer is therefore inclined to conclude that at least 90% of the uranium found in the Langer Heinrich deposit was sourced from the Bloedkoppie granite. The other 10% would have come from accessory sources in the area. Carlisle et al. (1978) has inferred the ancestral Tumas River to be draining from the area where the Abbabis Basement Complex is currently outcropping. It is therefore possible that part of the uranium deposited at Langer Heinrich was sourced from the Abbabis Basement complex. However field observations indicate that the Bloedkoppie granite has been the main catchment area from the Tertiary period to the present. The Abbabis metamorphic complex contains in the order of 5 ppm U on average (Marlow, 1981). During this study, the writer has sampled the Abbabis complex near Arandis (samples AB1 – AB5). The uranium values obtained here confirm the findings of Marlow (1981) that vanadium values ranged mainly between 20 – 70 ppm.

In carnotite, the ratio of U:V is about 4.7:1. Therefore to form the Langer Heinrich uranium deposit by eroding a source terrain with 10 ppm U, it means that only about 2 ppm V is required in the source terrain. This means the 15 ppm V in the Bloedkoppie granite and 140 ppm V in the Tinkas schist is more than the vanadium needed to form the Langer Heinrich deposit. This supports the writer's view that the unique abundance of vanadium in the Langer Heinrich catchment area played a significant role in the precipitation of carnotite.

7.2 Klein Trekkopje

Klein Trekkopje contains about 77 000 tons of U_3O_8 at 105 ppm (Macpherson et al., 2008). The study has shown that there is enough uranium and vanadium in the catchment area. The Klein Spitzkoppe and Gross Spitzkoppe granites together occupy an area of at least 50 km^2. It is known that the emplacement of both Klein Spitzkoppe and Gross Spitzkoppe granites is related to the same extensional event which resulted in the emplacement of Erongo granite (Trumbull et al., 2004). Since the Erongo Complex is capped by volcanics, it can be argued that the earth surface in the Spitzkoppe area was almost at the level where the volcanics are found today. Using this to estimate the amount of material eroded from Klein Spitzkoppe and Gross Spitzkoppe granites, there can be no doubt that these two granites contained sufficient U to produce the 77 000t U_3O_8 found at Klein Trekkopje. Without even considering uranium input from Damara aged granites, the two Spitzkoppe granites would have more than enough uranium for the Klein Trekkopje deposit today.

This study has shown that there are Damara-aged leucogranites in the vicinity of Marenica which have a uranium concentration in some cases exceeding 100 ppm and this is part of the wider catchment area for the Klein Trekkopje U deposit. According to Frindt et al. (2004b), the Spitzkoppe granites are subvolcanic intrusions. At present, the top of the Klein Spitzkoppe granite is about 1584 m above sea level. The top of the Gross Spitzkoppe granite is about 1728 m above sea level. Assuming that the current earth surface in the Spitzkoppe area is about 300 m above sea level, it is clear that more

than 1000 m of material has been eroded off the side of these two mountains to produce the conical shapes observed at present.

7.3 Summary

Mass balance calculations have shown that the Bloedkoppie granite alone was of such a volume that it could supply most of the U deposited at Langer Heinrich. Furthermore, the U-enriched granitoids upstream from the Klein Trekkopje deposit had more than enough U to contribute to what is today known as the Klein Trekkopje U deposit. With regard to V, there was more of it available in the catchment area compared to U because the former was sourced from both metapelites and granitoids, while U was only sourced from granitoids. It has been shown that to form carnotite, very little is required because the ratio of U to V is 4.7 to 1 while in the Bloedkoppie alone that ratio is roughly 1 to 1. Nevertheless, the more V in the system, the better.

CHAPTER 8 : GENERAL DISCUSSION

8.1 Proposed mechanisms of uranium precipitation

A combination of factors is usually responsible for the formation of a good calcrete hosted U deposit. In nature it is not very common that such factors are found together in one catchment area. Even if 95% of these factors are present in one catchment area, the missing 5% could prevent the formation of a good deposit.

8.1.1 Langer Heinrich Deposit

The characteristic erosional features displayed by the Bloedkoppie granite suggest that the mineralogy of the granite is amenable to chemical weathering. As discussed in earlier chapters the Bloedkoppie granite has about 10% Na-rich plagioclase and some amphiboles. Biotite, K-feldspars and quartz are the major minerals in this granite. The uniqueness of the Bloedkoppie granite, when comparing it to the Spitzkoppe granites, is that the former has more mafic minerals which decompose easily in the presence of water. The writer is of the opinion that the chemistry of this water is immaterial because these mafic minerals will decompose whenever they come into contact with any kind of water. K-feldspars also decompose but they are more resistant than plagioclase and amphiboles. The only resistant major mineral in the Bloedkoppie granite is quartz, which is not too important as a host of U in granite.

The texture for the Bloedkoppie granite is also conducive to weathering because it is largely coarse-grained, which means the water would percolate through the grains very easily and leach U. At Klein Spitzkoppe, there are fine-grained microgranite portions. This microgranite appears whitish in colour, which is an indication of its freshness. The coarse-grained varieties appear pinkish in colour, which may reflect the release of Fe from biotite and to a lesser extent from feldspars. In the Bloedkoppie granite, fresh fine-grained portions have not been reported and the writer has found none during this study. Analysis of the Bloedkoppie granite's geochemistry has shown that U in this granite is not trapped in refractory accessory minerals.

Therefore the writer is inclined to conclude that one single biggest positive factor in the formation of the Langer Heinrich deposit was the degree of readiness with which the Bloedkoppie granite was able to release U into the groundwater. The second positive factor was the abundance of V in the Tinkas schist. The third positive factor was the geomorphological features (e.g. Etusis quartzite) which formed mechanical traps for the fluids. The ultimate precipitation was smooth because the climate was arid enough and the rest of the other factors have already combined.

The fact that U mineralization at Langer Heinrich has been estimated at less than 100 000 yrs (Hambleton – Jones, 1976), is another indication that U has stayed in solution for a long period of time and only recently been precipitated. The leaching characteristics of the Bloedkoppie granite suggest that the period of leaching for the most part post-dated the wet period which was responsible for the formation of deep

valleys and the transportation of large fragments found in the conglomerates. The spherical hollows in the Bloedkoppie granite suggest that the fluid was eroding the granite with time and that there were non-flushing conditions during that time.

At Langer Heinrich the mode of carnotite precipitation is fairly simple and can be summed up as follows: firstly, there was a long period of weakly oxidizing groundwater conditions around the Bloedkoppie granite. This means there was an increase in the concentrations for ionic species such as K^+, Na^+, Mg^{2+}, Ca^{2+}, etc., which resulted in a massive mobilization of both U and V. Secondly, the groundwater conditions around Langer Heinrich became strongly oxidizing over time due to seasonal rains. Because there was sufficient supply of U, V and K into the groundwater and due to the fact that the oxidizing conditions were very long lasting and uninterrupted, carnotite was able to precipitate on a large scale.

The low channel gradient and the presence of well restricted perched ponds in the Langer Heinrich channel, coupled with an arid climate, created perfect conditions for carnotite precipitation. The lack of carbonate bedrock, such as Karibib marble, in the catchment area meant that there would be low level carbonate ion activity in the Langer Heinrich channel and as a result uranium solubility in the water was limited. This was good for carnotite precipitation because the bicarbonate ion would otherwise keep uranium in solution.

Considering the seven models of carnotite precipitation proposed by Mann and Deutscher (1978), it is obvious that formation of the commercially attractive Langer

Heinrich deposit was due to three fundamental reasons: 1) sufficient concentrations of ore forming elements in the catchment area, and 2) mechanical traps in the channel. These two controlling factors resulted in complete evolution of a weakly oxidizing fluid to a strongly oxidizing fluid. Other factors like proximity of source rocks to the site of deposition and arid climate also led to effective carnotite precipitation.

8.1.2 Klein Trekkopje Deposit

Unlike the Langer Heinrich deposit, the Klein Trekkopje deposit has a much more complicated genetic process. Firstly, the Spitzkoppe granites, which appear to be the main source of U for Klein Trekkopje, are about 40 km away from the site of deposition. This means part of the U could be lost on the way to the site of deposition. The leaching features observed in the Spitzkoppe granites, with a few exceptions, point to ordinary mechanical sedimentation. The site of U deposition, especially the western portion of the Klein Trekkopje deposit, is only about 50 km away from the shore line. This is quite close to the Ocean, which means it would be difficult for the groundwater conditions to become fully oxidizing and precipitate carnotite effectively. These factors alone already make this deposit different from the one at Langer Heinrich. Nevertheless, most of the mineralization at Klein Trekkopje is located at the confluence of two channels. This is an indication that carnotite precipitation was caused by the mixing of two fluids with a different chemistry.

The lack of good mechanical traps for U in the catchment area meant that U was transported for a long distance until it found more saline fluids which saw the uranyl

carbonate ion decomplexing, thereby concentrating U and forcing it to precipitate. Groundwater data and percussion drilling data from the area, examined in earlier chapters indicate that U mineralization at Klein Trekkopje was mainly triggered by a change in salinity. Therefore the models of Mann and Deutscher (1978) of common ion effect and decomplexing of the uranyl carbonate ion were both at play when the U-rich oxidized fluid reached an area of transitional salinity. However, there were too many negative factors in the process leading to U deposition at Klein Trekkopje. As mentioned earlier the leaching and mobilization of uranium in the main catchment area was poor and the volumes of water were too high, diluting anything in the channels.

The presence of a wide colour range for the V compounds in the ore suggests that oxidizing conditions were never really fully achieved. Oxidized V compounds are usually orange or bright yellow (Mann and Deutscher, 1978), therefore the observed greenish and greyish colours indicate that the U-rich groundwater was able to change from strongly oxidizing to weakly oxidizing at a salinity boundary or confluence. However, this water struggled to change back to a high oxidation state because the influence of marine fogs had become more prominent around the site of deposition, unlike in the main catchment area around the Spitzkoppe mountains.

It is not always the case that a range of colours in V compounds denote a continuous fluctuation between weakly oxidizing and fully oxidizing conditions as envisaged by Mann and Deutscher (1978). Sometimes it is simply a matter of a weakly oxidizing fluid unable to become fully oxidized.

8.2 General concepts governing the formation of both Langer Heinrich and Klein Trekkopje uranium deposits

In magmatic environments, V usually substitutes for Fe in minerals such as biotite. This study has shown that U minerals adsorb heavily onto the surfaces of biotite crystals during fractional crystallization of an ascending granitic magma. Laboratory experiments conducted by previous researchers have shown that clay minerals are quite important in concentrating not only U but also V in a sedimentary environment. This is due to the fact that clay particles have a powerful adsorption capacity, which enables them to capture a wide variety of ions and compounds in the groundwater.

Another experiment conducted on the interaction of U and V has revealed that when V, in its high oxidation state, is added to U compounds in the water, U is precipitated quickly as a yellow precipitate (Hostetler and Garrels, 1962). In nature this indicates that V is a powerful oxidant and its availability in the catchment area or in bedrock is therefore vital for the precipitation of carnotite.

Carnotite precipitation appears to be porosity-controlled because mineralization tends to be associated with fractures and clast surfaces, clearly reflecting the sites of water movement in an aquifer. The geochemistry of the deposits themselves provides a clue as to which elements had a controlling effect on uranium precipitation. In general, salinity plays a crucial role during the process of carnotite precipitation.

High salinity causes decomplexing of the uranyl carbonate complex. Aerated meteoric water entering the pond will then change the groundwater conditions from weakly oxidizing to strongly oxidizing. A continuous, strongly oxidizing environment in this pond will see carnotite precipitation taking place on a large scale. This was likely to have been the case during the formation of the Langer Heinrich deposit, where carnotite precipitation appears to have taken place for a long time without interruptions.

Frequent fluctuations in the redox conditions of the groundwater can either disrupt the process of decomplexing of uranyl carbonate complexes or the precipitation of V^{5+}. Such disruptions would result in the type of deposit found at Klein Trekkopje, where U grades are very low.

The main chemical traps at both the Langer Heinrich and Klein Trekkopje were the V-rich Tinkas schist, Kuiseb schist and saline brines close to the Atlantic Ocean. Some of these factors responsible for the formation of calcrete-hosted U deposits are interdependent. For instance evapo-transpiration depends on the geomorphological features of the channel bedrock. It is not always easy for these conditions to exist all at the same time.

The fact that the formation of a calcrete hosted U deposit is highly sensitive to a combination of factors mentioned above, demonstrates the low possibility of their existence in the Namib Desert and perhaps in other parts of the world.

In the Namib Desert, it is particularly difficult to form an attractive calcrete hosted uranium deposit because of the influence of marine fogs. A continuous inflow of fog into the channel may shift groundwater conditions towards a reducing environment, which means V^{4+} will find it difficult to transform into V^{5+}. By contrast, close to the escarpment, where the likelihood of good geomorphological features is high, groundwater conditions are likely to remain oxidizing throughout because of long distance from sea.

Too close to the sea, there will be endless, high salinity in the groundwater which is counterproductive because carnotite can only precipitate in sub-neutral, oxidizing conditions. A moderate degree of salinity is however necessary at the beginning of the deposit formation as it leads to the destabilization of uranyl carbonate complexes. If groundwater conditions are continuously oxidizing, it means U is likely to remain in solution and there is nothing to destabilize its complexes. These kinds of requirements suggest that the channel must just be in such a position that it is not too far from the escarpment and not too close to the sea.

Exploration for calcrete hosted U deposits could start with an investigation into the possible availability of V in the catchment area. Groundwater data from both Langer Heinrich and Klein Trekkopje areas have shown that high V concentrations in the water are usually associated with low U concentrations. This means V serves to precipitate U from solution, thereby lowering the U concentration in the groundwater. Percussion drilling data from the two deposits have also shown that high V concentrations in the

mineralized calcretes are associated with high U concentrations, again indicating the overwhelming influence of V on U mineralization.

Other ingredients like K, Mg, Sr, sulphate ion and chloride ion have all been found to have a minor effect on the precipitation of carnotite compared to V. Some factors like the availability of K and clay minerals control the precipitation of carnotite, but they are not critical to this study because in all likelihood they will always be available in nature. It has also emerged from this study that the evolution of fluids from a weakly oxidizing to a strongly oxidizing environment can only occur as a result of ponding. Fluids that are trapped in a pond for a long period of time will undergo evolution as fresh meteoric water continues to enter the pond. However ponding only occurs if the geomorphological features bounding the channel or on the channel floor are favourable.

An examination of results of borehole samples from the two U deposits has provided a clear link between the U grades and the depth. The data indicates that evapo-transpiration is one of the key controlling factors for carnotite precipitation. These areas of high U grades therefore represent the positions of the palaeo-water table because it is around the water table level that the groundwater conditions fluctuate between weakly oxidizing and strongly oxidizing. In general, an elevated water table (palaeo-high) will be exposed to more heat and will therefore see a higher degree of precipitation, not only for calcite or gypsum but also for carnotite.

Calcrete hosted U mineralization in the Namib Desert is of Quaternary age (Hambleton – Jones, 1976). Therefore these types of U deposits are likely to be still forming today. In fact, this has been demonstrated by previous researchers like Youlton (2006) who were able to show that in the groundwaters at both Langer Heinrich and Klein Trekkopje, carnotite precipitation predominates over dissolution. There is also a possibility that some calcrete hosted U deposits formed during the early days of aridification, might have been dismantled by subsequent high energy rivers heading seaward. This contributes to the rareness of these deposits.

The Langer Heinrich U deposit is very far from the shoreline and marine fogs would not reach it that easily. These fogs are not blown directly eastward because that is not the direction of the Benguela current. If the fogs were to be blown eastward, they would travel only about 100 km to reach Langer Heinrich but because of the general wind direction in the desert, it would take almost 130 km for these fogs to reach the Langer Heinrich area. Therefore disruption of strongly oxidizing conditions did not occur at Langer Heinrich.

Looking at the location of the Klein Trekkopje deposit, it can be seen that the marine fogs only had to travel about 70 km from the Swakopmund area to Klein Trekkopje. The Klein Trekkopje U deposit is located deeper into the desert compared to Langer Heinrich. This indicates there would be slightly more CO_2 and consequently more heat in the air directly above the Klein Trekkopje area. This could be the reason why there

are better developed gypcrete layers at Klein Trekkopje than at Langer Heinrich (Hambleton – Jones, 1976).

The Oligocene epoch was characterized by remarkable regression of the Atlantic Ocean and this has partly influenced erosion on the escarpment (Miller 2008). Although some researchers argue that the erosional episode might have started as early as 60 million years ago (Miller 2008), large-scale incision of the channels probably started around the Oligocene, triggered by the uplift over the escarpment. According to Hambleton-Jones (1976), the temperature for the Klein Trekkopje area has been slightly higher than that of Langer Heinrich area for the last 4 million years or so. U mineralization at both Klein Trekkopje and Langer Heinrich is younger than 100 000 years (Hambleton – Jones, 1976), which is long after the formation of first calcretes and gypcretes. The first calcretes and gypcretes are believed to have formed about 4 Ma (Wilkinson, 1990).

CHAPTER 9 : CONCLUSIONS

The mineralogy, geochemistry and texture for the Bloedkoppie granite are of such a nature that it weathers easily in the presence of water to release both U and some V. There is a slight possibility that a small proportion of uranium, possibly 10%, at Langer Heinrich was derived from the Abbabis Basement Complex via the ancestral Tumas River. An additional supply of V came from the Tinkas schist.

At Klein Trekkopje, there was a relatively larger volume of water and this created a dilution factor detrimental to the formation of a high grade deposit. The study also showed that there was a remarkable change in the Eh/pH conditions for the groundwater in the Langer Heinrich channel from the time of erosion to the time of carnotite precipitation. During erosion, the groundwater conditions were weakly oxidizing but the subsurface water went through a period of evolution to become strongly oxidizing. This evolution was mainly driven by the continuous interaction of groundwater with air and seasonal rains.

The study has outlined material differences between the two uranium deposits. Uranium mineralization at Langer Heinrich begins adjacent to the edge of the escarpment, while the Klein Trekkopje deposit is situated some 40 km to the west of the escarpment. This puts Klein Trekkopje at a disadvantage because part of the uranium gets precipitated along the way. The uranium deposited at Marenica and the 6000 ton U deposit a couple of hundred metres south of Klein Spitzkoppe granite should serve as a

classic example of how uranium is precipitated along the main channel system. Therefore in general, the further the deposit is from the escarpment, the poorer the grades.

The other significant outcome of the study is that the Langer Heinrich deposit is hosted by the V-rich Tinkas schist bedrock. V was found to be a key precipitant for uranium in the groundwater. Most of the V in the Klein Trekkopje deposit came from the Kuiseb schist. However, granitoids of both Damaran and post-Damaran age, also contributed V to the subsurface waters albeit to a lesser extent. While Klein Trekkopje is also hosted by the V rich Kuiseb schist in some areas, this is not always the case as other types of bedrock exist. These include Karibib marble, Karoo dolerite and Damara granites. Bedrock type is important from a geochemical point of view and it became an added advantage for U mineralization at Langer Heinrich.

The geomorphological features for two deposits are quite different. The Langer Heinrich area has a number of advantageous features which aid U mineralization, but which are not found at Klein Trekkopje. They include the Etusis and the Schieferberge schist, which are both highly resistant to erosion. The Etusis quartzite which bounds the Langer Heinrich deposit to the north does carry anomalous concentrations of U but it is highly resistant to erosion. These resistant lithologies have focused the fluids at Langer Heinrich along a narrow channel and have formed bedrock highs. The effect of bedrock highs is that the water table gets pushed closer to the surface and evapo-transpiration was enhanced, which results in effective carnotite precipitation.

The Klein Trekkopje area lacks these types of resistant lithologies. The dolerites around Klein Trekkopje which are highly resistant are limited in their regional distribution. The Karibib marble which resists erosion to a certain extent, cannot be compared to Etusis quartzite, for instance. As a result the fluids at Klein Trekkopje were poorly restricted and could not concentrate U along a single channel. A broad, unrestricted channel meant that the concentrations of ore forming ions would be diluted and carnotite saturation index would not be achieved easily. This partly explains the poor grades at Klein Trekkopje.

A further advantage at Langer Heinrich is that the deposit area has seen a lower influence of saline marine fogs during the Quaternary period. Since carnotite precipitation takes place in a strongly oxidizing environment, it was easier at Langer Heinrich to precipitate carnotite. At Klein Trekkopje, the influence of highly saline marine fogs prevented the groundwater conditions from becoming purely oxidizing. Although oxidizing conditions were achieved for the most part, the presence of green V compounds at Klein Trekkopje means that in certain parts of the channel, oxidizing conditions were not fully achieved.

The study found that moderate to high salinity leads to the decomplexing of uranyl carbonate complexes, which is a critical step towards carnotite precipitation. For carnotite to precipitate, groundwater salinity must evolve from a low oxidation state to a high oxidation state. Endless high salinity conditions can cause a persistently low oxidation state and even acidic conditions, which leads to the dissolution of carnotite.

Too close to the sea, marine fogs start to bring in counterproductive chemicals such as H_2S. This leads to a low Eh and acidic conditions in the groundwater, which inhibits carnotite precipitation. Therefore the closer towards the shoreline, the lower the chances of finding a good calcrete hosted U deposit.

From the conclusions above, it is obvious that during exploration, the Langer Heinrich type model will lead to the discovery of an attractive calcrete hosted U deposit. In the Namib Desert where marine fogs are active up to distances of 90 km from the shoreline, it will be impossible to find an attractive U deposit of this type within a distance of 30 km from the shoreline because in that zone V^{4+} can hardly transform into V^{5+}. Exploration for calcrete hosted deposits should therefore be focused on areas closer to the escarpment. Furthermore, exploration for these types of secondary deposits does not necessarily have to begin with radiometric surveys. It could start of by identifying the course of the channels on landsat images and identifying potential sources of U and V. To this end, rock chip sampling of the catchment area can start even before radiometric surveying, which is more costly. This will give an idea on whether there can be secondary U mineralization downdrainage. A quick investigation of geomorphological features will also be helpful because these types of deposits are, to a large extent, geomorphologically controlled. A flat looking landscape is not encouraging as it suggests a broad based, unrestricted flow. A rugged terrain, with channels dissecting it here and there, could be a good exploration target. After this exercise,

radiometric surveys and drilling can then follow if results from sampling of the catchment area are encouraging.

REFERENCES:

Ames, L. L., McGarrah, J. E. and Walker, B. E. (1983): Sorption of uranium and radium by biotite. *Clays and Clay Minerals, Vol. 31, No. 5, 343-351.*

Becker, E. and Hogarth, P. (2005): Mineral Deposit Retention License No. 2236, Langer Heinrich Uranium Project. Geological and Geotechnical Report for the period 16 August 1994 to 15 August 2005. Report prepared for the Ministry of Mines and Energy.

Becker, E. and Karner, K. (2007): Geological Setting of the Langer Heinrich Deposit, Namibia. IAEA-CN (ed.becker@paladinenergy.com.au).

Bittner, A. (2006): Electromagnetic Survey of the Palaeo-channel in the Trekkopje Uranium Mine Prospect area. *BIWAC-Hydrological Report for UraMin Namibia (Pty) Ltd.*

Bittner, A. (2009): Langer Heinrich Uranium Mine, Stage 3 Environmental Impact Assessment. Groundwater Specialist Input, Report No. 2009-11-V.D.2.

Bowell R.J., Barnes A., Grogan, J. (2009) Geochemical controls on secondary uranium mineralization in Namibian calcretes. *In: Lentz D. and Bowell, R.J. (eds) Special Issue 24th IAGS in Geochemistry, Exploration, Environment and Analysis. Volume 9. (In press).*

Bowell R.J., Laight T., Arthur J. & Barnes A., van Noort E. and Young J. (2010): Geochemical controls on uranium precipitation in palaeo-channel and pedogenic calcrete deposits, Marenica, Namibia. *In proceedings of Uranium Geology 2010. AusIMM conference, Adelaide. 21-24.*

Carlisle, D., Merifield, P., Orme, A. and Kolker, O., (1978): The distribution of calcretes and gypcretes in South – western United States and their uranium

favourability, based on a study of deposits in Western Australia and South West Africa. *U.S. Dep. Energy, Open File Rep GJBX 29 (78), 274 pp.*

Chetty, D., Kruger, S. J., Gould, D. G. and Pircalaboiu, G.: (1999): Pre-feasibility Study of the Trekkopje Uranium Deposits. *Inter-consult Namibia (Pty) Ltd and MINTEK, Report for Gulf Western Trading, Trekkopje Exclusive Prospecting License 2218.*

Cuney, M. (2008): The extreme diversity of uranium deposits. *Mineralium Depositor, www.Springerlink.com, accessed March 2010.*

Frindt, S., Haapala, I. and Pakkanen, L. (2004a): Anorogenic Gross Spitzkoppe granite stock in central western Namibia: Part I. Petrology and Geochemistry. *American Mineralogist, Volume 89, pages 841 – 856, 2004.*

Frindt S. and Haapala I., (2004b): Anorogenic Gross Spitzkoppe granite stock in central western Namibia: Part II. Structures and textures indicating crystallization from undercooled melt. *American Mineralogist, Volume 89, pages 857 – 866, 2004.*

Frindt, S., Robert B., Trumbull, Rolf L. Romer (2004c): Petrogenesis of the Gross Spitzkoppe topaz granite, central western Namibia: a geochemical and Nd-Sr-Pb isotope study. *Chemical Geology 206 (2004) 43-71.*

Ghabru, S. K., Mermut, A. R. and Arnaud, R.J.ST (1989): Layer-charge and cation-exchange characteristics of vermiculite (weathered biotite) isolated from a gray luvisol in north eastern Saskatchewan. *Clays and Clay Minerals, Vol. 37, No.2, 164-172, 1989.*

Hambleton-Jones, B.B. (1976): The Geology and Geochemistry of some epigenetic uranium deposits near the Swakop River, South-West Africa. –

University of Pretoria; Ph.D. Thesis; 306 p. *Nuclear Development Corporation of South Africa (Pty) Ltd, October 1983.*

Hambleton-Jones, B.B. (1984): Surficial Uranium Deposits in Namibia. In: Surficial Uranium Deposits: *Report of the working group on uranium geology; IAEA-TECDOC- 322; International Atomic Energy Agency; Vienna; pp. 205-216.*

Hartleb, J.W.O. (1988): The Langer Heinrich Uranium Deposit: Southwest Africa/Namibia. (*Ore geology reviews, vol. 3, 1998. P 277 – 287*).

Hobday, D.K. and Galloway, W.E., (1999): Groundwater processes and sedimentary uranium deposits. *Hydrogeology Journal, 7, 127-138.*

Hostetler, P. B. and R. M. Garrels, R.M., (1962): Transportation and precipitation of uranium and vanadium at low temperatures, with special reference to the sandstone type uranium deposits. *1962 Society of Economic Geologists, Inc. Economic Geology, v. 57, pp. 137-167.*

Huff, L. C. and Lesure, F. G. (1962): Diffusion features of uranium-vanadium deposits in Montezuma Canyon, Utah. *Economic Geology Vol. 57, 1962, pp. 226 – 237.*

Hussey, m. (2006): Langer Heinrich hyperspectral surveys, a poster prepared after surveys (Hyvista Corporation).

Kamona, F. (2011): Concentration of U and Th in the Bloedkoppie Granite, Namibia. *In Merkel, B., Schipek, M. (2011): The New Uranium Mining Boom, Challenge and Lessons learned, pp111 - 117.*

Kandara, J. R., (1998): Petrography and Geochemistry of the Klein Spitzkoppe Granite Complex, Central-western Namibia. *MSc Thesis, University of Helsinki, Finland.*

Maasen, L. (1982): Geochemistry of Sedimentary Uranium. *MSc. Mineral Exploration Seminars 1982 – Uranium Deposits.*

Macpherson I., Schnell H., Day P., Perie C., Limpitlaw D. and Mandziak T. (2008): *Presentation to the Ministry of Mines and Energy on Trekkopje Project – Introduction and Project Description.*

Mann, A. W. and Deutscher, R. L. (1978): Genesis principles for the precipitation of carnotite in the calcrete drainages in western Australia. *Economic Geology, Vol. 73, 1978, pp. 1724 – 1737.*

Marlow, A. G. (1981): Remobilization of and Primary Uranium Genesis in the Damaran Orogenic Belt, Namibia. *Ph.D thesis, Leeds University.*

Mc Dermott, P. F. (1986): Granite petrogenesis and crustal evolution studies in the Damara Pan-African Orogenic belt, Namibia. *PhD thesis, the Open University.*

Miller, R. (2008): The geology of Namibia, Volume 1 - 3. *Geological Survey of Namibia.*

Miller, R. (2009): How important was differentiation and deuteric recrystalization in modifying uranium distribution and apparent ages of Namibia's uraniferous alaskites. *A presentation given to the Geological society of Namibia..*

Moran, A. V., (2006): National Instrument 43-101 Technical Report. Initial Resource Estimate for the Trekkopje Uranium Project Feasibility Study.

Swakopmund and Karibib Districts, Erongo Region, Namibia. *Prepared for: UraMin Inc. 204 Rivona Road, Block A Morningside, Sandton, Gauteng 2057 South Africa. SRK Consulting report dated November 28, 2006.*

Notestein B. F., (1918): Some chemical experiments bearing on the origin of certain uranium-vanadium ores. *1918 Society of Economic Geologists, Inc. Economic Geology, v. 13, pp. 50-64.*

Skirrow, R. G., Jaireth, S., Huston, D. L., Bastrakov, E. N., Schofield, A., van der Wielen, S. E. & Barnicoat, A. C.: (2009). Uranium Mineral systems: Processes, exploration criteria and a new deposit framework. *Geoscience Australia, 2009/20, Geocat # 69124.*

Van Noort, E., (2010): Marenica Drilling data (uranium and vanadium). Hole ID's: MAR0133, MAR0147, MAR0148, etc.(i*n press).*

Ward, J. (1984): Aspects of the Cenozoic geology in the Kuiseb Valley, Central Namib Desert. *PhD thesis, University of Natal.*

Wilkinson, M. J. (1990): Palaeoenvironments in the Namib Desert: the lower Tumas Basin in the late Cenozoic. *University of Chicago, geography research paper; no. 231.*

World Nuclear Association (2010): Geology of Uranium Deposits. www.world-nuclear.org, accessed January 2010.

World Nuclear Association (2010): Uranium in Namibia. www.world-nuclear.org, accessed February 2010.

Youlton, B. (2006): Controls on uranium mineralization at the Klein Trekkopje prospect, Namibia. *Honours Project supervised by Prof. Judith Kinnaird and Prof. Richard Viljoen.*

www.paladinenery.com.au: →Project Status → Geology and Resources.

www.areva.com: Trekkopje uranium mine.

Google search: uranium sorption on biotite and clay minerals.

Appendix 1: Detection limits for ICP analysis by ALS Chemex Laboratory in Johannesburg.

Element	Symbol	Units	Lower Limit	Upper Limit
Silver	Ag	ppm	0.01	100
Aluminum	Al	%	0.01	50
Arsenic	As	ppm	0.2	10 000
Barium	Ba	ppm	10	10 000
Beryllium	Be	ppm	0.05	1 000
Bismuth	Bi	ppm	0.01	10 000
Calcium	Ca	%	0.01	50
Cadmium	Cd	ppm	0.02	1 000
Cerium	Ce	ppm	0.01	500
Cobalt	Co	ppm	0.1	10 000

Element	Symbol	Units	Lower Limit	Upper Limit
Chromium	Cr	ppm	1	10 000
Cesium	Cs	ppm	0.05	500
Copper	Cu	ppm	0.2	10 000
Iron	Fe	%	0.01	50
Gallium	Ga	ppm	0.05	10 000
Germanium	Ge	ppm	0.05	500
Hafnium	Hf	ppm	0.1	500
Indium	In	ppm	0.005	500
Potassium	K	%	0.01	10
Lanthanum	La	ppm	0.5	10 000
Lithium	Li	ppm	0.2	10 000
Magnesium	Mg	%	0.01	50

Element	Symbol	Units	Lower Limit	Upper Limit
Manganese	Mn	ppm	5	100 000
Molybdenum	Mo	ppm	0.05	10 000
Sodium	Na	%	0.01	10
Niobium	Nb	ppm	0.1	500
Nickel	Ni	ppm	0.2	10 000
Phosphorous	P	ppm	10	10 000
Lead	Pb	ppm	0.5	10 000
Rubidium	Rb	ppm	0.1	10 000
Rhenium	Re	ppm	0.002	50
Sulphur	S	%	0.01	10
Antimony	Sb	ppm	0.05	10 000
Scandium	Sc	ppm	0.1	10 000

Element	Symbol	Units	Lower Limit	Upper Limit
Selenium	Se	ppm	1	1 000
Tin	Sn	ppm	0.2	500
Strontium	Sr	ppm	0.2	10 000
Tantalum	Ta	ppm	0.05	100
Tellurium	Te	ppm	0.05	500
Thorium	Th	ppm	0.2	10 000
Titanium	Ti	%	0.005	10
Thallium	Tl	ppm	0.02	10 000
Uranium	U	ppm	0.1	10 000
Vanadium	V	ppm	1	10 000
Tungsten	W	ppm	0.1	10 000
Yttrium	Y	ppm	0.1	500

Element	Symbol	Units	Lower Limit	Upper Limit
Zinc	Zn	ppm	2	10 000
Zirconium	Zr	ppm	0.5	500
Dysprosium	Dy	ppm	0.05	1 000
Erbium	Er	ppm	0.03	1 000
Europium	Eu	ppm	0.03	1 000
Gadolinium	Gd	ppm	0.05	1 000
Holmium	Ho	ppm	0.01	1 000
Lutetium	Lu	ppm	0.01	1 000
Neodymium	Nd	ppm	0.1	1 000
Praseodymium	Pr	ppm	0.03	1 000
Samarium	Sm	ppm	0.03	1 000
Terbium	Tb	ppm	0.01	1 000

Element	Symbol	Units	Lower Limit	Upper Limit
Thulium	Tm	ppm	0.01	1 000
Ytterbium	Yb	ppm	0.03	1 000

Appendix 2: XRD analyses for samples LCALC1, Tink7, SP-CL-1, SP-CL-2, Bloed11 and SP4 (SP – CL stands for clay derived from the Klein Spitzkoppe granite, Geochemistry Laboratory, Geological Survey of Namibia).

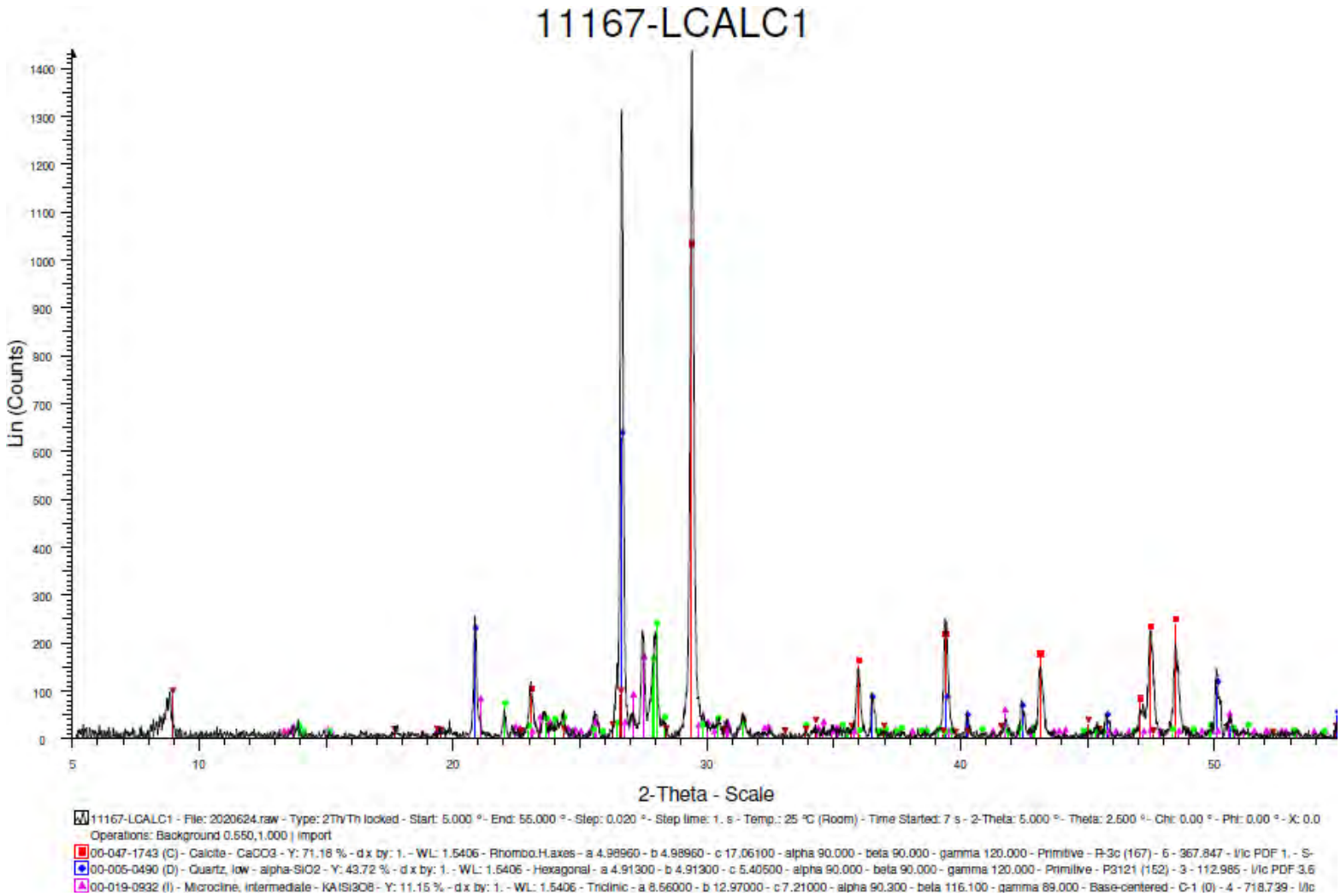

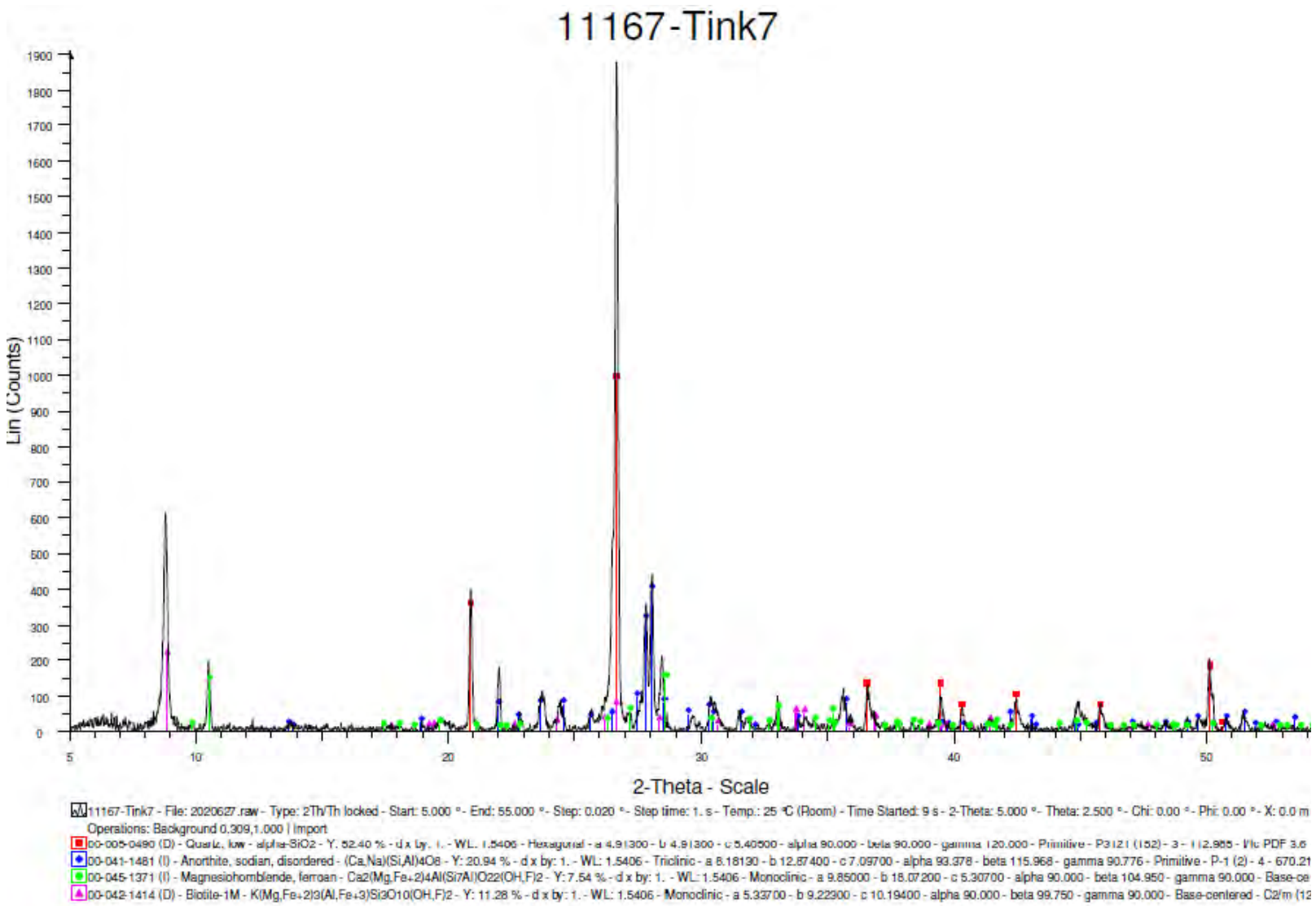
11167-Tink7
Lin (Counts)
2-Theta - Scale
11167-Tink7 - File: 20206Z7.raw - Type: 2Th/Th locked - Start: 5.000 °- End: 55.000 °- Step: 0.020 °- Step time: 1. s - Temp.: 25 °C (Room) - Time Started: 9 s - 2-Theta: 5.000 °- Theta: 2.500 °- Chi: 0.00 °- Phi: 0.00 °- X: 0.0 m
Operations: Background 0.309,1.000 | Import
00-005-0490 (D) - Quartz, low - alpha-SiO2 - Y: 52.40 % - d x by: 1. - WL: 1.5406 - Hexagonal - a 4.91300 - b 4.91300 - c 5.40500 - alpha 90.000 - beta 90.000 - gamma 120.000 - Primitive - P3121 (152) - 3 - 112.985 - I/Ic PDF 3.6
00-041-1481 (I) - Anorthite, sodian, disordered - (Ca,Na)(Si,Al)4O8 - Y: 20.94 % - d x by: 1. - WL: 1.5406 - Triclinic - a 8.18130 - b 12.87400 - c 7.09700 - alpha 93.378 - beta 115.968 - gamma 90.776 - Primitive - P-1 (2) - 4 - 670.21
00-045-1371 (I) - Magnesiohornblende, ferroan - Ca2(Mg,Fe+2)4Al(Si7Al)O22(OH,F)2 - Y: 7.54 % - d x by: 1. - WL: 1.5406 - Monoclinic - a 9.85000 - b 18.07200 - c 5.30700 - alpha 90.000 - beta 104.950 - gamma 90.000 - Base-ce
00-042-1414 (D) - Biotite-1M - K(Mg,Fe+2)3(Al,Fe+3)Si3O10(OH,F)2 - Y: 11.28 % - d x by: 1. - WL: 1.5406 - Monoclinic - a 5.33700 - b 9.22300 - c 10.19400 - alpha 90.000 - beta 99.750 - gamma 90.000 - Base-centered - C2/m (12

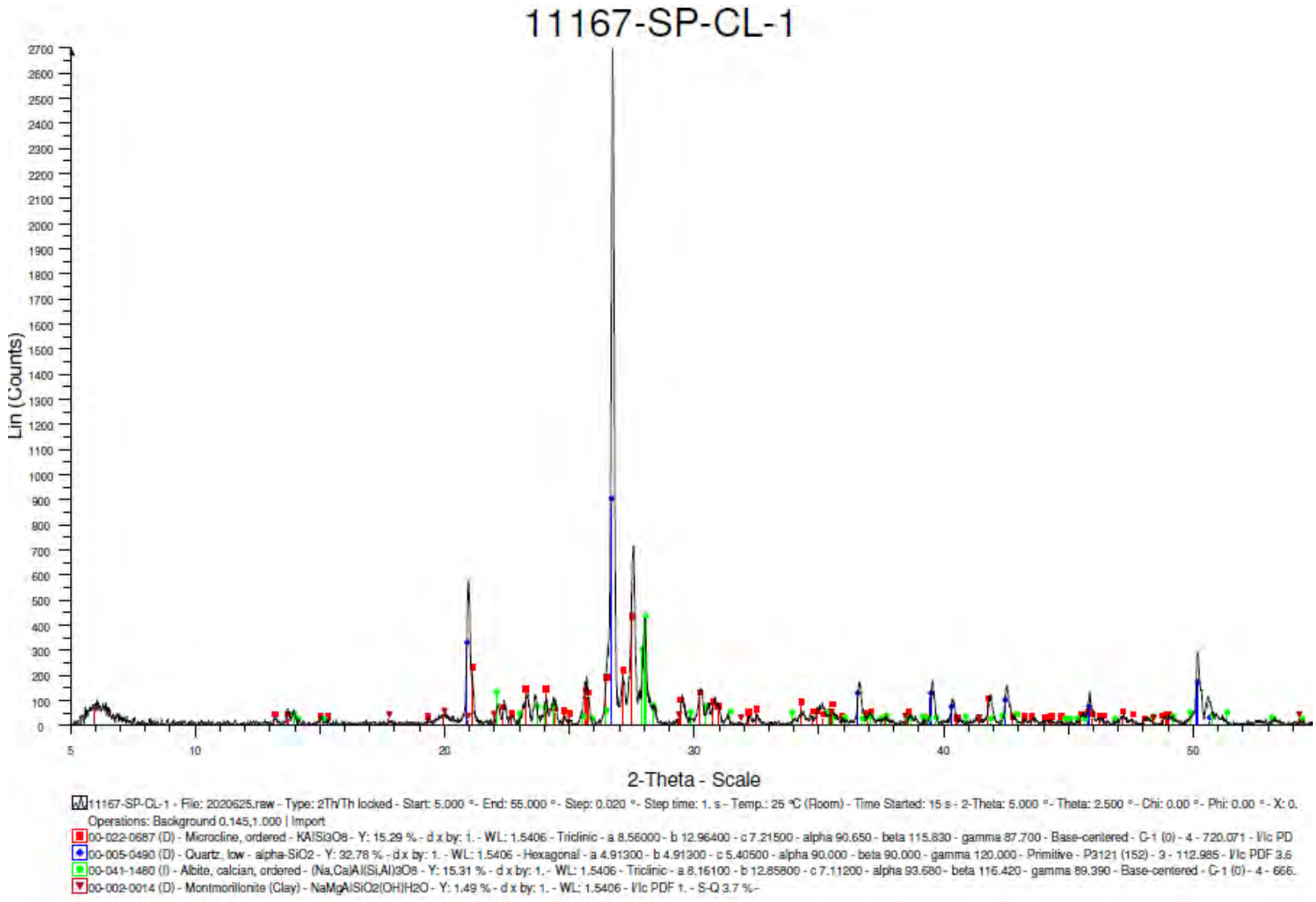
11167-SP-CL-1
Lin (Counts)
2-Theta - Scale
11167-SP-CL-1 - File: 2020625.raw - Type: 2Th/Th locked - Start: 5.000 ° - End: 55.000 ° - Step: 0.020 ° - Step time: 1. s - Temp.: 25 °C (Room) - Time Started: 15 s - 2-Theta: 5.000 ° - Theta: 2.500 ° - Chi: 0.00 ° - Phi: 0.00 ° - X: 0.
Operations: Background 0.145,1.000 | Import
00-022-0687 (D) - Microcline, ordered - KAlSi3O8 - Y: 15.29 % - d x by: 1. - WL: 1.5406 - Triclinic - a 8.56000 - b 12.96400 - c 7.21500 - alpha 90.650 - beta 115.830 - gamma 87.700 - Base-centered - C-1 (0) - 4 - 720.071 - I/Ic PD
00-005-0490 (D) - Quartz, low - alpha-SiO2 - Y: 32.78 % - d x by: 1. - WL: 1.5406 - Hexagonal - a 4.91300 - b 4.91300 - c 5.40500 - alpha 90.000 - beta 90.000 - gamma 120.000 - Primitive - P3121 (152) - 3 - 112.985 - I/Ic PDF 3.6
00-041-1480 (I) - Albite, calcian, ordered - (Na,Ca)Al(Si,Al)3O8 - Y: 15.31 % - d x by: 1. - WL: 1.5406 - Triclinic - a 8.16100 - b 12.85800 - c 7.11200 - alpha 93.680 - beta 116.420 - gamma 89.390 - Base-centered - C-1 (0) - 4 - 666.
00-002-0014 (D) - Montmorillonite (Clay) - NaMgAlSiO2(OH)H2O - Y: 1.49 % - d x by: 1. - WL: 1.5406 - I/Ic PDF 1. - S-Q 3.7 %-

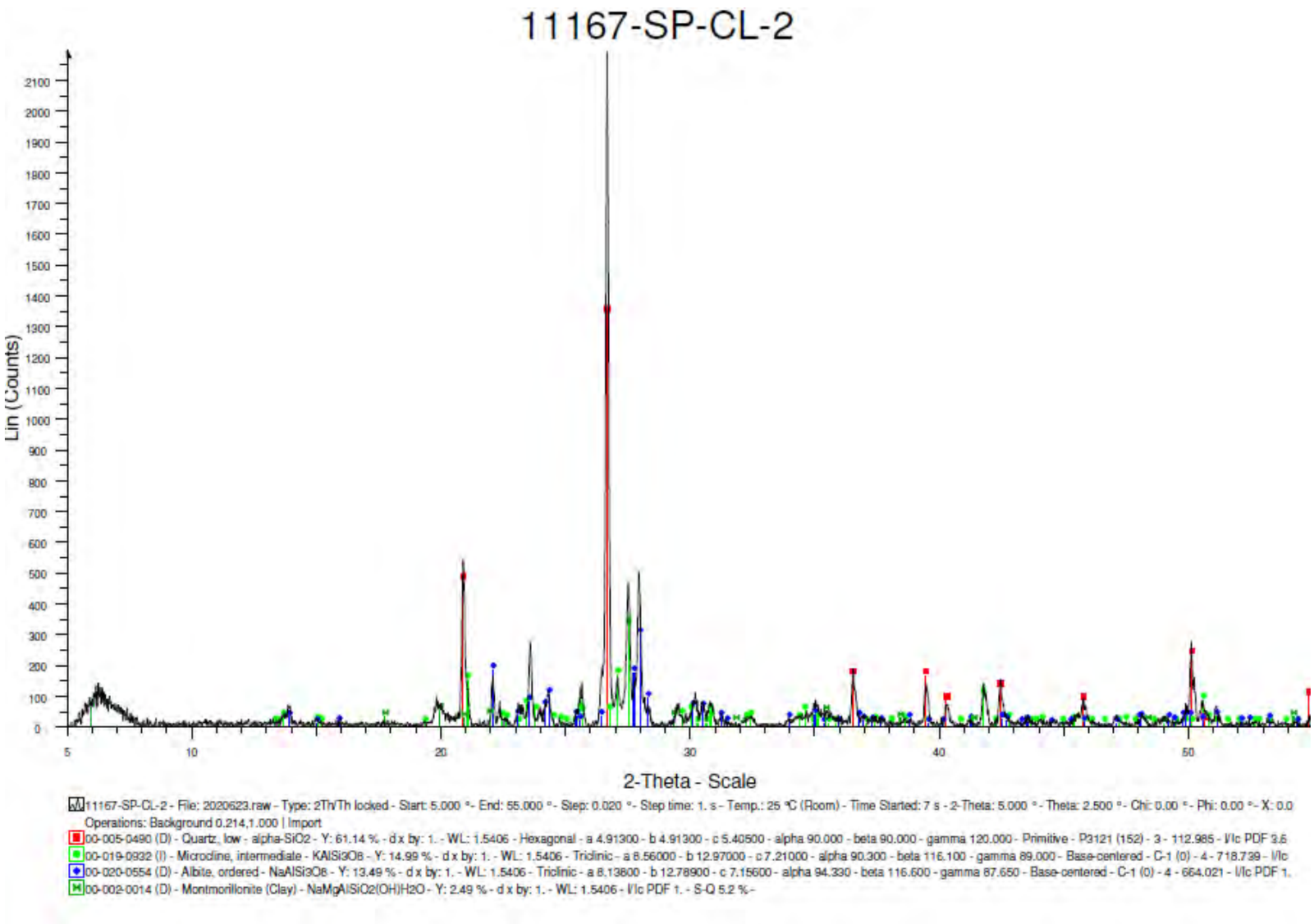
11167-SP-CL-2
Lin (Counts)
2-Theta - Scale
11167-SP-CL-2 - File: 2020623.raw - Type: 2Th/Th locked - Start: 5.000 ° - End: 55.000 ° - Step: 0.020 ° - Step time: 1. s - Temp.: 25 °C (Room) - Time Started: 7 s - 2-Theta: 5.000 ° - Theta: 2.500 ° - Chi: 0.00 ° - Phi: 0.00 ° - X: 0.0
Operations: Background 0.214,1.000 | Import
00-005-0490 (D) - Quartz, low - alpha-SiO2 - Y: 61.14 % - d x by: 1. - WL: 1.5406 - Hexagonal - a 4.91300 - b 4.91300 - c 5.40500 - alpha 90.000 - beta 90.000 - gamma 120.000 - Primitive - P3121 (152) - 3 - 112.985 - I/Ic PDF 3.6
00-019-0932 (I) - Microcline, intermediate - KAlSi3O8 - Y: 14.99 % - d x by: 1. - WL: 1.5406 - Triclinic - a 8.56000 - b 12.97000 - c 7.21000 - alpha 90.300 - beta 116.100 - gamma 89.000 - Base-centered - C-1 (0) - 4 - 718.739 - I/Ic
00-020-0554 (D) - Albite, ordered - NaAlSi3O8 - Y: 13.49 % - d x by: 1. - WL: 1.5406 - Triclinic - a 8.13800 - b 12.78900 - c 7.15600 - alpha 94.330 - beta 116.600 - gamma 87.650 - Base-centered - C-1 (0) - 4 - 664.021 - I/Ic PDF 1.
00-002-0014 (D) - Montmorillonite (Clay) - NaMgAlSiO2(OH)H2O - Y: 2.49 % - d x by: 1. - WL: 1.5406 - I/Ic PDF 1. - S-Q 5.2 %

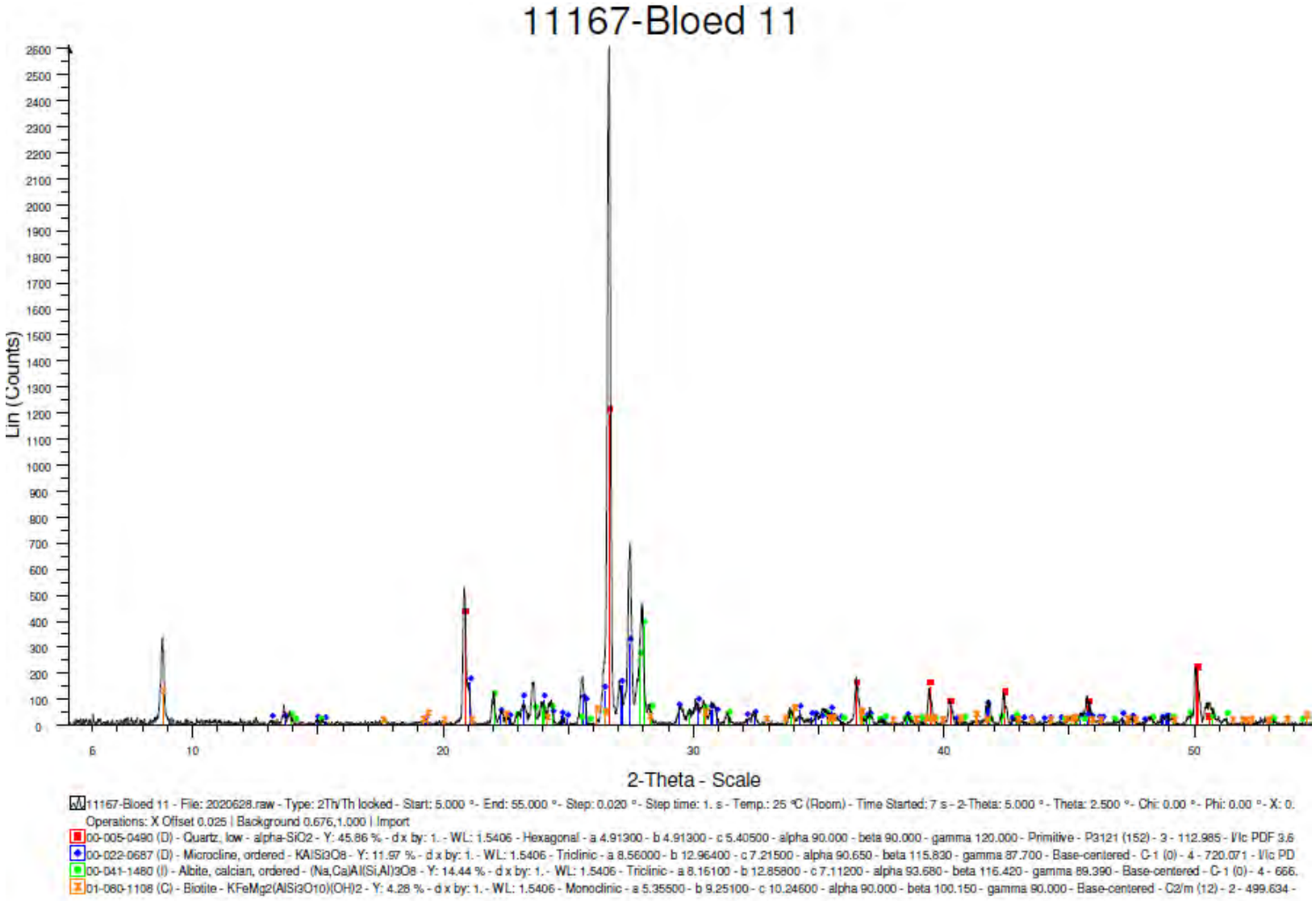
11167-Bloed 11
Lin (Counts)
2600
2500
2400
2300
2200
2100
2000
1900
1800
1700
1600
1500
1400
1300
1200
1100
1000
900
800
700
600
500
400
300
200
100
0
6
10
20
30
40
50
2-Theta - Scale
11167-Bloed 11 - File: 2020628.raw - Type: 2Th/Th locked - Start: 5.000 °- End: 55.000 °- Step: 0.020 °- Step time: 1. s - Temp.: 25 °C (Room) - Time Started: 7 s - 2-Theta: 5.000 °- Theta: 2.500 °- Chi: 0.00 °- Phi: 0.00 °- X: 0.
Operations: X Offset 0.025 | Background 0.676,1.000 | Import
00-005-0490 (D) - Quartz, low - alpha-SiO2 - Y: 45.86 % - d x by: 1. - WL: 1.5406 - Hexagonal - a 4.91300 - b 4.91300 - c 5.40500 - alpha 90.000 - beta 90.000 - gamma 120.000 - Primitive - P3121 (152) - 3 - 112.985 - I/Ic PDF 3.6
00-022-0687 (D) - Microcline, ordered - KAlSi3O8 - Y: 11.97 % - d x by: 1. - WL: 1.5406 - Triclinic - a 8.56000 - b 12.96400 - c 7.21500 - alpha 90.650 - beta 115.830 - gamma 87.700 - Base-centered - C-1 (0) - 4 - 720.071 - I/Ic PD
00-041-1480 (I) - Albite, calcian, ordered - (Na,Ca)Al(Si,Al)3O8 - Y: 14.44 % - d x by: 1. - WL: 1.5406 - Triclinic - a 8.16100 - b 12.85800 - c 7.11200 - alpha 93.680 - beta 116.420 - gamma 89.390 - Base-centered - C-1 (0) - 4 - 666.
01-080-1108 (C) - Biotite - KFeMg2(AlSi3O10)(OH)2 - Y: 4.28 % - d x by: 1. - WL: 1.5406 - Monoclinic - a 5.35500 - b 9.25100 - c 10.24600 - alpha 90.000 - beta 100.150 - gamma 90.000 - Base-centered - C2/m (12) - 2 - 499.634 -

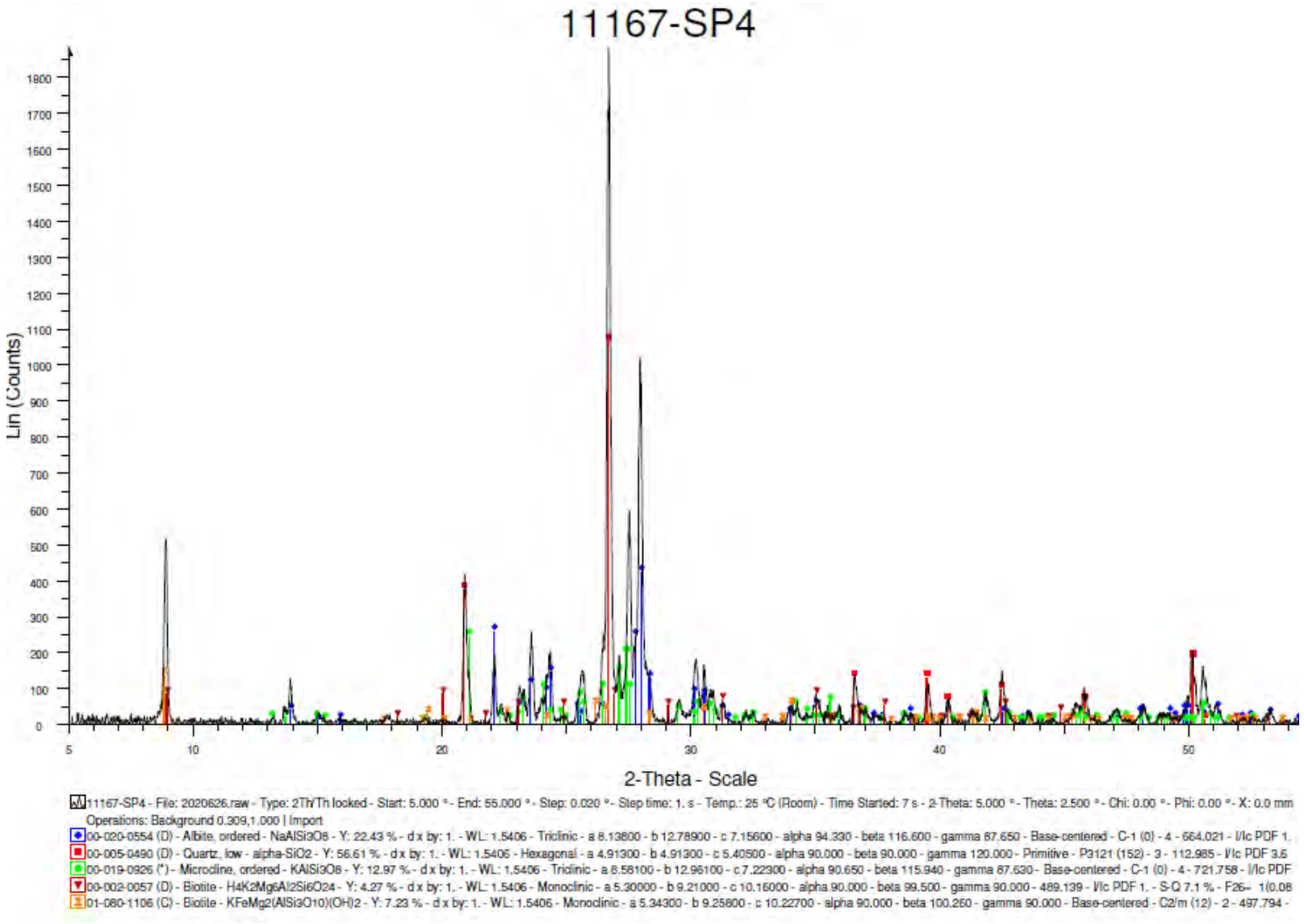
11167-SP4
Lin (Counts)
2-Theta - Scale
11167-SP4 - File: 2020626.raw - Type: 2Th/Th locked - Start: 5.000 ° - End: 55.000 ° - Step: 0.020 ° - Step time: 1. s - Temp.: 25 °C (Room) - Time Started: 7 s - 2-Theta: 5.000 ° - Theta: 2.500 ° - Chi: 0.00 ° - Phi: 0.00 ° - X: 0.0 mm
Operations: Background 0.309,1.000 | Import
00-020-0554 (D) - Albite, ordered - NaAlSi3O8 - Y: 22.43 % - d x by: 1. - WL: 1.5406 - Triclinic - a 8.13800 - b 12.78900 - c 7.15600 - alpha 94.330 - beta 116.600 - gamma 87.650 - Base-centered - C-1 (0) - 4 - 664.021 - I/Ic PDF 1.
00-005-0490 (D) - Quartz, low - alpha-SiO2 - Y: 56.61 % - d x by: 1. - WL: 1.5406 - Hexagonal - a 4.91300 - b 4.91300 - c 5.40500 - alpha 90.000 - beta 90.000 - gamma 120.000 - Primitive - P3121 (152) - 3 - 112.985 - I/Ic PDF 3.5
00-019-0926 (*) - Microcline, ordered - KAlSi3O8 - Y: 12.97 % - d x by: 1. - WL: 1.5406 - Triclinic - a 8.58100 - b 12.96100 - c 7.22300 - alpha 90.650 - beta 115.940 - gamma 87.630 - Base-centered - C-1 (0) - 4 - 721.758 - I/Ic PDF
00-002-0057 (D) - Biotite - H4K2Mg6Al2Si6O24 - Y: 4.27 % - d x by: 1. - WL: 1.5406 - Monoclinic - a 5.30000 - b 9.21000 - c 10.16000 - alpha 90.000 - beta 99.500 - gamma 90.000 - 489.139 - I/Ic PDF 1. - S-Q 7.1 % - F26= 1(0.08
01-080-1106 (C) - Biotite - KFeMg2(AlSi3O10)(OH)2 - Y: 7.23 % - d x by: 1. - WL: 1.5406 - Monoclinic - a 5.34300 - b 9.25800 - c 10.22700 - alpha 90.000 - beta 100.260 - gamma 90.000 - Base-centered - C2/m (12) - 2 - 497.794 -

Appendix 3: ICP-MS analyses for samples collected by the writer, ALS Chemex Laboratory, Johannesburg (see units in Appendix 1).

	Ag	Al	As	Ba	Be	Bi	Ca	Cd	Ce	Co	Cr	Cs	Cu	Fe	Ga	Ge	Hf	In	K	La	Li	Mg	Mn	Mo	Na	Nb	Ni	P	Pb	Rb	Re
SP1	0.03	6.21	<0.2	10	10.25	0.08	0.2	0.44	53.1	0.5	5	14.95	10.3	0.57	52.9	0.1	7.1	0.098	2.89	18.9	201	<0.01	193	0.34	3.09	58.1	2	10	64.6	870	<0.002
SP2	0.02	5.92	<0.2	10	10.85	0.15	0.19	0.42	54.2	0.4	7	13.55	7.7	0.55	50.4	0.1	6.7	0.094	2.87	18.5	198.5	<0.01	194	0.34	2.92	45.5	2	<10	65.7	860	<0.002
SP3	<0.01	6.28	<0.2	10	5.03	0.03	0.46	0.18	65.9	0.4	7	6.56	3.8	0.95	41.4	0.13	4.8	0.031	3.23	26.3	127.5	<0.01	148	0.49	2.57	99.6	2.2	<10	44.2	560	<0.002
SP4	<0.01	6.38	0.4	10	5.55	0.16	0.44	0.19	52	0.5	7	8.56	3.7	1.09	43.7	0.13	5.9	0.043	3.34	20.7	138.5	0.01	203	0.54	2.55	107	2.3	<10	58.8	610	<0.002
SP5	<0.01	6.5	0.8	20	6	0.1	0.47	0.25	67.5	0.5	6	8.86	3.9	1.22	45.3	0.16	4.5	0.043	3.46	26.5	168.5	0.01	363	1.07	2.63	102	1.9	<10	109	630	<0.002
SP6	<0.01	6.33	1.6	10	4.77	0.07	0.48	0.22	57.3	0.7	8	5.4	3.7	0.91	41.6	0.13	6.6	0.032	3.27	22.4	120.5	0.01	116	0.59	2.72	100.5	2.6	<10	47.7	540	<0.002
Gross 1	0.35	6.43	2.9	100	7.79	0.06	0.67	0.28	260	0.8	9	8.77	2.9	1.48	35.7	0.31	5.9	0.06	4.04	137.5	117	0.03	182	1.41	2.21	162.5	1.7	140	38	510	<0.002
Gross2	<0.01	5.9	2.9	110	11.35	0.05	0.68	0.27	255	1.2	7	7.72	3.4	1.57	32.2	0.31	5.6	0.053	3.54	135.5	104	0.03	199	1.12	2.02	141	3.3	400	31.9	440	<0.002
Gross3	<0.01	6.78	0.8	190	6.29	0.03	0.11	0.29	234	2.2	6	10.25	5.3	1.96	33.6	0.3	2.8	0.046	4.45	113.5	139.5	0.1	197	0.72	1.41	109	3.7	240	35.9	480	<0.002
TCalc1	0.05	6.63	<5	280	1.33	0.18	10.3	0.14	26.5	2.5	16	5.24	8.4	0.74	8.61	0.15	0.8	0.02	2.45	15	10.5	0.68	136	0.64	0.6	4.7	3.3	400	20.7	138	<0.002
TCalc2	0.05	3.11	<5	270	1.23	0.27	16.75	0.16	17.25	2.4	13	4.16	10.1	0.58	7.37	0.07	0.5	0.015	2.31	10.1	9.5	0.45	120	0.7	0.62	3.9	1	330	19.4	129.5	<0.002
SC1	0.11	5.7	<0.2	250	1.06	0.04	0.62	0.13	71.5	9.7	51	5.64	9.2	2.65	14.4	0.17	0.6	0.048	1.29	35.3	47.9	1.07	171	0.4	2.36	9.2	22.2	790	3.6	71.4	<0.002
SC2	0.06	5.96	<0.2	290	1.78	0.05	0.78	0.16	70.9	9.9	57	10.9	4.4	2.77	15.5	0.19	0.9	0.049	1.22	34.3	43.5	1.09	196	0.46	2.63	12.3	26.3	970	4.9	86	<0.002
SC3	0.05	5.78	4.4	330	3.02	0.11	0.83	0.21	77	9.9	54	10.4	1.6	2.87	15.45	0.2	0.7	0.059	1.17	37.9	43.4	1	364	0.39	2.45	14.8	23.7	840	4.8	80.6	<0.002
2Sc1	0.04	7.84	1.2	330	4.11	0.07	1.64	0.27	68	16.3	92	20	17.4	4.66	22.5	0.23	2.7	0.116	2.41	32.3	70.3	2.07	562	0.78	1.74	14.2	52.2	1060	6.9	159	<0.002
2Sc2	0.12	7.67	<0.2	410	3.81	0.08	1.58	0.25	77.5	12.3	95	19.7	6.6	4.44	22.4	0.28	2.6	0.104	2.56	35.7	77.6	2.03	464	0.5	1.87	13.6	47.8	1220	6.5	172	<0.002
2Sc3	0.11	8.24	2	390	3.87	0.08	1.9	0.25	62.6	16.7	102	14.7	1.4	4.43	25.2	0.25	1.2	0.099	2.31	28.5	94.3	1.97	492	0.44	2.58	14	42.1	760	7.1	98.7	<0.002
Sc4	0.08	5.82	4.2	250	2.11	0.04	0.82	0.15	74.1	8.7	47	8.56	6.5	2.11	15.3	0.21	0.4	0.04	1.07	36.6	39.7	1	163	0.29	2.62	9.1	23.4	710	6	72.4	<0.002
Sc5	0.06	5.66	11.9	280	2.02	0.04	0.89	0.17	86	10.1	61	8.8	5.8	2.79	15.2	0.24	1	0.05	1.15	41.2	40.7	1.01	290	0.48	2.36	13.7	26.2	1620	4.4	75.5	<0.002
AB1	0.04	7.62	2.6	1890	4.32	0.03	1.7	0.2	263	9	13	3.76	5.5	2.76	20.1	0.43	1.4	0.091	4.25	132.5	36.7	0.87	774	0.73	2.14	18.7	7.1	2070	32	284	<0.002

AB2	0.06	7.32	6.1	380	5.34	0.08	3.64	0.21	197	5.8	31	1.3	0.8	1.97	23.1	0.35	1	0.173	1.32	82.8	21.4	0.82	1080	0.77	3.2	27.6	9.2	1900	16.1	48.6	<0.002
AB3	0.04	7.37	3.1	1790	3.96	0.12	1.84	0.3	264	8.6	14	0.9	1.4	3.46	20.1	0.42	1.8	0.134	4.32	133.5	17.6	0.72	908	0.88	2.05	18.2	9.4	1690	54.6	195	<0.002
AB4	0.03	7.17	1.1	1270	1.56	0.02	0.73	0.04	22.3	1.4	7	3.38	3.3	0.39	14.8	0.09	1	0.006	5.34	12.4	19	0.1	131	0.34	1.5	2.5	2.8	610	45.5	281	<0.002
AB5	0.03	7.53	4.2	870	3.41	0.02	1.43	0.05	16.9	1	7	2.61	1.7	0.32	17.65	0.06	1.2	<0.005	4.49	10.3	20.9	0.06	89	0.32	2.11	1.4	2.1	400	35.4	230	<0.002
Bloed1	<0.01	6.6	1	70	14.8	0.18	0.53	0.1	9.51	2.4	7	7.43	3.3	0.65	24.4	0.06	2.2	0.015	2.22	7	44.3	0.04	450	0.51	3.04	53.6	5.8	100	45.4	248	<0.002
Bloed2	<0.01	6.66	1.4	80	12.25	0.09	0.4	0.08	19.85	1	7	9.16	2	0.76	24.5	0.11	2.6	0.013	3.27	13.2	65.5	0.05	286	0.44	2.56	63.8	2.4	170	62.9	380	<0.002
Bloed3	0.03	6.69	1.4	50	11.1	0.1	0.44	0.1	14.15	1	7	8.31	1.7	0.72	25.2	0.07	4	0.01	3.11	5.7	60	0.06	575	0.54	2.66	39.3	2.3	160	56.4	369	<0.002
Bloed4	<0.01	6.49	1.7	90	11	0.25	0.49	0.26	15.3	0.8	5	8.64	2.1	0.68	22.7	0.07	1.9	0.021	3.11	7.4	58.7	0.05	282	0.4	2.54	26.3	2.3	210	60	332	<0.002
Bloed5	<0.01	6.39	2.3	80	10.55	0.06	0.44	0.12	11.65	1	5	6.41	3.4	0.51	22.4	0.06	2.2	0.008	3.32	5.5	48.7	0.03	225	0.42	2.45	30	3	190	54.3	350	<0.002
Bloed6	<0.01	6.55	1.6	110	10.05	0.12	0.52	0.13	25.9	1.1	8	9.56	4.8	0.77	23	0.07	3.5	0.032	3.33	11.5	67.9	0.08	348	0.7	2.45	29.8	3.1	200	61.7	395	<0.002
Bloed7	0.03	7.11	2.7	660	6.18	0.18	0.92	0.19	91.8	3.4	9	9.47	5.3	1.73	22	0.21	2.8	0.058	3.9	46.3	48.3	0.21	512	0.52	2.21	26.5	4.2	510	41	264	<0.002
Bloed8	0.03	7.07	3.7	610	5.62	0.13	1.06	0.15	101	3.4	9	18.1	4.2	1.86	21.8	0.21	2.5	0.055	3.45	51.6	63.9	0.22	564	0.42	2.32	25.5	4.3	530	37	276	<0.002
Bloed9	0.03	6.86	2.1	210	3.44	0.09	0.38	0.07	20.1	1.6	5	4.7	11	0.84	17.95	0.1	1.3	0.019	4.86	7	24.3	0.08	211	0.44	1.53	13.6	2.8	170	53.2	288	<0.002
Bloed10	0.03	6.95	3.9	430	6.3	0.12	1.06	0.2	109.5	3.4	7	6.71	4.7	1.83	22.4	0.23	3.2	0.058	3.38	55.2	51	0.23	526	0.58	2.2	26.2	4.2	500	35.6	233	<0.002
Bloed11	0.06	6.93	4.1	620	6.18	0.26	0.99	0.19	98.6	3.4	9	14.25	1.6	1.7	21	0.22	3	0.064	3.71	50.6	57	0.21	539	0.36	2.23	28.2	4	400	40.5	250	<0.002
Bloed12	0.17	6.15	1	350	6.28	0.14	0.87	0.03	96.4	2.1	6	7.38	7.5	1.22	19.6	0.07	2.8	0.026	3.21	36.1	45.9	0.15	315	0.39	2.04	19.7	1.4	380	31	214	<0.002
Tink1	0.15	7.3	<0.2	580	1.93	0.17	9.74	0.1	71.8	24.4	74	6.87	37.3	5.05	20.9	0.17	2.5	0.073	2.12	28.5	47.6	2.2	966	0.7	0.81	12	41.2	740	10.9	101.5	<0.002
Tink2	0.23	7.41	1.1	530	2.63	0.43	3.74	0.07	60.8	33.1	86	6.69	106.5	6.14	24.3	0.17	3.6	0.105	2.02	23.9	87.5	2.51	713	0.87	1.4	13.9	67.6	720	18.7	41.4	<0.002
Tink3	0.15	7.25	5	590	1.86	0.19	10.65	0.14	56.3	16.6	70	2.87	43.4	5.41	21.3	0.15	1.8	0.064	1.76	22.5	34	2.41	745	0.51	0.43	10.6	36.8	900	10.1	91.4	<0.002
Tink4	0.11	5.39	7	250	1.38	0.19	16	0.14	53.8	19.5	61	0.76	8	3.06	13.5	0.08	1.8	0.051	0.66	23.2	11	1.35	1700	0.5	0.45	10.1	26.1	600	8.6	38.3	<0.002
Tink5	0.17	7.45	0.9	1540	1.79	0.36	1.75	0.03	57.5	24.1	86	19.2	24.4	5.17	23.9	0.15	3.6	0.039	4.87	25.2	91	2.39	478	0.69	1.22	13.3	55.8	710	18.9	217	<0.002
Tink6	0.17	7.76	0.8	620	2.16	0.16	6.08	0.11	66.6	27.2	81	8.4	79.2	5.89	23	0.18	2.9	0.062	2.51	26.8	61.4	2.15	788	1.51	1.72	12.2	60.3	1010	13.1	91.6	<0.002

Tink7	0.19	7.26	<0.2	530	2.48	0.33	4.55	0.07	71.3	25.6	88	5.74	61	5.24	21.6	0.15	3.2	0.058	1.73	26.5	82.9	2.34	702	1.05	1.12	12.5	58.3	750	13.2	83.4	<0.002
LCalc1	0.08	4.22	5	240	1.45	0.15	10.8	0.08	19.35	2.6	13	2.32	7.4	0.68	9.56	<0.05	1.2	0.006	2.03	10.7	11.3	0.31	130	0.41	1.25	3.2	5.9	270	21.4	82.1	<0.002
LCalc2	0.06	4.28	<0.2	250	1.49	0.14	9.6	0.07	19	2	12	2.34	7.9	0.76	9.69	<0.05	1.1	0.006	2.07	8.4	12.6	0.28	139	0.5	1.28	3.2	4.4	280	21	83.5	<0.002
LCalc3	0.09	3.81	<5	240	1.4	0.19	12.45	0.09	20.3	3.5	12	2.33	8.9	0.79	8.91	<0.05	1.2	0.006	1.87	8.7	12.1	0.29	221	1.09	1.1	3.4	5.3	320	23.8	77.5	<0.002
LCalc4	0.07	4.32	<5	270	1.49	0.21	10.3	0.09	20.2	3.1	14	2.57	8.5	0.88	9.78	<0.05	1.1	0.008	2.15	9.7	13.5	0.32	172	0.48	1.2	3.6	6.8	390	21.6	92.4	<0.002
LCalc5	0.07	4.24	<5	260	1.41	0.15	10.45	0.07	18.2	2.3	11	2.29	7.4	0.72	9.22	<0.05	1	0.005	2.21	10	11	0.26	117	0.47	1.24	3.3	5.2	310	22.6	85.3	<0.002
LCalc6	0.22	2.9	9	170	1.35	0.26	15.15	0.06	20.5	2.7	17	2.13	7.6	0.74	6.85	<0.05	1.3	0.007	1.7	9.6	18.6	0.38	128	2.91	0.79	3.3	5.5	600	26.9	66.3	<0.002

APPENDIX 3 CONTINUES…

	S	Sb	Sc	Se	Sn	Sr	Ta	Te	Th	Ti	Tl	U	V	W	Y	Zn	Zr	Dy	Er	Eu	Gd	Ho	Lu	Nd	Pr	Sm	Tb	Tm	Yb
SP1	<0.01	0.17	0.6	2	12.7	0.9	19.45	<0.05	21.8	0.005	4.07	11.3	1	3.5	66.3	65	53.1	12.1	10.35	<0.03	7.23	2.6	3.22	27.2	7.46	9	1.73	2.33	19.4
SP2	<0.01	0.11	0.6	2	12.1	0.8	16.3	<0.05	20.6	<0.005	4.11	10.7	<1	2.5	58.4	58	51.2	11.1	9.47	<0.03	6.77	2.38	2.84	27.4	7.58	8.92	1.59	2.07	16.9
SP3	<0.01	0.09	0.6	3	3.2	1.8	9.67	<0.05	61.7	0.021	2.59	11.6	1	2.7	157	60	73.4	18	14.5	0.07	11.8	4.08	2.82	37.4	9.12	11.75	2.59	2.56	17.8
SP4	<0.01	0.08	0.6	2	4	2	15.35	<0.05	56.6	0.02	2.66	9.3	5	3.7	162	77	85.8	15.5	12.8	0.08	10.25	3.56	2.61	29.6	7.12	10	2.23	2.28	16.1
SP5	<0.01	0.1	0.6	4	5.2	3.2	10.3	<0.05	50.3	0.022	2.94	7.2	1	2.8	234	92	64.4	21.5	17.8	0.08	14.25	4.93	3.81	41.1	9.56	14.2	3.1	3.24	23.1
SP6	<0.01	0.09	0.6	3	3.3	2.5	11.65	<0.05	64.9	0.02	2.53	7.8	4	2.8	184	101	98.4	18.85	15.75	0.07	11.75	4.36	3.25	33.5	7.97	11.5	2.65	2.83	20.1
Gross 1	<0.01	0.08	1.9	3	7.7	17.6	9.29	<0.05	94.3	0.073	2.43	16.9	3	2.5	164.5	74	137	21.1	15.8	0.35	19	4.69	2.46	94.5	28.5	19.45	3.32	2.48	15.9
Gross2	<0.01	0.09	1.8	3	7.2	17.8	8.43	<0.05	86.7	0.068	2.08	15.2	3	2.7	156.5	98	128.5	20.4	14.95	0.34	18.75	4.5	2.29	93.3	27.9	19.2	3.25	2.33	14.85
Gross3	<0.01	0.07	1.8	2	8.4	21.9	5.23	<0.05	92.3	0.108	2.47	11.4	9	4.1	49.7	55	81.4	11.15	6.96	0.39	14.6	2.19	0.88	84.3	23.8	17	2.09	0.99	6.05
TCalc1	0.02	0.06	2.7	<1	2.3	192.5	0.52	<0.05	6.1	0.067	0.78	1370	305	1.9	9	35	27.4	1.64	0.86	0.47	2.43	0.29	0.12	13.5	3.59	2.81	0.34	0.12	0.89
TCalc2	0.11	0.07	1.9	<1	1.9	218	0.63	<0.05	4.2	0.037	0.8	1450	321	2.1	6.8	27	19.1	1.27	0.69	0.41	1.72	0.23	0.11	9	2.42	1.94	0.26	0.1	0.67

SC1	0.01	0.08	10.9	1	3.2	63	0.68	<0.05	9.2	0.36	0.38	4.5	82	1.1	9.2	21	27.9	2.6	0.87	1.11	5.72	0.36	0.07	34.4	8.82	6.83	0.68	0.1	0.53
SC2	0.02	0.07	11.2	1	4.1	75.1	0.93	<0.05	10.6	0.44	0.51	4	82	2.3	11.6	23	37.5	3.09	1.19	1.09	5.93	0.45	0.1	34.5	8.74	6.96	0.75	0.11	0.74
SC3	0.01	0.14	11	<1	6.2	70.5	2.13	<0.05	10.7	0.446	0.45	6.7	87	2.8	11.8	46	32	3.12	1.18	1.09	5.99	0.46	0.1	36.6	9.4	7.22	0.74	0.12	0.74
2Sc1	0.01	<0.05	18.9	1	7.7	80.3	1.49	<0.05	9.2	0.487	1.42	3.3	168	3.3	13.7	45	106	3.65	1.34	1.12	6.33	0.55	0.13	35.1	8.69	7.57	0.84	0.14	0.87
2Sc2	0.01	<0.05	19.2	1	7.5	89.3	1.01	<0.05	9.9	0.502	1.67	3.7	171	2.8	15.3	34	100	4.28	1.56	1.27	7.29	0.64	0.14	40.8	10	8.85	0.99	0.16	1.02
2Sc3	0.01	<0.05	22.3	1	6.8	114	0.94	<0.05	9.1	0.502	1.03	3	198	3.1	10.8	42	51	3.1	1.11	1.43	5.7	0.46	0.09	33	8.14	6.95	0.74	0.11	0.65
Sc4	0.03	0.09	11.2	<1	3.4	83.4	0.68	<0.05	9.8	0.329	0.41	3.3	80	2	8.6	23	22.8	2.5	0.89	1.13	5.53	0.35	0.07	35.2	9	7.03	0.68	0.09	0.49
Sc5	0.01	0.1	12	1	3.9	57.9	1.06	<0.05	12.5	0.471	0.44	3.4	83	1.9	16.7	22	39.7	4.12	1.68	1.27	7.09	0.66	0.13	41.8	10.6	8.57	0.94	0.18	1.05
AB1	0.02	0.05	21	2	4.3	183.5	1.15	<0.05	30.8	0.435	1.07	4.2	52	0.5	42.4	118	53.1	8.44	4.54	2.99	14.95	1.54	0.48	107.5	30.1	17.75	1.82	0.55	3.22
AB2	<0.01	0.06	15	2	4.5	272	2.17	<0.05	31.7	0.569	0.28	2.4	75	0.2	43.5	68	29	8.18	5.08	2.07	12.1	1.61	0.74	83.4	22.5	14.05	1.61	0.71	4.63
AB3	0.01	0.07	16.8	2	3.5	196.5	1.34	<0.05	32.7	0.407	0.72	4.1	70	0.5	39.4	332	71.9	7.35	4.48	2.89	13.75	1.41	0.67	103	29.5	16.15	1.59	0.61	4.07
AB4	<0.01	<0.05	1.2	<1	0.8	133	0.18	<0.05	3.7	0.038	1.5	1.3	4	0.1	8.5	25	34.1	1.66	0.88	1.32	2.06	0.3	0.09	10	2.62	2.33	0.31	0.1	0.63
AB5	0.01	<0.05	0.9	<1	0.6	128	0.11	<0.05	2.2	0.025	0.99	0.7	3	0.1	5.8	18	38.8	1.16	0.62	1.01	1.36	0.21	0.08	6.5	1.81	1.44	0.21	0.08	0.52
Bloed1	<0.01	0.07	2.8	1	1.8	25.8	4.12	<0.05	13.3	0.024	1.03	7.6	5	1.7	40.2	38	43.3	6.21	4.09	0.33	3.71	1.32	0.64	7	1.66	2.71	0.89	0.62	3.99
Bloed2	0.01	0.07	3.3	2	1.6	31	5.08	<0.05	25.3	0.033	1.58	9	3	2	75.4	48	48	10.8	6.18	0.46	8.27	2.19	0.73	17.5	3.94	6.36	1.7	0.82	4.84
Bloed3	<0.01	0.06	4.6	1	1.4	17.1	5.21	<0.05	22.9	0.028	1.46	4.4	9	1.9	38.2	29	54.7	5.37	3.89	0.23	3.39	1.16	0.87	7.9	1.86	3.1	0.77	0.69	5.12
Bloed4	<0.01	0.07	3.1	1	2.1	49.5	3.18	<0.05	19.4	0.031	1.47	4.1	2	0.9	20.3	39	38.8	2.93	1.94	0.34	2.41	0.6	0.36	8.1	2	2.39	0.46	0.31	2.15
Bloed5	<0.01	0.06	2.2	1	1.1	30.7	3.69	<0.05	18.3	0.02	1.42	8.2	2	0.7	18.9	33	37.4	3.15	2.11	0.3	2.22	0.66	0.38	6.2	1.51	2.06	0.48	0.34	2.29
Bloed6	<0.01	0.07	3.7	1	2.5	37.6	4.22	<0.05	31.5	0.041	1.65	4.8	7	1.3	25.7	41	61.6	3.58	2.41	0.34	3.07	0.74	0.48	11.8	3.06	3.18	0.58	0.4	2.83
Bloed7	<0.01	0.07	4.7	1	5	125	2.88	<0.05	20.7	0.161	1.23	4.4	18	0.4	35.9	78	89.3	5.91	3.53	1.2	6.9	1.17	0.49	37.9	10.35	7.55	1.06	0.5	3.23
Bloed8	<0.01	0.07	4.7	1	3.9	126.5	1.94	<0.05	26.7	0.172	1.29	3.4	18	0.6	31.1	85	82.3	5.43	3	1.2	7.22	1.03	0.37	41.7	11.35	8.11	1.03	0.4	2.49
Bloed9	<0.01	0.06	2.1	1	1.6	62.6	0.9	<0.05	17.1	0.054	1.5	9.2	5	0.4	9	36	35.1	1.64	0.99	0.52	1.67	0.33	0.15	7	1.86	1.69	0.28	0.14	0.9
Bloed10	<0.01	0.07	5.2	1	4.6	115.5	2.38	<0.05	30.7	0.163	1.12	5	18	0.4	30.4	83	101	5.16	3.06	1.05	7.04	1	0.44	43.8	12.15	8.03	0.98	0.43	2.79

Bloed11	<0.01	0.07	4.6	1	4.7	124.5	2.27	<0.05	24.7	0.179	1.17	3.5	18	0.7	33.8	84	100	6.05	3.43	1.2	7.46	1.16	0.42	41.3	11.25	8.22	1.1	0.47	2.86
Bloed12	0.03	0.07	3.3	2	3.4	114	2.24	<0.05	18	0.115	0.96	2.4	12	0.5	25	65	77.7	4.39	2.61	0.93	5.62	0.72	0.27	32.1	8.84	6.2	0.89	0.35	2.33
Tink1	0.02	0.05	24.4	1	4.6	1010	0.93	0.05	9.8	0.416	0.55	3.3	134	1.5	33.6	101	78.1	5.8	3.36	1.32	6.7	0.92	0.36	32.8	8.3	7.15	1.16	0.44	3.06
Tink2	0.03	<0.05	23.4	1	3.4	406	1.1	0.06	7.3	0.454	0.57	3.1	164	1.3	27.1	120	119	5.4	3.15	1.12	6.09	0.86	0.36	28.8	7.35	6.36	1.06	0.42	2.89
Tink3	0.05	0.05	22.7	1	3.3	958	0.85	<0.05	8.9	0.4	0.33	3	124	1.4	29.3	106	54.6	5.03	3.01	1.2	5.7	0.82	0.33	27.1	6.68	6.2	1	0.4	2.72
Tink4	0.04	0.05	15.3	1	2.8	1490	0.82	<0.05	7.7	0.366	0.11	2.4	92	1.5	31.2	93	54	5.31	3.11	1.26	5.87	0.85	0.34	26.1	6.65	5.78	1.04	0.41	2.83
Tink5	0.02	<0.05	23.2	1	1.7	581	1.05	<0.05	8.9	0.448	1.39	3.6	151	1.1	15.4	111	116	3.11	1.93	1.37	4.54	0.52	0.23	26.4	6.97	5.05	0.68	0.25	1.8
Tink6	0.03	0.05	22.3	1	2.7	912	0.96	<0.05	9.6	0.447	0.68	6.5	164	1.6	24.3	133	91.3	4.25	2.61	1.16	5.54	0.69	0.3	28.8	7.51	5.99	0.89	0.34	2.48
Tink7	0.08	<0.05	23.6	1	2.8	553	0.99	<0.05	10.4	0.458	0.53	4.2	145	1.9	25.9	109	103	4.64	2.84	1.2	5.66	0.76	0.34	29.6	7.79	6.11	0.92	0.38	2.7
LCalc1	0.1	0.05	2.9	1	1.4	156.5	0.31	<0.05	3.6	0.068	0.44	154	53	0.8	6.3	21	34.8	1.34	0.65	0.51	1.91	0.18	0.07	10	2.69	2.08	0.29	0.08	0.59
LCalc2	0.06	0.05	2.9	2	1.4	163.5	0.31	<0.05	3.7	0.067	0.44	160	47	0.9	4.9	35	33.1	0.98	0.5	0.46	1.54	0.14	0.06	8.2	2.18	1.68	0.23	0.06	0.48
LCalc3	0.04	<0.05	3.1	1	1.3	163.5	0.33	<0.05	3.9	0.082	0.41	2260	511	2.6	6.3	16	37.6	1.19	0.63	0.47	1.69	0.18	0.07	8.5	2.29	1.79	0.26	0.08	0.57
LCalc4	0.03	0.05	3.3	1	1.5	163	0.37	<0.05	3.5	0.075	0.48	344	98	1.2	6.9	24	32.4	1.29	0.69	0.51	1.82	0.19	0.07	9.3	2.52	1.94	0.28	0.09	0.62
LCalc5	0.04	0.08	2.5	2	1.4	152.5	0.35	<0.05	3.6	0.06	0.45	284	79	1	5.8	32	30	1.14	0.57	0.51	1.74	0.16	0.06	9.2	2.48	1.89	0.28	0.07	0.54
LCalc6	0.04	0.05	2.8	<1	1	175	0.32	<0.05	4.2	0.091	0.32	>10000	2480	8.2	7.3	22	39.3	1.3	0.69	0.39	1.87	0.19	0.07	9.5	2.48	1.95	0.29	0.08	0.62

Appendix 4: U, V & Th data for various rocks around the Marenica uranium prospect (after van Noort, 2010).

Hole_ID	Depth_From	Depth_To	Sample_ID	U3O8_ppm_XRF75G	U_ppm_PP_XRFa	Th_ppm	V_ppm	Major_Rock1	Formation
MAR0132	0	1	MAR132-1		18	13.59	39	Calcrete	Recent
MAR0132	1	2	MAR132-2		45	11.52	97	Calcrete	Recent
MAR0132	2	3	MAR132-3		11	13.26	90	Calcrete	Recent
MAR0132	3	4	MAR132-4		-5	11.46	88	Calcrete	Recent
MAR0132	4	5	MAR132-5		17	11.95	82	Calcrete	Recent
MAR0132	5	6	MAR132-6		617	12.43	192	Calcrete	Recent
MAR0132	6	7	MAR132-7		7	10.66	78	Calcrete	Recent
MAR0132	7	8	MAR132-8		7	10.44	72	Calcrete	Recent
MAR0132	8	9	MAR132-9		-5	9.72	68	Calcrete	Recent
MAR0132	9	10	MAR132-10		87	0.09	87	Calcrete	Recent
MAR0132	10	11	MAR132-11		23	12.79	74	Calcrete	Recent
MAR0132	11	12	MAR132-12		-5	11.19	69	Calcrete	Recent
MAR0132	12	13	MAR132-13		-5	9.37	62	Calcrete	Recent
MAR0132	15	16	MAR132-16		-5	7.51	18	Calcrete	Recent
MAR0133	7	8	MAR133-8		14	13.71	72	Leucogranite	Damara
MAR0133	8	9	MAR133-9		46	14.88	95	Leucogranite	Damara
MAR0133	9	10	MAR133-10		84	13.91	99	Leucogranite	Damara
MAR0133	10	11	MAR133-11		42	12.5	84	Leucogranite	Damara

Hole_ID	Depth_From	Depth_To	Sample_ID	U3O8_ppm_XRF75G	U_ppm_PP_XRFa	Th_ppm	V_ppm	Major_Rock1	Formation
MAR0133	13	14	MAR133-14		10	11.49	60	Leucogranite	Damara
MAR0133	14	15	MAR133-15		20	9.51	113	Leucogranite	Damara
MAR0133	15	16	MAR133-16		31	10.87	59	Leucogranite	Damara
MAR0133	16	17	MAR133-17		5	9.33	75	Leucogranite	Damara
MAR0133	17	18	MAR133-18		-5	11.43	67	Leucogranite	Damara
MAR0133	18	19	MAR133-19		-5	10.77	58	Leucogranite	Damara
MAR0133	19	20	MAR133-20		-5	10.06	49	Leucogranite	Damara
MAR0133	20	21	MAR133-21		26	8.16	97	Leucogranite	Damara
MAR0133	21	22	MAR133-22		29	7.5	153	Leucogranite	Damara
MAR0133	22	23	MAR133-23		-5	6.87	168	Leucogranite	Damara
MAR0133	23	24	MAR133-24		-5	6.02	38	Leucogranite	Damara
MAR0133	24	25	MAR133-25		-5	4.22	22	Leucogranite	Damara
MAR0147	13	14	MAR147-14		11	9.48	155	Leucogranite	Damara
MAR0147	17	18	MAR147-18		-5	12.23	118	Leucogranite	Damara
MAR0148	4	5	MAR148-5		-5	3.41	22	Leucogranite	Damara

Hole_ID	Depth_From	Depth_To	Sample_ID	U3O8_ppm_XRF75G	U_ppm_PP_XRFa	Th_ppm	V_ppm	Major_Rock1	Formation
MAR0148	5	6	MAR148-6		7	3.53	33	Leucogranite	Damara
MAR0148	6	7	MAR148-7		-5	7.43	121	Leucogranite	Damara
MAR0148	9	10	MAR148-10		11	2.13	20	Leucogranite	Damara
MAR0149	40	41	MAR149-41		-5	4.75	4	Leucogranite	Damara
MAR0149	41	42	MAR149-42		-5	4.29	4	Leucogranite	Damara
MAR0149	42	43	MAR149-43		-5	4.46	5	Leucogranite	Damara
MAR0149	43	44	MAR149-44		-5	2.48	5	Leucogranite	Damara
MAR0150	8	9	MAR150-9		9	1.82	25	Leucogranite	Damara
MAR0150	9	10	MAR150-10		6	1.6	15	Leucogranite	Damara
MAR0150	10	11	MAR150-11		-5	1.45	13	Leucogranite	Damara
MAR0992	13	14	105420	-10		-10	123	Leucogranite	Damara
MAR0992	14	15	105421	-10		-10	83	Leucogranite	Damara
MAR0992	15	16	105422	-10		-10	21	Leucogranite	Damara
MAR0992	16	17	105423	-10		-10	184	Leucogranite	Damara
MAR1000	4	5	105434	31		-10	137	Leucogranite	Damara
MAR1000	10	11	105441	13		-10	85	Leucogranite	Damara
MAR1000	13	14	105444	-10		-10	84	Leucogranite	Damara
MAR1032	8	9	105505	-10		-10	120	Leucogranite	Damara
MAR1032	9	10	105506	-10		-10	115	Leucogranite	Damara
MAR1032	12	13	105509	-10		-10	101	Leucogranite	Damara
MAR1032	13	14	105510	-10		-10	136	Leucogranite	Damara

Hole_ID	Depth_From	Depth_To	Sample_ID	U3O8_ppm_XRF75G	U_ppm_PP_XRFa	Th_ppm	V_ppm	Major_Rock1	Formation
MAR1032	14	15	105511	-10		-10	143	Leucogranite	Damara
MAR1037	7	8	105520	29		-10	69	Leucogranite	Damara
MAR1037	8	9	105521	-10		-10	18	Leucogranite	Damara
MAR1037	9	10	105522	14		-10	13	Leucogranite	Damara
MAR1037	10	11	105526	13		-10	16	Leucogranite	Damara
MAR1037	11	12	105527	-10		-10	91	Leucogranite	Damara
MAR1045	0	1	105531	96		-10	63	Leucogranite	Damara
MAR1045	1	2	105532	236		-10	65	Leucogranite	Damara
MAR1045	11	12	105543	-10		-10	120	Leucogranite	Damara
MAR1045	12	13	105544	10		-10	80	Leucogranite	Damara
MAR1045	13	14	105545	-10		-10	18	Leucogranite	Damara
MAR1045	14	15	105546	-10		-10	-10	Leucogranite	Damara
MAR1058	0	1	105550	15		-10	84	Leucogranite	Damara
MAR1058	1	2	105551	11		-10	106	Leucogranite	Damara
MAR1058	2	3	105552	22		-10	153	Leucogranite	Damara
MAR1058	3	4	105553	46		-10	162	Leucogranite	Damara
MAR1058	4	5	105554	24		-10	182	Leucogranite	Damara
MAR1058	5	6	105555	10		-10	145	Leucogranite	Damara
MAR1058	8	9	105558	-10		-10	165	Leucogranite	Damara
MAR1058	9	10	105559	-10		-10	142	Leucogranite	Damara
MAR1058	10	11	105561	-10		-10	155	Leucogranite	Damara
MAR1058	11	12	105562	-10		-10	130	Leucogranite	Damara
MAR1058	13	14	105564	-10		-10	121	Leucogranite	Damara

Hole_ID	Depth_From	Depth_To	Sample_ID	U3O8_ppm_XRF75G	U_ppm_PP_XRFa	Th_ppm	V_ppm	Major_Rock1	Formation
MAR1058	14	15	105565	-10		-10	15	Leucogranite	Damara
MAR1069	1	2	105567	-10		10	88	Leucogranite	Damara
MAR1069	2	3	105568	-10		11	95	Leucogranite	Damara
MAR1069	4	5	105570	-10		-10	77	Leucogranite	Damara
MAR1069	5	6	105574	20		-10	68	Leucogranite	Damara
MAR1069	6	7	105575	13		-10	-10	Leucogranite	Damara
MAR1069	7	8	105576	51		-10	22	Leucogranite	Damara
MAR1069	8	9	105577	-10		-10	13	Leucogranite	Damara
MAR1069	9	10	105578	-10		-10	-10	Leucogranite	Damara
MAR1069	10	11	105579	-10		-10	-10	Leucogranite	Damara
MAR1069	11	12	105580	-10		-10	-10	Leucogranite	Damara
MAR1069	12	13	105581	-10		-10	-10	Leucogranite	Damara
MAR1069	13	14	105582	-10		-10	36	Leucogranite	Damara
MAR1069	14	15	105583	-10		-10	-10	Leucogranite	Damara
MAR1072	1	2	105586	12		-10	156	Leucogranite	Damara
MAR1072	2	3	105587	-10		-10	51	Leucogranite	Damara
MAR1072	4	5	105589	57		-10	230	Leucogranite	Damara
MAR1072	5	6	105590	92		-10	235	Leucogranite	Damara
MAR1072	6	7	105591	11		-10	81	Leucogranite	Damara
MAR1072	7	8	105592	27		-10	65	Leucogranite	Damara
MAR1072	8	9	105593	21		-10	54	Leucogranite	Damara
MAR1072	9	10	105594	38		-10	80	Leucogranite	Damara

MAR1072	10	11	105598	145		-10	116	Leucogranite	Damara
MAR1093	2	3	105634	322		-10	172	Leucogranite	Damara
MAR1105	4	5	105664	176		-10	118	Leucogranite	Damara
MAR1124	8	9	105699	-10		-10	115	Leucogranite	Damara
MAR1136	5	6	105709	275		-10	115	Leucogranite	Damara
MAR1136	6	7	105710	185		-10	125	Leucogranite	Damara
MAR1136	7	8	105711	14		-10	111	Leucogranite	Damara
MAR1136	17	18	105724	10		-10	136	Leucogranite	Damara
MAR1142	8	9	105734	81		-10	44	Leucogranite	Damara
MAR1142	9	10	105735	56		-10	29	Leucogranite	Damara
MAR1142	11	12	105737	168		-10	58	Leucogranite	Damara
MAR1142	12	13	105738	35		-10	76	Leucogranite	Damara
MAR1142	13	14	105742	12		-10	20	Leucogranite	Damara
MAR1142	14	15	105743	-10		-10	16	Leucogranite	Damara
MAR1142	15	16	105744	-10		-10	16	Leucogranite	Damara
MAR1142	16	17	105745	-10		-10	15	Leucogranite	Damara
MAR1147	1	2	105747	101		-10	91	Leucogranite	Damara
MAR1147	2	3	105748	44		-10	44	Leucogranite	Damara
MAR1147	3	4	105749	54		10	48	Leucogranite	Damara
MAR1147	4	5	105750	108		-10	60	Leucogranite	Damara
MAR1147	5	6	105751	46		-10	71	Leucogranite	Damara
MAR1147	6	7	105753	11		10	71	Leucogranite	Damara
MAR1147	7	8	105754	46		-10	91	Leucogranite	Damara
MAR1159	8	9	105770	74		-10	189	Leucogranite	Damara

Hole_ID	Depth_From	Depth_To	Sample_ID	U3O8_ppm_XRF75G	U_ppm_PP_XRFa	Th_ppm	V_ppm	Major_Rock1	Formation
MAR1159	9	10	105771	118		-10	156	Leucogranite	Damara
MAR1159	10	11	105772	16		-10	142	Leucogranite	Damara
MAR1159	13	14	105775	43		-10	104	Leucogranite	Damara
MAR1159	16	17	105779	12		-10	119	Leucogranite	Damara
MAR1175	4	5	105823	37		-10	90	Leucogranite	Damara
MAR1175	8	9	105828	38		-10	79	Leucogranite	Damara
MAR1175	9	10	105829	64		-10	48	Leucogranite	Damara
MAR1175	10	11	105830	83		-10	103	Leucogranite	Damara
MAR1175	13	14	105833	41		-10	32	Leucogranite	Damara
MAR1175	14	15	105834	-10		-10	12	Leucogranite	Damara
MAR1175	15	16	105838	-10		-10	50	Leucogranite	Damara
MAR1181	7	8	105847	26		-10	131	Leucogranite	Damara
MAR1181	8	9	105849	-10		-10	104	Leucogranite	Damara
MAR1181	9	10	105850	16		-10	120	Leucogranite	Damara
MAR1181	10	11	105851	21		-10	131	Leucogranite	Damara
MAR1181	12	13	105853	14		-10	156	Leucogranite	Damara
MAR1184	5	6	105869	32		-10	94	Leucogranite	Damara
MAR1184	6	7	105870	64		-10	77	Leucogranite	Damara
MAR1184	7	8	105871	184		-10	68	Leucogranite	Damara
MAR1184	10	11	105875	61		-10	77	Leucogranite	Damara
MAR1184	11	12	105876	43		-10	87	Leucogranite	Damara

Hole_ID	Depth_From	Depth_To	Sample_ID	U3O8_ppm_XRF75G	U_ppm_PP_XRFa	Th_ppm	V_ppm	Major_Rock1	Formation
MAR1204	9	10	105910	23		-10	91	Leucogranite	Damara
MAR1204	10	11	105911	-10		-10	138	Leucogranite	Damara
MAR1204	11	12	105912	-10		-10	133	Leucogranite	Damara
MAR1226	11	12	105959	159		-10	111	Leucogranite	Damara
MAR1226	12	13	105960	114		-10	76	Leucogranite	Damara
MAR1226	13	14	105961	52		-10	39	Leucogranite	Damara
MAR1226	14	15	105962	31		-10	49	Leucogranite	Damara
MAR1226	17	18	105965	18		-10	81	Leucogranite	Damara
MAR1226	18	19	105966	-10		10	60	Leucogranite	Damara
MAR1226	19	20	105967	-10		11	56	Leucogranite	Damara
MAR1226	20	21	105969	-10		-10	72	Leucogranite	Damara
MAR1226	21	22	105970	-10		12	82	Leucogranite	Damara
MAR1244	5	6	105991	89		-10	67	Leucogranite	Damara
MAR1244	10	11	105997	-10		-10	57	Leucogranite	Damara
MAR1244	11	12	105998	14		-10	45	Leucogranite	Damara
MAR1253	10	11	106012	-10		-10	118	Leucogranite	Damara
MAR1348	16	17	106331	59		-10	109	Leucogranite	Damara
MAR1348	22	23	106337	39		-10	105	Leucogranite	Damara
MAR1371	0	1	106364	20		-10	20	Leucogranite	Damara
MAR1371	1	2	106365	67		-10	51	Leucogranite	Damara
MAR1371	2	3	106366	282		-10	160	Leucogranite	Damara
MAR1371	8	9	106375	-10		-10	73	Leucogranite	Damara
MAR1371	9	10	106376	13		12	25	Leucogranite	Damara

MAR1379	0	1	106383	116		-10	40	Leucogranite	Damara
Hole_ID	Depth_From	Depth_To	Sample_ID	U3O8_ppm_XRF75G	U_ppm_PP_XRFa	Th_ppm	V_ppm	Major_Rock1	Formation
MAR1379	1	2	106384	206		-10	65	Leucogranite	Damara
MAR1379	2	3	106385	369		-10	128	Leucogranite	Damara
MAR1379	3	4	106386	595		-10	164	Leucogranite	Damara
MAR1448	24	25	106555	240		-10	83	Leucogranite	Damara
MAR1448	25	26	106556	48		-10	123	Leucogranite	Damara
MAR1512	3	4	106858	15		-10	101	Leucogranite	Damara
MAR1512	4	5	106859	36		-10	87	Leucogranite	Damara
MAR1512	5	6	106860	-10		-10	101	Leucogranite	Damara
MAR1512	13	14	106869	-10		-10	41	Leucogranite	Damara
MAR1520	12	13	106887	-10		-10	136	Leucogranite	Damara
MAR1552	1	2	106950	45		-10	34	Leucogranite	Damara
MAR1560	10	11	106981	-10		-10	106	Leucogranite	Damara
MAC0135	9	10	108334	11		-10	106	Leucogranite	Damara
MAC0148	2	3	108350	-10		-10	21	Leucogranite	Damara
MAC0185	2	3	108386	271		-10	177	Leucogranite	Damara
MAC0329	30	31	108446	-10		19	31	Leucogranite	Damara
MAC0344	2	3	108452	67		-10	109	Leucogranite	Damara
MAC0348	9	10	108475	-10		-10	73	Leucogranite	Damara
MAR0137	10	11	MAR137-11		24	10.82	143	Leucogranite	Damara
MAR0137	11	12	MAR137-12		-5	13.23	203	Leucogranite	Damara
MAR0137	12	13	MAR137-13		-5	12.29	180	Leucogranite	Damara
MAR0137	13	14	MAR137-14		-5	13.61	202	Leucogranite	Damara

Hole_ID	Depth_From	Depth_To	Sample_ID	U3O8_ppm_XRF75G	U_ppm_PP_XRFa	Th_ppm	V_ppm	Major_Rock1	Formation
MAR1142	1	2	105726	97		-10	100	Leucogranite	Damara
MAR1142	2	3	105727	48		-10	31	Leucogranite	Damara
MAR1142	3	4	105729	64		-10	43	Leucogranite	Damara
MAR1142	4	5	105730	38		-10	34	Leucogranite	Damara
MAR1142	5	6	105731	62		-10	43	Leucogranite	Damara
MAR1142	6	7	105732	44		-10	30	Leucogranite	Damara
MAR1142	7	8	105733	64		-10	39	Leucogranite	Damara
MAC0348	10	11	108476	10		-10	216	Dolerite	Cretaceous
MAR1077	7	8	105611	-10		-10	161	Dolerite	Cretaceous
MAR1077	8	9	105612	-10		-10	171	Dolerite	Cretaceous
MAR1077	10	11	105614	-10		-10	164	Dolerite	Cretaceous
MAR1077	11	12	105615	-10		-10	202	Dolerite	Cretaceous
MAR1093	4	5	105636	178		-10	251	Dolerite	Cretaceous
MAR1535	3	4	106915	281		-10	127	Psammite - biotite rich	Kuiseb
MAR1535	4	5	106916	160		-10	136	Psammite - biotite rich	Kuiseb
MAC0042	5	6	108160	132		-10	189	Biotite Schist	Kuiseb
MAC0063	2	3	108188	1997		-10	264	Biotite Schist	Kuiseb
MAC0063	3	4	108190	48		-10	123	Biotite Schist	Kuiseb
MAC0068	4	5	108206	-10		-10	162	Biotite Schist	Kuiseb
MAC0084	10	11	108228	12		-10	80	Biotite Schist	Kuiseb
MAC0084	11	12	108229	17		-10	79	Biotite Schist	Kuiseb
MAC0112	10	11	108281	-10		-10	139	Biotite Schist	Kuiseb

Hole_ID	Depth_From	Depth_To	Sample_ID	U3O8_ppm_XRF75G	U_ppm_PP_XRFa	Th_ppm	V_ppm	Major_Rock1	Formation
MAC0112	11	12	108282	-10		-10	142	Biotite Schist	Kuiseb
MAC0118	1	2	108284	13		-10	96	Biotite Schist	Kuiseb
MAC0118	2	3	108286	-10		11	124	Biotite Schist	Kuiseb
MAC0135	1	2	108325	-10		-10	124	Biotite Schist	Kuiseb
MAC0135	7	8	108331	-10		-10	150	Biotite Schist	Kuiseb
MAC0135	8	9	108332	15		-10	95	Biotite Schist	Kuiseb
MAC0142	3	4	108338	32		-10	93	Biotite Schist	Kuiseb
MAC0142	8	9	108343	-10		11	129	Biotite Schist	Kuiseb
MAC0142	9	10	108347	-10		-10	117	Biotite Schist	Kuiseb
MAC0158	7	8	108365	127		-10	148	Biotite Schist	Kuiseb
MAC0158	8	9	108366	13		-10	131	Biotite Schist	Kuiseb
MAC0167	1	2	108372	189		-10	75	Biotite Schist	Kuiseb
MAC0344	5	6	108456	23		11	136	Biotite Schist	Kuiseb
MAR0137	9	10	MAR137-10		14	12.97	98	Biotite Schist	Kuiseb
MAR0142	12	13	MAR142-13		-5	11.77	198	Biotite Schist	Kuiseb
MAR0142	13	14	MAR142-14		-5	8.36	128	Biotite Schist	Kuiseb
MAR0142	14	15	MAR142-15		-5	12.37	186	Biotite Schist	Kuiseb
MAR0142	17	18	MAR142-18		-5	8.05	103	Biotite Schist	Kuiseb
MAR0142	18	19	MAR142-19		-5	11.35	165	Biotite Schist	Kuiseb
MAR0143	5	6	MAR143-6		-5	11.87	172	Biotite Schist	Kuiseb
MAR0147	11	12	MAR147-12		-5	11.46	132	Biotite Schist	Kuiseb
MAR0147	12	13	MAR147-13		-5	10.75	141	Biotite Schist	Kuiseb
MAR0147	18	19	MAR147-19		-5	13.84	107	Biotite Schist	Kuiseb

Hole_ID	Depth_From	Depth_To	Sample_ID	U3O8_ppm_XRF75G	U_ppm_PP_XRFa	Th_ppm	V_ppm	Major_Rock1	Formation
MAR0147	19	20	MAR147-20		-5	15.53	109	Biotite Schist	Kuiseb
MAR0148	7	8	MAR148-8		18	10.15	173	Biotite Schist	Kuiseb
MAR0148	8	9	MAR148-9		-5	6.07	113	Biotite Schist	Kuiseb
MAR0148	10	11	MAR148-11		5	7.71	119	Biotite Schist	Kuiseb
MAR0148	11	12	MAR148-12		-5	10.14	138	Biotite Schist	Kuiseb
MAR0148	12	13	MAR148-13		-5	10.19	157	Biotite Schist	Kuiseb
MAR0148	13	14	MAR148-14		-5	10.29	164	Biotite Schist	Kuiseb
MAR0148	14	15	MAR148-15		-5	11.7	156	Biotite Schist	Kuiseb
MAR0149	19	20	MAR149-20		-5	10.25	117	Biotite Schist	Kuiseb
MAR0149	20	21	MAR149-21		-5	12.54	98	Biotite Schist	Kuiseb
MAR0149	21	22	MAR149-22		-5	11.11	132	Biotite Schist	Kuiseb
MAR0149	22	23	MAR149-23		-5	11.77	132	Biotite Schist	Kuiseb
MAR0149	23	24	MAR149-24		-5	11.04	133	Biotite Schist	Kuiseb
MAR0149	24	25	MAR149-25		-5	10.87	133	Biotite Schist	Kuiseb
MAR0149	44	45	MAR149-45		-5	9.14	111	Biotite Schist	Kuiseb
MAR0150	2	3	MAR150-3		-5	12.45	201	Biotite Schist	Kuiseb
MAR0150	3	4	MAR150-4		47	9.17	135	Biotite Schist	Kuiseb
MAR0150	4	5	MAR150-5		-5	9.85	140	Biotite Schist	Kuiseb
MAR0150	5	6	MAR150-6		-5	9.25	112	Biotite Schist	Kuiseb
MAR0150	6	7	MAR150-7		-5	7.68	132	Biotite Schist	Kuiseb
MAR0150	7	8	MAR150-8		23	8.59	179	Biotite Schist	Kuiseb
MAR0150	11	12	MAR150-12		23	3.41	57	Biotite Schist	Kuiseb
MAR0150	12	13	MAR150-13		-5	12.02	192	Biotite Schist	Kuiseb

MAR0150	13	14	MAR150-14		-5	12.69	193	Biotite Schist	Kuiseb
MAR0150	14	15	MAR150-15		16	8.04	114	Biotite Schist	Kuiseb
MAR0150	15	16	MAR150-16		-5	10.48	132	Biotite Schist	Kuiseb

Hole_ID	Depth_From	Depth_To	Sample_ID	U3O8_ppm_XRF75G	U_ppm_PP_XRFa	Th_ppm	V_ppm	Major_Rock1	Formation
MAR0150	17	18	MAR150-18		-5	11	190	Biotite Schist	Kuiseb
MAR0150	18	19	MAR150-19		281	10.75	227	Biotite Schist	Kuiseb
MAR0150	19	20	MAR150-20		-5	12.11	197	Biotite Schist	Kuiseb
MAR0150	20	21	MAR150-21		-5	12.14	210	Biotite Schist	Kuiseb
MAR0150	21	22	MAR150-22		-5	11.92	196	Biotite Schist	Kuiseb
MAR0150	22	23	MAR150-23		-5	11.02	195	Biotite Schist	Kuiseb
MAR0150	23	24	MAR150-24		-5	12.05	179	Biotite Schist	Kuiseb
MAR0150	24	25	MAR150-25		-5	12.92	186	Biotite Schist	Kuiseb
MAR0992	2	3	105408	51		-10	150	Biotite Schist	Kuiseb
MAR0992	3	4	105409	52		-10	193	Biotite Schist	Kuiseb
MAR0992	4	5	105410	16		-10	132	Biotite Schist	Kuiseb
MAR0992	5	6	105411	-10		-10	156	Biotite Schist	Kuiseb
MAR0992	6	7	105412	23		-10	145	Biotite Schist	Kuiseb
MAR0992	7	8	105413	-10		-10	164	Biotite Schist	Kuiseb
MAR0992	8	9	105414	-10		-10	192	Biotite Schist	Kuiseb
MAR0992	9	10	105415	-10		-10	169	Biotite Schist	Kuiseb
MAR0992	10	11	105417	-10		-10	145	Biotite Schist	Kuiseb
MAR0992	11	12	105418	-10		-10	156	Biotite Schist	Kuiseb
MAR0992	12	13	105419	-10		-10	143	Biotite Schist	Kuiseb

MAR0992	17	18	105424	-10		-10	128	Biotite Schist	Kuiseb

Hole_ID	Depth_From	Depth_To	Sample_ID	U3O8_ppm_XRF75G	U_ppm_PP_XRFa	Th_ppm	V_ppm	Major_Rock1	Formation
MAR0992	18	19	105425	-10		-10	149	Biotite Schist	Kuiseb
MAR0992	19	20	105426	-10		-10	131	Biotite Schist	Kuiseb
MAR1000	1	2	105431	14		-10	115	Biotite Schist	Kuiseb
MAR1000	2	3	105432	15		-10	150	Biotite Schist	Kuiseb
MAR1000	3	4	105433	23		-10	151	Biotite Schist	Kuiseb
MAR1000	5	6	105435	30		-10	141	Biotite Schist	Kuiseb
MAR1000	6	7	105436	37		-10	170	Biotite Schist	Kuiseb
MAR1000	7	8	105437	10		-10	157	Biotite Schist	Kuiseb
MAR1000	8	9	105438	47		-10	194	Biotite Schist	Kuiseb
MAR1000	9	10	105439	35		-10	188	Biotite Schist	Kuiseb
MAR1000	11	12	105442	-10		-10	119	Biotite Schist	Kuiseb
MAR1000	12	13	105443	-10		-10	109	Biotite Schist	Kuiseb
MAR1000	14	15	105445	-10		-10	100	Biotite Schist	Kuiseb
MAR1000	15	16	105446	-10		-10	95	Biotite Schist	Kuiseb
MAR1000	16	17	105447	-10		-10	92	Biotite Schist	Kuiseb
MAR1000	17	18	105448	-10		-10	120	Biotite Schist	Kuiseb
MAR1000	18	19	105449	-10		-10	132	Biotite Schist	Kuiseb
MAR1000	19	20	105450	-10		-10	96	Biotite Schist	Kuiseb
MAR1013	1	2	105455	64		-10	131	Biotite Schist	Kuiseb
MAR1013	2	3	105456	64		-10	120	Biotite Schist	Kuiseb
MAR1013	3	4	105457	-10		-10	122	Biotite Schist	Kuiseb

Hole_ID	Depth_From	Depth_To	Sample_ID	U3O8_ppm_XRF75G	U_ppm_PP_XRFa	Th_ppm	V_ppm	Major_Rock1	Formation
MAR1013	4	5	105458	50		-10	96	Biotite Schist	Kuiseb
MAR1013	5	6	105459	-10		-10	113	Biotite Schist	Kuiseb
MAR1013	6	7	105460	-10		-10	129	Biotite Schist	Kuiseb
MAR1013	7	8	105461	-10		-10	175	Biotite Schist	Kuiseb
MAR1013	8	9	105462	-10		-10	162	Biotite Schist	Kuiseb
MAR1013	9	10	105463	-10		-10	142	Biotite Schist	Kuiseb
MAR1013	10	11	105465	-10		-10	165	Biotite Schist	Kuiseb
MAR1013	11	12	105466	-10		-10	139	Biotite Schist	Kuiseb
MAR1013	12	13	105467	-10		-10	145	Biotite Schist	Kuiseb
MAR1013	13	14	105468	-10		-10	147	Biotite Schist	Kuiseb
MAR1013	14	15	105469	-10		-10	176	Biotite Schist	Kuiseb
MAR1013	15	16	105470	-10		-10	180	Biotite Schist	Kuiseb
MAR1013	16	17	105471	-10		-10	162	Biotite Schist	Kuiseb
MAR1013	17	18	105472	-10		-10	155	Biotite Schist	Kuiseb
MAR1013	18	19	105473	-10		-10	147	Biotite Schist	Kuiseb
MAR1013	19	20	105474	-10		-10	119	Biotite Schist	Kuiseb
MAR1021	0	1	105478	116		-10	92	Biotite Schist	Kuiseb
MAR1021	1	2	105479	95		-10	193	Biotite Schist	Kuiseb
MAR1021	2	3	105480	35		-10	155	Biotite Schist	Kuiseb
MAR1021	3	4	105481	21		-10	152	Biotite Schist	Kuiseb
MAR1021	4	5	105482	26		-10	165	Biotite Schist	Kuiseb
MAR1021	5	6	105483	-10		-10	111	Biotite Schist	Kuiseb
MAR1021	6	7	105484	12		-10	124	Biotite Schist	Kuiseb

Hole_ID	Depth_From	Depth_To	Sample_ID	U3O8_ppm_XRF75G	U_ppm_PP_XRFa	Th_ppm	V_ppm	Major_Rock1	Formation
MAR1021	7	8	105485	-10		-10	142	Biotite Schist	Kuiseb
MAR1021	8	9	105486	-10		10	128	Biotite Schist	Kuiseb
MAR1021	9	10	105487	-10		-10	142	Biotite Schist	Kuiseb
MAR1021	10	11	105489	-10		-10	127	Biotite Schist	Kuiseb
MAR1021	11	12	105490	-10		-10	97	Biotite Schist	Kuiseb
MAR1021	12	13	105491	-10		-10	81	Biotite Schist	Kuiseb
MAR1021	13	14	105492	-10		-10	76	Biotite Schist	Kuiseb
MAR1021	14	15	105493	-10		10	105	Biotite Schist	Kuiseb
MAR1032	2	3	105496	-10		-10	123	Biotite Schist	Kuiseb
MAR1032	3	4	105497	87		-10	156	Biotite Schist	Kuiseb
MAR1032	4	5	105498	61		-10	138	Biotite Schist	Kuiseb
MAR1032	5	6	105502	16		-10	95	Biotite Schist	Kuiseb
MAR1032	6	7	105503	15		-10	125	Biotite Schist	Kuiseb
MAR1032	7	8	105504	-10		-10	105	Biotite Schist	Kuiseb
MAR1032	10	11	105507	-10		-10	122	Biotite Schist	Kuiseb
MAR1032	11	12	105508	-10		-10	112	Biotite Schist	Kuiseb
MAR1037	4	5	105517	-10		-10	199	Biotite Schist	Kuiseb
MAR1037	5	6	105518	-10		-10	235	Biotite Schist	Kuiseb
MAR1037	6	7	105519	-10		-10	193	Biotite Schist	Kuiseb
MAR1037	12	13	105528	-10		-10	152	Biotite Schist	Kuiseb
MAR1037	13	14	105529	-10		-10	171	Biotite Schist	Kuiseb
MAR1037	14	15	105530	-10		-10	171	Biotite Schist	Kuiseb
MAR1045	3	4	105534	-10		-10	128	Biotite Schist	Kuiseb

Hole_ID	Depth_From	Depth_To	Sample_ID	U3O8_ppm_XRF75G	U_ppm_PP_XRFa	Th_ppm	V_ppm	Major_Rock1	Formation
MAR1045	4	5	105535	-10		-10	93	Biotite Schist	Kuiseb
MAR1045	5	6	105537	-10		-10	121	Biotite Schist	Kuiseb
MAR1045	6	7	105538	-10		-10	113	Biotite Schist	Kuiseb
MAR1045	10	11	105542	-10		-10	159	Biotite Schist	Kuiseb
MAR1069	0	1	105566	39		-10	62	Biotite Schist	Kuiseb
MAR1072	3	4	105588	-10		-10	171	Biotite Schist	Kuiseb
MAR1072	12	13	105600	24		-10	112	Biotite Schist	Kuiseb
MAR1072	13	14	105601	12		-10	169	Biotite Schist	Kuiseb
MAR1072	14	15	105602	-10		10	103	Biotite Schist	Kuiseb
MAR1077	1	2	105604	113		-10	203	Biotite Schist	Kuiseb
MAR1077	2	3	105605	119		-10	215	Biotite Schist	Kuiseb
MAR1077	3	4	105606	123		-10	174	Biotite Schist	Kuiseb
MAR1077	4	5	105607	282		-10	200	Biotite Schist	Kuiseb
MAR1077	5	6	105609	314		-10	213	Biotite Schist	Kuiseb
MAR1077	6	7	105610	18		-10	116	Biotite Schist	Kuiseb
MAR1077	9	10	105613	-10		11	135	Biotite Schist	Kuiseb
MAR1086	3	4	105622	80		-10	222	Biotite Schist	Kuiseb
MAR1086	4	5	105623	133		-10	242	Biotite Schist	Kuiseb
MAR1086	5	6	105624	39		-10	206	Biotite Schist	Kuiseb
MAR1086	6	7	105625	19		-10	202	Biotite Schist	Kuiseb
MAR1086	7	8	105626	10		-10	245	Biotite Schist	Kuiseb
MAR1093	3	4	105635	226		-10	145	Biotite Schist	Kuiseb
MAR1093	5	6	105637	141		-10	182	Biotite Schist	Kuiseb

MAR1093	6	7	105638	112		-10	138	Biotite Schist	Kuiseb
MAR1093	7	8	105639	13		-10	130	Biotite Schist	Kuiseb
MAR1093	8	9	105640	-10		-10	157	Biotite Schist	Kuiseb
Hole_ID	Depth_From	Depth_To	Sample_ID	U3O8_ppm_XRF75G	U_ppm_PP_XRFa	Th_ppm	V_ppm	Major_Rock1	Formation
MAR1093	9	10	105641	-10		-10	136	Biotite Schist	Kuiseb
MAR1093	10	11	105642	-10		-10	129	Biotite Schist	Kuiseb
MAR1093	11	12	105646	-10		-10	131	Biotite Schist	Kuiseb
MAR1100	1	2	105648	86		-10	128	Biotite Schist	Kuiseb
MAR1100	2	3	105649	41		-10	139	Biotite Schist	Kuiseb
MAR1100	3	4	105650	206		-10	161	Biotite Schist	Kuiseb
MAR1100	6	7	105653	67		-10	157	Biotite Schist	Kuiseb
MAR1100	7	8	105654	21		-10	125	Biotite Schist	Kuiseb
MAR1100	8	9	105655	-10		-10	174	Biotite Schist	Kuiseb
MAR1100	9	10	105657	-10		-10	229	Biotite Schist	Kuiseb
MAR1100	10	11	105658	-10		-10	161	Biotite Schist	Kuiseb
MAR1100	11	12	105659	-10		-10	169	Biotite Schist	Kuiseb
MAR1105	3	4	105663	228		-10	143	Biotite Schist	Kuiseb
MAR1105	5	6	105665	32		-10	127	Biotite Schist	Kuiseb
MAR1105	6	7	105666	-10		-10	132	Biotite Schist	Kuiseb
MAR1105	7	8	105670	13		-10	134	Biotite Schist	Kuiseb
MAR1105	8	9	105671	16		-10	193	Biotite Schist	Kuiseb
MAR1105	9	10	105672	-10		10	195	Biotite Schist	Kuiseb
MAR1105	10	11	105673	-10		-10	198	Biotite Schist	Kuiseb
MAR1105	11	12	105674	-10		-10	175	Biotite Schist	Kuiseb

MAR1113	4	5	105679	-10		-10	144	Biotite Schist	Kuiseb
MAR1113	5	6	105681	-10		-10	-10	Biotite Schist	Kuiseb
MAR1113	6	7	105682	-10		-10	12	Biotite Schist	Kuiseb
MAR1113	7	8	105683	-10		-10	99	Biotite Schist	Kuiseb
Hole_ID	Depth_From	Depth_To	Sample_ID	U3O8_ppm_XRF75G	U_ppm_PP_XRFa	Th_ppm	V_ppm	Major_Rock1	Formation
MAR1124	5	6	105696	15		-10	134	Biotite Schist	Kuiseb
MAR1124	6	7	105697	-10		-10	117	Biotite Schist	Kuiseb
MAR1124	7	8	105698	-10		-10	125	Biotite Schist	Kuiseb
MAR1124	9	10	105700	12		-10	109	Biotite Schist	Kuiseb
MAR1124	10	11	105701	-10		-10	94	Biotite Schist	Kuiseb
MAR1124	11	12	105702	-10		-10	108	Biotite Schist	Kuiseb
MAR1136	1	2	105705	168		-10	95	Biotite Schist	Kuiseb
MAR1136	2	3	105706	153		-10	108	Biotite Schist	Kuiseb
MAR1136	3	4	105707	446		-10	185	Biotite Schist	Kuiseb
MAR1136	4	5	105708	511		-10	183	Biotite Schist	Kuiseb
MAR1136	8	9	105712	52		-10	116	Biotite Schist	Kuiseb
MAR1136	9	10	105713	17		-10	96	Biotite Schist	Kuiseb
MAR1136	10	11	105714	118		-10	134	Biotite Schist	Kuiseb
MAR1136	11	12	105718	85		-10	121	Biotite Schist	Kuiseb
MAR1136	12	13	105719	133		-10	157	Biotite Schist	Kuiseb
MAR1136	13	14	105720	71		-10	147	Biotite Schist	Kuiseb
MAR1136	14	15	105721	73		-10	132	Biotite Schist	Kuiseb
MAR1136	16	17	105723	-10		-10	133	Biotite Schist	Kuiseb
MAR1147	8	9	105755	-10		-10	113	Biotite Schist	Kuiseb

Hole_ID	Depth_From	Depth_To	Sample_ID	U3O8_ppm_XRF75G	U_ppm_PP_XRFa	Th_ppm	V_ppm	Major_Rock1	Formation
MAR1147	9	10	105756	-10		-10	106	Biotite Schist	Kuiseb
MAR1147	10	11	105757	-10		-10	156	Biotite Schist	Kuiseb
MAR1147	11	12	105758	-10		-10	183	Biotite Schist	Kuiseb
MAR1159	2	3	105761	29		-10	118	Biotite Schist	Kuiseb
MAR1159	3	4	105762	23		-10	138	Biotite Schist	Kuiseb
MAR1159	4	5	105766	30		-10	147	Biotite Schist	Kuiseb
MAR1165	1	2	105784	159		-10	100	Biotite Schist	Kuiseb
MAR1165	9	10	105795	25		-10	78	Biotite Schist	Kuiseb
MAR1165	10	11	105796	18		-10	72	Biotite Schist	Kuiseb
MAR1165	11	12	105797	79		-10	81	Biotite Schist	Kuiseb
MAR1165	18	19	105805	-10		-10	74	Biotite Schist	Kuiseb
MAR1165	19	20	105806	-10		-10	89	Biotite Schist	Kuiseb
MAR1165	21	22	105808	15		-10	75	Biotite Schist	Kuiseb
MAR1165	22	23	105809	-10		-10	90	Biotite Schist	Kuiseb
MAR1165	23	24	105810	-10		-10	136	Biotite Schist	Kuiseb
MAR1165	25	26	105815	-10		-10	105	Biotite Schist	Kuiseb
MAR1165	26	27	105816	-10		-10	89	Biotite Schist	Kuiseb
MAR1165	27	28	105817	-10		-10	100	Biotite Schist	Kuiseb
MAR1165	28	29	105818	-10		-10	141	Biotite Schist	Kuiseb
MAR1181	11	12	105852	55		-10	178	Biotite Schist	Kuiseb
MAR1181	13	14	105854	-10		-10	82	Biotite Schist	Kuiseb
MAR1181	15	16	105856	-10		-10	159	Biotite Schist	Kuiseb
MAR1181	16	17	105857	-10		-10	167	Biotite Schist	Kuiseb

MAR1181	17	18	105858	-10		-10	160	Biotite Schist	Kuiseb
MAR1181	18	19	105862	-10		-10	151	Biotite Schist	Kuiseb
MAR1181	19	20	105863	-10		-10	136	Biotite Schist	Kuiseb
MAR1184	2	3	105866	87		-10	97	Biotite Schist	Kuiseb
MAR1184	13	14	105878	28		-10	116	Biotite Schist	Kuiseb
MAR1184	14	15	105879	-10		-10	113	Biotite Schist	Kuiseb
Hole_ID	Depth_From	Depth_To	Sample_ID	U3O8_ppm_XRF75G	U_ppm_PP_XRFa	Th_ppm	V_ppm	Major_Rock1	Formation
MAR1184	15	16	105880	23		-10	144	Biotite Schist	Kuiseb
MAR1184	16	17	105881	-10		-10	145	Biotite Schist	Kuiseb
MAR1192	9	10	105894	14		-10	123	Biotite Schist	Kuiseb
MAR1192	11	12	105897	-10		-10	141	Biotite Schist	Kuiseb
MAR1215	7	8	105921	13		-10	119	Biotite Schist	Kuiseb
MAR1215	8	9	105922	19		-10	119	Biotite Schist	Kuiseb
MAR1215	9	10	105923	40		-10	136	Biotite Schist	Kuiseb
MAR1215	10	11	105924	36		-10	133	Biotite Schist	Kuiseb
MAR1215	11	12	105925	-10		-10	115	Biotite Schist	Kuiseb
MAR1215	12	13	105926	-10		-10	131	Biotite Schist	Kuiseb
MAR1215	13	14	105927	-10		-10	141	Biotite Schist	Kuiseb
MAR1215	14	15	105928	-10		-10	181	Biotite Schist	Kuiseb
MAR1226	6	7	105951	62		-10	80	Biotite Schist	Kuiseb
MAR1253	11	12	106013	13		-10	104	Biotite Schist	Kuiseb
MAR1266	8	9	106054	58		-10	131	Biotite Schist	Kuiseb
MAR1266	9	10	106055	48		-10	101	Biotite Schist	Kuiseb
MAR1266	12	13	106058	40		-10	122	Biotite Schist	Kuiseb

MAR1266	13	14	106059	18		-10	134	Biotite Schist	Kuiseb
MAR1266	14	15	106060	49		-10	143	Biotite Schist	Kuiseb
MAR1348	20	21	106335	13		10	202	Biotite Schist	Kuiseb
MAR1348	21	22	106336	831		-10	175	Biotite Schist	Kuiseb
MAR1361	0	1	106348	124		-10	143	Biotite Schist	Kuiseb
MAR1361	5	6	106353	53		-10	149	Biotite Schist	Kuiseb
MAR1361	6	7	106354	-10		-10	145	Biotite Schist	Kuiseb
Hole_ID	Depth_From	Depth_To	Sample_ID	U3O8_ppm_XRF75G	U_ppm_PP_XRFa	Th_ppm	V_ppm	Major_Rock1	Formation
MAR1361	12	13	106361	-10		-10	112	Biotite Schist	Kuiseb
MAR1448	26	27	106557	-10		-10	160	Biotite Schist	Kuiseb
MAR1471	29	30	106632	-10		-10	85	Biotite Schist	Kuiseb
MAR1482	18	19	106655	-10		-10	193	Biotite Schist	Kuiseb
MAR1482	19	20	106656	-10		-10	168	Biotite Schist	Kuiseb
MAR1482	20	21	106660	17		-10	194	Biotite Schist	Kuiseb
MAR1485	33	34	106699	-10		-10	108	Biotite Schist	Kuiseb
MAR1506	2	3	106839	45		-10	96	Biotite Schist	Kuiseb
MAR1506	3	4	106840	193		-10	143	Biotite Schist	Kuiseb
MAR1506	14	15	106854	-10		-10	127	Biotite Schist	Kuiseb
MAR1512	14	15	106870	-10		-10	139	Biotite Schist	Kuiseb
MAR1520	6	7	106880	-10		-10	178	Biotite Schist	Kuiseb
MAR1520	11	12	106885	-10		-10	167	Biotite Schist	Kuiseb
MAR1529	1	2	106891	52		-10	149	Biotite Schist	Kuiseb
MAR1529	9	10	106902	43		-10	169	Biotite Schist	Kuiseb
MAR1541	4	5	106935	-10		-10	129	Biotite Schist	Kuiseb

MAR1541	10	11	106941	-10		-10	176	Biotite Schist	Kuiseb
MAR1560	0	1	106968	44		-10	48	Biotite Schist	Kuiseb
MAR1560	4	5	106975	24		11	143	Biotite Schist	Kuiseb

Appendix 5: Langer Heinrich groundwater data, (after Bittner 2009):

Langer Heinrich Uranium - Palaeo-channel groundwater within the mine lease Gawib River 8 km downstream mine												
	Sampling date	2005/07/30	2005/07/26	2005/07/26	2005/07/22	2005/07/20	2005/07/28	2005/08/17	2005/08/18	2005/08/19	2005/08/24	2006/10/12
	Your sample I.D.	**LH 1008**	**LH 1020**	**LH 1049**	**LH 1074**	**LH 1077**	**LH 1146**	**LH 1004**	**LH 1097**	**LH 1160**	**LH 1177**	**WW41180**
Major ions:	**Lab. #**	I050441/1	I050441/2	I050441/3	I050441/4	I050441/5	I050441/6	I050441/7	I050441/8	I050441/9	I050441/10	I060592/2
pH		7.0	7.1	7.0	7.1	7.0	7.0	6.9	7.0	7.0	6.9	7.2
Electrical Conductivity*	**mS/cm**	1817	1032	1149	1077	1436	1090	1953	1607	2481	1471	666
TDS (det.)	**mg/l**	11778	6292	7208	6603	9016	6671	12938	10277	16260	9345.4	3975
P-Alkalinity as $CaCO_3$	**mg/l**	0	0	0	0	0	0	0	0	0	0	0
M-Alkalinity as $CaCO_3$	**mg/l**	148	194	181	165	160	186	158	158	129	155	161

T-Hardness as $CaCO_3$	**mg/l**	2744	1606	2113	1699	3045	1727	2951	2656	3645	2474	992
Ca-Hardness as $CaCO_3$	**mg/l**	2053	1141	1446	1139	2167	1278	2222	2005	2834	1943	704
Mg-Hardness as $CaCO_3$	**mg/l**	692	465	667	560	877	449	729	651	811	531	288
Chloride as Cl^-	**mg/l**	5605	2981	3468	3278	4560	3064	5582	4560	7577	4347	1856
Fluoride as F^-	**mg/l**	2.4	2.0	1.8	2.2	2.0	1.8	3.0	2.9	2.8	2.3	1.8
Sulphate as SO_4^{2-}	**mg/l**	1119	604	628	417	574	686	1743	958	1389	780	460
Nitrate as N	**mg/l**	5.8	6.4	8.5	7.8	9.0	6.0	5.1	4.3	4.5	4.6	9.7
Nitrite as N	**mg/l**	0.02	0.01	0.01	0.01	0.01	0.01	0.01	0.01	0.02	0.02	0.01
Calcium as Ca	**mg/l**	822	457	579	456	868	512	890	803	1135	778	282
Magnesium as Mg	**mg/l**	168	113	162	136	213	109	177	158	197	129	70

Sodium as Na	**mg/l**	2744	1408	1462	1409	1972	1462	2844	2305	3738	2395	1039
Potassium as K	**mg/l**	208	103	109	109	143	110	249	196	284	152	61
Trace metal analysis:												
Iron as Fe	**µg/l**	<10	<10	50	<10	<10	<10	<10	<10	<10	<10	200
Manganese as Mn	**µg/l**	20	<10	<10	<10	<10	<10	90	110	330	50	70
Arsenic as As	**µg/l**	60	30	30	40	50	40	70	60	100	60	3
Bismuth as Bi	**µg/l**	<10	<10	<10	<10	<10	<10	<10	<10	<10	<10	<10
Cadmium as Cd	**µg/l**	<10	<10	<10	<10	<10	<10	<10	<10	<10	<10	<10
Copper as Cu	**µg/l**	590	510	550	610	840	540	520	490	580	460	<10
Mercury as Hg	**µg/l**	<10	<10	<10	<10	<10	<10	<10	<10	<10	<10	<10
Antimony as Sb	**µg/l**	<10	<10	<10	<10	<10	<10	<10	<10	<10	<10	<10

Selenium as Se	**µg/l**	210	120	140	130	160	120	180	150	250	160	10
Tellurium as Te	**µg/l**	<10	<10	<10	<10	<10	<10	<10	<10	<10	<10	<10
Uranium as U	**µg/l**	90	150	120	160	160	130	180	140	60	110	60
Uranium as U_3O_8 calc.	**µg/l**	107	179	143	190	190	155	214	167	71	131	71
Vanadium as V	**µg/l**	300	190	230	190	200	200	340	290	330	250	50

Appendix 6: Some groundwater data for the area around the Klein Trekkopje uranium deposit, (after Youlton 2006).

U(ppm)	Mg (ppm)	V(ppm)	Sr(ppm)	K(ppm)	Ca(ppm)
0	0.0545	0.0045	0.0035	0.1365	0.5955
0.48	42.3425	0.0645	14.5455	135.4655	191.6985
0.272	217.3775	0.1685	36.3245	255.8375	838.1925
0.147	185.3225	0.1155	25.0165	126.8375	497.3375
0.144	190.5635	0.1165	25.2975	129.9835	500.8685
0.176	139.1785	0.1155	21.6665	113.6265	482.5315
0.1	332.3725	0.0895	25.8195	132.8615	570.9405
0.164	80.4765	0.0855	20.7075	118.1655	483.7065
0.405	91.0125	0.0625	25.7885	146.1725	475.7985
0.229	240.6395	0.1885	57.4565	285.1985	1182.159
0.237	166.6735	0.1045	33.3355	107.7205	844.4955
0.119	37.5695	0.0925	6.8955	87.7815	181.2785
0.708	385.0305	0.1025	43.7965	215.4885	721.8215
0.117	153.2835	0.1375	24.0805	175.6055	748.7225
0.15	98.9965	0.0885	14.5255	63.0015	426.5015

0.421	218.7665	0.0755	30.8155	108.3945	557.6255
0.52	245.6375	0.1215	28.0915	120.4345	588.5265
0.511	244.0935	0.1225	27.8865	121.0405	597.9405
0.313	145.1675	0.1405	22.6475	91.4725	593.1145
0.09	504.7985	0.2485	46.0165	427.8025	1152.513
0.013	161.7475	0.2775	18.7975	176.7475	579.0205
0.358	235.4595	0.1795	28.0335	127.8475	775.8155
0.178	113.9835	0.1275	15.5235	66.2695	497.8735
0.213	131.5615	0.1295	18.1705	137.3415	561.7795
0.687	411.8705	0.1175	37.9365	184.1365	799.8335
0.212	140.1895	0.1305	18.1535	124.6125	548.9025
0.091	425.4005	0.1725	39.5675	250.1645	1087.48
0.118	633.5095	0.1865	50.7545	174.8145	1391.429
0.057	294.8505	0.2165	34.9345	147.4385	1166.488
0.443	69.2525	0.1265	10.4285	108.4145	301.1685
0.443	69.6035	0.1285	10.6275	108.1785	290.8435
0.596	203.7415	0.1735	32.3215	205.1715	825.1605
0.33	174.6385	0.1675	22.6035	218.4695	666.3305

0.101	53.5965	0.0645	16.1275	73.8135	374.0955
0.244	111.7165	0.0765	21.1555	142.7235	553.7635
0.243	109.7035	0.0805	21.2405	141.5645	549.1065
0.097	120.9055	0.1125	11.8525	97.3965	306.4595
0.364	74.5115	0.0905	10.5545	111.7505	383.3555
0.175	93.5375	0.1055	14.8685	113.9965	530.1565
0.257	128.4825	0.1565	18.1065	74.2895	594.7575
0.139	286.6365	0.1685	33.2935	214.9105	772.5515
0.137	100.2505	0.1495	20.7395	114.4765	780.2195
0.262	294.8485	0.2205	35.6805	162.1885	1151.671
0.72	454.8795	0.1325	39.3205	189.8725	921.6745
0.047	440.4285	0.2175	39.2635	178.8335	1502.494
0.747	148.7065	0.1215	23.9245	139.9335	667.4345
0.037	331.4785	0.1695	33.3655	137.6905	965.8105